

Some parts of this thesis may have been removed for copyright restrictions.

If you have discovered material in AURA which is unlawful e.g. breaches copyright, (either yours or that of a third party) or any other law, including but not limited to those relating to patent, trademark, confidentiality, data protection, obscenity, defamation, libel, then please read our [Takedown Policy](#) and [contact the service](#) immediately

GLOBAL OPTIMISATION OF COLD-FORMED STEEL SECTIONS

Tuan Dinh Tran, *BEng, MEng*

Doctor of Philosophy



School of Engineering and Applied Science

Aston University

Birmingham, UK

2007

This copy of the thesis has been supplied on condition that anyone who consults it is understood to recognize that its copyright rests with its author and that no quotation from the thesis and no information derived from it may be published without proper acknowledgement.

GLOBAL OPTIMISATION OF COLD-FORMED STEEL SECTIONS

Tuan Dinh Tran, *BEng, MEng*
Doctor of Philosophy
2007

SUMMARY

Cold-formed steel members provide substantial savings due to their high strength-to-weight ratio. As a result, they have become very popular in the construction of industrial, commercial, and agricultural buildings. An important advantage of cold-formed steel is the greater flexibility of cross-sectional shapes and sizes available to the structural steel designer. However, the lack of standard optimised shapes makes the selection of the most economical shape very difficult. This task is further complicated by the complex and highly nonlinear nature of the rules that govern their designs. In this thesis, standard algorithms are used to carry out the optimisation of cold-formed steel purlins such as zed, channel and sigma sections, which are assumed to be simply supported and subjected to a gravity load.

The optimisation problem of the cold-formed steel sections is a highly nonlinear problem in which the objective function is a nonlinear function of the multi-design variables and the constraints are also nonlinear inequality. The constraints of the optimisation problem in the cold-formed steel section consist of strength, deflection and stability requirement as well as the practical geometric constraint of the design variables. For zed, channel and sigma section, the local buckling, distortional buckling and lateral-torsional buckling are considered respectively herein. Currently, the local buckling is based on the BS 5950-5:1998 and EN 1993-1-3:2006. The distortional buckling is calculated by the direct strength method employing the elastic distortional buckling which is calculated by three available approaches such as Hancock (1995), Schafer and Pekoz (1998), Yu (2005). In the optimisation program, the lateral-torsional buckling based on BS 5950-5:1998, AISI and analytical model of Li (2004) are investigated. For the optimisation program, the programming codes are written for optimisation of channel, zed and sigma beam. The full study has been coded into a computer-based analysis program (MATLAB)

Keywords: cold-formed steel section, optimisation, standard algorithms, zed-shape purlin, channel-shape purlin, sigma-shape purlin

ACKNOWLEDGEMENTS

First and foremost, it is difficult to overstate my gratitude to my Ph.D. supervisor, Dr. Long-Yuan Li. With his enthusiasm, his inspiration, and his great efforts to explain things clearly and simply, to provide me an excellent study and working environment I would like to thank him for directing me into this challenging and interesting research field. Throughout my thesis-writing period, he provided encouragement, sound advice, good teaching, good company, and lots of good ideas. Without his consistent encouragement and help, this work would have never been completed.

I would like to acknowledge the financial support provided partly by the committee of Vice-Chancellor and Principals of the Universities of the U.K. through the Overseas Research Studentship (ORS) awards and by DTA Consultants Company Ltd.

I am most honoured to have been enrolled in the Group of Civil Engineering and Logistics of Aston University, as the support the Group helps postgraduate students to make the PhD process a more successful one. Many thanks go to Dr Purkiss who provided a lot of helpful discussions and comments for my first-year report.

I am most grateful to Rob Poole, who helped me with numerous computer and network problems, and to the secretaries and librarians at Aston University, for helping the departments to run smoothly and for assisting me in many different ways, special thanks go to Sharen Lloyd, Research Student Co-ordinator for her kind assistance.

I wish to thank my postgrad colleagues and dear friends, Mrs Xiao-ting Chu, Mr Baisen He, who gave me generous support at various stages, whether direct advice about my subject or help with personal problems. I enjoyed the time being with them. I also acknowledge the kindness provided by my colleague, particularly Betty Tam in MB171 from Bio-mechanical Engineering. Thanks also to the Vietnamese society in Aston University. I felt warm and happy with them during my studies in the UK.

Finally, my sincere appreciation is attributed to my family. My wife, Thuy Cam Duong provided great support, encouragement and understanding throughout the whole period of my study. But most importantly, I would like to give my best acknowledgement and honour to my parents for their love.

CONTENTS

1	INTRODUCTION	1
1.1	OVERVIEW OF COLD-FORMED STEEL	1
1.2	BACKGROUND OF PROJECT	2
1.3	AIMS OF THE THESIS	3
1.4	ORDER OF PRESENTATION	5
2	LITERATURE REVIEW	7
2.1	COLD-FORMED STEEL SECTION	7
2.1.1	Definition	7
2.1.2	Characteristics of cold-formed steel section	7
2.2	METHOD OF FORMING	9
2.3	OPTIMISATION OF COLD-FORMED STEEL MEMBERS	11
2.3.1	Neural network	13
2.3.2	Genetic algorithms	16
2.4	LOCAL BUCKLING BEHAVIOUR	19
2.4.1	Effective width approach	19
2.4.2	Effective cross section	21
2.4.3	Design specification	22
2.5	DISTORTIONAL BUCKLING BEHAVIOUR	24
2.5.1	Model for distortional buckling in column	24
2.5.2	Model for distortional buckling in beam	25
2.6	LATERAL-TORSIONAL BUCKLING BEHAVIOUR	31
2.6.1	Recent study in lateral-torsional buckling	31
2.6.2	Analytical model for lateral-torsional buckling	33
2.7	CALCULATION OF DEFLECTION	40
2.8	FINITE STRIP METHOD	41
2.8.1	Initial stiffness matrix for plates	44
2.8.2	Geometrical stiffness matrix for plates	48
2.8.3	The finite strip solution method	49

2.8.4	The limitation of finite strip method	50
3	OPTIMISATION PROBLEM	51
3.1	INTRODUCTION	51
3.2	DESCRIPTION OF THE OPTIMISATION PROBLEM	52
3.3	STANDARD ALGORITHM OPTIMISATION BUILT IN MATLAB.....	57
4	CONSTRAINTS IN THE OPTIMISATION PROBLEM.....	72
4.1	GENERAL	72
4.2	GEOMETRICAL CONSTRAINTS	72
4.3	STRENGTH CONSTRAINTS	74
4.3.1	Local buckling.....	74
4.3.1.1	British standard BS 5950-5:1998.....	74
4.3.1.2	Eurocode EN 1993-1-3:2006	77
4.3.2	Distortional buckling.....	80
4.3.2.1	Hancock's model.....	80
4.3.2.2	Direct strength method.....	81
4.3.2.3	Distortional buckling based on EN 1993-1-3:2006	88
4.3.3	Lateral-torsional buckling	91
4.3.3.1	Lateral-torsional buckling based on BS 5950-5:1998.....	91
4.3.3.2	Lateral-torsional buckling based on AISI specification.....	94
4.3.3.3	Lateral-torsional buckling based on Li's model.....	96
4.3.4	Deflection constraint.....	97
4.3.5	Shear strength in web.....	98
4.4	SUMMARY	99
5	OPTIMISATION OF CHANNEL SECTION PURLINS.....	100
5.1	BEHAVIOUR OF SINGLE SPAN CHANNEL PURLIN	100
5.1.1	Introduction.....	100
5.1.2	Effects of dimensions changes on the cross-sections local buckling resistance	101
5.1.3	Effects of dimension changes on the lateral-torsional buckling based on BS 5950-5:1998	105
5.1.4	Effects of the dimensions changes on deflection of the purlin based on BS 5950-5:1998	106
5.1.5	Investigation of the distortional buckling resistance of purlin.....	107

5.1.6	Comparisons lateral-torsional buckling moment of resistance based on different calculation methods.....	109
5.2	OPTIMISATION PROCEDURE	112
5.2.1	Description of problems.....	112
5.2.2	Optimisation process in MATLAB programme	113
5.3	SELECTION OF PARAMETERS	115
5.4	NUMERICAL OPTIMISATION RESULTS	115
5.4.1	Optimisation result based on BS 5950-5:1998	115
5.4.2	Optimisation result based on BS 5950-5:1998 considering distortional buckling.....	121
5.5	CONCLUSION	128
6	OPTIMISATION OF ZED PURLIN SECTIONS.....	129
6.1	BEHAVIOUR OF SINGLE SPAN ZED PURLIN	129
6.1.1	Introduction.....	129
6.1.2	Design zed purlin subjected to bending	130
6.1.3	Effects of dimensions changes on the cross section local buckling resistance	130
6.1.4	Effects of dimensions changes on the lateral-torsional buckling.....	132
6.1.5	Effects of dimensions changes on the deflection of the zed purlin....	133
6.1.6	Distortional buckling.....	134
6.1.7	Comparison of lateral-torsional buckling results	135
6.2	SELECTION OF PARAMETERS OF OPTIMISATION PROBLEM.....	138
6.3	NUMERICAL OPTIMISATION RESULTS	139
6.3.1	Optimisation results based on BS 5950-5:1998.....	139
6.3.2	Optimisation results based on BS 5950-5:1998 considering distortional buckling.....	145
6.4	CONCLUSION.....	151
7	OPTIMISATION OF THE SIGMA PURLIN SECTION	153

7.1	BEHAVIOUR OF A SINGLE SPAN SIGMA PURLIN	153
7.1.1	Introduction	153
7.1.2	Effect of the depth of the web stiffener in the plane perpendicular to the web on local buckling	154
7.1.3	Effect of the depth of web stiffener in plane of web on local buckling resistance	156
7.2	DESIGN OF SIGMA SECTION PURLIN BASED ON BS 5950-5:1998	157
7.2.1	General	157
7.2.2	Determination of moment capacity based on the local buckling	157
7.2.3	Effect of dimensions changes on the moment capacity	158
7.2.4	Calculation of lateral-torsional buckling of sigma section	159
7.2.5	Comparison of the lateral-torsional buckling results	160
7.2.6	Distortional buckling.....	162
7.3	OPTIMISATION OF SIGMA PURLIN.....	166
7.3.1	Selection of parameters.....	166
7.3.2	Optimisation results based on BS 5950-5:1998.....	167
7.3.3	Optimisation result based on BS 5950-5:1998 and considering distortional buckling	173
7.4	CONCLUSION.....	179
8	CONCLUSIONS AND FUTURE RESEARCH.....	180
8.1	CHAPTER SYNOPSIS.....	180
8.2	MATHEMATICAL MODELLING OF THE OPTIMISATION PROBLEM 180	
8.3	DESIGN CONSTRAINTS OF OPTIMISATION.....	181
8.4	OPTIMISATION RESULTS OF CHANNEL SECTION.....	181
8.5	OPTIMISATION RESULTS OF ZED SECTION	182
8.6	OPTIMISATION RESULTS OF SIGMA SECTION	183
8.7	HOW TO APPLY THE RESEARCH RESULTS IN PRACTICAL DESIGN	184

8.8	DISCUSSION FOR FUTURE RESEARCH.....	185
	REFERENCE.....	187
	APPENDIX.....	195
A.1	FINITE STRIP METHOD.....	195
A.1.1	Plane stress stiffness matrix.....	195
A.1.2	Bending stiffness matrix.....	196
A.1.3	Geometric stiffness matrix (CUFSM).....	197
A.1.4	Coupled geometric stiffness matrix of semi-analytical finite strip method.....	198
A.1.5	Finite strip programme scheme.....	199
A.2	EXPRESSIONS OF SECTION PROPERTIES.....	200
A.2.1	Zed sections.....	200
A.2.2	Channel sections.....	202
A.2.3	Sigma section or arbitrary open section.....	204
A.3	NUMERICAL OPTIMISATION RESULTS.....	211
A.3.1	Steel lipped channel wall stud in compression based on EN 1993-1- 3:2006.....	211
A.3.2	Simple steel lipped channel purlin in bending based on EN 1993-1-3:2006	214
A.4	PUBLICATIONS.....	217

LIST OF FIGURES & TABLES

Fig. 2.1: Cold roll forming machine.....	10
Fig. 2.2: Press brake machine.	10
Fig. 2.3: Neural network with one hidden layer (El-Kassas, 2001).	15
Fig. 2.4: Flow chart for the neural network training and operation stages.	16
Fig. 2.5: Structure of the GA.....	18
Fig. 2.6: Buckling in a cassette section column (Davies, 2000).	20
Fig. 2.7: Effective width of plane element stiffened along both edges.....	20
Fig. 2.8: Distortional buckling models (Hancock,1997).....	24
Fig. 2.9: Analytical distortional buckling model (Hancock, 1997).	26
Fig. 2.10: Lip-flange component geometric properties.....	28
Fig. 2.11: An analytical model for lateral-torsional buckling analysis.	34
Fig. 2.12: Displacement field for typical simply supported finite strip.	44
Fig. 2.13: Strip with compression stress distribution.....	44
Fig. 3.1: Simply supported beam subjected to uniformly-distributed transverse loading.....	55
Fig.3.2: Graphical optimisation representation.....	56
Fig. 3.3: Three-dimensional plot (P. Venkataraman, 2002).....	62
Fig. 4.1: Behaviour of the member in bending.	74
Fig. 4.2: Distortional buckling mode of flexural members.....	80
Fig. 4.3: Analytical model for flange (Yu 2005)	82
Fig.4.4: Element with simple lip edge stiffener.	86
Fig. 4.5: Development of simple expression for distortional buckling k_d of C and Z- section based on closed-form solution (Yu, 2005).....	87
Fig. 4.6: Determination of spring stiffness.....	89
Fig. 4.7: Compression resistance of a flange with an edge stiffener (Fig 5.8 in EN 1993-1-3:2006).....	91
Fig. 4.8: Deformation of lateral-torsional buckling.....	92
Fig. 4.9: Single and double curvature bending.	93
Fig. 5.1: Dimension and model analysis of single span channel purlin under vertical uniformly distributed load.....	100
Fig. 5.2: Comparison between local buckling moment and yielding moment...102	
Fig. 5.3: Moment efficiency based on BS 5950-5:1998.	102
Fig. 5.4: Comparison between local buckling moment and yielding moment..103	
Fig. 5.5: Moment efficiency based on EN 1993-1-3:2006.....	103
Fig. 5.6: Comparison of local buckling moment between BS 5950-5:1998 and	104
Fig. 5.7: Comparison of local buckling moment between BS 5950-5:1998 and	104
Fig. 5.8: Effects of the dimensions on the moment of lateral-torsional buckling based on BS 5950-5:1998.	106
Fig. 5.9: Effects of the dimensions on moment resistance taking into account of deflection based on BS 5950-5:1998.	107
Fig. 5.10: Distortional buckling comparison.....	109
Fig. 5.11: Lateral-torsional buckling with the variation of the width of flange.110	
Fig. 5.12: Lateral-torsional buckling with the variation of the depth of web. ...111	
Fig. 5.13: Lateral-torsional buckling with the variation of the span length.....111	
Fig. 5.14: Lateral-torsional buckling with the variation of the depth of lip.....112	

Fig. 5.15: The computational procedure of the optimisation programme.....	114
Fig. 5.16: Curves of optimum thickness over span length for un-braced channel beams based on BS 5950-5:1998.....	116
Fig. 5.17: Curves of optimum web depth over span length for un-braced channel beams based on BS 5950-5:1998.....	116
Fig. 5.18: Curves of optimum flange width over span length for un-braced channel beams based on BS 5950-5:1998.....	117
Fig. 5.19: Curves of optimum lip depth over span length for un-braced channel beams based on BS 5950-5:1998.....	118
Fig. 5.20: Curves of optimum gross area section over span length for un-braced channel beams based on BS 5950-5:1998.....	118
Fig. 5.21: Moment capacities of the optimised section over span length for un-braced channel beams based on BS 5950-5:1998 for $q= 2$ kN/m.....	119
Fig. 5.22: Moment capacities of the optimised section over span length for un-braced channel beams based on BS 5950-5:1998 for $q= 3$ kN/m.....	119
Fig. 5.23: Moment capacities of the optimised section over span length for un-braced channel beams based on BS 5950-5:1998 for $q= 4$ kN/m.....	120
Fig. 5.24: Curves of optimum thickness over span length for un-braced channel beams based on BS 5950-5:1998 taking into account distortional buckling.....	122
Fig. 5.25: Curves of optimum web depth over span length for un-braced channel beams based on BS 5950-5:1998 taking into account distortional buckling.....	123
Fig. 5.26: Curves of optimum flange width span length for un-braced channel beams based on BS 5950-5:1998 taking into account distortional buckling.....	124
Fig. 5.27: Curves of optimum lip depth over span length for un-braced channel beams based on BS 5950-5:1998 taking into account distortional buckling.....	125
Fig. 5.28: Curves of optimum gross area section over span length for un-braced channel beams based on BS 5950-5:1998 taking into account distortional buckling (DB).	126
Fig. 5.29: Moment capacities of the optimised section over span length for un-braced channel beams based on BS 5950-5:1998 taking into account DB for $q= 2$ kN/m.....	126
Fig. 5.30: Moment capacities of the optimised section over span length for un-braced channel beams based on BS 5950-5:1998 taking into account DB for $q= 3$ kN/m.....	127
Fig. 5.31: Moment capacities of the optimised section over span length for un-braced channel beams based on BS 5950-5:1998 taking into account DB for $q= 4$ kN/m.....	127
Fig. 6.1: Zed purlin in the slope roof system.....	129
Fig. 6.2: Effects of the dimensions on the moment capacity.....	131
Fig. 6.3: Effects of the dimensions on the moment efficiency.....	132
Fig. 6.4: Effects of the dimensions on the moment of lateral-torsional buckling based on BS 5950-5:1998.....	133
Fig. 6.5: Effects of the dimensions on the moment resistance taking into account of deflection.....	134
Fig. 6.6: Distortional buckling comparison.....	135
Fig. 6.7: Lateral-torsional buckling with variation of the flange width.....	136

Fig. 6.8: Lateral-torsional buckling with variation of the web depth.....	137
Fig. 6.9: Lateral-torsional buckling with variation of the span.....	137
Fig. 6.10: Lateral-torsional buckling with variation of the the lip.	138
Fig. 6.11: Global optimum design thickness versus span length for un-braced zed beams based on BS 5950-5:1998.	139
Fig. 6.12: Global optimum design web depth versus span length for un-braced zed beams based on BS 5950-5:1998.....	140
Fig. 6.13: Global optimum design flange width versus span length for un-braced zed beams based on BS 5950-5:1998.....	141
Fig. 6.14: Global optimum design lip depth versus span length for un-braced zed beams based on BS 5950-5:1998.	142
Fig. 6.15: Global optimum design cross area section versus span length for un-braced zed beams based on BS 5950-5:1998.	143
Fig. 6.16: Moment capacities of the optimised section over span length for un-braced zed beams based on BS 5950-5:1998 for $q= 2\text{kN/m}$	143
Fig. 6.17: Moment capacities of the optimised section over span length for un-braced zed beams based on BS 5950-5:1998 for $q= 3\text{kN/m}$	144
Fig. 6.18: Moment capacities of the optimised section over span length for un-braced zed beams based on BS 5950-5:1998 for $q= 4\text{kN/m}$	144
Fig. 6.19: Global optimum design thickness versus span length for un-braced zed beam based on BS 5950-5:1998 taking into account distortional buckling.	146
Fig. 6.20: Global optimum design web depth versus span length for un-braced zed beam based on BS 5950-5:1998 taking into account distortional buckling.....	147
Fig. 6.21: Global optimum design flange width versus span length for un-braced zed beam based on BS 5950-5:1998 taking into account distortional buckling.....	148
Fig. 6.22: Global optimum design lip depth versus span length for un-braced Zed beam based on BS 5950-5:1998 taking into account distortional buckling.	149
Fig. 6.23: Global optimum design cross area section versus span length for un-braced zed beams based on BS 5950-5:1998 taking into account distortional buckling.....	149
Fig. 6.24: Moment capacities of the optimised section over span length for un-braced zed beam based on BS 5950-5:1998 taking into account DB for $q=2\text{kN/m}$	150
Fig. 6.25: Moment capacities of the optimised section over span length for un-braced zed beam based on BS 5950-5:1998 taking into account DB for $q=3\text{kN/m}$	150
Fig. 6.26: Moment capacities of the optimised section over span length for un-braced zed beam based on BS 5950-5:1998 taking into account DB for $q=4\text{kN/m}$	151
Fig.7.1: Dimension of the cross-section of the Σ Shape purlin.	153
Fig. 7.2: Effect of depth of the web stiffener on local buckling mode shape. ...	154
Fig. 7.3: Effect of the web stiffener on the load factor of the sigma purlin section.	155
Fig. 7.4: Comparison between section with stiffener and without stiffener.	155
Fig.7.5: Buckling mode shape of the section with h_2 from 10 to 30mm.....	156
Fig. 7.6: Effective section of the Sigma purlin.	158

Fig. 7.7: Effect of position of web stiffener on the moment capacity.....	159
Fig.7.8: Effect of the flange to the lateral-torsional buckling.	161
Fig. 7.9: Effect of the position of the web stiffener.	161
Fig. 7.10: Distortional buckling shape mode of sigma section.	162
Fig.7.11: Effect of the flange width on distortional buckling of sigma section calculated by direct strength method.....	163
Fig.7.12: Effect of web stiffener position on the elastic distortional buckling strength.....	164
Fig. 7.13: Effect of depth of lip on the distortional buckling resistance.	165
Fig. 7.14: Effect of lip depth on the distortional buckling strength.	166
Fig.7.15: Global optimum design thickness versus span length for un-braced sigma beams based on BS 5950-5:1998.	167
Fig.7.16: Global optimum design web depth versus span length for un-braced sigma beams based on BS 5950-5:1998.	168
Fig.7.17: Global optimum design flange width versus span length for un-braced sigma beams based on BS 5950-5:1998.	169
Fig.7.18: Global optimum design position of web stiffener in plane of web versus span length for sigma beams based on BS 5950-5:1998.	169
Fig.7.19: Global optimum design web stiffener depth versus span length for sigma beams based on BS 5950-5:1998.	170
Fig.7.20: Optimum crosses sectional area versus span length for sigma beams based on BS 5950-5:1998.	171
Fig.7.21: Moment capacity of the optimum section versus span length for sigma beam based on BS 5950-5:1998 for $q=2\text{kN/m}$	172
Fig.7.22: Moment capacity of the optimum section versus span length for sigma beam based on BS 5950-5:1998 for $q=3\text{kN/m}$	172
Fig.7.23: Moment capacity of the optimum section versus span length for sigma beam based on BS 5950-5:1998 for $q=4\text{kN/m}$	173
Fig.7.24: Optimum design thickness of sigma section with and without distortional buckling (DB).	174
Fig. 7.25: Optimum design web depth of sigma section with and without distortional buckling (DB).	174
Fig.7.26: Optimum design flange width of sigma section with and without distortional buckling (DB).	175
Fig.7.27: Optimum location of web stiffener of sigma section with and without distortional buckling (DB).	176
Fig.7.28: Optimum design depth of web stiffener of sigma section with and without distortional buckling.	176
Fig.7.29: Optimum design depth of lip of sigma section with and without distortional buckling.	177
Fig.7.30: Moment capacity of the optimised section for un-braced sigma beams based on BS 5950-5:1998 considering distortional buckling for $q=2\text{kN/m}$	177
Fig.7.31: Moment capacity of the optimised section for un-braced sigma beams based on BS 5950-5:1998 considering distortional buckling for $q=3\text{kN/m}$	178
Fig. 7.32: Moment capacity of the optimised section for un-braced sigma beams based on BS 5950-5:1998 considering distortional buckling for $q=3\text{kN/m}$	178

Table 4.1: Internal compression elements.....	79
Table 4.2: Out-stand compression elements	79
Table 4.3: Geometrical flange properties for C and Z-section (Schafer, 1997).	83
Table 5.1: Comparison of optimisation results	121

NOMENCLATURE

Roman Characters

A_e	effective area of the cross section (mm^2)
A_g	gross area of the cross section (mm^2)
A_f	gross area of flange and lip (mm^2)
b	flange width along the middle line (mm)
b_o	overall width of flange (mm)
b_{e1}, b_{e2}, b_{eff}	effective width (mm)
b_{elem}	Element flat width (m)
c	lip length along the middle line (mm)
c_o	overall lip length (mm)
c_{eff}	effective length of the stiffening lip (mm)
C_w	warping constant (mm^6)
$C_i(x)$	equality and inequality constraints of optimisation problem
C_b	bending coefficient
$\{d\}$	vector of nodal degrees of freedom
D_w	section property (mm^6)
$[D]$	plate rigidities matrix
E	modulus of elasticity ($\text{MPa}=\text{N}/\text{mm}^2$)
f_c	extreme compression fibre in section
f_d	elastic distortional buckling stress
f_1, f_2	linear edge stresses (MPa)
$f_i(x, x_i)$	spline interpolation function
$\{f\}$	vector of nodal forces
$F(X)$	objective function of optimisation problem
G	shear modulus (MPa)
h	web depth along the middle line (mm)
h_o	overall depth of the cross section (mm)
I_y, I_z	second moments of the cross-section area about y and z axes (mm^4)
I_{xf}, I_{yf}	second moment of flange lip about axis through intersection between flange and web (mm^4)
I_{yz}	product moment of the cross-section area (mm^4)
I_{xyf}	Product moment of flange lip about axis through intersection between flange and web (mm^4)
I_ω	warping constant calculated based on the sectional coordinate with respect to the centroid (mm^6)
$I_{\omega z}$	sectorial product of inertia with respect to z axis calculated based on the

	sectional coordinate with respect to the centroid (mm^5)
J	torsion constant (mm^4)
J_f	torsion constant of flange and lip (mm^4)
k_x, k_z	translational spring stiffness along x and z axis (MPa)
k_ϕ	rotational spring stiffness (N)
k_σ	buckling factor
$[K]$	initial stiffness matrix
$[K_g]$	geometric stiffness
$[K_{gmn}]$, $[K_{gmm}]$	coupled global geometric stiffness matrix associated with wave number m and n
$[K_M]$, $[K_{gMM}]$	global stiffness matrix and global geometric stiffness matrix associated with wave number M
$[K_{uv}]$, $[K_{w\theta}]$	initial stiffness submatrices for plane stress and bending
L	span length of the beam (mm)
L_b, L_u	lower and upper limit of the length of strip
L_{strip}	Length of strip
M_c	moment capacity
M_{cr}	critical buckling moment (MPa)
M_{crd}	critical elastic distortional buckling moment (N mm)
M_E	Elastic lateral-torsional buckling moment resistance (N mm)
M_{cre}	critical elastic lateral-torsional buckling moment (N mm)
M_{crl}	critical elastic local buckling moment (N mm)
M_n	nominal flexural strength (N mm)
M_{nd}	nominal flexural strength for distortional buckling (N mm)
M_{ne}	nominal flexural strength for lateral-torsional buckling (N mm)
M_{nl}	nominal flexural strength for local buckling (N mm)
M_T	twisting moment (N mm)
M_{Oy} , M_{Oz}	pre-buckling moment about y and z axes (N mm)
M_y , M_z	bending moments about y and z axis (N mm)
M_{yield}	yielding moment (N mm)
M_{y0} , M_{y1} , M_{z0} , M_{z1}	concentrated moments about y and z axes, applied at the ends of the purlin (N mm)
M_ω	warping moment (N mm)
N	number of modes
$[N]$	shape functions
$[N']$	appropriate derivatives of the shape functions $[N]$
p_o	limiting compression stress (MPa)
P	yield stress

p_{cr}	local buckling stress (MPa)
q_y	density of uniformly distributed load (N/mm)
R_y, R_z	radii of curvature of the centroidal axis in the xz and xy planes
s	distance from some chosen origin to the point along the section's middle line (mm)
S_e	section modulus of effective section
S_f	gross section modulus referenced to the extreme compression fibre
t	thickness (mm)
T_1, T_2	tractions (N/mm)
$u(x,y),$ $v(x,y),$ $w(x,y)$	displacements of a finite strip at a point (x,y) (mm)
$\bar{u}(x, y, z),$ $u_b(x)$	longitudinal displacements of the beam at points (x,y,z) and $(x,0,0)$ (mm)
$[u]$	nodal displacement column matrix
U	total strain energy (N mm)
U_0	total strain energy (N mm)
U_1	strain energy generated by the buckling displacements (N mm)
U_{0_beam}	strain energy of the beam due to deflections and rotation (N mm)
U_{0_k}	strain energy stored in two rotational springs over the supports (N mm)
U_{0_spring}	strain energy stored in two springs (N mm)
U_{1_beam}	strain energy due to the deflections and rotation when buckling occurs (N mm)
U_{1_k}	strain energy stored in two rotational springs over the support when buckling occurs (N mm)
U_{1_spring}	strain energy stored in two springs when buckling occurs (N mm)
v, w	pre-buckling deflections of the beam in y and z directions (mm)
v_b, w_b	buckling deflections of the beam in y and z directions respectively (mm)
v_i, w_i	to-be-determined horizontal and vertical deflections at interpolation points x_i (mm)
$\{v_i\}, \{w_i\}$	deflections of the purin centroid at $x=x_i$ (mm)
\bar{v}, \bar{w}	deflections of the beam at point (x,y,z) during the buckling (mm)
W	strain energy generated by the membrane stresses through the nonlinear strains of the buckling displacements (N mm)
W_0	strain energy generated by the load (N mm)
W_1	strain energy generated by the pre-buckling longitudinal stresses through the second-order strains (N mm)
$W_{\alpha b}, W_{\alpha w}$	strain energy generated by bending stress and done by warping stress respectively (N mm)

W_q	strain energy generated by the load due to the load that is not acting at the shear centre (N mm)
\bar{x}, \bar{y}	distance from shear centre of flange to junction between web and flange (mm)
x_i	spline interpolation points
Y_m	depth of compression zone (mm)

Greek Characters

α_1	imperfection factor
$\beta(y,z)$	warping function of St. Venant torsion
β	Ratio of the small end moment to the larger end moment
$\epsilon_x, \gamma_{xy}, \gamma_{xz}$	longitudinal strain and shear strains generated by the buckling displacements
$\epsilon_{x2}, \gamma_{xy2}, \gamma_{xz2}$	second-order non-linear longitudinal strain and shear strains
χ	reduction factor for buckling with respect to the unbuckled capacity
ϕ	angle of twist
ϕ_b	buckling angle of twist
ϕ_i	to-be-determined angle of twist at interpolation points
Δ	deflection for given loading system (mm)
Δ_c	deflection corresponding to M_c (mm)
Δ_{cr}	deflection corresponding to critical bending moment M_{cr} (mm)
Δ_{max}	maximum deflection of beam (mm)
Δ_{lim}	deflection limitation of member based on codes (mm)
∇f	gradient
λ	half buckling wavelength
$\bar{\lambda}$	relative slenderness in the relevant buckling mode
λ_m	distance between restraints which limit the rotation of the lip/flange (mm)
$\bar{\lambda}_p$	plate slenderness
$\omega, \bar{\omega}$	sectional coordinate (mm ²) and corresponding average value (mm ³) with respect to the centroid
$\omega_s, \bar{\omega}_s$	sectional coordinate (mm ²) and corresponding average value (mm ³) with respect to the shear centre
ν	Poisson's ratio
σ_c	maximum compressive stress in the plate element (MPa)

σ_{cr}	critical stress for elastic buckling (MPa)
σ_{eff}	maximum compressive stress in the plate element (MPa)
σ_x	pre-buckling longitudinal stress (MPa)
δ_i	Lagrange multipliers
σ_{xb}, σ_{xw}	longitudinal stresses generated by the bending and twisting moments respectively (MPa)

Chapter 1

1 INTRODUCTION

1.1 OVERVIEW OF COLD-FORMED STEEL

Cold-formed steel products are made by bending a flat sheet of steel at room temperature into a shape that will support more load than the flat sheet itself. Cold-formed steel has been produced and widely used as corrugated sheets for farm buildings, industrial and commercial buildings, sheeting and cladding, and secondary structural members to support. Trapezoidal sheeting is usually fixed to the members in order to enclose the building. The shapes of the cross-section of the members are mostly that of zed, channel or sigma.

Cold-formed steel members have been increasingly used recently in various buildings because of advantages such as lightness, high strength and stiffness, fast and easy erection, economy in transportation and handling. Although not yet so evident in the UK, in other parts of the developed world there is an extremely rapid development in use of cold-formed framing systems for houses and other low-rise construction (Davies, 2000). In USA, It has been reported that about 500 homes were built in light gauge steel in 1992, increasing to 15,000 in 1993 and 75,000 in 1994. By 2002 the increase had reached to a further five-fold.

The increases use of higher-strength steel has inevitably led to reduction in the thickness of the section and therefore, considerations of the local stability has lead logically to the development of the highly stiffened section with more folds and rolled in stiffeners. Consequently, design procedures are becoming more complicated and engineers will experience difficulty if they try to obtain results by hand calculation. In

addition, the optimum cross section should also be considered in terms of the increase of the load capacity of the members and saving materials.

1.2 BACKGROUND OF PROJECT

Cold-formed steel members provide substantial savings due to their high strength-to-weight ratio. As a result, they have become very popular in the construction of industrial, commercial and agricultural buildings. An important advantage of cold-formed steel is the greater flexibility of cross-sectional shapes and sizes available to the structural steel designer. Through cold-forming operations, steel sheets, strips or plates can be shaped easily and sized to meet a large variety of design options. Such a large number of design possibilities create a very important challenge in choosing the most economical cold-formed shape in the design of steel structures.

The basic problem of an economic design is to achieve the least expensive construction that satisfies the design requirements. One of the conditions required for the low cost of erected structure is that the weight of the material should be kept to a minimum, which is associated with a maximum structural efficiency. It has been shown by numerous investigators that for a given loading system, the maximum efficiency can be obtained when all the possible modes of failure (overall and local instabilities, yielding of material, etc.) occur at the same time (Yu WW, 1985). In practice, such ideal conditions may not be easily obtained due to unavoidable limitations such as pre-selected shapes and specific dimensional limitations. However, it can be shown that in some cases there may be a possible mode of failure which will result in a maximum efficiency within the practical limitations. The efficiency of the use of high grade steel depends on the type of failure mode. Under certain conditions,

such as long columns having large slenderness ratios, the failure mode is usually dominated by overall elastic buckling. For sections that have an un-stiffened compression flange with an unusually large width-to-thickness ratio, the failure is usually dominated by local buckling in the elastic range. In such cases, the use of high-strength steel may not result in an economic design because the performance of structural members under these conditions may be the same for different grades of steel. For this reason, the use of high-strength steel in these cases may not be justified as far as the overall cost is concerned. *Therefore, this project focuses on finding out the optimum shapes of cross section, which satisfy the design requirements.*

1.3 AIMS OF THE THESIS

Cold-formed steel is widely used as structural steel for building. The most common applications of cold-formed steel members are used as purlins or rails, the intermediate members between the main structural frame and the corrugated roof or wall sheeting. These members normally work as simple beam subjected to the concentrated load or the uniformly distributed load. Thus, the primary aim of this thesis is to investigate the behaviour of cold-formed steel purlins and to find a suitable design method for the designers amongst the current methods. The main task is to develop a programme to optimise the simply supported purlin sections subjected to the uniformly distributed transverse load based on the conservative and more accurate design method.

Furthermore, the purpose of this thesis is not only to focus on the optimisation of channel, zed and sigma simply supported purlin, but the programme in this study is

used as basic programme to develop the general open access codes used in MATLAB to optimise different kinds of cold-formed steel section. The remaining task for MATLAB users is to define the constraints and objective function of the optimisation problem.

The main aim can be further subdivided into the five sub-sections listed below:

1. To investigate the mechanism of failure of the purlin subjected to the uniformly distributed load, understanding the essential factors in improving the strength capacity of the section.
2. To explore the current effective design approaches for cold-formed steel purlin, identifying the advantages, disadvantages and limitations of these approaches in order to help the structural designer to use the most accurate method in the individual situation.
3. To find the optimum shape of the cross section, in order to inspect the influence of the dimension of each element in the section that plays an integral role in the preliminary optimisation stage.
4. To illustrate the robust optimisation tool of the programming language MATLAB, understanding fully the algorithm structure of the optimisation programme and its applicability in the optimisation of simply supported cold-formed steel purlin.
5. To focus on improving the more precise analysis as well as design method applied to the popular cross sections such as channel, zed beams and the new

proposed sigma section. The numerical optimisation results of those section shapes are presented here.

1.4 ORDER OF PRESENTATION

Chapter 1

Provides an introductory overview of cold-formed steel structures and its applications in structure of the building and the importance of optimisation in the design of sections.

Chapter 2

The findings of recent research about the optimisation of cold-formed steel members are presented herein: a literature review of the failure mode of cold-formed steel members, the current design methods, as well as a discussion of the advantages and disadvantages of these methods.

Chapter 3

Describes the optimisation problem in cold-formed steel structures and presents the application of the robust optimisation tool of the programming language MATLAB in optimising cold-formed sections. An overview of the standard algorithm optimisation is demonstrated.

Chapter 4

In this chapter, the discussion about the constraints of optimisation problem in terms of geometry and strength of the section is described in detail. Furthermore, the different calculation methods are presented to find out the more accurate and

conservative method for the structural designer, which can be used in the optimisation programme.

Chapter 5 and 6

The behaviour of the simply supported channel beam and zed beam is investigated under uniformly distributed transverse loading. The numerical results of the global optimum dimension of those sections are illustrated under a global curve of optimum dimension with the different spans of the beam and the various intensity of the loading.

Chapter 7

This chapter contains a full investigation of the behaviour of the sections with and without stiffener in which the numerical optimisation results are presented. The importance of the stiffener in the web of sigma section in increasing the strength capacity of the section is studied and optimised in order to get the best shape in terms of geometry and strength capacity.

Chapter 8

The optimum results for each kind of section in this study are provided, to provide sufficient information for industrial designers and manufacturers to find the proper nominal dimensions. A conclusion and suggestions for future research are provided.

Chapter 2

2 LITERATURE REVIEW

2.1 COLD-FORMED STEEL SECTION

2.1.1 Definition

In construction, steel members are used quite a lot as the main structural support members. There are two main families of structural members. One is the familiar group of hot-rolled sections which are normally used to carry heavy loads. Other members are called cold-formed steel members which are built up of plates. The cold-formed steel sections are less familiar in steel construction, but nowadays, it is growing very quickly. It is composed of sections of cold-formed from steel sheets, strips, plates, or flat bars in a roll-forming machine or by press brake or bending brake operations. Cold-formed steel has been produced and widely used as corrugated sheets for agricultural farm buildings, industrial and commercial buildings, sheeting and cladding, and secondary structural members to support.

2.1.2 Characteristics of cold-formed steel section

In general, cold-formed steel structural members provide the following advantages in building construction (Yu, 1985):

- As compared with thicker hot-rolled sections, cold-formed light members can be manufactured for relatively light loads and/or short spans;
- Unusual sectional configurations can be produced economically by cold-forming operations and, consequently, favourable strength-to-weight ratios can be obtained;
- Nestable sections can be produced, allowing for compact packaging and shipping;

- Load-carrying panels and decks can provide useful surfaces for floor, roof, and wall construction, and in other cases, they can also provide enclosed cells for electrical and HVAC conduits;
- Load-carrying panels and decks not only withstand loads normal to their surfaces, but they can also act as shear diaphragms to resist force in their own planes if they are adequately interconnected to each other and to supporting members.

Compared with other materials such as timber and concrete, the cold-formed steel structural members have the following qualities:

- Lightness;
- High strength and stiffness;
- Ease of prefabrication and mass production;
- Fast and easy erection and installation;
- Substantial elimination of delays due to weather;
- More accurate detailing;
- Non-shrinking and non-creeping at ambient temperature;
- Uniform quality;
- Economy in transportation and handling.

However, because cold-formed members are usually thin-walled, special care must be given to design. Compared to classical hot-rolled sections, they are characterized by some peculiarities, e.g.:

- Large width to thickness ratios;
- Singly symmetrical or unsymmetrical shapes;

- Un-stiffened or partially un-stiffened parts of sections, which can lead to complicated buckling problems;
- Combined torsional and flexural buckling;
- Local plate buckling;
- Distortional buckling;
- Interaction between local and global buckling;
- Fire resistance.

Also, connections must be designed with care because of the thinness of the members that can lead to local failures. For these reasons, dedicated specifications have been published in the United States first, followed by Europe, Australia and other countries to cover these important questions.

At this moment, cold-formed steels are made through cold forming of a thin plate which is normally from 1.2mm to 6.4mm thick and has a yield stress in the range of 280 to 550N/mm².

2.2 METHOD OF FORMING

Three methods are generally used in the manufacturing of cold-formed sections, such as cold roll forming shown in Fig. 2.1, press brake operation shown in Fig. 2.2, and bending brake operation (Yu, 1985). The method of cold roll forming has been widely used for production of building components as individual structural members for roof, floor and wall panels. The machine used in the cold roll forming consists of pairs of rolls which progressively form strips into the final required shape. A simple section may be produced by a few pairs of rolls. However, a complex section may require more sets of rolls. The speed of the rolling process ranges from 6 to 92m/min. At the

end, the completed section is usually cut to required lengths by an automatic cut-off tool without stopping the machine.

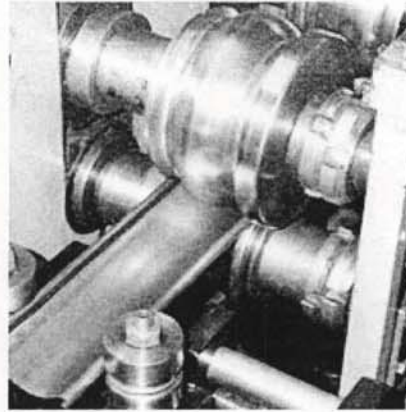


Fig. 2.1: Cold roll forming machine.

For the press brake operation, the section is normally a simple configuration to be produced relatively wider such as roof sheets and decking units. The equipment used in a press brake operation consists essentially of a moving top beam and a stationary bottom bed on which the dies applicable to the particular required product are mounted. Simple sections such as angles, channel or Z-section are formed by press brake operation from sheets, strips, plates or bars in not more than two operations. More complicated sections may take several operations.

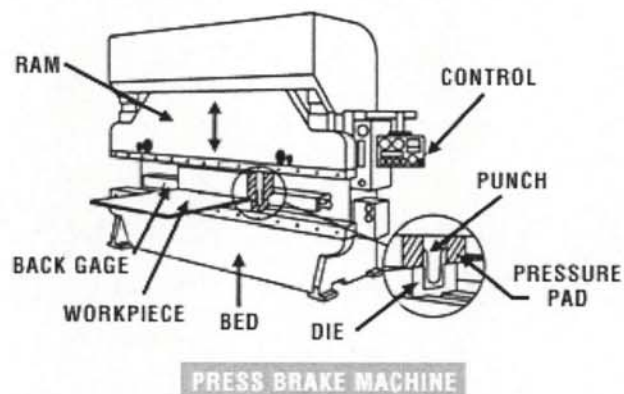


Fig. 2.2: Press brake machine.

2.3 OPTIMISATION OF COLD-FORMED STEEL MEMBERS

Cold-formed steel members provide considerable savings due to their high strength-to-weight ratio. They are very popular in the steel construction of industrial, commercial, and agricultural buildings. An essential advantage of cold-formed steel is the greater flexibility of the cross sectional profiles and sizes available to the structural steel designer. Steel sheets, strips or plates can be shaped easily and sized to meet a large variety of design options through the cold forming operations or press brake operation.

However, this flexibility, in addition to the complex behaviour that dominates cold-formed members design, makes the selection of the most economical section for the particular situation more difficult.

Through structural engineering and computational journals, there are few papers on the optimisation of cold-formed steel structures. The optimisation of cold-formed steel using the computational neural network model has been performed by Karimm and Adeli (1999), but only applied for the Z-shape beam with un-stiffened flange based on the AISI specification. El-Kassas and Mackie (2001) demonstrate the potential of using neural networks to optimise a cold-formed steel channel, lipped channel and hat shape. Nagy (2000) used the genetic algorithm to obtain the optimum shape of trapezoidal sheeting profiles. Tian and Lu (2004) introduced a combined theoretical and experimental study on the minimum weight and associated optimal geometric dimensions of an open-channel steel section subjected to the axial compressive load. The result obtained using nonlinearly constrained optimisation method are compared with those estimated from a simple-minded optimisation

procedure that assumes the simultaneous occurrence of all failure modes including yielding, flexural buckling, torsional flexural buckling, and local buckling. Lu (2003) employed the genetic algorithm to optimise the Zed, Channel and Sigma section based on the Eurocode 3. Recently, Lee (2004) used the Micro Genetic Algorithm to find the optimum cross-section of simply supported cold-formed steel channel beams under uniformly distributed loading. The Micro Genetic Algorithm is one of the improved forms of Genetic Algorithm, to reduce iteration and computing resources by using small populations.

The optimisation problem in structural engineering can be defined mathematically as (Fletcher, 1987):

$$C_i(x) = 0 (i = 1, \dots, m_e) \quad (2.1)$$

$$C_i(x) \leq 0 (i = m_{e+1}, \dots, m) \quad (2.2)$$

$$Z = F(\{X\}) \rightarrow \min. \quad (2.3)$$

where $\{X\}$ the vector of the design variables such as material, topology, configuration or geometric layout, and cross-sectional design variables, $C_i(x)$ are the equality and inequality constraints, m are the number of inequality and equality constraints. $Z = F(\{X\})$ is the objective function and may represent the weight, the cost of structure or any other criterion. The aim of the optimisation problem is to find the design variables in the design space under the constraints, which minimise the objective function. In the practice, the design variables of the optimisation problem in structural engineering are discrete variables. Many mathematical linear and non-linear

programming methods have been developed for solving these optimisation problems. However, no single method has been found to be entirely efficient and robust for all different kinds of engineering optimisation problems. With these methods, if there is more than one local optimum in the problem, the result will depend on the choice of the starting point, and the global optimum cannot be guaranteed. Furthermore, when the objective function and constraints have multiple or sharp peaks, gradient search becomes difficult and unstable (Adeli et al, 1993).

Currently, there are two robust methods of optimisation which have been used to optimise cold-formed steel members such as the Neural Network and the Genetic Algorithm method. Each method has different advantages and disadvantages which will be described in the following part.

2.3.1 Neural network

Neural networks are artificial intelligence algorithms for cognitive tasks, such as learning and optimisation. Neural networks are of interest because of their ability to learn, to make decisions, and to draw conclusions from examples without knowledge of underlying rules. The motivation for neural networks came from attempts to simulate the processes of the human brain, and so to enhance the capabilities of the computer. In terms of internal construction, a neural network is made up of a large number of interconnected processing units (called nodes) that seek to emulate the human neuron. Each node receives input from other nodes to which it is connected, carries out a process, and transmits the output to other nodes. The most popular type neural network is the multilayer perception network (Kassas, 2001).

Commonly, the network is arranged in at least three layers of nodes as shown in Fig. 2.3:

- An input layer that receives input values.
- An output layer that reports the final answer.
- One or more hidden layers between the input and output layers.

Before using the network, it needs to be adequately trained using a carefully selected and large set of solved examples (sets of given input and output values) that effectively cover the range of variables likely to be encountered. The network uses these examples to adjust the weight of its inter-node links so that the error in the output is minimised. A technique called the back propagation is most widely used technique in this optimisation process to improve the network's accuracy, though conjugate gradient methods and genetic algorithms have been also used. In the back propagation technique, the error found at the output layer is propagated back through the network to the input layer, and subsequently, this process of calculating the error and the propagating it back is repeated until the error is reduced to a specific low value, and once this has been achieved, training is considered to be complete, the inter-node link weights are registered and kept unchanged and the networks is considered ready to handle new problems. The neural network training and operation stages are illustrated in the Fig. 2.4.

Neural networks possess a number of advantages which can be summarised as follows:

- Neural networks can learn by training from a series of examples (without knowledge of underlying rules) to produce meaningful solutions to problems.
- Data presented for training neural networks can be theoretical data, experimental data, empirical data based on good and reliable past experience, expert knowledge or a combination of these.
- Neural networks can encapsulate a great deal of knowledge in a very efficient manner, and can take account of factors that are not easily quantifiable (non-numeric) such as ease of construction, failure mode and availability.

However, the data using in training neural network is based on the good and reliable experience, expert knowledge. Therefore, the results of optimisation problem depend on a lot of experience of user. That is the limitation of neural network method.



Fig. 2.3: Neural network with one hidden layer (El-Kassas, 2001).

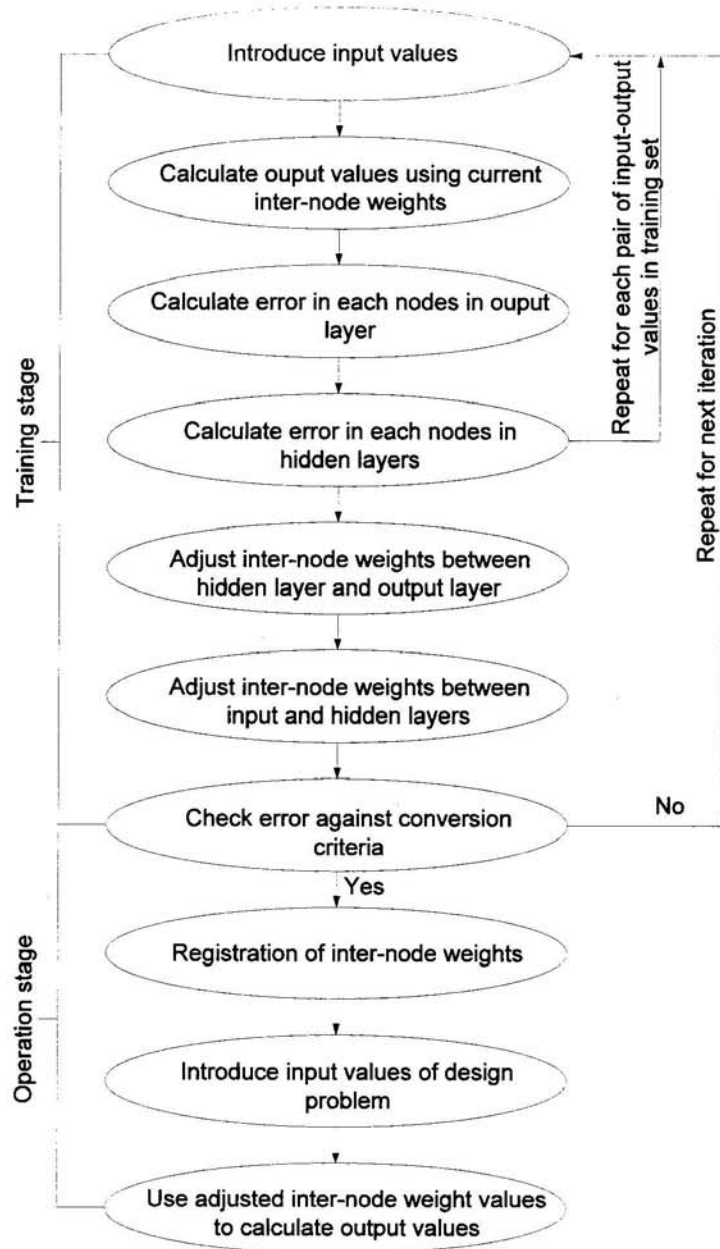


Fig. 2.4: Flow chart for the neural network training and operation stages.

2.3.2 Genetic algorithms

The Genetic Algorithms (GA) were invented by John Holland (1960) and developed by Holland and his students and colleagues at University of Michigan. GA is a search

technique used in computer science to find approximate solutions to optimisation and search problems. Genetic algorithms are a particular class of evolutionary algorithms that use techniques inspired by evolutionary biology such as inheritance, mutation, natural selection, and recombination (or crossover). Genetic algorithms are typically implemented as a computer simulation in which a population of abstract representations (called chromosomes) of candidate solutions (called individuals) to an optimisation problem evolves toward better solutions. Traditionally, solutions are represented in binary as strings of 0s and 1s, but different encodings are also possible. The evolution starts from a population of completely random individuals and happens in generations. In each generation, the fitness of the whole population is evaluated, multiple individuals are stochastically selected from the current population (based on their fitness), modified (mutated or recombined) to form a new population, which becomes current in the next iteration of the algorithm. GA performs a multi-directional search by maintaining a population of potential solution and encourages information formation and exchange between these directions. As compared to other search and optimisation algorithms, GA has the following features:

- GA search a set of points in parallel, not only at a single point;
- GA does not require derivative information or other auxiliary knowledge. Only the objective function and corresponding fitness affect the direction of search;
- GA use probability rules;
- GA provides a number of potential solutions to a given problem. The final choice is left to user.

Holland's GA is a method for moving from one population of chromosomes to a new population by using a kind of natural selection together with the genetics inspired

operators of crossover, mutation and inversion. The structure of the GA is shown in Fig. 2.5:

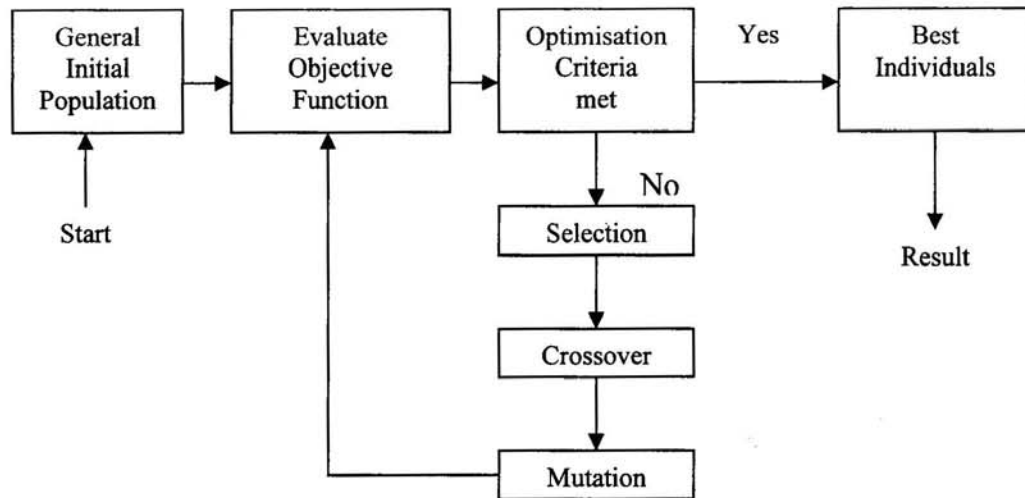


Fig. 2.5: Structure of the GA.

However, there are several general observations about the generation of solutions via a genetic algorithm:

- In many problems with sufficient complexity, GAs may have a tendency to converge towards local optima rather than the global optimum of the problem;
- Operating on dynamic data sets is difficult, as genomes begin to converge early on towards solutions which may no longer be valid for later data;
- GAs cannot effectively solve problems in which there is no way to judge the fitness of an answer other than right/wrong, as there is no-way to converge on the solution.
- GA is used for solving an unconstrained optimisation problem. The constrained optimisation should be transformed into an unconstrained problem by including a

penalty function. Therefore, the optimum results depend on the penalty function and maybe not unique values.

2.4 LOCAL BUCKLING BEHAVIOUR

2.4.1 Effective width approach

Local buckling is a failure mode involving plate flexure alone without transverse deformation of the line or lines of intersection of adjoining plates. Local buckling of thin-walled sections has been known for many years and has been well understood. For such plate elements, local buckling is not the same as overall beam or column buckling. Although the element begins to deflect out of its original straight or plane shape, it does not fail when the initial buckling stress is reached. On the contrary, it can still resist increasing compression stresses often well in excess of those at which local buckling first appears.

The fundamental phenomenon of local buckling is illustrated in Fig. 2.6 which shows local buckling behaviour in a cassette column with an intermediate stiffener in the wide flange. As can be seen from Fig. 2.6, plate elements that are adequately stiffened along both longitudinal edges tend to buckle into approximately square waves. For economic design purpose, it is necessary to consider the post-buckled condition and the primary analytical model of concept of effective width illustrated in Fig. 2.7.



Aston University

Illustration removed for copyright restrictions

Fig. 2.6: Buckling in a cassette section column (Davies, 2000).

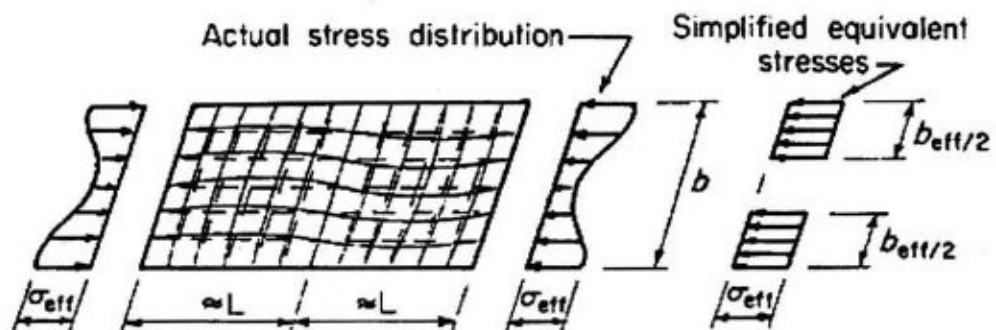


Fig. 2.7: Effective width of plane element stiffened along both edges.

Considering the element as the compression flange of some member (see Fig. 2.7), the total compressive force is the area under this stress distribution curve, times the thickness of the element. What is needed in design, really, is only this total compressive force. It is convenient to replace the actual variable stress distribution with a fictitious uniform stress distribution, of the same intensity of the edge stress, σ_{eff} as in the real element.

In order to get the same total compression force in the fictitious as in the real distribution, the areas under the two must be equal. This means adjusting the width of each of the two fictitious rectangles $b_{\text{eff}}/2$ until the combined area of the two rectangles is equal to that under the solid curve. This width is known as the effective width b_{eff} .

Once this effective width b_{eff} is known, structural members, such as beams or columns can be designed simply by replacing the real width b of each compression element by its effective width b_{eff} . Then, effective section properties, such as area, section modulus and second moment of area can be calculated by using for each compression element its effective width b_{eff} instead of its real width b .

2.4.2 Effective cross section

The effects of local buckling shall be taken into account in the determination of the design strength and stiffness of the members. Using the concept of effective width of individual elements to be prone to local buckling, the effective cross-sectional properties can be calculated. The first step is to evaluate the effective width of the compression elements of the section, based on the appropriate stress distribution over the cross-section; the next step is to calculate the geometric properties of the effective section, taking into account the shift of the neutral axis caused by disregarding the ineffective parts of the section. In general, the resistance of a thin-walled effective cross-section is limited by the design yield design stress at any part of the section, based on an elastic analysis. Deviations from this rule are only permitted in special cases.

2.4.3 Design specification

Elastic local buckling is typically treated by ignoring any interaction between elements (flanges and web). Each element is considered independently and classical plate buckling equations based on isolated simply supported plates are generally used. The result of this approach is that each element of the section is predicted to buckle at a different stress. This approach, called the element model, can lead to rather conservative predictions.

The critical stress of the each element is given by the well-known Von Karman formula:

$$\sigma_{cr} = k_{\sigma} \frac{\pi^2 E}{12(1-\nu^2)} \left(\frac{t}{b}\right)^2 \quad (2.4)$$

where b is the width of the considered element; k_{σ} is the buckling factor which depends on the type of element and of the stress distribution on the element. The buckling factor k_{σ} is equal to 4 for a stiffened element and to 0.43 for un-stiffened element under uniform compression and is given in the different specifications for non-uniform stress distributions;

For the determination of the design strength under local buckling, the effective width and effective cross-section properties are generally used. The semi-empirical formula, due to Winter (1947), is generally used in the specification:

$$\begin{aligned} \text{if } \lambda_p \leq 0.673 & \quad b_{\text{eff}} = b \\ \text{if } \lambda_p > 0.673 & \quad b_{\text{eff}} = \left(1 - \frac{0.22}{\lambda_p}\right) \frac{b}{\lambda_p} \end{aligned} \quad (2.5)$$

where, the plate slenderness $\overline{\lambda}_p$ is given by:

$$\overline{\lambda}_p = \sqrt{\frac{\sigma_c}{\sigma_{cr}}} = 1.052 \frac{b}{t} \sqrt{\frac{\sigma_c}{Ek_\sigma}} \quad (2.6)$$

where σ_c is the maximum compressive stress in the plate element; σ_{cr} is the critical stress for elastic buckling of the plate element given by the well-known Von Karmen formula.

A stiffened element on one side only is much less stable and can also be treated by an analogous effective width approach. However, such un-stiffened elements rarely arise in practice because lips usually restrain the free edges. The modern tendency is to use compound lips (Davies,2000).

EN 1993-1-3:2006 gives some comprehensive rules for the determination of effective widths under different stress conditions. In principle, the effective widths of the individual plate elements may be combined to give an effective section and member design completed using conventional techniques. However, this apparent simplicity conceals a number of difficulties. As illustrated by Fig. 2.6, individual plate elements do not buckle in isolation but interact with each other. Although some codes (e.g. BS 5950-5:1998) give an approximate treatment of this phenomenon, it can only be dealt with accurately by a whole-section analysis.

Furthermore, Fig. 2.6 suggests that both the intermediate stiffener in the wide flange and the compound lip stiffeners are “fully effective” so that they remain straight during local buckling of the plate elements. With modern highly stiffened sections,

this is often not the case. Stiffeners may be partially effective so that stiffener buckling interacts with local plate buckling. EN 1993-1-3:2006 gives some design rules for more general situations but these are complicated to use and not particularly accurate (Kesti, Davies, 1999). Evidently, this is the situation where the design based on an analysis of the whole section is to be preferred.

2.5 DISTORTIONAL BUCKLING BEHAVIOUR

2.5.1 Model for distortional buckling in column



Fig. 2.8: Distortional buckling models (Hancock,1997).

Distortional buckling of compression members such as lipped channels usually involves rotation of each flange and lip about the flange-web junction in opposite directions as shown in Fig. 2.88. The web undergoes flexure at the same half-wavelength as the flange buckles, and the whole section may translate in a direction normal to the web also at the same half-wavelength as the flange and web buckling deformations. The web buckling involves single curvature transverse bending of the web.

A simplified analytical expressions for the distortional elastic buckling stress was originally developed by Lau and Hancock (1997), as is shown in Fig. 2.89, which were based on a flange buckling model in which the flange was treated as a compression member restrained by a rotational and a translational spring. The rotational spring stiffness k_ϕ represents the torsional restraint from the web and the translational spring stiffness k_x represents the restraint to translational movement of the cross section.

In Lau and Hancock's analysis (1997), it is shown that the translational spring stiffness k_x does not have much influence on the buckling mode under consideration and the value of k_x was thus assumed to be zero. The key to evaluating this model is to consider the rotational spring stiffness k_ϕ and the half buckling wavelength λ , while taking account of symmetry. Lau and Hancock (1997) give a detailed analysis in which the effect of the local buckling stress in the web and of shear and flange distortion were taken into account in determining expressions for k_ϕ and λ . This gave rise to a rather long and detailed series of explicit equations for the distortional buckling stress. Notwithstanding their cumbersome nature, these are now included in the Australian code (AS/NZS 4600).

2.5.2 Model for distortional buckling in beam

Analytical expressions for the distortional buckling of thin-walled beams of general section geometry under a pure bending moment about the major axis have been developed by Hancock (1997). These analytical expressions were based on the simple flange buckling model shown in Fig. 2.9, in which the flange was treated as a

compression member with both rotational and translational spring restraints in the longitudinal direction. The rotational spring stiffness k_ϕ and the translational spring stiffness k_x represent the torsional restraint and translational restraint from the web respectively. In his analysis, Hancock again assumed the translational spring stiffness k_x to be zero.



Fig. 2.9: Analytical distortional buckling model (Hancock, 1997).

These beam models are, of course, directly analogous to the column model shown in Fig. 2.89. The only significant difference lies in the stiffness of the rotational spring and the necessary modifications to the design expressions for the rotational spring stiffness k_ϕ and the buckling length λ are given in Hancock's paper (1997). This then leads to the similar equations for the critical stress for distortional buckling.

Hancock provided distortional buckling formulae for channel columns based upon a simple flange buckling model where the flange is treated as a thin-walled compression members undergoing flexural torsional buckling. The rotational spring stiffness k_ϕ represents the flexural restraint provided by web which is in pure compression, and translational spring stiffness k_x represents the resistance to translational movement of the section in the buckling mode. As a result of the compressive stress in the web, the

model included a reduction in the flexural restraint provided by the web. In the Hancock model, it is assumed that the value of the translational spring stiffness k_x is zero so that the flange is free to translate in the x direction in the buckling mode. The equation for the rotational spring stiffness k_ϕ is given in Lau & Hancock:

$$k_\phi = \frac{Et^3}{5.46(h + 0.06\lambda)} \left[1 - \frac{1.11f_{ed}'}{Et^2} \left(\frac{h^2\lambda}{h^2 + \lambda^2} \right)^2 \right] \quad (2.7)$$

where λ is the half-wavelength of the distortional buckle given by:

$$\lambda = 4.8 \left(\frac{I_x b^2 h}{2t^3} \right)^{0.25} \quad (2.8)$$

An analytical method for the prediction of short half-wavelength distortional buckling has recently been presented by Hancock(1995). The method is similar to that of Lau & Hancock for compression members, but involves modified torsional restraint stiffness, k_ϕ at the flange/web corner. The modified torsional restraint stiffness is calculated on the basis of an assumed elastic distortional buckling stress, f_{ed}' , of the lip/flange component, and the compressive stress distribution in the web element. The section in which the compressive lip/flange component torsionally restrains the web element, i.e. develop negative torsional restraint stiffness, typically have large web slenderness ratios, i.e. $h/t > 150$, and tend to fail by flange/web distortional buckling. However, it is also possible to observe experimentally flange/web distortional buckling of sections which have low positive torsional restraint stiffness values. The procedure used to calculate the assumed elastic distortional buckling stress and the resulting torsional restraint stiffness is given below:

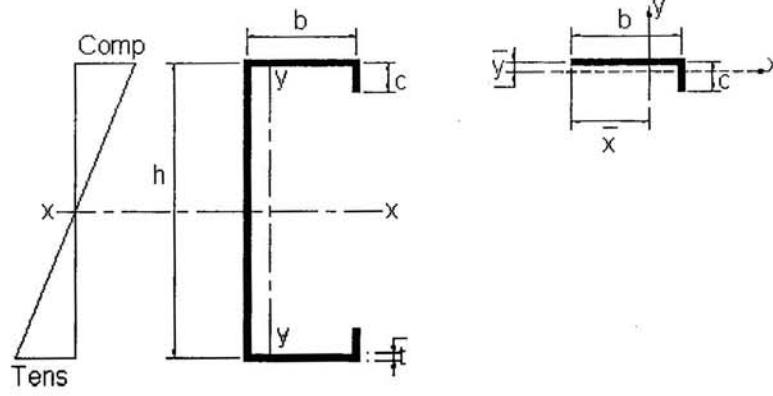


Fig. 2.10: Lip-flange component geometric properties.

$$A_f = t(b+c) \quad (2.9)$$

$$\bar{y} = \frac{c^2/2}{b+c} \quad (2.10)$$

$$\bar{x} = \frac{b^2/2+bc}{b+c} \quad (2.11)$$

$$J_f = \frac{t^3}{3}(b+c) \quad (2.12)$$

$$I_{xf} = \frac{bt^3}{12} + \frac{tc^3}{12} + bt\bar{y}^2 + ct(c/2-\bar{y})^2 \quad (2.13)$$

$$I_{yf} = \frac{tb^3}{12} + \frac{ct^3}{12} + bt(\bar{x}-b/2)^2 + ct(b-\bar{x})^2 \quad (2.14)$$

$$I_{xyf} = bt(b/2-\bar{x})(-\bar{y}) + ct(c/2-\bar{y})(b-\bar{x}) \quad (2.15)$$

Step 1

$$\beta_1 = \bar{x}^2 + \left(\frac{I_{xf} + I_{yf}}{A_f}\right) \quad (2.16)$$

$$\lambda_d = 4.8 \left(\frac{I_{xf} b^2 h}{2t^3}\right)^{0.25} \quad \text{if } \lambda_m < \lambda_d \text{ then } \lambda_d = \lambda_m \quad (2.17)$$

$$\eta = \left(\frac{\pi}{\lambda_d}\right)^2 \quad (2.18)$$

$$\alpha_1 = \frac{\eta}{\beta_1} (I_{yf} b^2 + 0.039 J_f \lambda_d^2) \quad (2.19)$$

$$\alpha_2 = \eta \left(I_{yf} + \frac{2}{\beta_1} \bar{y} b I_{xyf} \right) \quad (2.20)$$

$$\alpha_3 = \eta \left(\alpha_1 I_{yf} - \frac{\eta}{\beta_1} I_{xyf}^2 b^2 \right) \quad (2.21)$$

$$f_{ed}' = \frac{E}{2A_f} \{ (\alpha_1 + \alpha_2) \pm \sqrt{(\alpha_1 + \alpha_2)^2 - 4\alpha_3} \} \text{ smaller positive value} \quad (2.22)$$

$$k_\phi = \frac{2Et^3}{5.46(h + 0.06\lambda_d)} \left[1 - \frac{1.11f_{ed}'}{Et^2} \left(\frac{h^4 \lambda_d^2}{12.56\lambda_d^4 + 2.192h^4 + 13.39\lambda_d^2 h^2} \right) \right] \quad (2.23)$$

Step 2

If $k_\phi \geq 0$ then

$$\alpha_1 = \frac{\eta}{\beta_1} (I_{yf} b^2 + 0.039 J_f \lambda_d^2) + \frac{k_\phi}{\beta_1 \eta E} \quad (2.24)$$

$$\alpha_3 = \eta \left(\alpha_1 I_{yf} - \frac{\eta}{\beta_1} I_{xyf}^2 b^2 \right) \quad (2.25)$$

$$f_{ed}' = \frac{E}{2A_f} \{ (\alpha_1 + \alpha_2) \pm \sqrt{(\alpha_1 + \alpha_2)^2 - 4\alpha_3} \} \text{ smaller positive value} \quad (2.26)$$

If $k_\phi \leq 0$ then

$$k_\phi = \frac{2Et^2}{5.46(h + 0.06\lambda_d)} \quad (2.27)$$

$$\alpha_1 = \frac{\eta}{\beta_1} (I_{yf} b^2 + 0.039 J_f \lambda_d^2) + \frac{k_\phi}{\beta_1 \eta E} \quad (2.28)$$

$$\alpha_3 = \eta \left(\alpha_1 I_{yf} - \frac{\eta}{\beta_1} I_{xyf}^2 b^2 \right) \quad (2.29)$$

$$f_{ed}' = \frac{E}{2A_f} \{ (\alpha_1 + \alpha_2) \pm \sqrt{(\alpha_1 + \alpha_2)^2 - 4\alpha_3} \} \text{ smaller positive value} \quad (2.30)$$

Strength curve 1

For $f_{ed}' > 2.2f_y$

$$f_c = f_y \quad (2.31)$$

For $f_{ed}' \leq 2.2f_y$

$$f_c = f_y \sqrt{\frac{f_{ed}'}{f_y}} \left(1 - 0.22 \sqrt{\frac{f_{ed}'}{f_y}} \right) \quad (2.32)$$

Strength curve 2

For $f_{ed}' > 3.18f_y$

$$f_c = f_y \quad (2.33)$$

For $f_{ed}' \leq 3.18f_y$

$$f_c = f_y \left(\frac{f_{ed}'}{f_y} \right)^{0.6} \left(1 - 0.25 \left(\frac{f_{ed}'}{f_y} \right)^{0.6} \right) \quad (2.34)$$

Nominal moment resistance

If $k_\phi \geq 0$ then

$$M_n = S_f f_c \quad (2.35)$$

If $k_\phi < 0$ then

$$M_n = S_e f_c \quad (2.36)$$

where S_f is section modulus of the full unreduced section for the extreme compression fibre; S_e is section modulus of the effective section calculated as stress f_c in the extreme compression fibre, with $k_\sigma = 4$ for the stiffened flange, and $f = f_c$ for the edge stiffener; λ_m is distance between restraints which limit rotation of the lip/flange component about the flange/web corner.

2.6 LATERAL-TORSIONAL BUCKLING BEHAVIOUR

2.6.1 Recent study in lateral-torsional buckling

The lateral-torsional buckling is characterized by the mode of rigid body movements of the whole member in which individual cross-sections rotate and translate but do not distort in shape. It is well known that long beams with low lateral stiffness and low torsional stiffness are very prone to buckling laterally. Further, the sections are often loaded eccentrically from their shear centres. Because of the geometry of the cross section, which gives great flexural rigidity about one axis at the expense of low torsional rigidity and low flexural rigidity about a perpendicular axis, cold-formed members are particularly susceptible to lateral-torsional buckling.

Comparing to the local and distortional buckling, the lateral-torsional buckling has been little concerned. This is partly because cold-formed steel members are usually used together with metal sheeting that restrains the lateral movement of the members and thus reduces the possibility of the occurrence of lateral-torsional buckling, and partly because the lateral-torsional buckling is traditionally prevented by the use of inexpensive anti-sag bars.

Recently, there have been many experimental, numerical and analytical studies of torsion and lateral-torsional buckling (Davies, 2000; Gotluru et al., 2000; Hancock, 2003). Put et al. (1998) performed lateral buckling tests on un-braced, simply supported cold-formed lipped channel beams. Experiments on braced cold-formed steel channels and zed purlin beams were also undertaken at Cornell University (Schafer, 2001b). Pi et al. (1998) investigated the lateral buckling and biaxial bending behaviour of both channel and zed sections using finite element methods. A pilot

study of laterally braced C-sections as used in wall studs was performed by Beshara and LaBoube (2001). The effect of a lateral brace at the middle of span to restrain the C-section from rotation was investigated experimentally.

Channel and Zed-sections are the most common members used as purlins and girders in roof and wall systems with sheeting attached and so the effect of the sheeting in preventing torsion and lateral-torsional buckling needs to be quantified. Considerable research has been performed in this area over many years. Lucas et al. (1997a & 1997b) investigated the influence of sheeting on the performance of the cold-formed sections using the finite element method. Linder and Aschinger (1994) proposed some alternative design procedures for the load-carrying capacity of cold-formed beams subjected to overall lateral-torsional buckling and local plate buckling. Laine and Tuomala (1999) studied Z, Zeta, C and Hat shaped sections to determine experimentally the influence of internal supports and sheeting on the top flange for purlins under gravity load. In design specifications such as BS 5950-5:1998 the lateral-torsional buckling of cold-formed members is calculated based on the theory of a detached beam, the result of which is obviously too conservative as it neglects the influence of sheeting restraints.

The recently developed finite strip analysis packages are aimed to predict more accurate elastic buckling stresses related to local, distortional, and lateral-torsional buckling (Loughlan, 1996; Hancock, 1997a; Schafer, 2001c&2003a; Ye, 2002). However, at the present, these packages can be only applied to the case where the member is subjected to pure compression and pure bending. For local buckling, it may be acceptable to assume constant stresses along the longitudinal axis because of its relatively short half-wavelength. For distortional buckling and particularly for

lateral-torsional buckling, however, the stress gradient along the longitudinal axis should be considered if the result of finite strip analysis is going to be used for the design purpose.

Recently, Li (2004) developed an analytical model for predicting the lateral-torsional buckling of cold-formed zed-purlins partially restrained by metal sheeting for both downward and uplift loadings. The calculation details are given in the following part.

2.6.2 Analytical model for lateral-torsional buckling

An analytical model for predicting the lateral-torsional buckling of cold-formed steel members is presented by Li (2004). The model is constructed for the practical case where the cold-formed member is subjected to transverse loads and is restrained partial-laterally by sheeting and interval anti-sag bars. The focus is to investigate the influence of the restraints provided by the sheeting and by the interval anti-sag bars, and the variation of moment along the longitudinal axis on the lateral-torsional buckling behaviour of the cold-formed steel member.

Consider a purlin that is partially restrained by the sheeting on its upper flange. The restraint of the sheeting can be simplified by one translational spring and one rotational spring, as shown in Fig. 2.11. Let the origin of the coordinate system (x, y, z) be the centroid of the cross-section, with x axis being along the longitudinal direction of the beam, and y and z axes taken in the plane of the cross-section. For an arbitrary axis system, the relationship between bending moments and radii of curvature can be expressed as:

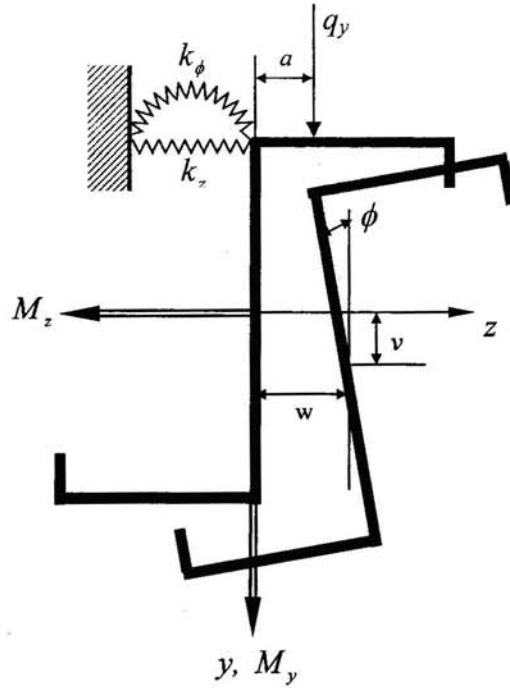


Fig. 2.11: An analytical model for lateral-torsional buckling analysis.

$$\begin{Bmatrix} M_y \\ M_z \end{Bmatrix} = E \begin{bmatrix} I_y & I_{yz} \\ I_{yz} & I_z \end{bmatrix} \begin{Bmatrix} 1/R_z \\ 1/R_y \end{Bmatrix} \quad (2.37)$$

where M_y and M_z are the bending moments about y and z axes; I_y and I_z are the second moments of the cross-section area about y and z axes; I_{yz} is the product moment of the cross-section area; R_y and R_z are the radii of curvature of the centroidal axis in the xz and xy planes, respectively.

The moment in Eq.(2.37) is defined as positive if it creates a tensile stress for positive y and z values. Thus, M_y has the same direction as y axis, while M_z has an opposite direction to z axis.

Note that for small deflections the radii of curvature can be expressed in terms of deflections of the centroidal axis as follows:

$$\frac{1}{R_y} = -\frac{d^2 v}{dx^2}; \frac{1}{R_z} = -\frac{d^2 w}{dx^2} \quad (2.38)$$

where v and w are the deflections of the beam centroidal axis in y and z directions, respectively.

The strain energy of the beam due to deflections and rotation can be expressed as:

$$U_{0_beam} = \frac{1}{2} \int_0^l \left(\frac{M_y}{R_z} + \frac{M_z}{R_y} \right) dx + \frac{GJ}{2} \int_0^l \left(\frac{d\phi}{dx} \right)^2 dx + \frac{EC_w}{2} \int_0^l \left(\frac{d^2\phi}{dx^2} \right)^2 dx \quad (2.39)$$

where G is the modulus of elasticity in shear; J is the torsion constant; C_w is the warping constant; ϕ is the angle of twist; l is the span length of the beam.

The first term in Eq.(2.39) represents the strain energy due to bending about y and z axes, the second term represents the strain energy due to twisting, and the third term represents the warping strain energy, respectively.

The strain energy stored in the two springs due to the deformation of the beam can be expressed by

$$U_{0_Spring} = \frac{k_z}{2} \int_0^l \left(w - \frac{d\phi}{2} \right)^2 dx + \frac{k_\phi}{2} \int_0^l \phi^2 dx \quad (2.40)$$

where k_z and k_ϕ are the per-unit length stiffness constants of the translational and rotational springs; d is the depth of the section.

It is assumed that the purlin is subjected to the external loads of a vertical uniformly distributed load within the span and concentrated moments at its ends. The potential

energy generated by these external loads can be expressed by

$$W_o = \int_0^l q_y (v - a\phi) dx + \left(M_{yo} \frac{dw}{dx} \Big|_{x=0} - M_{yl} \frac{dw}{dx} \Big|_{x=l} \right) + \left(M_{zo} \frac{dv}{dx} \Big|_{x=0} - M_{zl} \frac{dv}{dx} \Big|_{x=l} \right) \quad (2.41)$$

where q_y is the density of uniformly distributed load; a is the distance between loading line and web central line; $M_{yo}, M_{yl}, M_{zo}, M_{zl}$ are the concentrated moments about y and z axes, applied at the ends of the purlin.

The deflections, $v(x)$ and $w(x)$, and the angle of twist, $\phi(x)$ due to the externally applied loads can be determined by employing the stationary principle as follows:

$$\delta(U_o - W_o) = \delta(U_{o_beam} + U_{o_spring} - W_o) = 0 \quad (2.42)$$

After the deflections and rotation are determined the pre-buckling moment distributions along the longitudinal axis can then be calculated using Eq.(2.37).

The analysis of linear elastic buckling can be done using a similar energy method. Let M_{oy} and M_{oz} be the pre-buckling moment distributions that are obtained from the pre-buckling stress analysis. The pre-buckling longitudinal stress due to M_{oy} and M_{oz} can be calculated by using the bending formula of the asymmetric beam:

$$\sigma_x(x, y, z) = \frac{M_{oz} I_y - M_{oy} I_{yz}}{I_y I_z - I_{yz}^2} y + \frac{M_{oy} I_z - M_{oz} I_{yz}}{I_y I_z - I_{yz}^2} z \quad (2.43)$$

Note that σ_x is the function of y and z as well as of x . Now, let $v(x)$ and $w(x)$ be the buckling deflections of the beam centroidal axis in y and z directions and $\phi(x)$ as the buckling twisting about x axis. Thus, the strain energy generated by the buckling

displacements can be calculated using Eq.(2.39) for the purlin and Eq.(2.40) for the springs.

The buckling deflections of the beam at any point x during buckling can be expressed in terms of the buckling displacements of the beam centroidal axis, v_b , w_b and ϕ_b , as follows (Li, 2004):

$$\begin{aligned}\bar{v}(x, y, z) &= v_b - z \sin \phi_b + y(\cos \phi_b - 1) \approx v_b - z\phi_b - \frac{1}{2}y\phi_b^2 \\ \bar{w}(x, y, z) &= w_b + z(\cos \phi_b - 1) + y \sin \phi_b \approx w_b + y\phi_b - \frac{1}{2}z\phi_b^2\end{aligned}\quad (2.44)$$

where $\bar{v}(x, y, z)$ and $\bar{w}(x, y, z)$ are the deflections of the beam at point (x, y, z) during the buckling.

The longitudinal displacement at point (x, y, z) can be expressed as follows:

$$\begin{aligned}\bar{u}(x, y, z) &= u_b - (y \cos \phi_b - z \sin \phi_b) \frac{dv_b}{dx} - (z \cos \phi_b + y \sin \phi_b) \frac{dw_b}{dx} + \beta(y, z) \frac{d\phi_b}{dx} \\ &\approx u_b - y \frac{dv_b}{dx} - z \frac{dw_b}{dx} + \beta \frac{d\phi_b}{dx} + z\phi_b \frac{dv_b}{dx} - y\phi_b \frac{dw_b}{dx}\end{aligned}\quad (2.45)$$

where $\beta(y, z)$ is the warping function of St. Venant torsion; $\bar{u}(x, y, z)$ and $u(x)$ are the longitudinal displacements of the beam at points (x, y, z) and $(x, 0, 0)$, respectively.

The longitudinal strain and shear strains generated by the buckling displacements can be calculated by

$$\begin{aligned}
\varepsilon_x(x, y, z) &= \frac{\partial \bar{u}}{\partial x} + \frac{1}{2} \left[\left(\frac{\partial \bar{v}}{\partial x} \right)^2 + \left(\frac{\partial \bar{w}}{\partial x} \right)^2 \right] \\
\gamma_{xy}(x, y, z) &= \frac{\partial \bar{u}}{\partial y} + \frac{\partial \bar{v}}{\partial x} + \frac{\partial \bar{w}}{\partial x} \frac{\partial \bar{w}}{\partial y} \\
\gamma_{xz}(x, y, z) &= \frac{\partial \bar{u}}{\partial z} + \frac{\partial \bar{w}}{\partial x} + \frac{\partial \bar{v}}{\partial x} \frac{\partial \bar{v}}{\partial z}
\end{aligned} \tag{2.46}$$

Substituting Eqs.(2.44) and (2.45) into (2.46) and splitting them into linear and nonlinear terms in terms of the buckling displacements, it leads to the following second-order nonlinear strains:

$$\begin{aligned}
\varepsilon_{x2}(x, y, z) &= \frac{1}{2} \left[\left(\frac{dv}{dx} \right)^2 + \left(\frac{dw}{dx} \right)^2 + (y^2 + z^2) \left(\frac{d\phi}{dx} \right)^2 \right] + z\phi \frac{d^2v}{dx^2} - y\phi \frac{d^2w}{dx^2} \\
\gamma_{xy2} &= 0 \\
\gamma_{xz2} &= 0
\end{aligned} \tag{2.47}$$

The non-linear strain energy generated by the pre-buckling longitudinal stress through the second-order strains is calculated by:

$$W_{\sigma_{xb}} = - \int_0^l \int_A \sigma_x(x, y, z) \varepsilon_{x2}(x, y, z) dA dx \tag{2.48}$$

where A = the area of the cross section.

The negative sign in Eq.(2.48) is because σ_x and ε_{x2} are in opposite direction.

Substituting Eq.(2.47) into Eq.(2.48) and noting that for the zed purlin that is symmetric about its centroid.

$$\int_A \sigma_x(x, y, z) dA = 0$$

$$\int_A \sigma_x(x, y, z)(y^2 + z^2) dA = 0 \quad (2.49)$$

the following equation is obtained,

$$W_{\sigma_{xb}} = \int_0^l \int_A \sigma_x(x, y, z) \left(y \frac{d^2 w}{dx^2} - z \frac{d^2 v}{dx^2} \right) \phi dA dx = \int_0^l \phi \left(M_{oz} \frac{d^2 w}{dx^2} - M_{oy} \frac{d^2 v}{dx^2} \right) dx \quad (2.50)$$

Note that $W_{\sigma_{xb}}$ does not include the strain energy generated due to the lowering of the distributed load during the rotation which is due to the load that is not acting at the shear center (Timoshenko & Gere, 1961). When this is considered the strain energy should be expressed by

$$W_1 = W_{\sigma_{xb}} + W_q = \int_0^l \phi \left(M_{oz} \frac{d^2 w}{dx^2} - M_{oy} \frac{d^2 v}{dx^2} \right) dx + \frac{d}{4} \int_0^l q_y \phi^2 dx \quad (2.51)$$

It is known that for any infinitesimal buckling displacements, if the strain energy generated by the buckling displacements is less than the strain energy generated by the pre-buckling stresses then buckling will occur. Mathematically, this indicates that buckling occurs at:

$$\lambda W_1 = \lambda(W_{\sigma_{xb}} + W_q) \geq U_1 = U_{1_spring} + U_{1_beam} \quad (2.52)$$

where λ is the critical load factor; U_1 is the total strain energy of the system;

U_{1_beam} and U_{1_spring} are the strain energy of the beam when the buckling occurs, which

have the same expressions as U_{0_beam} and U_{0_spring} , except now that the deflections and the angle of twist are the buckling deflections and the buckling angle of twist.

The minimum buckling critical load thus is calculated from

$$\delta(U - \lambda W) = 0 \quad (2.53)$$

2.7 CALCULATION OF DEFLECTION

In evaluation of the deflection for such a beam, the question arises: which section properties should be used? Using the full second moment of area predicts deflections, which seriously underestimates the real deflections. Using the reduced second moment of area overestimates the deflections considerably, and will cause over-conservatism if the design is governed by deflection. Therefore, if the displacements are required with reasonable accuracy, some attempt must be made to give consideration to both pre-buckling and post-buckling effects on deflection behaviour.

The recommended deflection limitations for beams are given in cl.2.4.2 of BS 5950-5:1998. The deflection, in the plane of loading, of a laterally stable beam or one which is adequately restrained against twisting and which does not utilise the plastic capacity, may be calculated as follows:

- a- For M or $M_c \leq M_{cr}$, the full cross-section should be used in evaluating the second moment of area and the deflection calculated using simple beam theory;

b- $M_{cr} < M \leq M_c$, either M or Δ is determined from a specified value of the other quantity using the equation:

$$\frac{M - M_{cr}}{M_c - M_{cr}} = \frac{\Delta - \Delta_{cr}}{\Delta_c - \Delta_{cr}} \quad (2.54)$$

where M is the bending moment for a given loading system; Δ is the deflection for the given loading system; M_c is the moment capacity determined in accordance with cl.5.2.2 of BS 5950-5:1998. Δ_c is the deflection corresponding to M_c calculated using the reduced cross-section; Δ_{cr} is the deflection of the beam corresponding to M_{cr} calculated using the full cross-section; M_{cr} is the critical bending moment given by:

$$M_{cr} = 0.59EK(t/b)^2 Z_c \quad (2.55)$$

where K is the buckling coefficient of the compression flange, values of K for different sections and conditions are given in the annex B of BS 5950-5:1998; Z_c is the elastic modulus of the gross cross-section with respect to the compression flange.

2.8 FINITE STRIP METHOD

The best known numerical method developed for analysing thin-walled beams based on the separation of variables is perhaps the finite strip method. In the finite strip method, the displacement interpolation is built-up of two parts, a polynomial defined on a cross-section and a truncated Fourier-series part governing the behaviour of the displacement function in the axial direction with the latter satisfying a priori the boundary conditions at the ends of the beam. This provides “whole section” solutions for the full range of buckling phenomena, leading to relatively new design procedures.

If the thin-walled beam is prismatic and the boundary and loading conditions are suitable, the finite strip method is quite economical with respect to computational efficiency. Several well-known researchers have developed user-friendly computer software (Schafer, 2001c & 2003a) for this calculation, which is available to practical designers.

Unfortunately, the applications of the finite strip method to various geometries or boundary and loading conditions are not fully developed. In the buckling analysis of thin-walled beams using the finite strip method difficulties are experienced, for example, when dealing with non-periodic buckling modes or unequal loading in the axial direction.

A brief introduction to the finite strip model employed in the open access software CUFSM (Schafer, 2001c & 2003a) is presented in the section below:

The finite strip method is applicable to elastic local, distortional and global buckling of the structures with uniform stress distribution along the longitudinal axis of the member. The finite strip method falls into the category of numerical methods that are specifically designed for prismatic members. Cold-formed sections are generally prismatic and the finite strip method has the advantage over finite element method of requiring less computer time and memory as well as less data preparation.

From the practical point of view, the second-order finite strip method is particularly important because bifurcation buckling solutions may be obtained relatively easily using simple half sine wave displacement functions. This provides "whole section" solutions for the full range of buckling phenomena, leading to relatively new design

procedures which will be considered later. Several well-known researchers (e.g. Hancock, Pekoz, Rhodes) have developed user-friendly computer software for this calculation which is available to practical designers.

Cheung (1976) originally developed the finite strip method and an excellent summary of the method, and the theory behind it, can be found in his book. The use of the finite strip method to understand and predict the behaviour of hot-rolled steel members and cold-formed steel members has been greatly extended by Hancock (1994). Hancock used the stiffness matrices derived in Cheung's book, and with some modification, created BFINST- a computer programme for solution of the elastic buckling problem of open thin-walled members via finite strip. His early work in the field on I-beams led to the acceptance and understanding of the use of finite strip method, which was further developed particularly on cold-formed steel design.

A basic introduction to the finite strip model employed in the programme CUFSM is presented here, which includes theoretical development and derivation of the initial stiffness and geometric stiffness within the finite strip method (Schafer, 2001c, 2003a). The coordinate directions and degrees of freedom for a typical strip are shown in Fig. 2.12. Please note the rather unusual choice of the x-z coordinate system which is consistent with Cheung's original derivation.

Since a box structure may be considered as an assembly of rectangular plates, which are capable of undergoing both bending and in-plane deformations; in a linear elastic analysis, it is assumed that no interaction takes place between these two systems. The stiffness and force matrices for a finite strip in the analysis of box structures can therefore be obtained by combining the bending and in plane analysis.

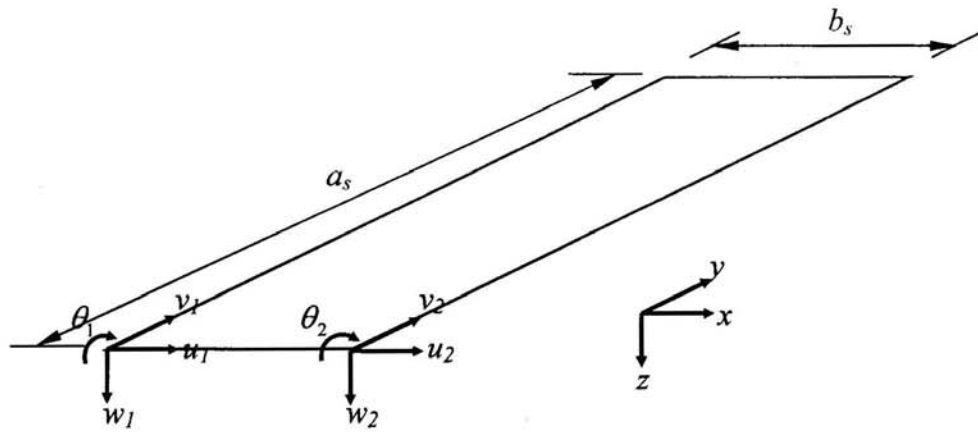


Fig. 2.12: Displacement field for typical simply supported finite strip.

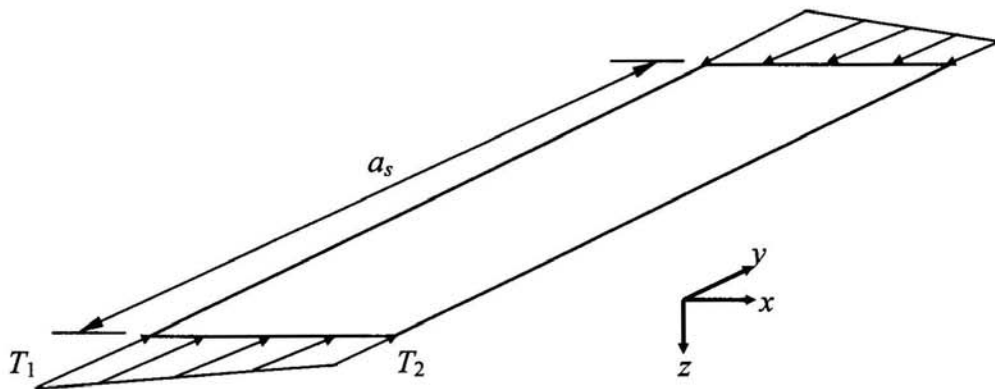


Fig. 2.13: Strip with compression stress distribution.

2.8.1 Initial stiffness matrix for plates

The standard definition of an initial stiffness matrix is apparent from $\{f\}=[K]\{d\}$, or, expanded to explicitly show the nodal forces, nodal degrees of freedom, and the initial stiffness sub matrices: $[K_{uv}]$ (plane stress) and $[K_{w\phi}]$ (bending) are:

$$\begin{Bmatrix} F_{u_1} \\ F_{v_1} \\ F_{u_2} \\ F_{v_2} \\ F_{w_1} \\ M_{\theta_1} \\ F_{w_2} \\ M_{\theta_2} \end{Bmatrix} = \begin{bmatrix} [K_{uv}] & 0 & 0 & 0 & 0 \\ 0 & 0 & 0 & 0 & 0 \\ 0 & 0 & 0 & 0 & 0 \\ 0 & 0 & 0 & 0 & 0 \\ 0 & 0 & 0 & 0 & 0 \\ 0 & 0 & 0 & 0 & [K_{w\theta}] \\ 0 & 0 & 0 & 0 & 0 \\ 0 & 0 & 0 & 0 & 0 \end{bmatrix} \begin{Bmatrix} u_1 \\ v_1 \\ u_2 \\ v_2 \\ w_1 \\ \theta_1 \\ w_2 \\ \theta_2 \end{Bmatrix} \quad (2.56)$$

The initial stiffness matrix may be expressed as:

$$[K] = \int [B]^T [D] [B] dV \text{ or } \int [N']^T [D] [N] dV \quad (2.57)$$

where $[B]$ or $[N']$ is the appropriate derivatives of the shape functions $[N]$, which is defined from $(u, v, w)^T = [N] \{d\}$, where $(u, v, w)^T$ is the displacement field and $\{d\}$ is a vector of the nodal degrees of freedom.

For an orthotropic plate, and assuming no variation in the thickness (t) of the strip,

$[K]$ may be expressed as: $[K] = t \int [B]^T [D] [B] dA$, where the plate rigidities are defined

as:

$$[D] = \begin{bmatrix} D_x & D_1 & 0 \\ D_1 & D_y & 0 \\ 0 & 0 & D_{xy} \end{bmatrix} \quad (2.58)$$

$$D_x = \frac{E_x t^3}{12(1-\nu_x \nu_y)}, D_y = \frac{E_y t^3}{12(1-\nu_x \nu_y)}, D_{xy} = \frac{G t^3}{12}, D_1 = \frac{\nu_y E_x t^3}{12(1-\nu_x \nu_y)} = \frac{\nu_x E_y t^3}{12(1-\nu_x \nu_y)}$$

The finite strip solution used employs a polynomial in the transverse direction and a harmonic function in the longitudinal direction. In this derivation, the longitudinal direction is assumed to take the form of a half sine wave. This is consistent with the boundary condition of simply supported ends. The advantage of such an assumption is that the integrals used in forming the stiffness matrix decouple, and the solution is simplified.

The derivation of the initial stiffness matrix is in two completely decoupled parts. A pure plane stress conditions is assumed for the in-plane u and v degrees of freedom. The w , θ degrees of freedom are derived using classical small deflection plate theory to arrive at the bending initial stiffness matrix. The two matrices $[K_{uv}]$ and $[K_{w\theta}]$ are combined to form the total initial stiffness matrix.

- **Plane stress initial stiffness matrix $[K_{uv}]$**

The shape functions for use in determining the in-plane stiffness matrix are:

$$\begin{aligned} u &= \begin{bmatrix} (1-\frac{x}{b}) & (\frac{x}{b}) \end{bmatrix} \begin{Bmatrix} u_1 \\ u_2 \end{Bmatrix} Y_m \\ v &= \begin{bmatrix} (1-\frac{x}{b}) & (\frac{x}{b}) \end{bmatrix} \begin{Bmatrix} v_1 \\ v_2 \end{Bmatrix} \frac{a}{m\pi} Y'_m \end{aligned} \quad Y_m = \sin\left(\frac{m\pi y}{a}\right) \quad (2.59)$$

The expressions can be put in the general form $[N]$ such that:

$$\begin{Bmatrix} u \\ v \end{Bmatrix} = [N] \begin{Bmatrix} u_1 \\ v_1 \\ u_2 \\ v_2 \end{Bmatrix} = [N] \{d\} \quad (2.60)$$

With the shape functions in that form, the strain-displacement matrix [B] can be written in terms of derivatives of [N]:

$$\begin{Bmatrix} \varepsilon_x \\ \varepsilon_y \\ \gamma_{xy} \end{Bmatrix} = \begin{Bmatrix} \partial u / \partial x \\ \partial v / \partial y \\ \partial u / \partial y + \partial v / \partial x \end{Bmatrix} = [B] \{d\} = [N'] \{d\} \quad (2.61)$$

Using these definitions, and performing the necessary substitutions into the expression for the stiffness matrix presented before, the explicit plane stress matrix for an element, or strip is given in Appendix A.1.

- **Bending initial stiffness matrix $[K_{w\phi}]$**

The shape functions for use in determining the bending stiffness matrix are:

$$w = Y_m \left[\left(1 - \frac{3x^2}{b^2} + \frac{2x^3}{b^3}\right) \quad x\left(1 - \frac{2x}{b} + \frac{x^2}{b^2}\right) \quad \left(\frac{3x^2}{b^2} - \frac{2x^3}{b^3}\right) \quad x\left(\frac{x^2}{b^2} - \frac{x}{b}\right) \right] \begin{Bmatrix} w_1 \\ \theta_1 \\ w_2 \\ \theta_2 \end{Bmatrix} \quad (2.62)$$

With the shape functions in this form, the strain-displacement matrix [B] can be written in terms of derivatives of [N]:

$$\{\varepsilon\} = \begin{Bmatrix} -\partial^2 w / \partial x^2 \\ -\partial^2 w / \partial y^2 \\ \partial^2 w / \partial xy \end{Bmatrix} = [B] \{d\} = [N'] \{d\} \quad (2.63)$$

The explicit bending stiffness matrix for an element or strip is also given in Appendix A.1.

2.8.2 Geometrical stiffness matrix for plates

The geometric stiffness matrix for a plate strip subjected to linearly varying edge traction can be determined by either directly considering the higher order strain terms, or equivalently by forming the potential energy due to in-plane forces.

Consider a strip with linear edge traction as shown in Fig. 2.13. The tractions corresponding to linear edge stresses f_1, f_2 are T_1 and T_2 .

The expression for the potential energy (U) due to the in-plane forces is

$$U = \frac{1}{2} \int_0^a \int_0^b \left[T_1 - (T_1 - T_2) \frac{x}{b_s} \right] \left(\left[\frac{\partial u}{\partial y} \quad \frac{\partial v}{\partial y} \quad \frac{\partial w}{\partial y} \right] \left\{ \frac{\partial u}{\partial y} \quad \frac{\partial v}{\partial y} \quad \frac{\partial w}{\partial y} \right\}^T \right) dx dy \quad (2.64)$$

The derivatives in the expression for U , may be expressed in terms of the nodal degrees of freedom $\{d\}$. The matrix resulting from differentiating the shape functions in this case is called $[G]$, for which we have

$$\left\{ \frac{\partial u}{\partial y} \quad \frac{\partial v}{\partial y} \quad \frac{\partial w}{\partial y} \right\}^T = [G] \{d\} \quad (2.65)$$

The potential energy may now be expressed in terms of $\{d\}$ and a matrix known as the geometric stiffness $[k_g]$,

$$U = \frac{1}{2} \{d\}^T [k_g] \{d\}, [k_g] = \int_0^a \int_0^b (T_1 - (T_1 - T_2) \frac{x}{b_s}) [G]^T dx dy \quad (2.66)$$

Its explicit form is given in Appendix A.1.

2.8.3 The finite strip solution method

In the previous two sections explicit matrices are given for the initial stiffness and geometric stiffness of a discrete finite strip. For a member composed of multiple strips the contribution of each strip must be formed into a global initial stiffness geometric stiffness. Thus:

$$[K] = \sum_{n=1}^{\#strips} [k]_n \text{ and } [K_g] = \sum_{n=1}^{\#strips} [k_g]_n \quad (2.67)$$

The summation implies proper coordinate transformations and correct addition of the stiffness terms in the global coordinates according to the degrees of freedom. The elastic buckling problem is a standard eigenvalue problem of the following form:

$$[K] \{d\} = \lambda [K_g] \{d\} \quad (2.68)$$

Where the eigenvalues λ , are the buckling load factor, and the eigenvectors are the buckling modes. Solution of such an eigenvalue problem may readily be solved in programmes such as MATLAB.

Both $[K]$ and $[K_g]$ are a function of the modelling length. Therefore, the elastic buckling stress and the corresponding buckling modes are also a function of the length. The problem can be solved for several lengths and thus a complete picture of

the elastic buckling stress and modes can be determined. The minima of such of curve could be considered as the critical buckling loads and modes for the member.

2.8.4 The limitation of finite strip method

It should be mentioned here that in the finite strip method the stress distribution is assumed as constant along the half wavelength, while in the practical case the longitudinal stress varies along the member span. However, it is conceivable that for a beam subjected to a varying stress distribution along its span the local and distortional buckling will occur only at a worst location such as mid span. Obviously, the finite strip method is not suitable for analysing global buckling of the structures with a varying stress distribution along its span.

However, local buckling can be carried out by finite strip method if the pre-buckling stress distribution on the cross-section at the worst place is known, since it has a relatively short half wavelength.

Chapter 3

3 OPTIMISATION PROBLEM

3.1 INTRODUCTION

Nowadays, optimisation has become a necessary design trend in all major disciplines. The motivation to produce economically relevant products with embedded quality is the principal reason for optimisation. Optimisation is frequently associated with engineering design, especially in structure civil engineering.

Cold-formed steel members provide substantial savings due to their high strength-to-weight ratio. As a result, they have become very popular in the construction of industrial, commercial, and agricultural buildings. An important advantage of cold-formed steel is the greater flexibility of cross-sectional shapes and sizes available to the structural steel designer. The shape of the cross-section of the members is mostly that of zed, channel or sigma. These types of cross sections are popular and suitable for the connection with other structure parts for buildings such as Zed and Channel, Sigma sections which are used in roof and wall systems, as purlins and girt, or sometimes as beams or columns.

The basic problem of the economical design of structures is to achieve the least expensive construction that satisfies the design requirements. One of the conditions required for a low-cost erected structure is the minimum weight of the material, which is associated with the maximum structural efficiency (Yu, 1991). Cold-formed steel structural members provide various kinds of cross sections, and can be produced economically by forming operations. They provide a much larger variety of choices for steel designers.

In this study, the MATLAB programme for optimising the cross-sectional area of cold-formed steel beams such as channel, zed and sigma purlin, subjected to the uniformly distributed vertical load is presented here. The optimised beams are assumed to be simply supported with no lateral restraint. The design variables include thickness, web depth, flange width, lip length and dimension of stiffener. Parametric studies are carried out for different span lengths and loading intensities.

3.2 DESCRIPTION OF THE OPTIMISATION PROBLEM

The aim of the optimisation of cold-formed steel members is to minimise the weight of material which is described by the gross area of the cross section A_g when the design variables reach their constraints. In general, the optimum design problem of thin-walled open cross sections can be expressed as below:

$$\min F = f(x_i) \quad (3.1)$$

where $f(x_i)$ is the objective function which represent the area of the cross section and x_i represents the design variables, which consists of the cross sectional dimensions such as the wall thickness t , web depth h_o , flange width b_o and lip length c_o or the dimension of the stiffener of the section, which are chosen to minimise the objective function $f(x_i)$ under some equality or inequality structural performance constraints and geometric constraints of the design variables.

The structural performance constraints for cold-formed section beams generally include strength, deflection and stability requirements as well as geometric

constraints. There might exist some types of fabrication constraints in some practical applications. For instance, the length of strip L_{strip} , which is used to form the desired shape of the cross section, should be in the range of design variables that the manufacturer provides. In general, the constraints of optimisation in cold-formed steel beams $C_i(x)$ can be expressed as follows:

$$C_i(x) = \left\{ \begin{array}{l} M_{\max} - M_c \\ M_{\max} - \min \{ M_{\text{cr,d}}, M_{\text{cr,g}}, M_{\text{cr,sh}} \} \\ \Delta_{\max} - \Delta_{\text{lim}} \end{array} \right\} \leq 0 \quad (3.2)$$

where M_{\max} and Δ_{\max} are the actual maximum moment design and maximum deflection occurring in the beam when it is subjected to a uniformly distributed transverse load, which is calculated based on the bending theory of the beam; M_c is the moment capacity of the section, which is calculated based on the design codes; Δ_{lim} is the deflection limit which is also specified in design codes; $M_{\text{cr,d}}$, $M_{\text{cr,g}}$ and $M_{\text{cr,sh}}$ are the moment capacities corresponding to distortional buckling, lateral-torsional buckling and shear buckling, which are also calculated based on design codes and currently available approaches.

Geometrical constraints of design variables are applied based on the EN 1993-1-3:2006 as below:

$$L_l \leq L_{\text{strip}} \leq L_u \quad (3.3)$$

$$\frac{h_o}{t} \leq 500; \frac{b_o}{t} \leq 60; 0.2 \leq \frac{c_o}{b_o} \leq 0.6; \frac{c_o}{t} \leq 50 \quad (3.4)$$

where L_l and L_u are the lower and upper limit of the strip length which is provided by the manufacturer.

These geometrical proportions are assumed to represent the field for which sufficient experience and verification by testing are already available. Cross sections with larger width-to-thickness ratio are also used, provided that their resistance at ultimate limit states and their behaviour at serviceability limit states are verified by testing and/or by calculations and the results are confirmed by an appropriate number of tests.

In general, the above optimisation problem is a nonlinear problem in which both objective function and constraints are nonlinear functions of the design variables. The nonlinear character of the objective function and the constraints will be expressed in greater detail in the next chapters with regard to different kinds of sections that are to be optimised.

In this study, the optimisation problem is solved using the trust-region method which is based on a standard optimisation algorithm medium scale built in MATLAB. The requirement inputs for using this kind of optimisation tool are to create the objective function and constraint functions for each individual optimisation problem. The computational procedure and the mechanism of the optimisation programme are described in the following section.

In order to demonstrate the overview picture of the general algorithm and its process towards a solution of the optimisation problem, an example of the optimisation problem with two design variables will be presented here as a good demonstration of nonlinearity and the solution method when there are many variables.

The problem is to design simply supported, plain channel beams under a uniformly distributed load, and minimise the cross-sectional area, as shown in the Fig 3.1. The design parameters are modulus of elasticity $E=205000 \text{ N/m}^2$, yielding stress $p_y = 350 \text{ N/m}^2$, span length $L=4\text{m}$, thickness of section $t=3 \text{ mm}$, load intensity $q = 4\text{kN/m}$. The design variables are the width of flange (X_1) and the depth of web (X_2). In this example, we assume the only two critical design criteria are bending strength and a deflection limit of beam. Hence we have two nonlinear constraints, and for practical engineering we have a geometric constraint for the section as the depth of web is greater or equal to twice the width of flange. So the optimisation problem can be described as follows:

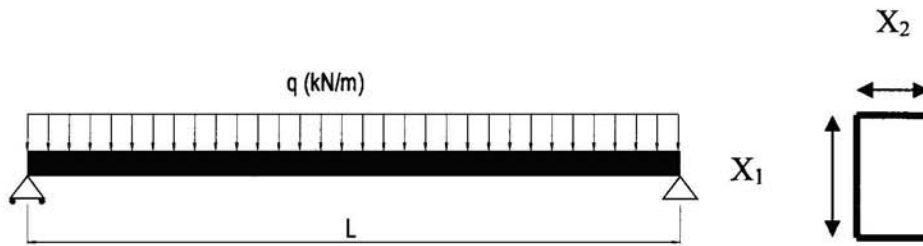


Fig. 3.1: Simply supported beam subjected to uniformly-distributed transverse loading

Objective function:

$$\text{Minimise } f(X_1, X_2) = t(2X_1 + X_2 - t). \quad (3.5)$$

Subjected to:

$$C_1(X_1, X_2): \sigma_{\text{design}} \leq p_y \quad (3.6)$$

$$C_2(X_1, X_2): \Delta_{\text{max}} \leq \Delta_{\text{lim}} \quad (3.7)$$

$$C_3(X_1, X_2): 2X_1 - X_2 \leq 0 \quad (3.8)$$

Dimension constraints are: $50\text{mm} \leq X_1 \leq 300\text{mm}; 50\text{mm} \leq X_2 \leq 300\text{mm}$

where σ_{design} is the maximum stress in the section due to the applied design load;
 Δ_{max} is the maximum deflection at mid span due to the applied design load; Δ_{lim} is the allowable limit deflection in the beam equal to $L/300$.

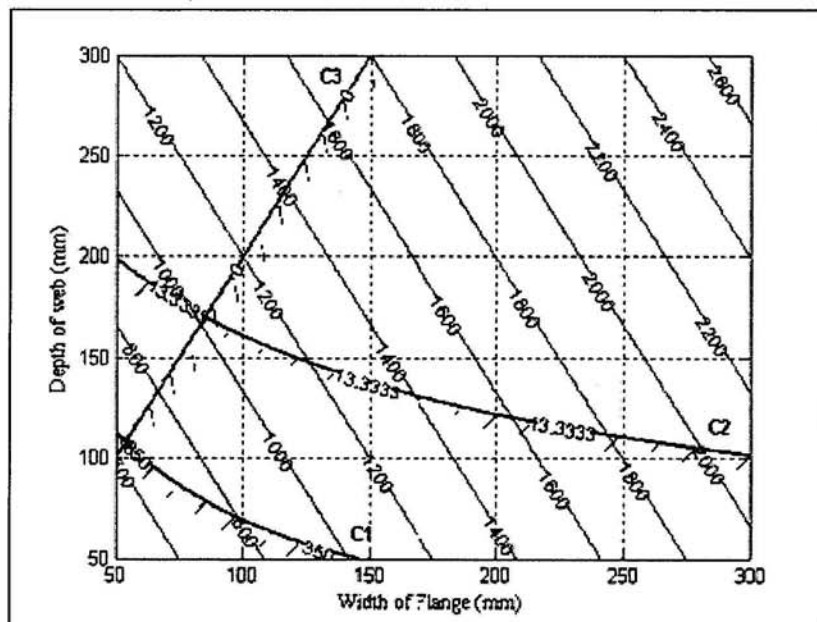


Fig.3.2: Graphical optimisation representation

The two inequalities of nonlinear constraints are shown as (C1) and (C2) curves and linear constraint is given by as line (C3). The labels on the constraints curves is the limitation of constraint such as allowable stress and limit deflection of beam. Hash lines on the side of the inequalities of constraint establish the disallowable region for the design variables. The constraints are drawn thicker for emphasis. The scaled objective function is represented through several labelled contours. Each contour is associated with a fixed value of the objective function and these values are shown on Fig.3.2. The range of two axes establishes the web and flange dimension constraints. The problem represented in Fig.3.2 provides an opportunity to identify the graphical solution. First, the feasible region is identified. In Fig.3.2, the region above the linear

constraint (C3) and nonlinear curve constraint (C2) is a feasible and optimal region. Any solution from this region is an acceptable solution. There are usually a large number of such solutions so-called infinite solutions. If optimisation is involved, then these choices must be reduced to the best one with respect to some criteria (the objective). In this example, the smallest value of objective function $f(X_1, X_2)$ is desired. The lowest values of $f(X_1, X_2)$ must be bigger than the contour value of 800 and less than the contour value of 1000. It is the intersection of constraint C2 and dimension constraint for the depth of web. Hence the value of $f(X_1, X_2)$ needs to be calculated. The optimal values of the design variables read from Fig.3.2, are 200mm for web depth and 50mm for flange width. Another significant item of information obtained from Fig.3.2 is that C1, C2 and C3 are active constraints. While there are infinite feasible solutions to the problem, the optimal solution is unique.

3.3 STANDARD ALGORITHM OPTIMISATION BUILT IN MATLAB

Standard Algorithm provides an introduction to the different optimisation problem formulations, and describes the medium-scale algorithms used in the toolbox functions. These algorithms have been chosen for their robustness and iterative efficiency. The choice of problem formulation (e.g., unconstrained, least-squares, constrained, multi-objective, or goal attainment) depends on the problem being considered and the required execution efficiency.

Optimisation techniques are used to find a set of design parameters, $x = \{x_1, x_2, \dots, x_n\}$, that can in some way be defined as optimal. In a simple case this might be the minimisation or maximisation of some system characteristic that is dependent on design variables x_i . In a more advanced formulation the objective

function, $f(x_i)$, to be minimised or maximised, might be subject to constraints in the form of equality constraints, $C_i(x) = 0 (i = 1, \dots, m_e)$, inequality constraints, $C_i(x) \leq 0 (i = m_{e+1}, \dots, m)$; and x_l, x_u are the parameter bounds of the variables design.

A general problem description is stated as

$$\text{minimise } f(x) \tag{3.9}$$

Subject to

$$C_i(x) = 0 (i = 1, \dots, m_e) \tag{3.10}$$

$$C_i(x) \leq 0 (i = m_{e+1}, \dots, m) \tag{3.11}$$

where x is the vector of n design variables parameters; $f(x)$ is the objective function, which returns a scalar value, and the vector function $C(x)$ returns a vector of length m containing the values of the equality and inequality constraints evaluated at x .

An efficient and accurate solution to this problem depends not only on the size of the problem in terms of the number of constraints and design variables, but also on characteristics of the objective function and constraints. For the optimisation problem of the cold-formed steel section, because of nonlinear characteristics of the objective function and constraints, the optimisation problem for the cold-formed beam is described as a nonlinear optimisation problem (NLP). A solution of the nonlinear problem generally requires an iterative procedure to establish a direction of search at major iteration and is obtained through numerical analysis. Through computer code, numerical analysis becomes a numerical technique. The methods or techniques for finding the solution to optimisation problems are called search methods. In applied mathematics and numerical techniques these are referred to as interactive techniques.

Implicitly, this means several tries will be necessary before the solution can be obtained. Also implied is that each try or search is executed in a consistent manner. The information from the previous iteration is employed in the computation of values in the present sequence. This consistent process, by which the search is performed and the solution determined, is called an algorithm. The search process is started typically by trying to guess the initial design solution. The designer can base this selection on his experience. On several occasions the success of optimisation may hinge on his ability to choose a good initial estimate to the required solution. The search method, even when used consistently, corresponds differently to the particular problem that is being solved. The degree and type of nonlinearity may frequently cause the method to fail.

In constrained optimisation the general aim is to transform the problem into an easier sub-problem that can then be solved and used as the basis of an iterative process. A characteristic of a large class of early methods is the translation of the constrained problem to a basic unconstrained problem by using a penalty function for constraints that are near or beyond the constraint boundary. In this way the constrained problem is solved using a sequence of parameterised unconstrained optimisations, which in the limit converge to the constrained problem.

Minimise $F = f(x)$ (if Required Strength \leq Allowable Strength)

$$\begin{aligned}
 &F = f(x) + \text{penalty}(x) \\
 &\text{(if Required Strength} > \text{Allowable Strength)}
 \end{aligned}
 \tag{3.12}$$

The penalty is equal to the sum of square of all the constraints and is therefore greater than zero when any constraint is violated and is zero when the point is feasible.

$$Penalty(X) = r \cdot \sum C_i^2 \quad (3.13)$$

where r is a positive penalty constant.

This method is now considered relatively inefficient and has been replaced by a method that has focused on the solution of the Kuhn-Tucker (KT) equations (Venka. The KT equations are necessary conditions for optimality of constrained optimisation problems. If the problem is a so-called convex programming problem, that is, $f(x)$ and $C_i(x) (i = m_{e+1}, \dots, m)$, are convex functions, then the KT equations are both necessary and sufficient for a global solution point.

Referring to the general mathematical problem in Eq.(3.9), the Kuhn-Tucker expressions can be stated as

$$\begin{aligned} \nabla f(X^*) + \sum_{i=1}^m \delta_i^* \cdot \nabla C_i(X^*) &= 0 \\ \delta_i^* \cdot C_i(X^*) &= 0 \quad i = 1, \dots, m \\ \delta_i^* &\geq 0 \quad i = m_e + 1, \dots, m \end{aligned} \quad (3.14)$$

The first equation describes a cancelling of the gradients between the objective function and the active constraints at the solution point. For the gradients to be cancelled, Lagrange multipliers $\delta_i, i = 1, \dots, m$ are necessary to balance the deviations in magnitude of the objective function and constraint gradients. Because only active constraints are included in this cancelling operation, the constraints which are not active must not be included in this operation and so are given Lagrange multipliers equal to zero. This is stated implicitly in the last two relationships to Eq.(3.14)

The gradient of the function is a vector which presents the change of the function per unit change in the variables and at any point represents the direction in which the

function will increase most rapidly. Examining the conventional objective function of nonlinear problem minimisation of objective functions, the gradient has a natural part to play in the development of methods to solve the problem. The gradient is composed of the partial derivatives organised as a vector. It is defined by:

$$\nabla f = \left[\frac{\partial f}{\partial x_1} \quad \frac{\partial f}{\partial x_2} \quad \frac{\partial f}{\partial x_3} \quad \dots \quad \frac{\partial f}{\partial x_n} \right]^T \quad (3.15)$$

For mathematical concepts of nonlinear optimisation problems, the unconstrained problems are discussed first followed by constrained problems. For constrained problems the equality constrained problem is discussed first. A similar technique will be applied to the inequality-constrained problem.

- Unconstrained problems

To illustrate the mathematical concepts of the unconstrained problem, we use an example of two design variables and the nonlinear objective function defined as below:

$$\text{Minimise } f(x_1, x_2) = (x_1 - 1)^2 + (x_2 - 1)^2 - x_1 x_2 \quad (3.16)$$

$$0 \leq x_1 \leq 3; \quad 0 \leq x_2 \leq 3 \quad (3.17)$$



Fig. 3.3: Three-dimensional plot (P. Venkataraman, 2002)

Fig. 3.3 gives the contour plot solution and is used to identify the properties of the function $f(x_1, x_2)$. A tangent plane is drawn at the minimum for emphasis. The minimum value of function is identified by X^* or $[x_1^*, x_2^*]$. From Fig. 3.3 the minimum value of the function is equal to -2, while the design variables x_1^*, x_2^* are both equal to 2. If the design variables move a slight amount away from the optimum value, in any direction, the value of the function $f(x_1, x_2)$ will definitely increase because X^* is the lowest location of the concave surface representing the function $f(x_1, x_2)$. Corresponding to the displacement from the optimum values of variables as ΔX , the change in the function value from the optimum value as Δf , from the direct observation, it is evident that the optimum solution must be a point which satisfies

$$\Delta f > 0, \text{ for all } \Delta X \quad (3.18)$$

The same suggestion can be applied in the limit, such as for extreme small displacement dx_1 and dx_2 about X^* . The function itself can be approximated by a plane tangent to the function at the optimum solution as in Fig. 3.3. Moving to any point in the plane from the optimum will not change the value of the function, therefore $df = 0$. Moving away from optimum variables that dx_1 , dx_2 are not zero. The changes in functions occur due to changes in the variables. From calculation of the differential change in $f(x_1, x_2)$ (df) due to the differential change in the variables x_1 (dx_1) and x_2 (dx_2) is expressed as

$$df = \frac{\partial f}{\partial x_1} dx_1 + \frac{\partial f}{\partial x_2} dx_2 = 0$$

$$df = \begin{bmatrix} \frac{\partial f}{\partial x_1} & \frac{\partial f}{\partial x_2} \end{bmatrix} \begin{bmatrix} dx_1 \\ dx_2 \end{bmatrix} \quad (3.19)$$

This should be applied for all locations in the plane $dx_1 \neq 0$ and $dx_2 \neq 0$

Therefore,

$$\frac{\partial f}{\partial x_1} = 0, \quad \frac{\partial f}{\partial x_2} = 0$$

or the gradient of $f(x_1, x_2)$ at the optimum must be zero. That is,

$$\nabla f(x_1^*, x_2^*) = 0$$

For n variables, X^* , this expression becomes:

$$\nabla f(X^*) = 0 \quad (3.20)$$

Eq.(3.20) expresses the necessary condition, or first order condition, for unconstrained optimisation. This equation is used to identify the possible solutions to the optimisation problem. The solution for the variables will be at the same value of the design variable. Eq.(3.20) by itself will not determine the minimum value of the

function. Additional considerations are necessary to ensure that the solution established by the first order conditions is optimum value.

The second order conditions are usually considered as sufficient conditions. It can be assumed that these conditions will involve a second derivative of the function. The second-order condition is often gained through the Taylor expression of the function. The Taylor series is a useful mechanism to approximate the value of the function $f(x)$ at the point $(x_p + \Delta x)$ if the function is completely known at point x_p . The expansion is for finite n :

$$f(x_p + \Delta x) \cong f(x_p) + \left. \frac{df}{dx} \right|_{x_p} (\Delta x) + \frac{1}{2!} \left. \frac{d^2 f}{dx^2} \right|_{x_p} (\Delta x)^2 + \dots + \frac{1}{n!} \left. \frac{d^n f}{dx^n} \right|_{x_p} (\Delta x)^n \quad (3.21)$$

The series is widely used in most disciplines to establish continuous models. It is the basis of many numerical techniques, including those in optimisation. The equation is usually truncated to the first two or three terms, understanding that the approximation will suffer some error:

$$f(x_p + \Delta x) \cong f(x_p) + \left. \frac{df}{dx} \right|_{x_p} (\Delta x) + \frac{1}{2!} \left. \frac{d^2 f}{dx^2} \right|_{x_p} (\Delta x)^2 + 0.(\Delta x)^3 \quad (3.22)$$

Moving the first term of the right hand side to the left hand side, ignoring the error term, the Eq.(3.22) can be written as:

$$\Delta f = f(x_p + \Delta x) - f(x_p) = \left. \frac{df}{dx} \right|_{x_p} (\Delta x) + \frac{1}{2!} \left. \frac{d^2 f}{dx^2} \right|_{x_p} (\Delta x)^2 \quad (3.23)$$

For n variables, with X_p the current point and ΔX the displacement vector,

$$f(X_p + \Delta X) = f(X_p) + \nabla f(X_p)^T \Delta X + \frac{1}{2} \Delta X^T H(X_p) \Delta X \quad (3.24)$$

where $H(X_p)$, the Hessian matrix is the same as the matrix of second derivatives of a function of n variables:

$$[H] = \begin{bmatrix} \frac{\partial^2 f}{\partial x_1^2} & \frac{\partial^2 f}{\partial x_1 \partial x_2} & \cdots & \frac{\partial^2 f}{\partial x_1 \partial x_n} \\ \frac{\partial^2 f}{\partial x_2 \partial x_1} & \frac{\partial^2 f}{\partial x_2^2} & & \cdots \\ \vdots & & \ddots & \\ \frac{\partial^2 f}{\partial x_n \partial x_1} & & & \frac{\partial^2 f}{\partial x_n^2} \end{bmatrix} \quad (3.25)$$

If X^* is the solution, and ΔX represents the change of the variables from the optimum value which will lead a change Δf , then

$$\Delta f = f(X^* + \Delta X) - f(X^*) = \nabla f(X^*)^T \Delta X + \frac{1}{2} \Delta X^T H(X^*) \Delta X \quad (3.26)$$

Δf must be greater than zero. By substituting the first order condition in Eq.(3.26) the first term on the right hand side of this equation is zero, and we have the following inequality:

$$\Delta f = \frac{1}{2} \Delta X^T H(X^*) \Delta X > 0 \quad (3.27)$$

Hence, the second-order condition to ensure that the solution established by the first-order condition is optimum is expressed in Eq.(3.27).

- Equality-constrained problem

For the equality-constrained problem, it is said that at the optimum solution, the gradients of the objective function and the constraint are parallel and oppositely directed. There may exist a proportional relationship between the gradients at the

solution. Using the constant of proportionality δ_1 (a positive value) the relationship between the gradient can be expressed as:

$$\nabla f = -\delta_1 \nabla C \text{ or } \nabla f + \delta_1 \nabla C = 0 \quad (3.28)$$

Eq.(3.28) is usually obtained in a more formal way using the method of Lagrange multipliers. In this method, the problem is transformed by introducing an increased function, called the Lagrangian, as the objective function subjected to the same equality constraints. The Lagrangian is defined as the sum of the original objective function and a linear combination of the constraints. The coefficients of this linear combination are known as the Lagrange multipliers. Therefore the objective function becomes as below:

$$\begin{aligned} \text{Minimise } F(X, \delta) &= f(X) + \delta C \\ \text{Subject to equality constraint } &C \end{aligned} \quad (3.29)$$

The solution to Eq.(3.29) is the same as the solution to Eq.(3.16). This is because, if the design variable is feasible, the equality constraint is satisfied and the objective function returns to the original expression. If it is not feasible, then by definition there is no solution anyway. Applying the first-order condition, we obtained:

$$\nabla F = \nabla f + \delta \nabla C = 0 \quad (3.30)$$

The Lagrange multiplier method is an elegant formulation to gain the solution to a constrained problem. In overview, it seems out of the ordinary that we have to introduce an additional unknown δ to solve the constrained problem. This breaks the conventional rule for nonlinear problems in which the problem with fewer variables

are normally easier to obtain the solution. As illustrated above, the Lagrangian allows the transformation of a constrained problem into an unconstrained problem. The Lagrange multiplier also has a physical significance. At the solution, it expresses the ratio of the change in the objective function to the change in the constraint value.

$$F(X, \delta) = f(X) + \delta C \Rightarrow dF = df + \delta dC \quad (3.31)$$

At the solution, the first order condition supposes that $dF = 0$. Hence,

$$\delta = -\frac{df}{dC} = -\frac{\Delta f}{\Delta C} \quad (3.32)$$

At the solution determined by first order condition, to ensure having the optimum solution, the second-order condition can be expected to satisfy the following relations:

$$\begin{aligned} \Delta F = F(X^* + \Delta X) - F(X^*) &= \nabla F(X^*) + \frac{1}{2} \Delta X^T [\nabla^2 F(X^*)] \Delta X > 0 \\ \nabla C^T \Delta X &= 0 \end{aligned} \quad (3.33)$$

where $[\nabla^2 F(X^*)]$ is the Hessian of Lagrangian, with respect to the design variables only evaluated at the solution. Also, the first order condition requires that $\nabla F(X^*) = 0$.

- Inequality-constrained problem

The inequality-constrained problem is described by Eq.(3.9) and Eq.(3.11). We saw above how the equality-constrained problems can be solved. If the inequality-constrained problem can be equally transformed to an equivalent equality-constrained problem, then we have a solution. The standard transformation approach requires a

slack variable s_j for each inequality constraint C_j . Unlike linear problems, the slack variable for nonlinear problems is not restricted in sign. Therefore, the square of the new variable is added to the left-hand side of the corresponding constraint. This adds a positive value to the left-hand side to bring the constraint up to zero. Evidently a zero value of slack will be added if the constraint is already zero. Therefore, the new equality-constrained problem is defined as below:

$$\begin{aligned} \text{Minimise} \quad & f(X) \\ \text{Subject to} \quad & C(X) + s^2 = 0 \end{aligned} \quad (3.34)$$

This is a valid equality-constrained problem. The Lagrange multiplier method can be applied to this transformation. To distinguish the multipliers associated with inequality constraints, the symbol β is used. The augmented function or Lagrangian is:

$$\text{Minimise } F(X, s, \beta) = f(X) + \beta[C(X) + s^2] \quad (3.35)$$

If the Lagrangian is considered as an unconstrained objective function, the first order conditions are:

$$\begin{aligned} \frac{\partial F}{\partial X} &= \frac{\partial f}{\partial X} + \beta \frac{\partial C}{\partial X} = 0 \\ \frac{\partial F}{\partial s} &= \frac{\partial f}{\partial s} + \beta \frac{\partial C}{\partial s} - 2\beta s = 0 \\ \frac{\partial F}{\partial \beta} &= C + s^2 = 0 \end{aligned} \quad (3.36)$$

It is noted that X is the vector of design variables, C is vector of constrained function and s is the vector of slack variables for each inequality constraint C_j .

By combining the last two relationships in Eq.(3.36), the first order condition can be restated as:

$$\begin{aligned} \frac{\partial F}{\partial X} = \frac{\partial f}{\partial X} + \beta \frac{\partial C}{\partial X} = 0 \\ \beta C = 0 \end{aligned} \tag{3.37}$$

These equations have to be solved for X^*, β^* . Note that the slacks s^* are not being determined. It suggests that they can be removed from the problem altogether in the first order condition. The last equation of Eq.(3.37) presents a definite feature for a nontrivial solution, either β is zero (and $C \neq 0$) or C is zero ($\beta \neq 0$). Since simultaneous equations are being solved, the conditions on the multipliers and constraints must be satisfied simultaneously. If $\beta \neq 0$ (or corresponding $C = 0$), then the corresponding constraint is an equality. Therefore, we are going to pretend slack s never existed; the Lagrangian is reformed without the slack variables as

$$\text{Minimise } F(X, \beta) = f(X) + \beta C \tag{3.38}$$

This equation is the same formulation as in the equality-constrained problem. The slack variable was introduced to provide the transformation to an equality constraint. It is evident that the construction of the Lagrangian function is insensitive to the type of constraint. Since the multipliers tie to the inequality constraints are required to be positive, those corresponding to the equality constraint are not. Hence the first order condition for the problem can be rewritten as Eq.(3.37). These equations are used to solve unknown variables. The best design solution is decided by scanning several solutions. The sign of the multiplier in the solution is not a sufficient condition for the inequality-constrained problem. Formally verifying a minimum solution requires consideration of the second derivative of the Lagrangian. In practical situations, if the problem is well defined, the positive value of the multiplier usually suggests a minimum solution.

- General optimisation problem

The general optimisation problem is described as below:

$$\begin{aligned}
& \text{Minimise } f(x_1, x_2, \dots, x_n) \\
& \text{Subject to } E_k(x_1, x_2, \dots, x_n) = 0 \quad k=1, 2, \dots, l \\
& \quad \quad C_j(x_1, x_2, \dots, x_n) \leq 0 \quad j=1, 2, \dots, m \\
& \quad \quad x_i^{\text{low}} \leq x_i \leq x_i^{\text{upper}} \quad i=1, 2, \dots, n
\end{aligned} \tag{3.39}$$

The Lagrangian:

$$\begin{aligned}
& \text{Minimise } F(x_1, \dots, x_n, \delta_1, \dots, \delta_l, \beta_1, \dots, \beta_m) = \\
& \quad f(x_1, \dots, x_n) + \delta_1 E_1 + \dots + \delta_l E_l + \beta_1 C_1 + \dots + \beta_m C_m
\end{aligned} \tag{3.40}$$

The first order condition associated with the general optimisation problem is called the Kuhn-Tucker condition. There are $n+l+m$ unknowns. The same numbers of equations are required to solve the problem. They are provided by the Kuhn-Tucker condition:

$$\frac{\partial F}{\partial x_i} = \frac{\partial f}{\partial x_i} + \delta_1 \frac{\partial E_1}{\partial x_i} + \dots + \delta_l \frac{\partial E_l}{\partial x_i} + \beta_1 \frac{\partial C_1}{\partial x_i} + \dots + \beta_m \frac{\partial C_m}{\partial x_i} = 0; \quad i = 1, 2, \dots, n \tag{3.41}$$

$$E_k(x_1, x_2, \dots, x_n) = 0 \quad k = 1, 2, \dots, l \tag{3.42}$$

It is evident that n equations are obtained by Eq.(3.41), l equations are obtained directly through the equality constraints Eq.(3.42) and m equations are applied through the 2^m cases. This indicates that there are 2^m possible solutions. These solutions must include Eq.(3.41) and Eq.(3.42). Each case sets the multiplier β_j or the corresponding inequality constraint C_j to zero. If the multiplier is set to zero, then the corresponding constraint must be feasible for an acceptable solution. If the constraint is set to zero, then the corresponding multiplier must be positive for a minimum.

Therefore, the m equations can be expressed as below:

$$\begin{aligned} \beta_j C_j = 0 \rightarrow & \text{if } \beta_j = 0 \text{ then } C_j < 0 \\ & \text{if } C_j = 0 \text{ then } \beta_j > 0 \end{aligned} \quad (3.43)$$

If conditions Eq.(3.43) are not met, the design is not acceptable. For each case a simultaneous total of m values and equalities must be assigned. Once these first order conditions determine a possible solution, the side or boundary constraints of variable design have to be checked.

The solution of the equations forms the basis to many nonlinear programming algorithms. These algorithms attempt to compute the Lagrange multipliers directly. Constrained quasi-Newton methods guarantee super-linear convergence by accumulating second order information regarding the KT equations using a quasi-Newton updating procedure.

Chapter 4

4 CONSTRAINTS IN THE OPTIMISATION PROBLEM

4.1 GENERAL

The optimisation of cold-formed steel sections is a highly nonlinear problem. As seen in Chapter 3 the objective function is a quadratic nonlinear function of the multi-design variables, and the constraints are also nonlinear. The constraints of the optimisation problem in cold-formed steel sections consist of strength, deflection and stability requirements, as well as the practical geometrical constraints of the design variables. These constraints will be discussed in the following sections.

4.2 GEOMETRICAL CONSTRAINTS

In this study, the three types of cold formed steel purlins studied are the C channel, the Zed section and the Sigma section. Depending on the design specification of each country, the geometrical constraints of the cold-formed steel section are different. For example, following the EN 1993-1-3:2006, the dimensions of the section are specified as:

$$\frac{h_o}{t} \leq 500; \frac{b_o}{t} \leq 60; 0.2 \leq \frac{c_o}{b_o} \leq 0.6; \frac{c_o}{t} \leq 50 \quad (4.1)$$

where b_o , c_o and h_o are the overall width of a flange, a lip and a web, respectively, measured from the face of the section.

In the British Standard BS 5950-5:1998, the maximum ratios of the element flat width b_{elem} to the thickness t are determined for different kind of elements and compression elements are given as follows;

Stiffened elements having one longitudinal edge connected to a flange or web element

$$(b_{\text{elem}} / t)_{\text{max}} = 60 \quad (4.2)$$

Stiffened element with both longitudinal edges connected to other stiffened elements

$$(b_{\text{elem}} / t)_{\text{max}} = 500 \quad (4.3)$$

Un-stiffened compression elements

$$(b_{\text{elem}} / t)_{\text{max}} = 60 \quad (4.4)$$

According to AISI, the geometrical constraint of the flange is the same as BS 5950-5:1998 above, but for the flexural member maximum depth-to-thickness ratio of web should not exceed the following limitations:

For un-reinforced webs

$$(h_o / t)_{\text{max}} = 200 \quad (4.5)$$

For web with intermediate stiffener

$$(h_o / t)_{\text{max}} = 300 \quad (4.6)$$

In this thesis, the geometrical constraints based on EN 1993-1-3:2006 will be used in the optimisation process. However, depending on the purpose of the design, these constraints can be changed to suite the design requirement.

4.3 STRENGTH CONSTRAINTS

In designing simple cold-formed steel purlins subjected to the uniformly distributed load, the constraints in the strength of the members are based on the three main modes of failure as local buckling, distortional buckling and the lateral-torsional buckling. Additionally, the serviceability limit state of the member such as the maximum deflection is also considered as one of the design constraints. The calculation of these constraints will be presented herein under several methods based on the different codes and recent research deliverables. The purpose of this section is to illustrate the currently available approaches that are used to investigate the behaviour of the cold-formed steel beams and are used for optimisation programming.

4.3.1 Local buckling

4.3.1.1 British standard BS 5950-5:1998

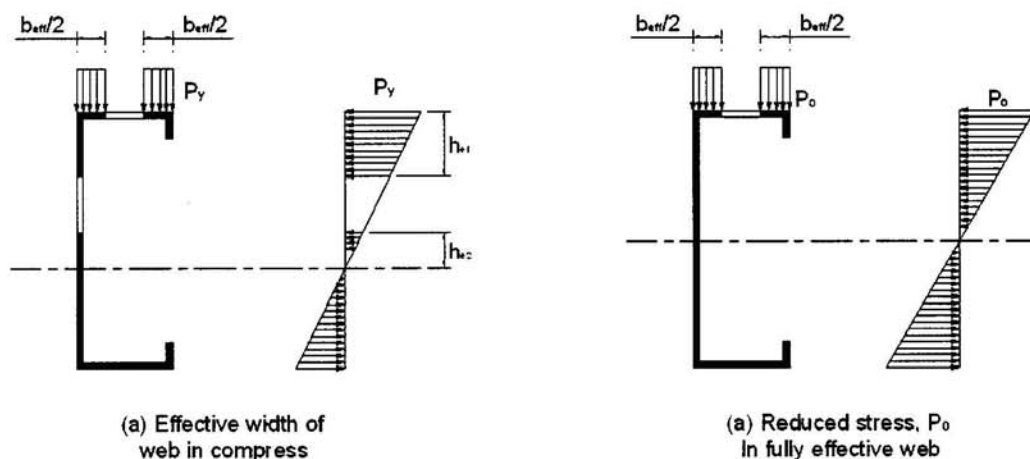


Fig. 4.1: Behaviour of the member in bending.

The elastic properties of sections in bending are determined by considering the effective widths of compression elements, as illustrated in Fig. 4.1. The neutral axis of

the section is determined by balancing tension and a compression zone. The elastic section modulus is then calculated based on the final axis position. Multiplying the elastic section modulus by the design yielding strength of the steel leads directly to the elastic moment capacity. Both the neutral axis position and the elastic section modulus are therefore functions of the operating stress in the compression flange.

For symmetric sections, the elastic section modulus in compression is not higher than that in tension and therefore compression yielding occurs first. However, for those sections that are un-symmetric about the axis of bending, tension yielding may occur first, causing plasticity to occur in the web. This local yielding as illustrated in Fig. 4.1, and is permitted provided that this stress in the compression plate does not exceed the yield value.

The moment capacity of the section is computed based on the effective section. In BS 5950-5:1998, the moment capacity is determined on the basis of a limiting compressive stress in the webs p_o , determined in accordance with Cl.5.2.2.2 and Cl.5.2.2.3. This stress is used to determine the effective widths of compression elements, and hence the reduced section properties, and in the determination of the moment capacity M_c .

The procedure of the calculation of effective section based on BS 5950-5:1998 is listed as follows:

Limiting compressive stress in the web:

$$p_o = p_y \min(1, k) \quad (4.7)$$

where:

$$k = 1.13 - 0.0019 \left(\frac{d_w}{t} \right) \sqrt{\frac{p_y}{280}}$$

$d_w = \max(h, 2Y_m)$; h is depth of web along the middle line; p_y is yield stress, given in Table 3.1 BS 5950-5:1998; Y_m is depth of compression zone ($=0.5h$);

Effective width of the compressed flange (with stiffening lip):

The local buckling stress of an element is calculated by E.q.(4.8):

$$p_{cr} = \frac{\pi^2 E}{12(1-\nu^2)} k_\sigma \left(\frac{t}{b} \right)^2 = 0.904 E k_\sigma \left(\frac{t}{b} \right)^2 \quad (4.8)$$

where

$$k_\sigma = 5.4 - \frac{1.4(h/b)}{0.6 + h/b} - 0.02 \left(\frac{h}{b} \right)^3 \quad (4.9)$$

Compressive stress on the effective flange:

$$f_c = p_o \quad (4.10)$$

Effective width of the flange:

$$b_{e1} = b_{e2} = 0.5 b_{eff} \quad (4.11)$$

where

$$b_{eff} = b \left[1 + 14 \left(\sqrt{\frac{f_c}{p_{cr}}} - 0.35 \right)^4 \right]^{-0.2} \quad \text{if } f_c / p_{cr} > 0.123$$

$$b_{eff} = b \quad \text{if } f_c / p_{cr} \leq 0.123 \quad (4.12)$$

Effective length of the compressed stiffening lip:

The local buckling stress:

$$p_{cr} = \frac{\pi^2 E}{12(1-\nu^2)} k_\sigma \left(\frac{t}{c} \right)^2 \quad (4.13)$$

where

$$k_{\sigma} = \frac{1.7}{3 + f_{cs}/f_{cf}}; f_{cs} = p_o; f_{cf} = f_{cs} \frac{Y_m - c}{Y_m}$$

c is lip length along middle line

$$\text{Average compression stress in the stiffening lip: } f_c = (f_{cs} + f_{cf})/2 \quad (4.14)$$

where f_{cf} and f_{cs} are compression stress at two end of lip.

Effective length of the stiffening lip:

$$c_{\text{eff}} = c \quad \text{if } f_c / p_{cr} \leq 0.123$$

$$c_{\text{eff}} = c_1 \left\{ 0.89 \left[1 + 14 \left(\sqrt{\frac{f_c}{p_{cr}}} - 0.35 \right)^4 \right]^{-0.2} + 0.11 \right\} \quad \text{if } f_c / p_{cr} > 0.123 \quad (4.15)$$

⇒ Calculation of the new position of the neutral axis

$$Y_n = \frac{\frac{c_{\text{eff}}^2}{2} + \frac{h^2}{2} + bh + c \left(h - \frac{c}{2} \right)}{c_{\text{eff}} + b_{\text{eff}} + h + b + c} \quad (4.16)$$

4.3.1.2 Eurocode EN 1993-1-3:2006

EN 1993-1-3:2006 gives some comprehensive rule for the determination of effective widths under different stress conditions. In practice, the effective width of individual plate elements may be combined to give an effective section and member design completed using conventional techniques. The procedure of calculating of the effective width of an individual plane element is described detail in EN 1993-1-5:2006. For plane elements without stiffeners, the effective width of un-stiffened elements such as lip element of channel should be obtained by using the notional flat

width reduced by the reduction factor ρ for plate buckling based on the plate slenderness $\bar{\lambda}_p$. For plane elements such as flange element with edge or intermediate stiffener, the design of a compression element should be based on the assumption that the stiffener behaves as a full restraint.

We therefore have for plate element i that:

$$b_{\text{eff},i} = \rho \cdot \bar{b}_i \quad (4.17)$$

The calculation of the effective width of a compression element is summarised here:

Internal compression elements:

$$\begin{aligned} \bar{\lambda}_p \leq 0.673 & \quad \rho = 1.0 \\ \bar{\lambda}_p > 0.673 & \quad \rho = \frac{\bar{\lambda}_p - 0.055(3 + \psi)}{\bar{\lambda}_p^2} \leq 1, \text{ where } (3 + \psi) \geq 0 \end{aligned} \quad (4.18)$$

Out-stand compression elements:

$$\begin{aligned} \bar{\lambda}_p \leq 0.748 & \quad \rho = 1 \\ \bar{\lambda}_p > 0.748 & \quad \rho = \frac{\bar{\lambda}_p - 0.188}{\bar{\lambda}_p^2} \leq 1 \end{aligned} \quad (4.19)$$

$$\begin{aligned} \bar{\lambda}_p &= \sqrt{\frac{f_y}{\sigma_{cr}}} = \frac{\bar{b}_i / t}{28.4 \varepsilon \sqrt{k_\sigma}} \\ \varepsilon &= \sqrt{\frac{235}{f_y}} \end{aligned} \quad (4.20)$$

where k_σ is buckling factor corresponding to the stress ratio ψ and boundary conditions

ρ is the reduction factor

\bar{b}_i is notional flat width of a plane element

f_y is the basic yield strength

σ_{cr} is the elastic critical plate buckling stress

The effective widths of compression element under different stress conditions are summarised in the Table 4.1 and Table 4.2.

Table 4.1: Internal compression elements

Stress distribution (compression positive)			Effective ^p width b_{eff}			
			$\psi = 1$: $b_{eff} = \rho \bar{b}$ $b_{e1} = 0.5 b_{eff}$ $b_{e2} = 0.5 b_{eff}$			
			$1 > \psi > 0$: $b_{eff} = \rho \bar{b}$ $b_{e1} = \frac{2}{5 - \psi} b_{eff}$ $b_{e2} = b_{eff} - b_{e1}$			
			$\psi < 0$: $b_{eff} = \rho b_c = \rho \bar{b} / (1 - \psi)$ $b_{e1} = 0.4 b_{eff}$ $b_{e2} = 0.6 b_{eff}$			
$\psi = \sigma_2 / \sigma_1$	1	$1 > \psi > 0$	0	$0 > \psi > -1$	-1	$-1 > \psi > -3$
Buckling factor k_c	4.0	$8.2 / (1.05 + \psi)$	7.81	$7.81 - 6.29\psi + 9.78\psi^2$	23.9	$5.98 (1 - \psi)^2$

Table 4.2: Out-stand compression elements

Stress distribution (compression positive)			Effective ^p width b_{eff}		
			$1 > \psi > 0$: $b_{eff} = \rho c$		
			$\psi < 0$: $b_{eff} = \rho b_c = \rho c / (1 - \psi)$		
$\psi = \sigma_2 / \sigma_1$	1	0	-1	$1 \geq \psi \geq -3$	
Buckling factor k_c	0.43	0.57	0.85	$0.57 - 0.21\psi + 0.07\psi^2$	
			$1 > \psi > 0$: $b_{eff} = \rho c$		
			$\psi < 0$: $b_{eff} = \rho b_c = \rho c / (1 - \psi)$		
$\psi = \sigma_2 / \sigma_1$	1	$1 > \psi > 0$	0	$0 > \psi > -1$	-1
Buckling factor k_c	0.43	$0.578 / (\psi + 0.34)$	1.70	$1.7 - 5\psi + 17.1\psi^2$	23.8

4.3.2 Distortional buckling

4.3.2.1 Hancock's model

Distortional buckling of flexural members such as C channel and Z sections usually involves rotation of only the compression flange and lip about the flange-web junction. The web undergoes flexure at the same half-wavelength as the flange buckle, and the compression flange may translate in a direction normal to the web, also at the same half-wavelength as the flange and web buckling deformations. The web buckle involves double curvature transverse bending.

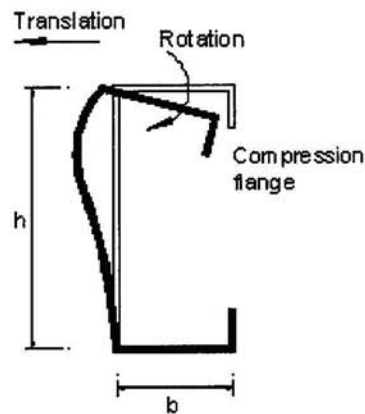


Fig. 4.2: Distortional buckling mode of flexural members.

Analytical expressions for the distortional buckling of thin-walled beams of general section geometry under a constant bending moment about the major axis had been developed by Hancock (1995). These analytical expressions were based on the simple flange buckling model, with an improvement proposed by Davies and Jiang (1996) in which the flange was again treated as a compression member with both rotational and translational spring restraints in the longitudinal direction. The rotational spring stiffness k_ϕ and the translational spring stiffness k_x represent the torsional restraint and translational restraint from the web respectively. In this analysis, Hancock

assumes the translational spring stiffness k_x to be zero so that the flange is free to translate in direction perpendicular to web plane. This gives a conservative prediction for the buckling load.

Detailed explicit expressions for the determination of the distortional buckling strength of flexural members have been presented in the literature review, and are thus not discussed further here.

4.3.2.2 Direct strength method

Schafer and Pekoz (1998) proposed a new approach that works only with gross properties of a member, and can take into account not only the interaction between local and global buckling but also the interaction between distortional and global buckling.

The Direct Strength Method (DSM) employs strength curves for an entire section to predict the load carrying capacity. The strength curves were initiated from the Winter's curve and have been modified by a number of experimental results on cold-formed steel structural members. The current provisions (AISI) for the distortional buckling of beams give the nominal flexural strength M_{nd} as:

$$M_{nd} / M_y = \begin{cases} 1 & \sqrt{M_y / M_{crd}} \leq 0.673 \\ [1 - 0.22(\frac{M_{crd}}{M_y})^{0.5}](\frac{M_{crd}}{M_y})^{0.5} & \sqrt{M_y / M_{crd}} > 0.673 \end{cases} \quad (4.21)$$

where M_{crd} is the critical elastic distortional buckling moment. M_{crd} can be obtained by using finite element analysis or finite strip analysis (ABAQUS, ANSYS and CUFSM). Modelling and simulation by such computational method is often too complicated for the practitioner to use effectively. For this reason, Schafer and Pekoz proposed closed form expressions as Eq 4.22 to Eq 4.24 giving the elastic distortional buckling. Yu (2005) simplified the closed form expressions, and proposed empirical expressions which are more applicable to C and Z sections with simple lip edge stiffeners.

Analytical model for distortional buckling of cold-formed steel members

For design purposes, closed-form solutions for elastic buckling moment are often desired.



Fig. 4.3: Analytical model for flange (Yu 2005)

Since distortional buckling mainly involves the rotation of the flange, the distortional buckling of an entire section can be obtained by considering the lateral-torsional buckling of the compression flange. As shown Fig. 4.3, the flange is modelled as an undistorted column with springs along one edge. The three springs represent the effect of the web. By considering equilibrium of forces in the x and y direction and

equilibrium of the moments about the shear centre axis, the governing differential equations are:

$$EI_{yf} \frac{d^4 u}{dz^4} + EI_{xyf} \frac{d^4 v}{dz^4} + P \left(\frac{d^2 u}{dz^2} + y_o \frac{d^2 \phi}{dz^2} \right) + k_{yf} \left(u + (y_o - h_y) \phi \right) = 0 \quad (4.22)$$

$$EI_{yf} \frac{d^4 v}{dz^4} + EI_{xyf} \frac{d^4 u}{dz^4} + P \left(\frac{d^2 v}{dz^2} + x_o \frac{d^2 \phi}{dz^2} \right) + k_{yf} \left(v + (x_o - h_x) \phi \right) = 0 \quad (4.23)$$

$$EC_{wf} \frac{d^4 \phi}{dz^4} - \left(GJ_f - \frac{I_{of}}{A_f} P \right) \frac{d^2 \phi}{dz^2} - P \left(x_o \frac{d^2 v}{dz^2} - y_o \frac{d^2 u}{dz^2} \right) + k_{yf} \left(u + (y_o - h_y) \phi \right) (y_o - h_y) - k_{yf} \left(v - (x_o - h_x) \phi \right) (x_o - h_x) + k_{\phi f} \phi = 0 \quad (4.24)$$

where I_{of} , I_{xf} , I_{yf} , I_{xyf} , C_{wf} , J_f and A_f are section properties of the flange, k_{yf} , k_{yf} , and $k_{\phi f}$ are the springs stiffness, x_o and y_o are the distances from the centroid to the shear centre, h_x and h_y are the distances from the centroid to the springs. The geometrical flange properties for C and Z sections are determined from Table 4.3.

Table 4.3: Geometrical flange properties for C and Z-section (Schafer, 1997).



Illustration removed for copyright restrictions

This flange model has been applied successfully by Lau and Hancock (1987) for compression members, Hancock (1995) for flexural members, Schafer and Pekoz (1999) for flexural members, and Schafer (2001) for compression members. The work by Schafer and Pekoz proposed an explicit treatment of the role of the elastic and geometric rotational stiffness at the web-flange junction and the method can account for the cases where the buckling is initiated by web instability. The elastic distortional buckling solutions of Schafer and Pekoz (1999) are summarised here:

The elastic distortional buckling stress f_d is:

$$f_d = \frac{k_{\phi_e} + k_{\phi_{ve}}}{k_{\phi_g} + k_{\phi_{vg}}} \quad (4.25)$$

where the flange rotational stiffness is:

$$k_{\phi fe} = \left(\frac{\pi}{L}\right)^4 \left(EI_{xf} (x_o - h_x)^2 + EC_{wf} - E \frac{I_{xyf}^2}{I_{yf}} (x_o - h_x)^2 \right) + \left(\frac{\pi}{L}\right)^2 GJ_f \quad (4.26)$$

$$\overline{k_{\phi fg}} = \left(\frac{\pi}{L}\right)^2 \left(A_f (x_o - h_x)^2 \left(\frac{I_{xyf}}{I_{yf}}\right)^2 - 2y_o (x_o - h_x) \left(\frac{I_{xyf}}{I_{yf}}\right) + h_x^2 + y_o^2 \right) + I_{xf} + I_{yf} \quad (4.27)$$

And the web rotational stiffness is:

$$k_{\phi ve} = \frac{Et^3}{12(1-\nu^2)} \left(\frac{3}{h} + \left(\frac{\pi}{L}\right)^2 \frac{19h}{60} + \left(\frac{\pi}{L}\right)^4 \frac{h^3}{240} \right) \quad (4.28)$$

$$\overline{k_{\phi vg}} = \frac{ht\pi^2}{13440} \left(\frac{45360(1-\xi_{web}) + 62160\left(\frac{L}{h}\right)^2 + 448\pi^2 + \left(\frac{h}{L}\right)^2 (53 + 3(1-\xi_{web}))\pi^4}{\pi^4 + 28\pi^2\left(\frac{L}{h}\right)^2 + 420\left(\frac{L}{h}\right)^4} \right) \quad (4.29)$$

where, L is defined as the minimum of the critical distortional buckling length L_{cr} .

ξ_{web} is stress gradient in the web defined as $(f_1 - f_2)/f_1$ in which f_1 and f_2 are the stresses at the opposite ends of the web. The critical buckling lengths L_{cr} can be determined by minimising the elastic buckling stress f_d with respect to the L . The general solution for L_{cr} is:

$$L_{cr} = \left(\frac{4\pi^4 h(1-\nu^2)}{t^3} \left(I_{xf} (x_o - h_x)^2 + C_{wf} - \frac{I_{xyf}^2}{I_{yf}} (x_o - h_x)^2 \right) + \frac{\pi^4 h^4}{720} \right)^{1/4} \quad (4.30)$$

The closed-form solutions for the buckling stress f_d and critical buckling length L_{cr} were previously proposed and verified, but the expressions are still complicated. Therefore, simple empirical expressions are proposed herein, applicable for C and Z-sections with simple lip edge stiffeners within the following dimensional limits:

$$50 \leq h_o/t \leq 200; 25 \leq b_o/t \leq 100; 6.25 < D/t < 50$$

$$45 \text{ deg} \leq \theta < 90; 2 \leq h_o/b_o \leq 8; 0.04 \leq D \sin(\theta)/b_o \leq 0.5$$

where h_o is out-to-out dimension of web;

b_o is out-to-out dimension of the flange;

D and θ are defined as in the Fig.4.4;

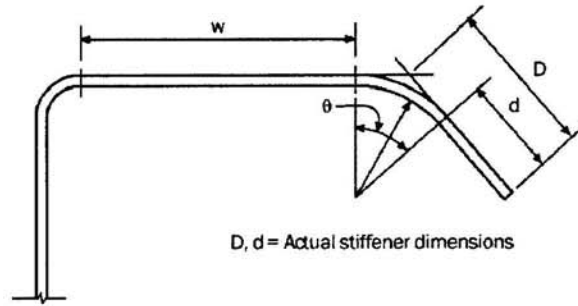


Fig.4.4: Element with simple lip edge stiffener.

The proposed simple expressions are:

$$f_d = \alpha \cdot k_d \frac{\pi^2 E}{12(1-\nu^2)} \left(\frac{t}{b_o} \right)^2 \quad (4.31)$$

$$k_d = 0.5 \leq 0.6 \left(\frac{b_o D \sin \theta}{h_o t} \right)^{0.7} \leq 8 \quad (4.32)$$

where α accounts for bracing as follow:

$$\text{if } L_m \geq L_{cr}, \alpha = 1$$

$$\text{if } L_m < L_{cr}, \alpha = \left(\frac{L_m}{L_{cr}} \right)^{\ln \left(\frac{L_m}{L_{cr}} \right)} \quad (4.33)$$

Where L_m is the distance between restraints which restrict distortional buckling and

L_{cr} is critical distortional buckling wave-length given by

$$L_{cr} = 1.2h_o \left(\frac{b_o D \sin \theta}{h_o t} \right)^{0.6} \leq 10h_o \quad (4.34)$$

The simplified provisions have been verified by Yu (2005) by way of an extensive parametric study using 7251 different geometries for C and Z section (Yu, 2005). The results show that the simple expression of Eq 4.32 give a lower bound approximation solutions as shown in Fig 4.5. Hence, the simple empirical expressions will be used in the optimisation programme to determine the load capacity of the section against failure by the distortional buckling mode failure.



Fig. 4.5: Development of simple expression for distortional buckling k_d of C and Z- section based on closed-form solution (Yu, 2005).

For the case where the member is subjected to a moment gradient, the closed-form solution can be modified by multiplying by a factor β , to take into account the moment gradient effect. The modified formulae are:

$$f_d = \beta \frac{k_{\phi e} + k_{\phi w e}}{k_{\phi g} + k_{\phi w g}} \quad (4.35)$$

$$f_d = \alpha \beta k_d \frac{\pi^2 E}{12(1-\nu^2)} \left(\frac{t}{b_o} \right)^2 \quad (4.36)$$

where $\beta = 1.0 \leq 1 + 0.4(L_d / L_m)^{0.7} (1 - M_1 / M_2)^{0.7} \leq 1.3$

$$|M_2| > |M_1|$$

M_1 / M_2 is positive for single curvature;

where, M_2 and M_1 are the largest moment at the distance between restraints that do restrict distortional buckling.

In case of partial restraint by a panel, the closed form solution for distortional buckling can be modified to be:

$$f_d = \beta \frac{k_{\phi e} + k_{\phi ve} + k_p}{k_{\phi g} + k_{\phi vg}} \quad (4.37)$$

where k_p is the elastic rotational stiffness provided by the panel.

Because the optimisation analysis does not consider attached panel case, hence then expression for k_p is not presented now.

4.3.2.3 Distortional buckling based on EN 1993-1-3:2006

Distortional buckling for elements with edge or intermediate stiffener is described in Cl.5.5.3 of EN 1993-1-3:2006. The design of compression elements with edge or intermediate stiffener should be based on the assumption that the stiffener behaves as a compression member with continuous partial restraint, with a spring stiffness that depends on the boundary conditions and the flexural stiffness of adjacent plane

elements. The spring stiffness of the stiffener should be determined by applying a unit load per unit length u as illustrated in Fig. 4.6.

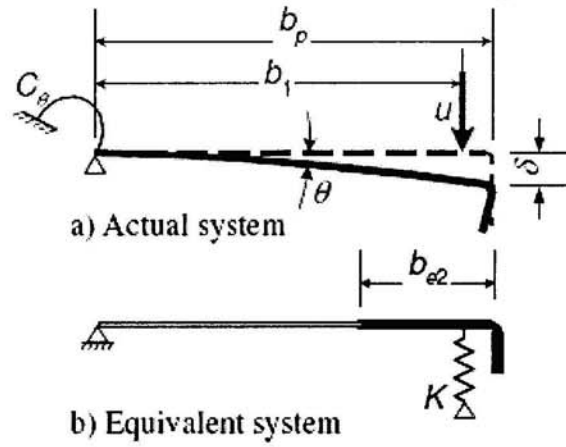


Fig. 4.6: Determination of spring stiffness.

The spring stiffness K per unit length may be determined from:

$$K = u / \delta \quad (4.38)$$

where δ is the deflection of the stiffener due to the unit load u acting in the centroid of the effective area of the edge stiffener of flange.

In the case of the edge stiffener of a lipped C section and a lipped Z section, the spring stiffness K of the compression flange is given by:

$$K = \frac{Et^3}{4(1-\nu^2)} \cdot \frac{1}{b_1^2 h + b_1^3} \quad (4.39)$$

where b_1 is the distance from the web to flange junction to the centre of gravity of the effective area of the edge stiffener of flange, and h is the depth of the web.

The reduction factor χ_d for determining the distortional buckling resistance should be

obtained from the relative slenderness $\bar{\lambda}_d$ given from:

$$\begin{aligned}
\chi_d &= 1 && \text{if } \bar{\lambda}_d \leq 0.65 \\
\chi_d &= 1.47 - 0.723\bar{\lambda}_d && \text{if } 0.65 < \bar{\lambda}_d \leq 1.38 \\
\chi_d &= \frac{0.66}{\bar{\lambda}_d} && \text{if } \bar{\lambda}_d \geq 1.38
\end{aligned} \tag{4.40}$$

$$\bar{\lambda}_d = \sqrt{f_y / \sigma_{cr,s}}$$

where $\sigma_{cr,s}$ is the elastic critical stress of the stiffener calculated by Eq 4.41 .

The general procedure to calculate the effective properties of the compression flange and lip taking into account distortional buckling has the following three steps :

Step 1:

Obtain an initial effective cross section for stiffeners, using effective widths of flange determined by assuming that the compression flange is doubly supported, the edge stiffener lip gives full restraint ($K = \infty$) and the design strength is not reduced (f_{yb}).

The initial values of the effective widths of flange (b_{e1}, b_{e2}) should be determined from Cl.5.5.2 in EN 1993-1-5:2006. The initial value of an effective lip depth is calculated from Cl.5.5.3.2 in EN 1993-1-3:2006.

Step 2:

Use the initial effective cross section of the stiffener to determine the reduction factor for distortional buckling. The elastic critical buckling stress $\sigma_{cr,s}$ for an edge stiffener should be obtained from:

$$\sigma_{cr,s} = \frac{2\sqrt{K.E.I_s}}{A_s} \tag{4.41}$$

where I_s is the effective second moment of area of the stiffener, taken as that of its effective area A_s about the centroidal axis of its effective cross section.

Step 3:

Optionally repeat step 1 by calculating the effective width with a reduced compressive stress $\sigma_{com,Ed} = \chi_d \cdot f_{yb} / \gamma_{M0}$ with χ_d from previous iteration, continuing until χ_d converge. Adopt an effective cross section with b_{e2}, c_{eff} and reduced thickness t_{red} corresponding to $\chi_{d,n}$

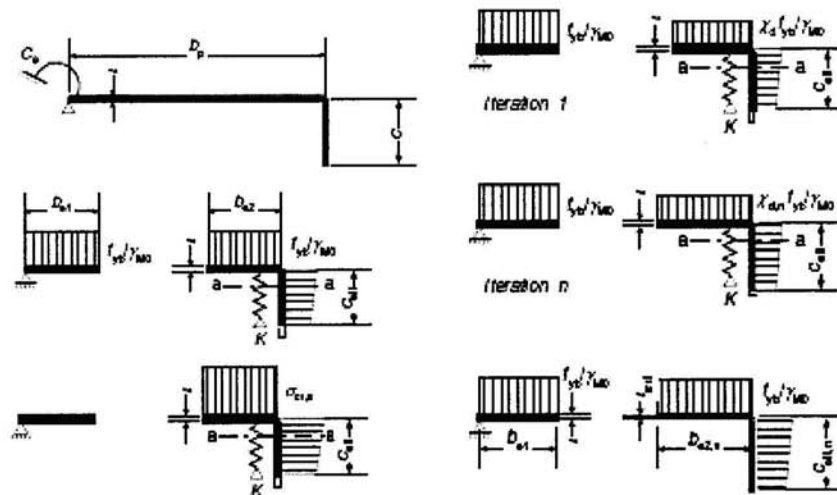


Fig. 4.7: Compression resistance of a flange with an edge stiffener (Fig 5.8 in EN 1993-1-3:2006).

4.3.3 Lateral-torsional buckling

In the design of cold-formed steel flexural members, when the load is applied in the plane of the web, the members may twist and deflect laterally, as well as vertically, if braces are not adequately provided. In design the moment capacity is not only ruled by the section strength of the cross section but is also limited by the lateral buckling strength of the member. This sub-section presents the current methods to design cold-formed steel flexural members which will be discussed and used as the constraints in the optimisation programme.

4.3.3.1 Lateral-torsional buckling based on BS 5950-5:1998

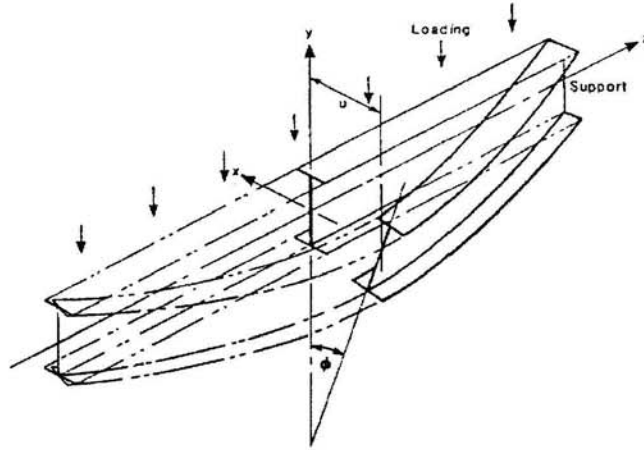


Fig. 4.8: Deformation of lateral-torsional buckling.

The buckling moment resistance of flexural members M_b is calculated as follows:

$$M_b = \frac{M_E M_Y}{\phi_B + \sqrt{\phi_B^2 - M_E M_Y}} \quad (4.42)$$

$$\phi_B = \frac{M_y + (1 + \eta)M_E}{2} \quad (4.43)$$

where M_c is the moment capacity of the section.

M_y is the yield moment of the section, that is the product of the design strength p_y and the elastic section modulus of the gross cross-section with respect to the compression flange Z_c .

M_E is the elastic lateral-torsional buckling moment resistance.

η is the Perry coefficient which is determined as followings

$$\text{When } L_E / r_y < 40C_b \quad \eta = 0$$

$$\text{When } L_E / r_y > 40C_b \quad \eta = 0.002 \left(\frac{L_E}{r_y} - 40C_b \right)$$

where L_e is the effective length in accordance with Cl.5.6.3 in BS 5950-5:1998. r_y is the radius of gyration of the section about the y axis. C_b is a coefficient which may be conservatively assumed to be unity, or can be calculated using $C_b = 1.75 - 1.05\beta + 0.3\beta^2 \leq 2.3$. β is the ratio of the smaller end moment to the larger end moment, M , in the un-braced length of a beam. β is taken as positive in the case of single curvature bending and negative in the case of double curvature bending. The bending curves are shown in Fig. 4.9. When the bending moment at any point within the span is greater than M , C_b should be taken as unity.

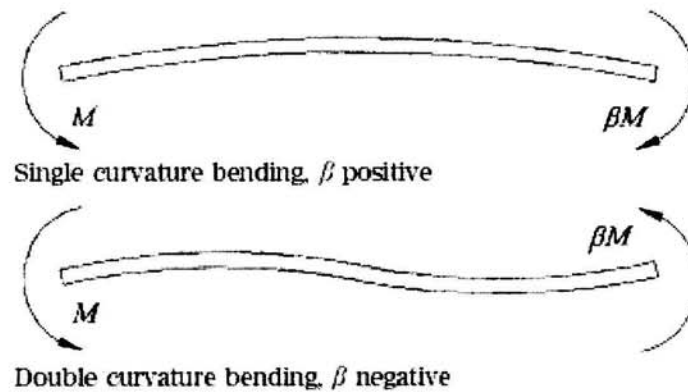


Fig. 4.9: Single and double curvature bending.

When the buckling moment resistance M_b exceeds M_c , the ultimate moment should be taken as M_c .

For the channel section which is torsionally restrained at the end support points, it may be considered to be loaded through the shear centre. The elastic lateral-torsional buckling moment resistance M_E can be determined from clause 5.6.2.2 in BS 5950-5:1998:

$$M_E = \frac{\pi^2 AEh_o}{2(L_E/r_y)^2} C_b \left\{ 1 + \frac{1}{20} \left(\frac{L_E t}{r_y h_o} \right)^2 \right\}^{\frac{1}{2}} \quad (4.44)$$

For Z-section beams which are bent in the plane of the web:

$$M_E = \frac{\pi^2 AEh_o}{4(L_E/r_y)^2} C_b \left\{ 1 + \frac{1}{20} \left(\frac{L_E t}{r_y h_o} \right)^2 \right\}^{\frac{1}{2}} \quad (4.45)$$

4.3.3.2 Lateral-torsional buckling based on AISI specification

For the laterally un-braced segment of singly and/or doubly symmetric sections in which the compression flange is laterally braced by the sheeting steel, subject to lateral buckling M_n shall be determined as follows:

$$M_n = S_e \frac{M_c}{S_f} \quad (4.46)$$

where S_f is the elastic section modulus of the full section for the extreme compression fibre; S_e is the elastic section modulus of the effective section calculated at a stress M_c / S_f in the extreme compression fibre;

M_c is the critical moment calculated according to:

For $M_e > 0.5M_y$

$$M_c = M_y \left(1 - \frac{M_y}{4M_e} \right) \quad (4.47)$$

For $M_e \leq 0.5M_y$

$$M_c = M_e \quad (4.48)$$

where M_y is the moment causing initial yield at the extreme compression fibre of the full section;

$$M_y = S_f \cdot F_y \quad (4.49)$$

M_e is the elastic critical moment computed from:

$$M_e = C_b r_o \sqrt{\sigma_{ey} \sigma_t} \quad (4.50)$$

$$\sigma_{ey} = \frac{\pi^2 \cdot E}{(K_y L_y / r_y)^2} \quad (4.51)$$

$$\sigma_t = \frac{1}{A r_o^2} \left[G \cdot J + \frac{\pi^2 \cdot E \cdot C_w}{(K_t \cdot L_t)^2} \right] \quad (4.52)$$

where C_b is bending coefficient which can conservatively be taken as unity or calculated from:

$$C_b = 1.75 + 1.05 \left[\left(\frac{M_1}{M_2} \right) \right] + 0.3 \left[\left(\frac{M_1}{M_2} \right) \right]^2 \leq 2.3 \quad (4.53)$$

where M_1 is the smaller and M_2 the larger bending moment at the ends of un-braced length, taken about the strong axis of the member, and where M_1 / M_2 the ratio of end moments is positive when M_1 and M_2 have the same sign (reverse curvature bending) and negative when they are of opposite sign (single curvature bending). When the bending moment at any point within an un-braced length is larger than that at both

ends of this length, and for members subject to combined axial load and bending moment, C_b shall be taken as unity

r_o is polar radius of gyration of the cross section about the shear centre

$$r_o = \sqrt{r_x^2 + r_y^2 + x_o^2} \quad (4.54)$$

where r_x, r_y are radii of gyration of the cross section about the centroidal principal axes; K_x, K_y, K_t are effective length factors for bending about the x and y axes and for twisting; L_x, L_y, L_t are un-braced lengths of compression member for bending about the x and y axes and for twisting; x_o is distance from the shear centre to the centroid along the principal x-axis taken as negative.

4.3.3.3 Lateral-torsional buckling based on Li's model

Recently, Li (2004) developed an analytical model for predicting the lateral-torsional buckling of cold-formed C channel and Z purlins partially restrained by metal sheeting for both downward and upward loadings. The model is constructed for the practical case where the member is subjected to transverse loads and is restrained partial-laterally by sheeting and interval anti-sag bars. The focus is to investigate the influence of the restraints provided by the sheeting and by the interval anti-sag bars, and the variation of moment along the longitudinal axis on the lateral-torsional buckling behaviour resistance. In design specification such as BS 5950-5:1998, lateral-torsional buckling of cold-formed steel members is calculated based on the theory of unrestrained beam, the result of which is obviously conservative as it neglects the influence of sheeting restraints. In the analytical model of Li (2004), the

relations between the sheeting and the beam have been considered. As a result of that, the calculation of lateral-torsional buckling is improved and it illustrated the real behaviour of the structure. The explicit detail of this calculation was presented in the literature review.

4.3.4 Deflection constraint

In the design of flexural beams, with a given loading condition, the deflection of flexural members depends on the magnitude, location, and type of the applied load, the span length, and the elastic bending stiffness.

Similar to the bending strength calculation, the determination of the second moment I for calculating the deflection of steel beams is based on the effective areas of the compression flange and beam web, for which the effective widths are computed for the compressive stress developed from the bending. If the compression flange and the web of beam are fully effective, the second moment of the beam section is obviously based on the full section. In this case, the second moment is constant value along the entire beam length. Otherwise, if the second moment is based on the effective areas of the compression flange and the web of beam, the second moment may vary along the beam span because the bending moment usually varies along the beam length.

In design the method to be used for deflection calculation is based on the accuracy desired in the analysis. If more exact deflection is required, a computer programme or a numerical method such as finite element method may be used. The deflection calculation is too complicated for hand calculation. If an approximate analysis is used, such as assuming the full constant second moment determined for maximum bending moment, the deflection result is too conservative. Thus, some attempt must be made

to give consideration to both pre-buckling and post-buckling effects on deflection behaviour. The recommended deflection limitations for beams given in Cl.2.4.2 of BS 5950-5:1998 are chosen as being appropriate. In this study, we apply this concept in the deflection constraint for the optimisation programme of C channel, Z zed and sigma purlins. The detailed expressions of the calculation are described in sub-section 2.7 in Chapter 2.

The recommended deflection limitation for beam is limited to maximum of span/200. However, the limit of deflection should be specified by the designer.

4.3.5 Shear strength in web

For simply supported beam subjected to the uniformly distributed load, the shear force in the web at the supports is quite significant, as the section could fail in the event of an over shear stress in the web. According to BS 5950-5:1998, a separate calculation should be made for maximum and average stresses. The maximum shear stress is calculated based on the principle of an accepted method of elastic analysis, which should not be greater than $0.7p_y$, where here p_y is the for design strength. The average shear stress should not exceed the lesser of the shear yield strength p_v or the shear buckling strength q_{cr} , obtained as follows:

$$\begin{aligned}
 p_v &= 0.6p_y \\
 q_{cr} &= \left(\frac{1000t}{h_o} \right)^2 \quad N/mm^2
 \end{aligned}
 \tag{4.55}$$

The design strength value p_y is from Table 4 of BS 5950-5:1998

4.4 SUMMARY

The summary of constraints of the optimisation problem in cold-formed steel purlin which consists of strength, deflection and stability requirements, as well as the practical geometrical constraint of the design variables have been presented here. Structural designer can freely modify these constraints to suit the different design codes and the purpose of the client. The purpose of this chapter is to demonstrate the general constraints of the optimisation problem of C channel, Z zed and Σ sigma simply supported purlin subjected to uniformly distributed load. For more complicated shape sections and others loading condition, the constraints may be amended and revised accordingly.

Chapter 5

5 OPTIMISATION OF CHANNEL SECTION PURLINS

5.1 BEHAVIOUR OF SINGLE SPAN CHANNEL PURLIN

5.1.1 Introduction

Channel section are widely used as purlins or rails, the secondary member between main the structural frame and the outer cladding material, such as corrugated roof or wall sheeting, such as that used agricultural and industrial buildings. Generally, the purlin works as a simply supported beam subjected to uniformly distributed load. The loading, the span and the dimensions of cross-section are illustrated in Fig. 5.1. In Fig.5.1, b_o is the overall width of flange; c_o is the depth of lip; t is the thickness of cross-section, h_o is the overall height of cross-section and L is the span of purlin.

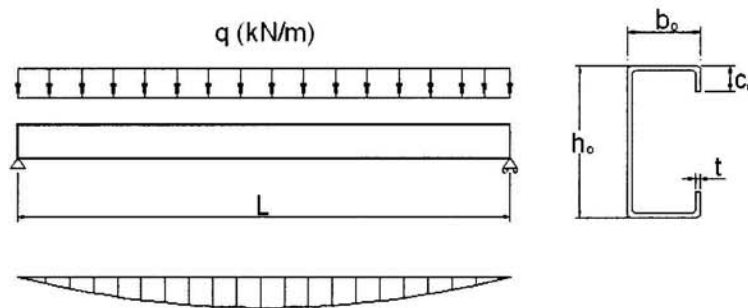


Fig. 5.1: Dimension and model analysis of single span channel purlin under vertical uniformly distributed load.

In this section, the effects of dimension changes on the effective section properties are investigated in order to obtain the first information to find the optimum section. The investigations are based on BS 5950-5:1998, EN 1993-1-3:2006, and AISI or AS4600.

The investigation is performed for section with b_o increased from 40 to 100mm, in 10mm increments. The depth of web, h_o , is also increased from 100 to 300mm, in 100mm increments. The thickness of section is assumed to vary from 1 to 3 mm in 0.1mm increments. The span of purlin is maintained at a constant value of 4 m. The yield strength is 350MPa with modulus of elasticity of 205GPa.

5.1.2 Effects of dimensions changes on the cross-sections local buckling resistance

In this part, the effects of dimension changes on local buckling resistance are investigated. The calculations are based on BS 5950-5:1998. In this thesis the specimen labelling is shown as h200-02 which illustrate h_o and the ratio c_o/b_o of 0.2.

Fig. 5.2 shows the comparison between local buckling moment resistance and yielding moment capacity of section which are presented in Chapter 4. As can be seen from Fig. 5.2, the yield moment resistance of section is always higher than that of the local buckling moment. The yield moment varies linearly with the increase of b_o , whereas the local buckling moment varies nonlinearly with the increase of the flange width. Fig. 5.2 shows that local buckling has a significant effect on the resistance of the channel section. Furthermore, the local buckling moment increases more rapidly for flange width from 40 to 65mm and less rapidly for b_o from 65 to 100mm. This is due to the fact that the effective width of a large flange is less than that of full flange width of small section. While effective width of flange of small section is equal or closes to the full width of flange. It indicates that local buckling tends to occur when the flange is reasonably large. We also found that b_o from 40 to 60mm local buckling

moment and yielding moment are very close. It proves that the local buckling occur rarely with small width of flange.

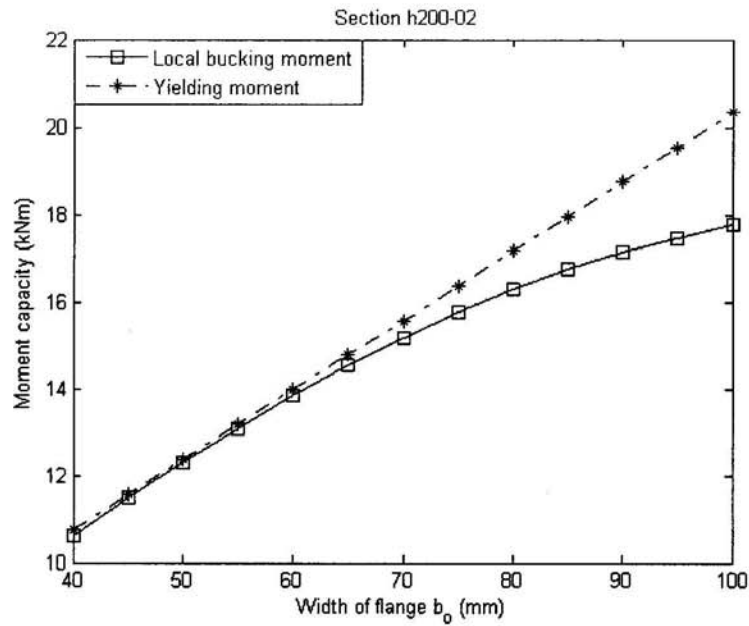


Fig. 5.2: Comparison between local buckling moment and yielding moment (BS 5950-5:1998).

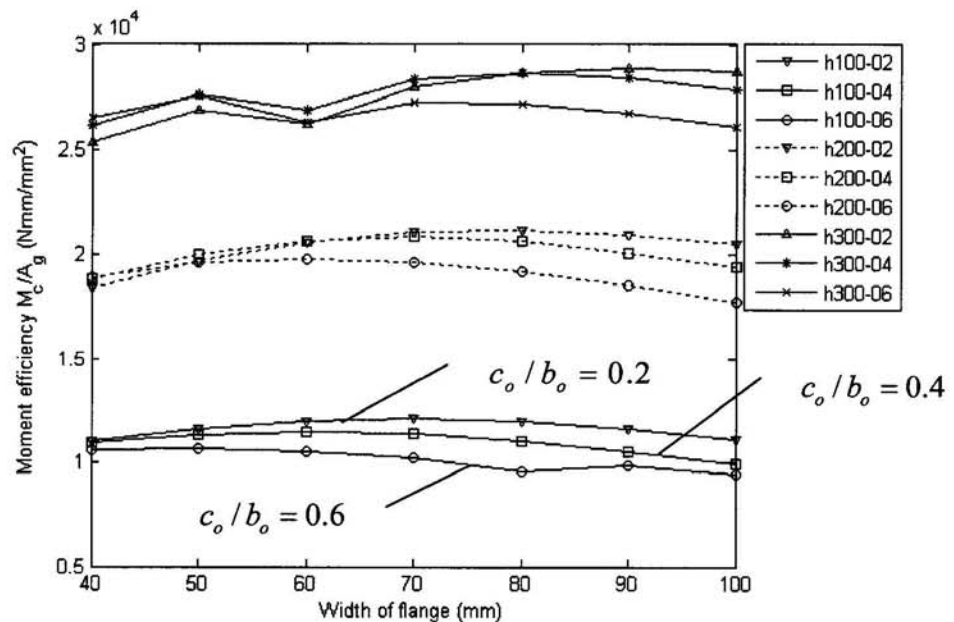


Fig. 5.3: Moment efficiency based on BS 5950-5:1998.

Fig. 5.3 shows the effects of dimension changes on the moment efficiency. This is defined as the ratio of the moment capacity to the gross area of cross section. As far as

the moment efficiency M_c / A_g is concerned, its value decreases when b_o is more than 80mm. Thus, the maximum value of moment efficiency does not correspond to the widest flange and the largest ratio c_o / b_o .

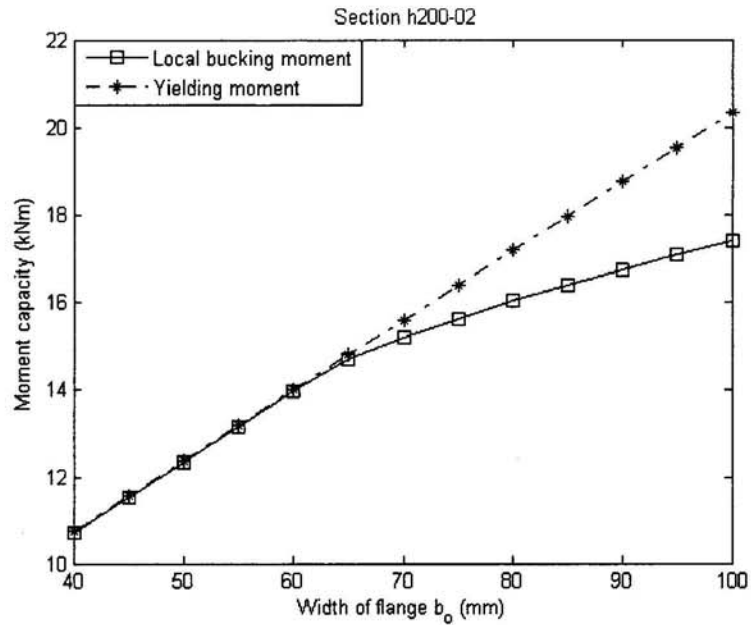


Fig. 5.4: Comparison between local buckling moment and yielding moment (EN 1993-1-3:2006).

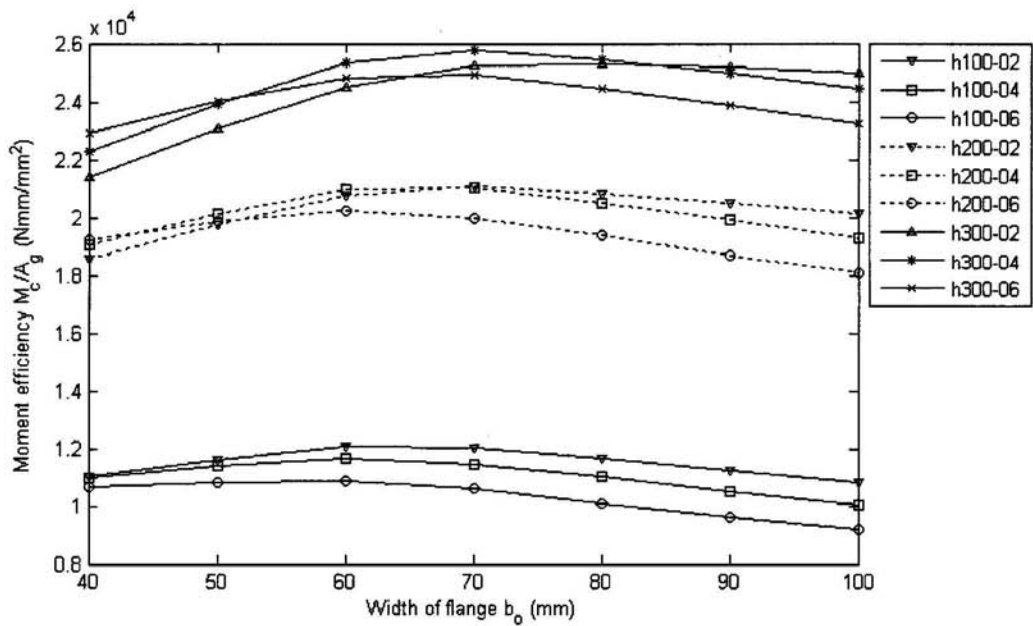


Fig. 5.5: Moment efficiency based on EN 1993-1-3:2006.

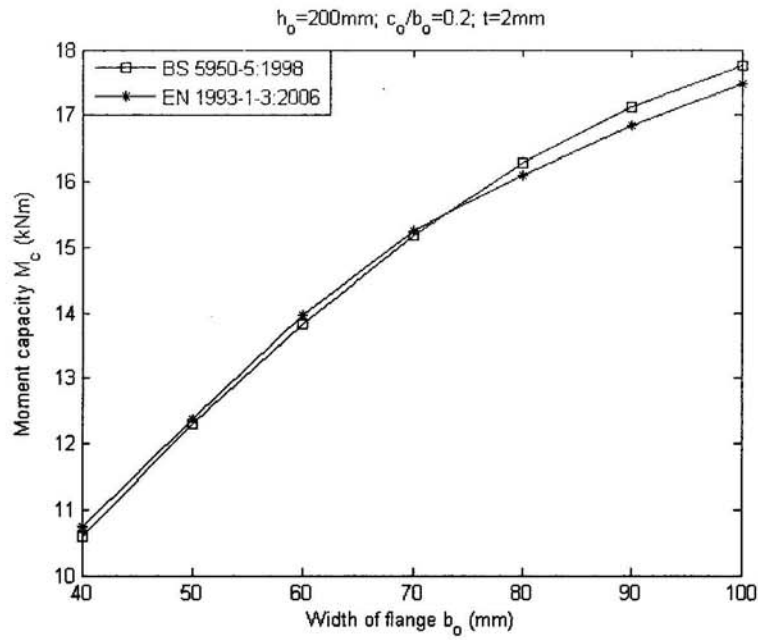


Fig. 5.6: Comparison of local buckling moment between BS 5950-5:1998 and EN 1993-1-3:2006 based on variation of flange width.

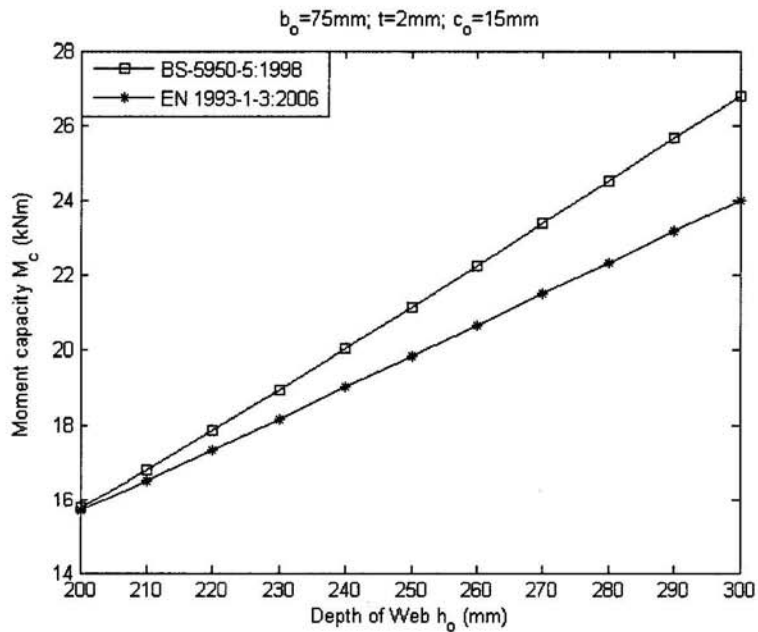


Fig. 5.7: Comparison of local buckling moment between BS 5950-5:1998 and EN 1993-1-3:2006 based on variation of web depth.

The same effect can be seen on the moment capacity calculated using the EN 1993-1-3:2006 shown in Fig. 5.4. When b_o is small enough, the flange is has a full effective

width, and local buckling does not occur. But when the width of flange is more than 65mm, local buckling of flange starts to occur. From Fig. 5.6, it is found that the local buckling moments calculated by BS 5950-5:1998 and EN 1993-1-3:2006 are very convergent. However, the moment capacity computed by EN 1993-1-3:2006 is always smaller than that by BS 5950-5:1998 when h_o varies, it can be seen clearly from Fig. 5.7. This is due to the fact that local buckling in the compression part of web is considered in EN 1993-1-3:2006, whilst there is a limiting compression stress p_o of the web in BS 5950-5:1998. This comparison demonstrates that local buckling calculated by EN 1993-1-3:2006 is more conservative than BS 5950-5:1998.

5.1.3 Effects of dimension changes on the lateral-torsional buckling based on BS 5950-5:1998

Fig. 5.8 gives plots to show the effects of dimension changes on the lateral-torsional buckling moment based on BS 5950-5:1998. As can be seen from Fig. 5.8, the increase of b_o leads to an increase of moment resistance of lateral-torsional buckling, because the minor second moment of area of the cross section is increased and the position of shear centre is shifted in vicinity of the centroid of the section. Similarly, the lateral-torsional buckling moment is improved significantly with an increase in the depth of lip. The lip will improve the torsional rigidity of the channel section, which is often very weak to torsion force. Thus, Fig. 5.8 illustrates the true behaviour of a channel section, the moment resistance increases as result of the increase of c_o . As can be seen also in Fig. 5.8, with the deep h_o , the lateral-torsional buckling moment resistance is greater than that of the section with shallow h_o due to the increase of th

yield moment of section which is a product of the yielding stress p_y and the elastic section modulus of the gross cross-section.

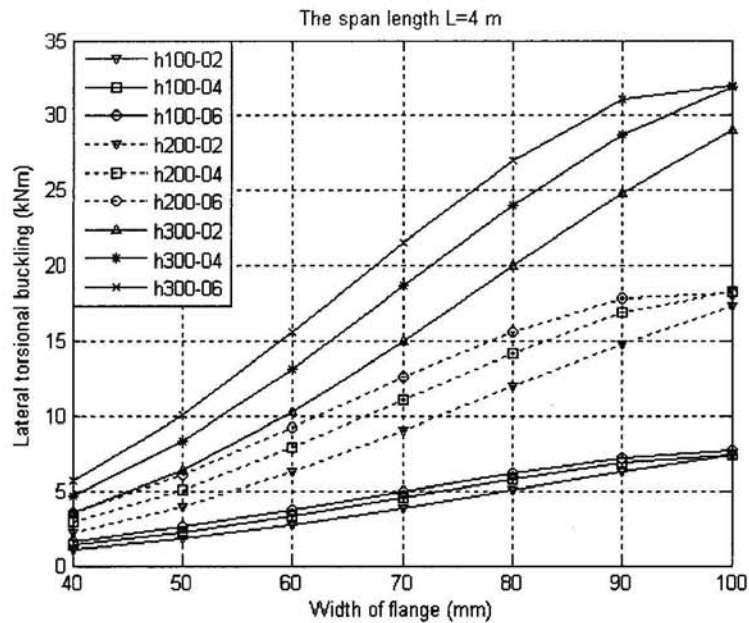


Fig. 5.8: Effects of the dimensions on the moment of lateral-torsional buckling based on BS 5950-5:1998.

5.1.4 Effects of the dimensions changes on deflection of the purlin based on BS 5950-5:1998

As can be seen from the plots in Fig. 5.9 that the moment resistance considering the deflection constraint increases with the increase of b_o , because of the full second moment of area of section increases. Similarly, with the increase of h_o , the moment resistance against deflection increases also. Observing the lowest group of three curves, when $h_o = 100\text{mm}$, the influence of c_o on the section capacity of deflection is insignificant. But for the deepest section with $h_o = 300\text{mm}$, we can see that the c_o does have a significant effect on the moment resistance. This is due to the fact that the full cross section is used in evaluating the second moment of area for the shallow section for example $h_o = 100\text{mm}$. Hence an increase of c_o does not help to increase the

capacity of section to resist deflection. However, in the deep section, the effective section may be used to calculate the second moment of area due to the local buckling. In such case, the depth of lip will improve significantly the cross sections capacity to resist deflection.

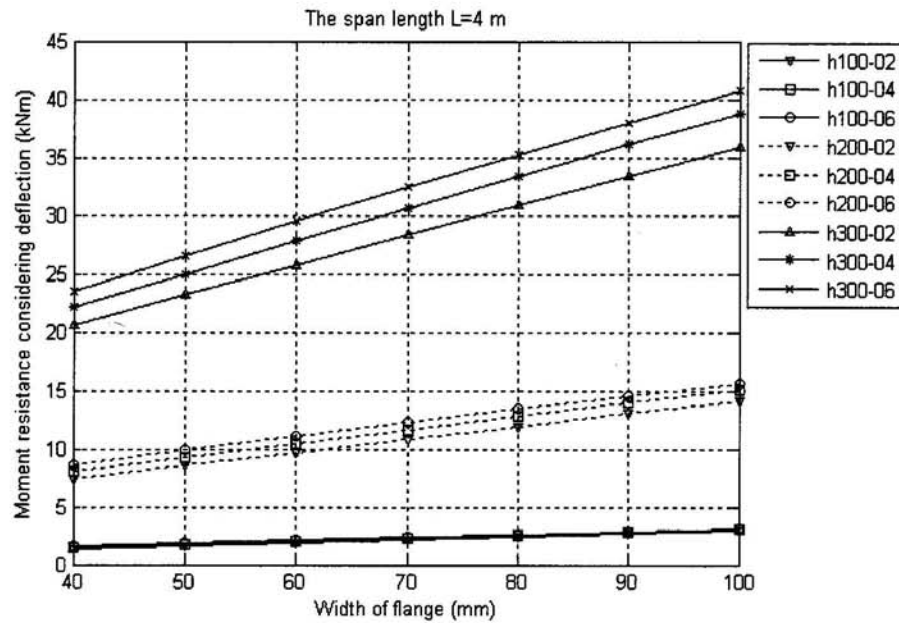


Fig. 5.9: Effects of the dimensions on moment resistance taking into account of deflection based on BS 5950-5:1998.

5.1.5 Investigation of the distortional buckling resistance of purlin

In BS 5950-5:1998 the purlin section is designed without considering the effect of distortional buckling. Currently, there are two efficient approaches for calculating distortional buckling of flexural members. The first approach is Hancock's method (1995) in which analytical expressions were based on the simple flange buckling model, the flange was treated as a compression member with rotational and translational spring restraints at junction between web and flange. The rotational spring stiffness k_ϕ and the translational spring stiffness k_x represent the torsional restraint and translational restraint from the web, respectively. Hancock assumes the

translational spring stiffness k_x to be zero. The second method by Schafer and Pekoz's (1999) is the direct strength method. It is a new approach which works with the gross properties of member and can take into account not only the interaction between local and global buckling but also the interaction between distortional buckling and global buckling.

The direct strength method employs the elastic distortional buckling moment which can be obtained by numerical methods such as finite element analysis or finite strip analysis (CUFSM, ABAQUS, and ANSYS). However, those methods are sometimes complicated or not practical for the designer. For this reason, Schafer and Pekoz proposed the expression for close form solutions of elastic distortional buckling. Recently, Cheng Yu (2005) simplified this expression and produced empirical expressions which are applicable for C and Z sections with lip edge stiffeners.

The comparison between the two methods is performed based on the calculation of the distortional buckling of the channel purlin with h_o of 200mm and the width of flange varying from 40 to 100mm, the thickness of 2mm in order to evaluate the efficiency and applicability of each approach in terms of design. Fig. 5.10 shows that the moment resistance of distortional buckling calculated by the direct strength method which is smaller than that by Hancock's analysis. Thus we will use the direct strength method to calculate distortional buckling in the optimisation programme of channel purlin, because the results are more conservative.

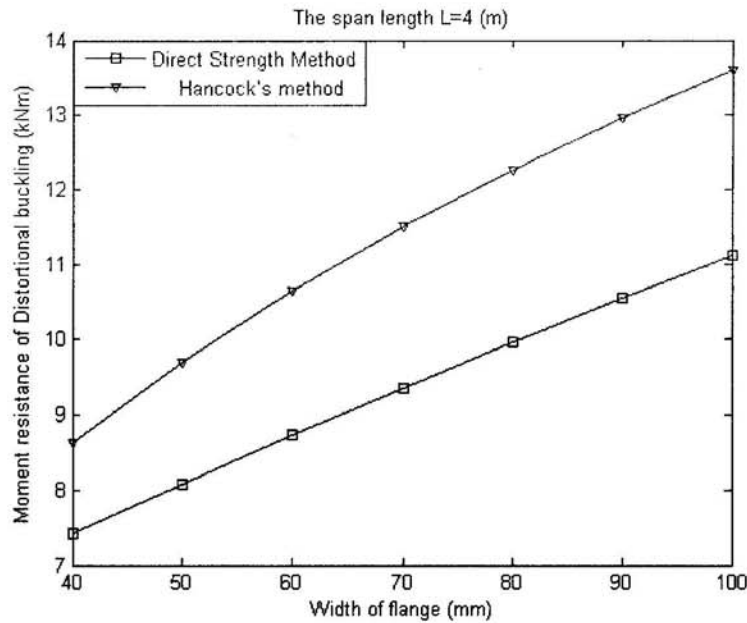


Fig. 5.10: Distortional buckling comparison.

5.1.6 Comparisons lateral-torsional buckling moment of resistance based on different calculation methods

Comparison is carried out for four different analyses with variation of dimensions and span length. First, we shall consider a simply supported channel purlin with a span length of 4m, which is restrained rotationally in all directions at the supports. The web depth is maintained at 200mm, the section thickness of 2 mm and ratio c_0/b_0 of 0.2. The width of flange varies from 40 to 100 mm. Fig. 5.11 shows that the moment resistance of lateral-torsional buckling increases with the increase of the width of flange in all four methods(BS 5950-5:1998 , Li's model and AISI, and AS4600 standard). Such increase is due to the increase of minor second moment of section. However, Fig. 5.11 illustrates that the results of Li's model are always higher than other methods, because Li's model computes lateral-torsional buckling taking into account the explicit gradient moment of members subjected to the uniform distributed load instead of using approximate bending coefficient C_b to consider the gradient

distributed moment of the simple beam or considering pure bending moment. AS4600 results are the most conservative due to the assumption that the section is subjected to a pure bending moment. Similarly with the variations of h_o , span length and c_o , the moment resistance calculated by Li's model is always higher than other methods. The plots for these comparisons are given in Fig. 5.12, Fig. 5.13 and Fig. 5.14. It shows that the Li's model illustrates more accurate behaviour of the channel purlin. However for practical design, we tend to use the more conservative result, because it inclines toward the safety.

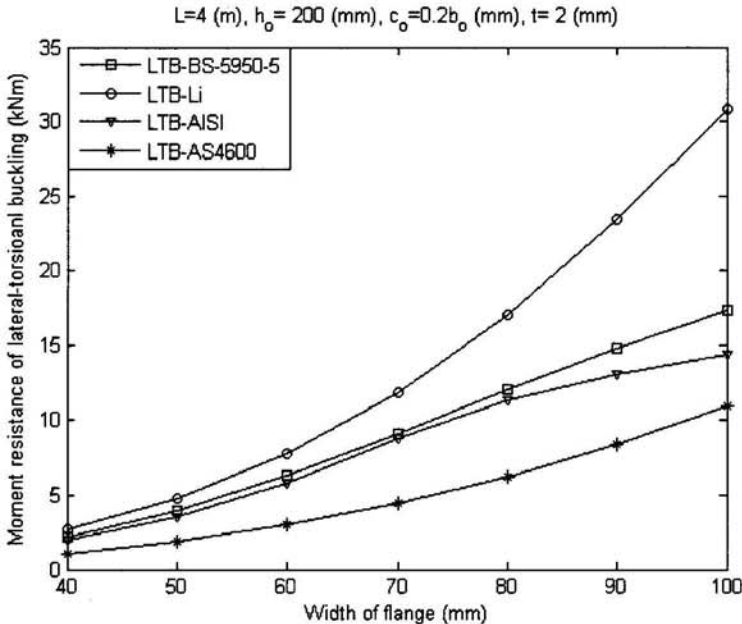


Fig. 5.11: Lateral-torsional buckling with the variation of the width of flange.

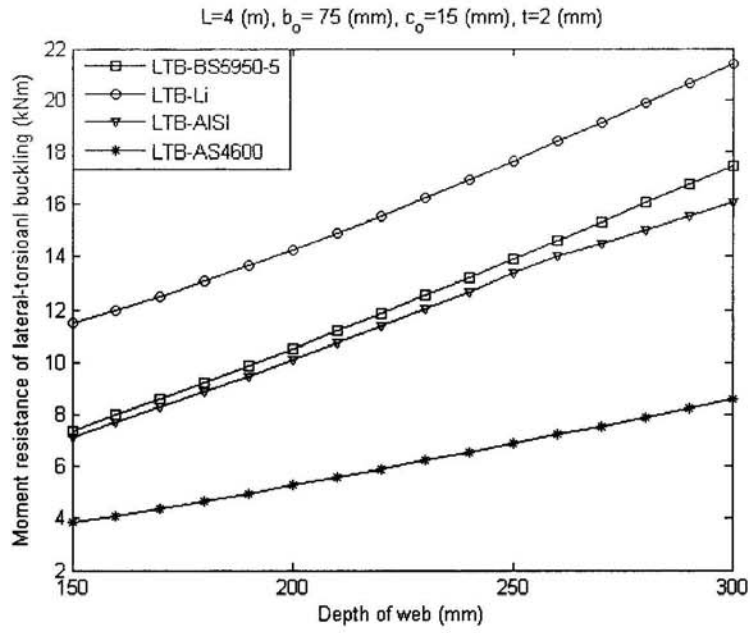


Fig. 5.12: Lateral-torsional buckling with the variation of the depth of web.

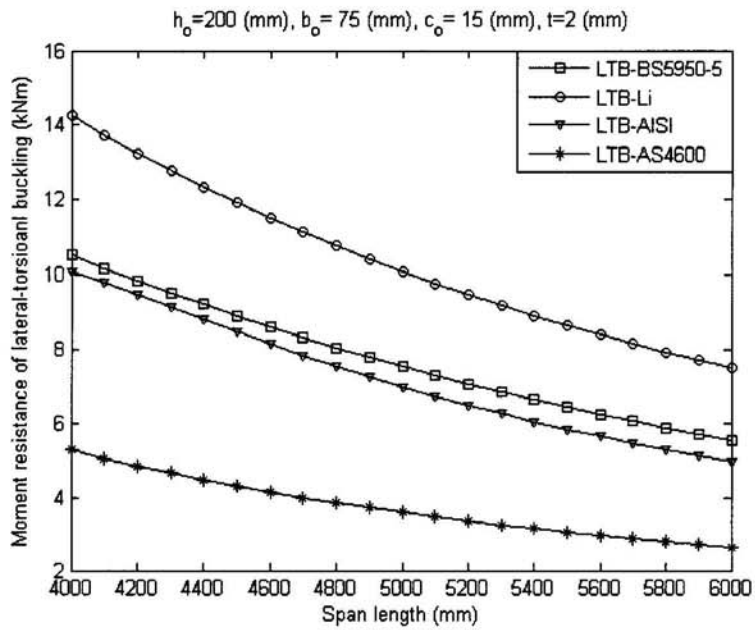


Fig. 5.13: Lateral-torsional buckling with the variation of the span length.

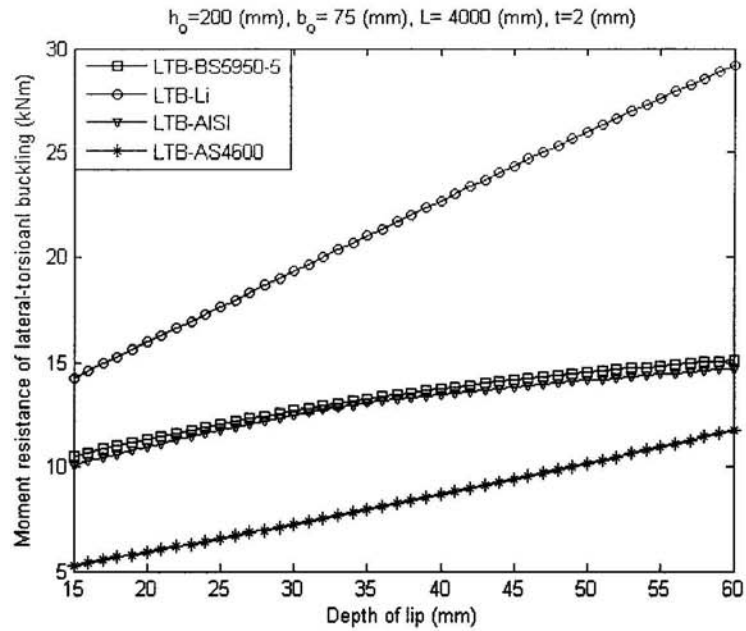


Fig. 5.14: Lateral-torsional buckling with the variation of the depth of lip.

5.2 OPTIMISATION PROCEDURE

5.2.1 Description of problems

For a given span length, the minimisation of weight of the beam is equivalent to minimisation of its cross-sectional area. Hence the objective function of the optimisation problem can be expressed as:

$$F(h_o, b_o, c_o, t) = h_o t + 2(b_o - t)t + 2(c_o - t)t \quad (5.1)$$

where h_o , b_o , c_o and t are the dimensions of cross section and so-called the design variables which are chosen to minimise the objective function F under some structural performance constraints and the geometric constraints of the design variables.

The structural performance constraints for cold-formed section beams generally include strength, deflection and stability requirement and the geometrical constraints; these have been discussed in Chapter 4.

5.2.2 Optimisation process in MATLAB programme

In this section, the dimensions of the channel purlins used in Section 5.1 are optimised by using the optimisation toolbox in MATLAB. The toolbox includes routines for many types of optimisation, including constrained nonlinear minimisation.

The cold-formed steel optimisation is the nonlinear optimisation problem with nonlinear constraints and multi-design variables such as the geometrical dimension constraints and the structural performance constraints. The procedure using the optimisation toolbox of MATLAB is introduced:

The called function for the optimisation problem is:

$$(x, Fval) = fmincon(F(x), x_o, A, b, A_{eq}, b_{eq}, L_b, U_b, Nonlcon) \quad (5.2)$$

where *fmincon* function attempts to find a constrained minimum of a scalar function of several variables starting at an initial population of design variables. This is generally referred to as constrained nonlinear optimisation or nonlinear programming; $F(x)$ is the objective function defined by Eq.(5.1); x_o is the initial population of the design variables; A , b and A_{eq} , b_{eq} are the parameters of the linear constraints, in our problem the constraint is a nonlinear functions, hence those parameters can be set to null; L_b and U_b are the lower and upper bounds of the design variables such as the overall depth of section, the overall width of flange, the depth of lip and the thickness of section; *Nonlcon* are nonlinear constraints of the problem including the geometrical constraints and the strength constraints; x and *Fval* are the optimum design variables and the optimum value of the objective function.

In the present study, the optimisation problem is solved using the trust-region method which is based on a standard optimisation algorithm built into MATLAB. The requirement for using this kind of optimisation tool is to create the objective function and constraints functions. The computational procedure of optimisation is summarised in the flowchart given in Fig. 5.15.

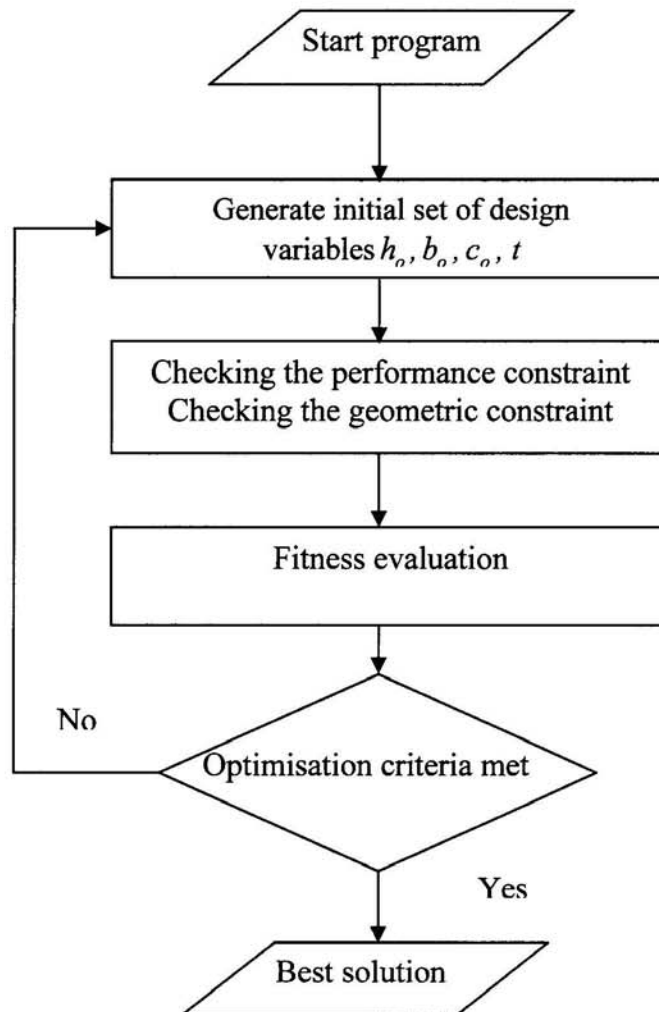


Fig. 5.15: The computational procedure of the optimisation programme.

5.3 SELECTION OF PARAMETERS

The optimisation is performed for simply supported channel beams subjected to a uniformly distributed load from 2kN/m to 4kN/m with span length between 3m and 6m. The modulus of elasticity and the yield strength of steel are taken as $E = 205 \text{ GPa}$ and $p_y = 350 \text{ MPa}$. The optimisation is carried out with different constraint conditions. Firstly, we perform the optimisation based on BS 5950-5:1998 in which the local buckling, lateral-torsional buckling and deflection constraints are considered. Secondly, due to the lack of the calculation of distortional buckling calculation in BS 5950-5:1998, we take consideration of the distortional buckling calculation in the optimisation problem.

5.4 NUMERICAL OPTIMISATION RESULTS

5.4.1 Optimisation result based on BS 5950-5:1998

The optimum dimensions h_o , b_o and c_o are given in Fig. 5.16 to 5.19 and that the minimum cross section area is given in Fig. 5.20. The optimum dimensions are read from graphical curve in accordance with specific span and loading value. For example with span $L=4500\text{mm}$ and $q=3\text{kN/m}$, the optimum dimensions are $h_o = 270\text{mm}$, $b_o = 84\text{mm}$, $c_o = 17.5\text{mm}$ and $t = 1.47\text{mm}$.

Fig. 5.16 shows that the wall thickness has a slight influence on the resistance of section. It is especially so for small load cases such as 2kN/m, although spans of the beam vary from 3m to 6m, the thickness of section just changes in the range of 1mm to 1.5mm. For higher loads, the wall thickness does not increase significantly. It

indicates that in terms of material saving, the thickness of section is not an important design factor.

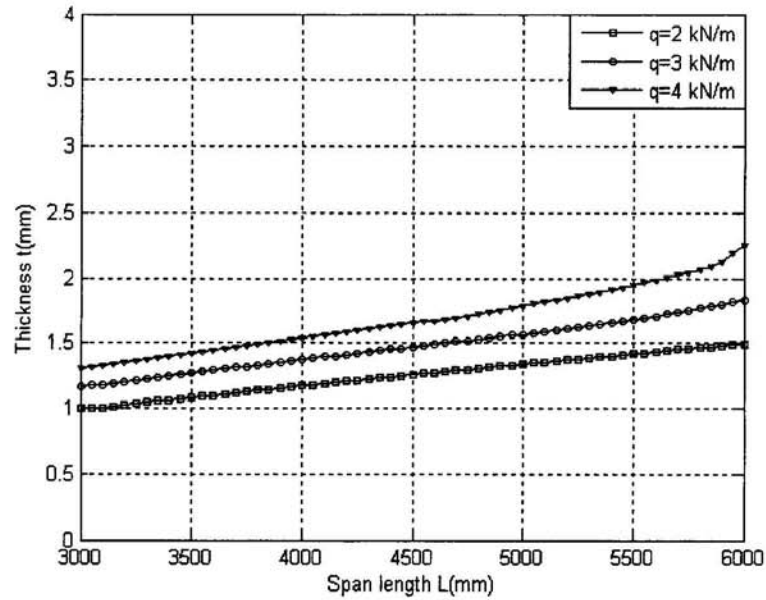


Fig. 5.16: Curves of optimum thickness over span length for un-braced channel beams based on BS 5950-5:1998.

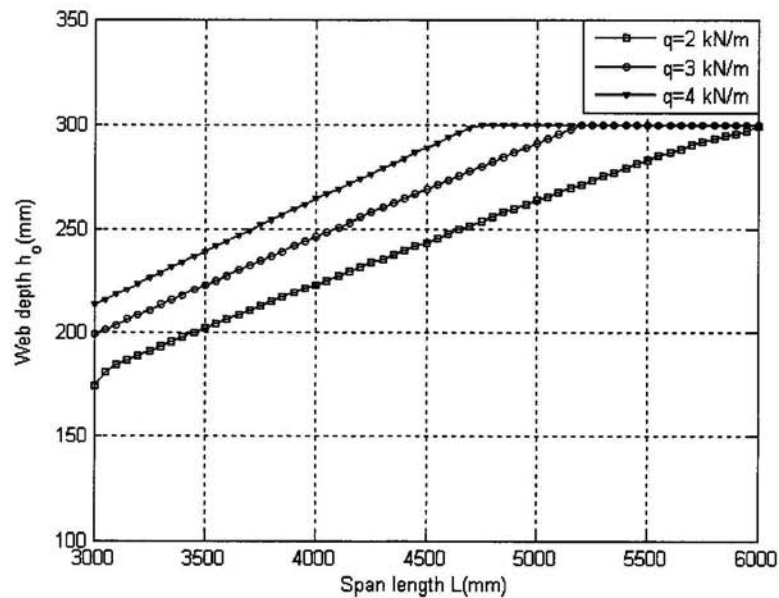


Fig. 5.17: Curves of optimum web depth over span length for un-braced channel beams based on BS 5950-5:1998.

From Fig. 5.17, we can see that h_o increases rapidly according to large load case, for instance, load case of 4kN/m, at 4.7m span length, h_o attains the maximum bound value of 300mm. Whereas for small load case such as 2kN/m, the depth of web increases gradually and slowly and reaches the maximum bound value at 6m span. It is due to the fact that for large load cases with unrestrained beams, the lateral-torsional buckling starts to control the capacity of section, so it evidently leads to an increase of h_o in order to improve the lateral-torsional buckling resistance.

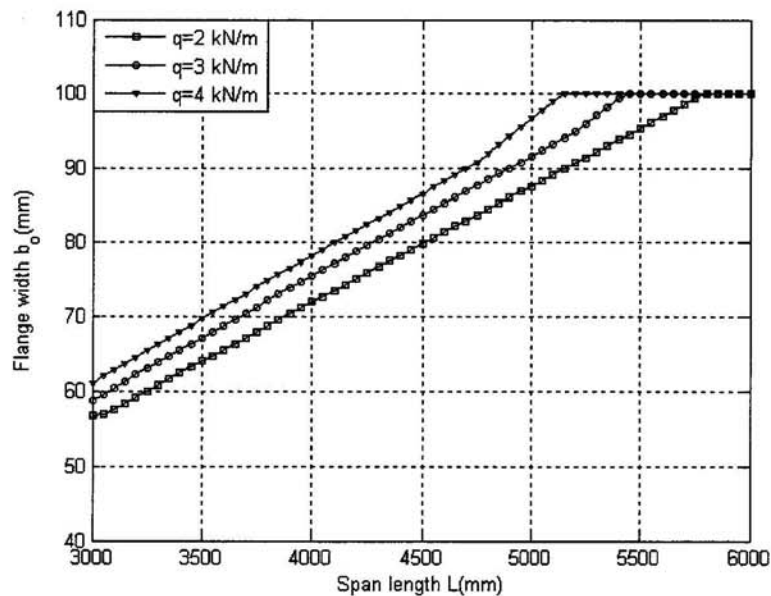


Fig. 5.18: Curves of optimum flange width over span length for un-braced channel beams based on BS 5950-5:1998.

Fig. 5.18 shows the optimum flange width over span length. The lateral-torsional buckling is an instability mode with lateral movement of section in plane of the minor axis and torsion around the longitudinal axis of member. In order to improve the resistance of lateral-torsional buckling, there are two trends. Firstly, we can increase the second moment of area about the minor axis by increasing the width of flange. Secondly, we can increase the depth of lip which will help to change the performance

of open section, like plain channel, to closed section form which has greater resistance of torsion. It is illustrated in Fig. 5.19, the depth of lip increases dramatically for long span for all load case.

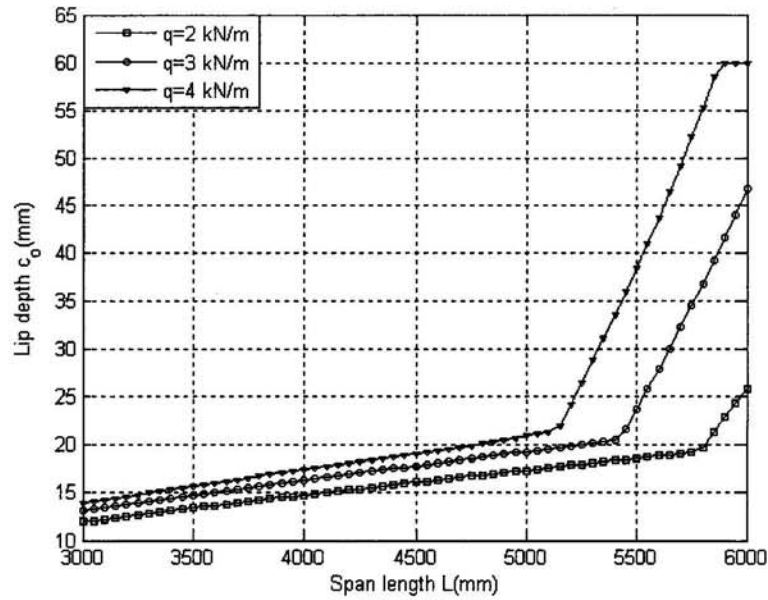


Fig. 5.19: Curves of optimum lip depth over span length for un-braced channel beams based on BS 5950-5:1998.

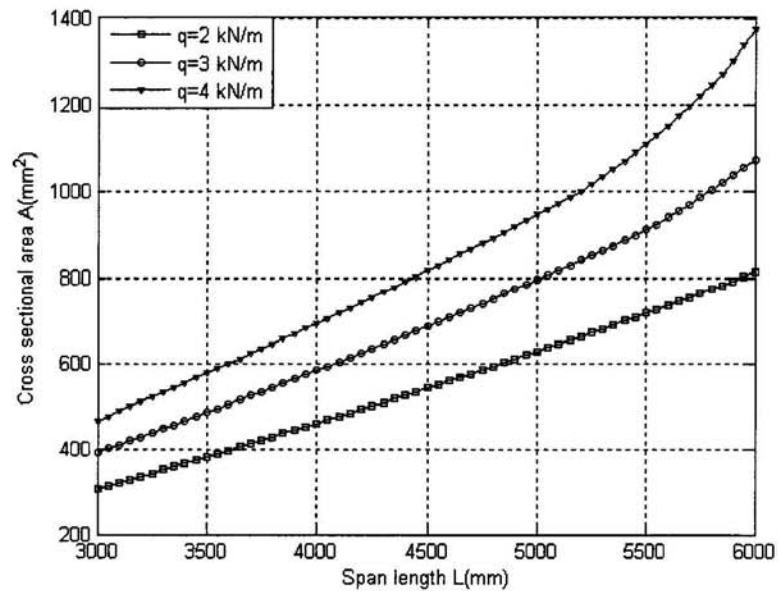


Fig. 5.20: Curves of optimum gross area section over span length for un-braced channel beams based on BS 5950-5:1998.

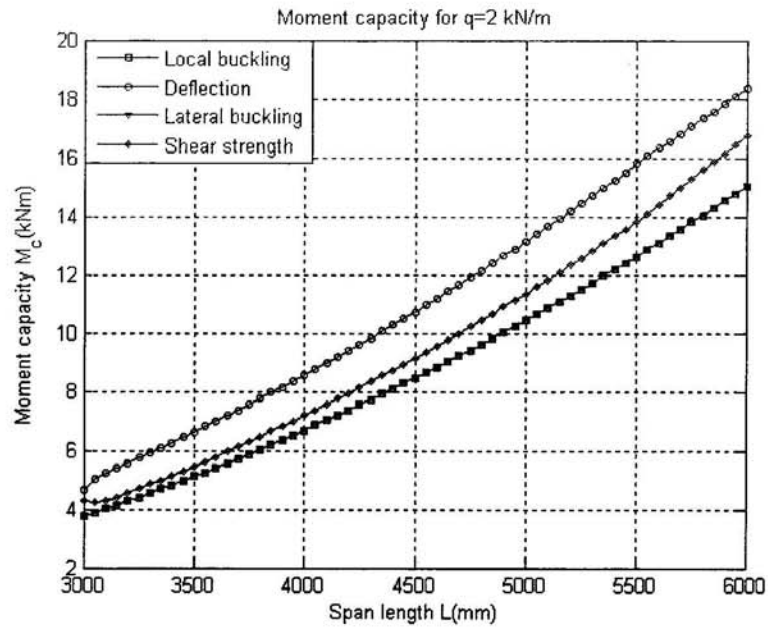


Fig. 5.21: Moment capacities of the optimised section over span length for unbraced channel beams based on BS 5950-5:1998 for $q= 2$ kN/m.

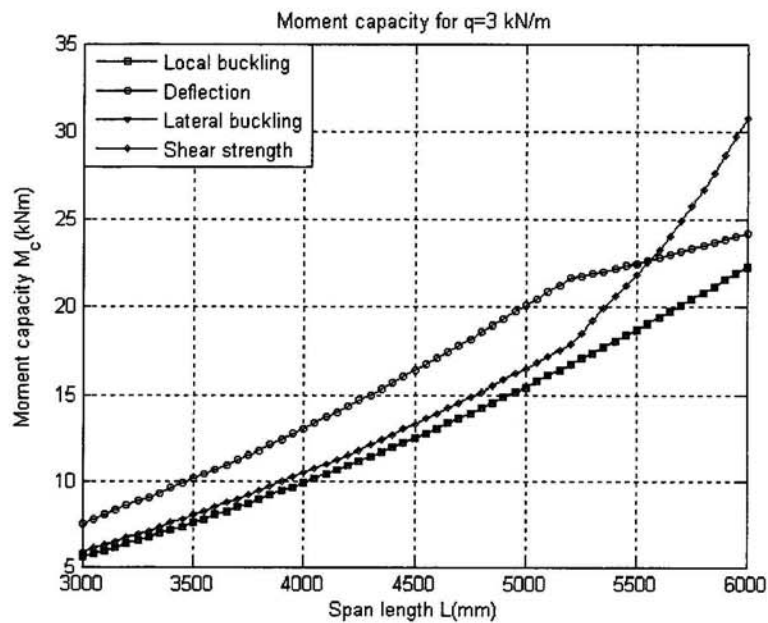


Fig. 5.22: Moment capacities of the optimised section over span length for unbraced channel beams based on BS 5950-5:1998 for $q= 3$ kN/m.

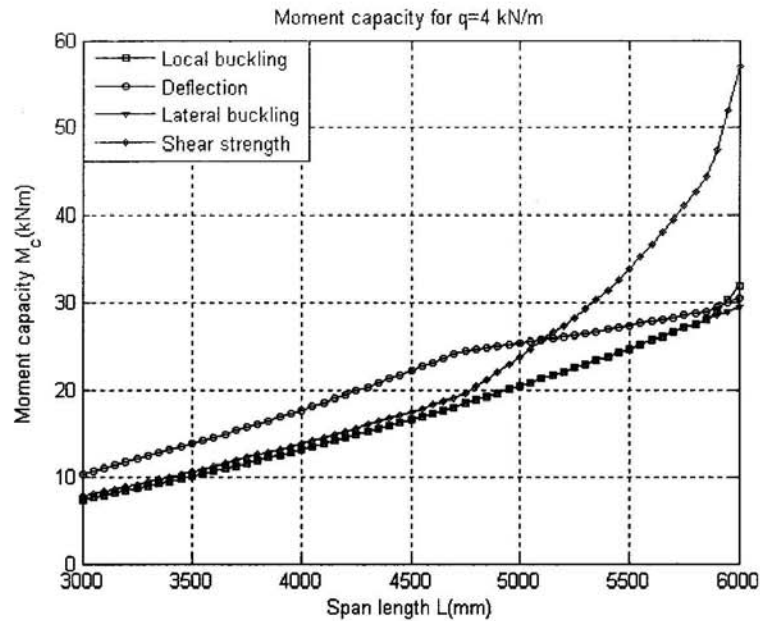


Fig. 5.23: Moment capacities of the optimised section over span length for unbraced channel beams based on BS 5950-5:1998 for $q=4$ kN/m.

From Fig. 5.21 to 5.23, we know which design criterion controls the strength capacity of the beam. It obviously can be seen that the optimum section of the unrestrained beam are found when lateral-torsional buckling and local buckling coincide. It satisfies the hypothesis of optimisation problem that we discussed in the Chapter 2. The optimum section is a section which satisfies the hypothesis that all buckling mode happen at the same time. However, because of geometrical constraint, it is impossible to make all mode of failure occurring at the same time.

In order to verify the optimisation method, general method of optimisation process is used. This method is effective with less design variable. The inputs of optimisation of the channel section are b_o from 50mm to 150mm, and the ratio c_o/b_o of 0.2, h_o of 202mm and the thickness is 2mm. The span length of beam is 4m. The beam is designed based on the geometrical constraints and strength constraints identified by local buckling and lateral-torsional buckling. The beam is subjected to uniformly

distributed load of 5kN/m. The comparison of optimum dimensions for two methods are shown in Table 5.1:

In the table, ‘Opt-GO’ is the general optimisation procedure; ‘Opt-STA’ is the standard algorithm procedure using the trust-region method. The corresponding optimum dimensions are quite close in both methods. Thus the computer programme for optimisation using standard algorithms is verified and can be used for further analysis.

Table 5.1: Comparison of optimisation results

Optimisation methods	h_o (mm)	b_o (mm)	c_o (mm)	t (mm)	A_g (mm ²)
Opt-GO	202	96.1	19.22	2	849.28
Opt-STA	202	95.7	19.10	2	847.22

5.4.2 Optimisation result based on BS 5950-5:1998 considering distortional buckling

Currently, the distortional buckling is not considered in BS 5950-5:1998. Therefore, the distortional buckling will be considered in the optimisation programme of the flexural channel section based on BS 5950-5:1998. As above-mentioned in 5.1.5, the investigation of the distortional buckling failure of channel section is calculated by Hancock’s method and direct strength method (DSM). Fig. 5.10 shows that the moment resistance of distortional buckling computed by DSM is always smaller than by Hancock’s value, because DSM employs elastic distortional buckling which is considered for the flexural beam under gradient moment and the interaction between

flange element and web element instead of pure bending and assuming the lateral restraint from the web to compression flange is zero in Hancock's model. Hence, in this part the calculation of distortional buckling based on DSM is used for the optimisation programme for safety reason and numerical results.

Although, the distortional buckling is included in the optimisation programme, the plots of optimum thickness are 0.5% different from the case without considering distortional buckling. It indicates that the thickness of section has a small influence on the optimum design section.

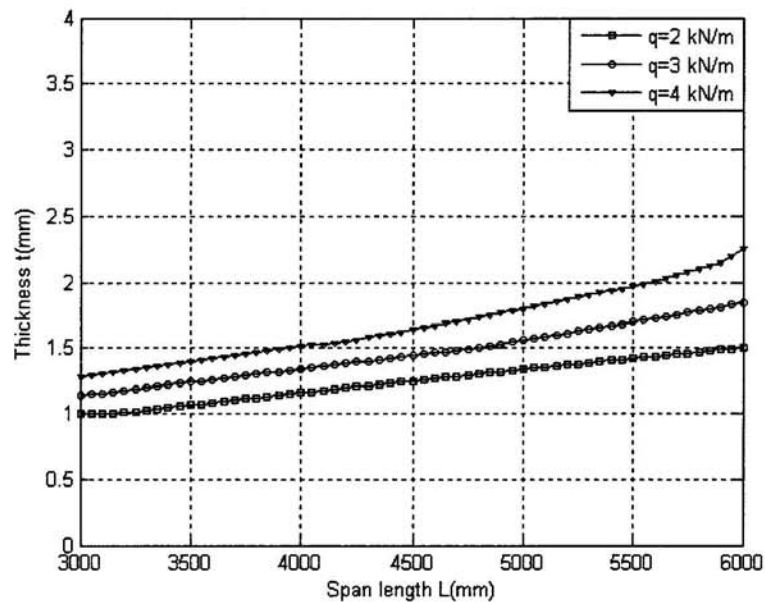


Fig. 5.24: Curves of optimum thickness over span length for un-braced channel beams based on BS 5950-5:1998 taking into account distortional buckling.

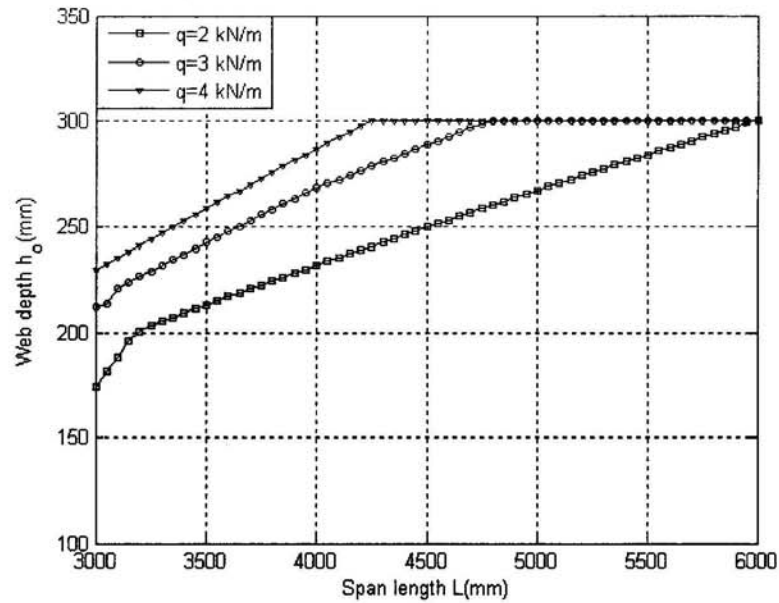


Fig. 5.25: Curves of optimum web depth over span length for un-braced channel beams based on BS 5950-5:1998 taking into account distortional buckling.

As can be seen from Fig. 5.25, it has the same trend compared with the case without taking into account distortional buckling. However, for load cases of 3 and 4kN/m, the depth of web increases with increase of span to attain the upper bound of 300mm more quickly than that in Fig 5.17 when distortional buckling is not considered. It indicates that the distortional buckling has evolved to control in the optimisation process and hence it should be included in the design procedure of section.

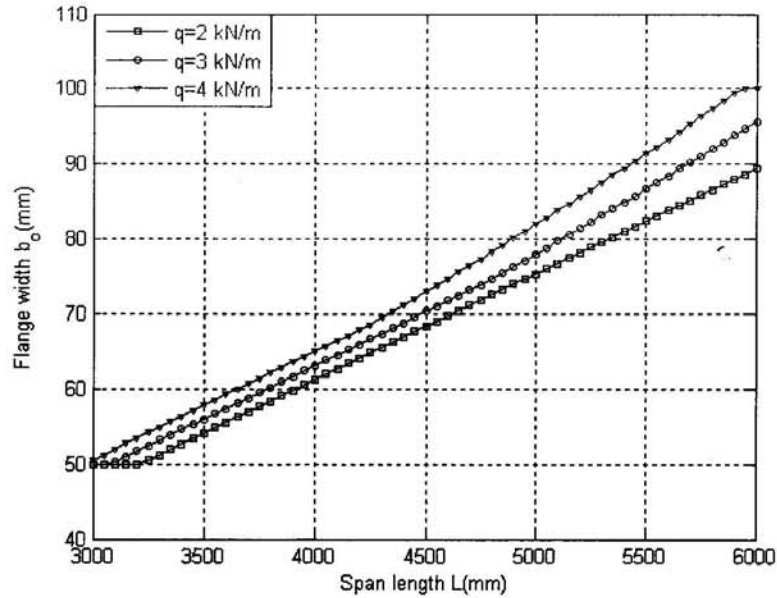


Fig. 5.26: Curves of optimum flange width span length for un-braced channel beams based on BS 5950-5:1998 taking into account distortional buckling.

Contrary to the depth of web, Fig. 5.26 shows that as the width of flange increases gradually it reaches its upper bound of 100mm more slowly than that in Fig. 5.18 when the distortional buckling is not considered. It proves that there is a reciprocal relation between the web depth and flange width in designing process. When considering distortional buckling in design, h_o provides a greater contribution to increase the rotational spring stiffness k_ϕ at the junction between the web and the flange, in order to increase the resistance of distortional buckling. The increase of h_o induces the slow increase of the flange width. Furthermore, the optimum design section is controlled by distortional buckling as showed in Fig. 5.29 to Fig. 5.31. On the other hand, when the distortional buckling is not considered in Fig. 5.18, b_o tends to increase more quickly due to the fact that the lateral-torsional buckling or local buckling governs the design section, hence this leads to the a quicker increase in flange width.

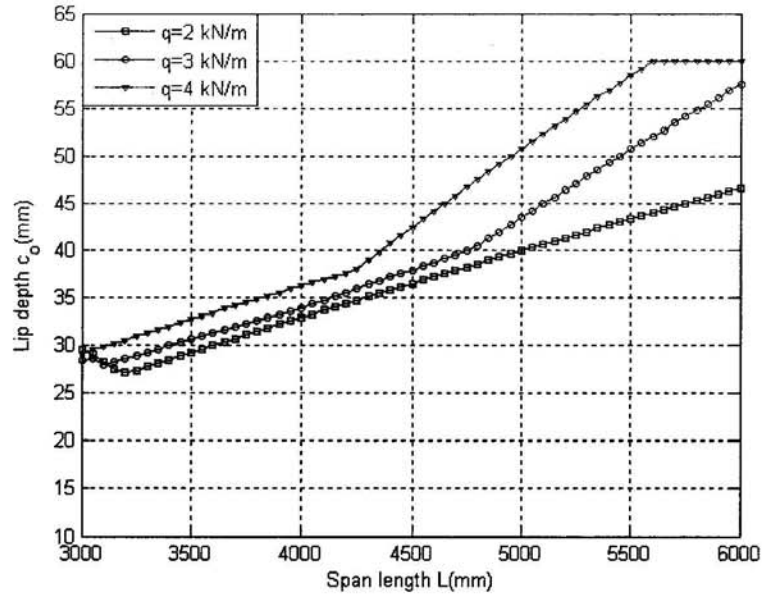


Fig. 5.27: Curves of optimum lip depth over span length for un-braced channel beams based on BS 5950-5:1998 taking into account distortional buckling.

As can be seen from Fig. 5.27, we find that the depth of lip becomes the important factor in the distortional buckling resistance. The depth of lip starts at the higher value of 27mm instead of 12mm in Fig. 5.19 and increases significantly up to the upper bound of 60mm.

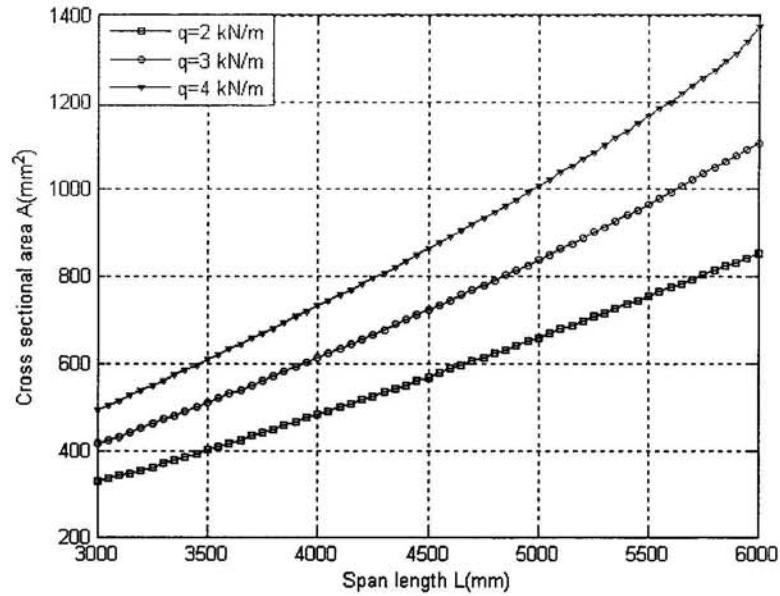


Fig. 5.28: Curves of optimum gross area section over span length for un-braced channel beams based on BS 5950-5:1998 taking into account distortional buckling (DB).

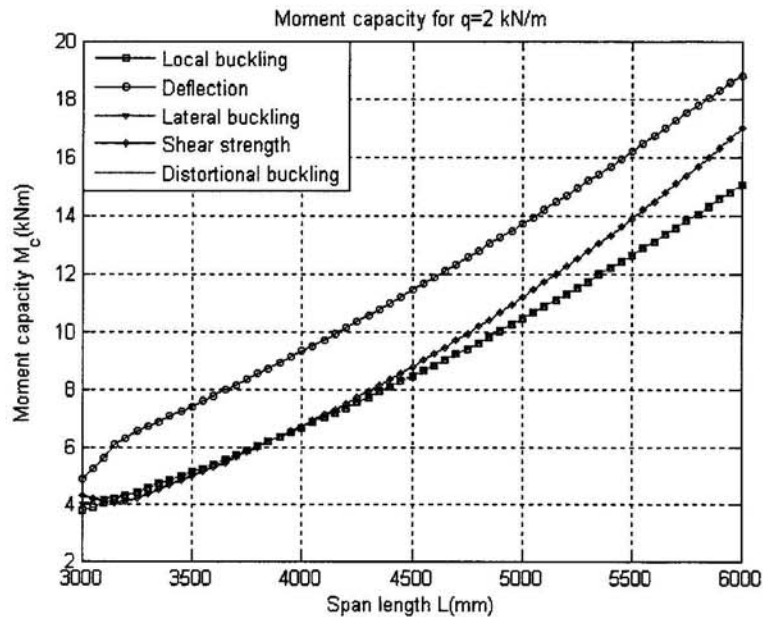


Fig. 5.29: Moment capacities of the optimised section over span length for un-braced channel beams based on BS 5950-5:1998 taking into account DB for $q=2$ kN/m.

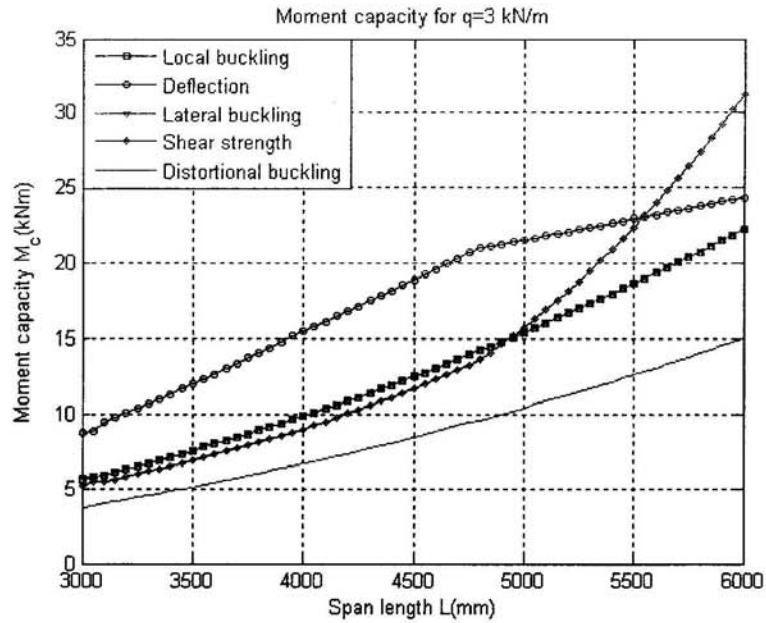


Fig. 5.30: Moment capacities of the optimised section over span length for unbraced channel beams based on BS 5950-5:1998 taking into account DB for $q=3$ kN/m.

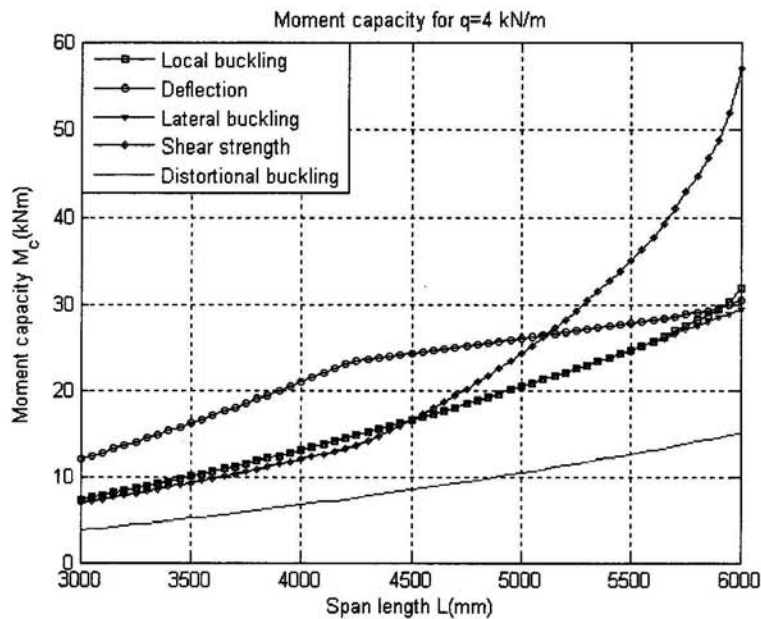


Fig. 5.31: Moment capacities of the optimised section over span length for unbraced channel beams based on BS 5950-5:1998 taking into account DB for $q=4$ kN/m.

Figs. 5.29 to 5.31 show the plots of moment capacity of five design constraints and show the lowest M_c that governs the optimum design solution.

5.5 CONCLUSION

The optimum dimensions section of simply supported lipped channel beams subjected uniform distributed load, and without internal restraint have been calculated. The numerical results of the optimisation were performed for two cases based on BS 5950-5:1998 without distortional buckling calculation and with distortional buckling calculation. We found that the optimum thicknesses for the both cases with different load intensities are similar. It indicates that the wall thickness has a slight influence on distortional buckling. On the contrary, the distortional buckling affects the other dimensions of the section such as the depth of web, the width of flange and depth of lip. Furthermore, it can be seen that the optimum design section is controlled by the moment of distortional buckling when distortional buckling is considered in the design calculation.

In conclusion, the global optimum dimensions of a simply supported lipped channel purlin without restraints in span subjected uniformly distributed load are presented here. The plots can be used for concept design by the structural engineer. For other standards or other design constraint conditions such as with intermediate restraints, the optimisation programme can easily be amended to find the plots for global optimum section dimensions.

Chapter 6

6 OPTIMISATION OF ZED PURLIN SECTIONS

6.1 BEHAVIOUR OF SINGLE SPAN ZED PURLIN

6.1.1 Introduction

Similar to the channel section, zed section is used often as a purlin on the roof system, to be connected to the trapezoidal sheeting at the top flange. However, the channel section is employed more in the flat roof, since its principal axes of the section are perpendicular to the flange and the web of the section instead of zed section in which the major axis makes an angle with the web plane. Thus, we tend to use the zed section in a slope roof system to avoid the torsion of the section subjected to the vertical load.



Illustration removed for copyright restrictions

The behaviour of the zed purlin section will be investigated with parametric studies where flange width b_o varies from 40 to 100 mm in 10mm increments, and depth of the web h_o varies from 100 to 300mm in 100mm increments. The thickness of the cross section is assumed to vary from 2 mm to 3mm. The span of the purlin is to be 4m. The steel properties are design strength of 350MPa and of modulus of elasticity

of 205GPa. The current available design method as BS 5950-5:1998, EN 1993-1-3:2006, and AISI will be employed in this investigation.

6.1.2 Design zed purlin subjected to bending

In general, cold-formed Zed sections may undergo the modes of failure listed as below:

- Flexural failure involving local buckling in compression zone.
- Lateral-torsional buckling due to insufficient lateral restraints.
- Distortional buckling of the compression flange.
- Shear failure at support.
- Web crushing under direct loads or reactions.
- Combined effects between bending and web crushing, and bending and shear.
- Excessive deflection at the mid span.

In this study, we consider a simply supported zed purlin subjected to vertical uniformly distributed load applied through the shear centre of section without internal lateral restraints and no concentrated load applied to the beam. Therefore, the design criteria for the combinations between bending and web crushing and bending and shear are omitted. The detail formulas for beam design based on BS 5950-5:1998 were presented in the Chapter 2.

6.1.3 Effects of dimensions changes on the cross section local buckling resistance

The influence of local buckling failure of a flexural beam is illustrated under moment capacity of section. In BS 5950-5:1998, the limiting maximum compressive stress p_c in the web is employed, thus the entire web depth is considered fully effective under

p_o , only the effective width of compression flange is required. Fig. 6.2 shows the moment capacity of section with variation of b_o and ratio c_o/b_o , it can be seen that the moment capacity increases with the increase of b_o . The effective width of flange b_{eff} is smaller than b_o , for example $b_o = 70\text{mm}$ then $b_{eff} = 65\text{mm}$, the width of flange decrease 7.15%. Furthermore, with the increase of web depth, the moment capacity of section increases also due to the increase of second moment of area of the section. For shallow sections such as $h_o = 100\text{mm}$, the depth of lip has insignificant influence on the moment capacity while c_o has considerable influence on the moment capacity in deep sections such as h_o above 200mm.

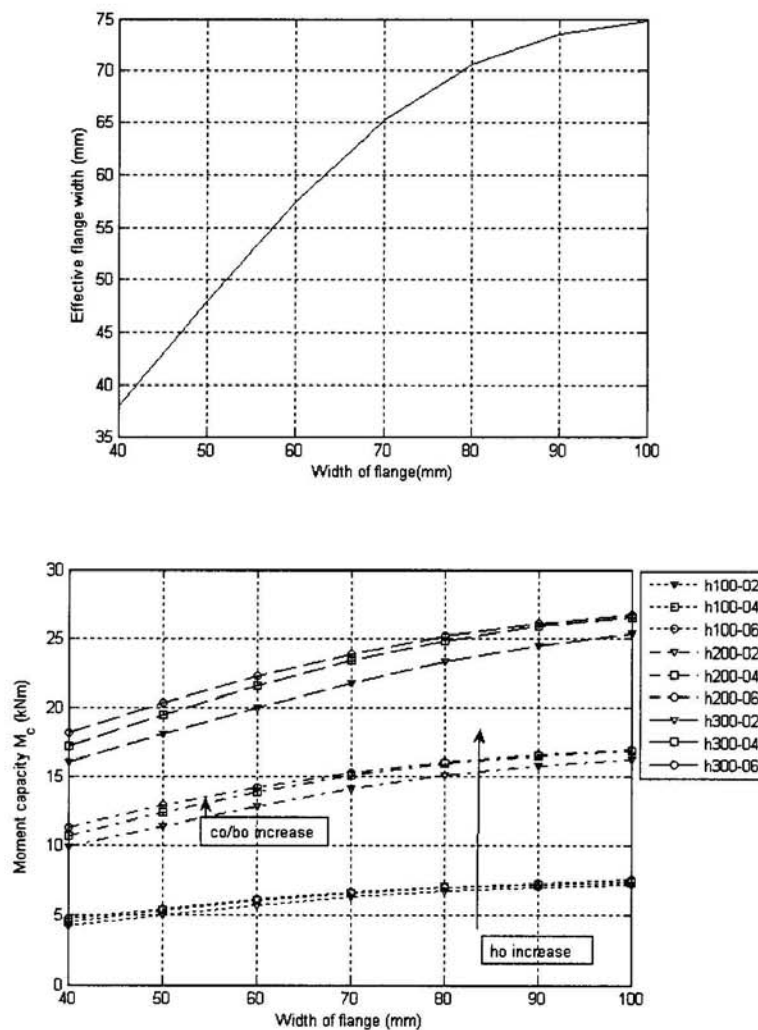


Fig. 6.2: Effects of the dimensions on the moment capacity.

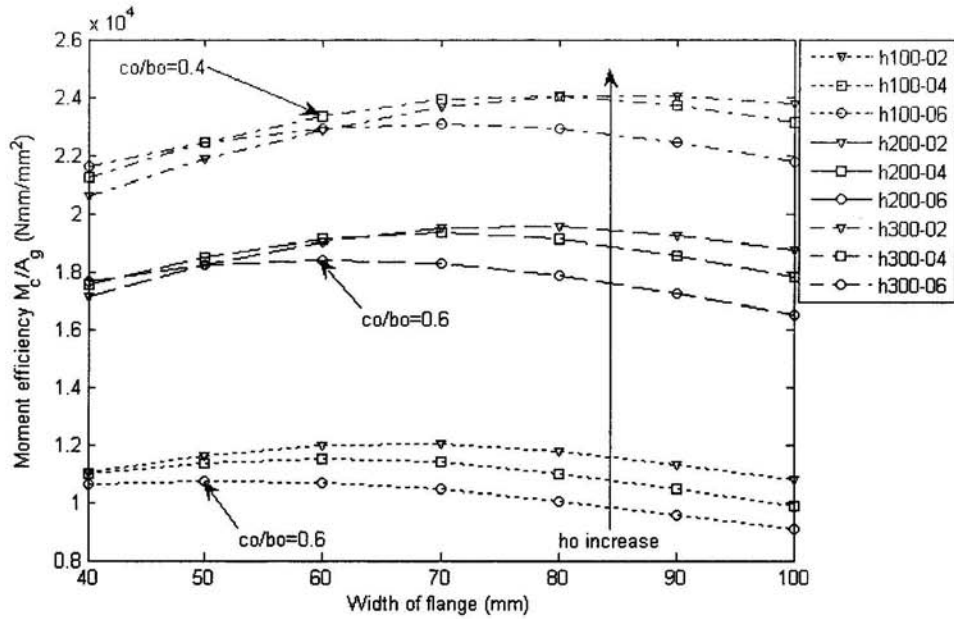


Fig. 6.3: Effects of the dimensions on the moment efficiency.

The effect of section dimensions on local buckling is also demonstrated under the moment efficiency, which is defined as the ratio of moment capacity to the gross area of section. As far as the moment efficiency is concerned, as can be seen from Fig. 6.3, when b_0 starts increasing, the maximum value of moment efficiency is found not to correspond to the widest flange width and the largest ratio c_0/b_0 . For example with $h_0 = 200\text{mm}$ and $c_0/b_0 = 0.2$, the M_c/A_g is maximum when b_0 is 80mm.

6.1.4 Effects of dimensions changes on the lateral-torsional buckling

The effect of section dimensions on the lateral-torsional buckling of the zed section is slightly different compared with the channel section analysed in Chapter 5. Fig. 6.4 demonstrates the effect of section dimension changes on the moment of lateral-torsional buckling, it can be seen that for shallow sections such as $h_0 = 100\text{mm}$, the lateral-torsional buckling increases gradually with the increase of b_0 and c_0 . This

illustrates that for shallow sections the change of b_o and c_o do not contribute very much to the lateral-torsional buckling resistance. On the contrary, for deep sections h_o above 200mm, the width of flange and the depth of lip have a significant contribution to increase resistance of lateral torsional buckling.

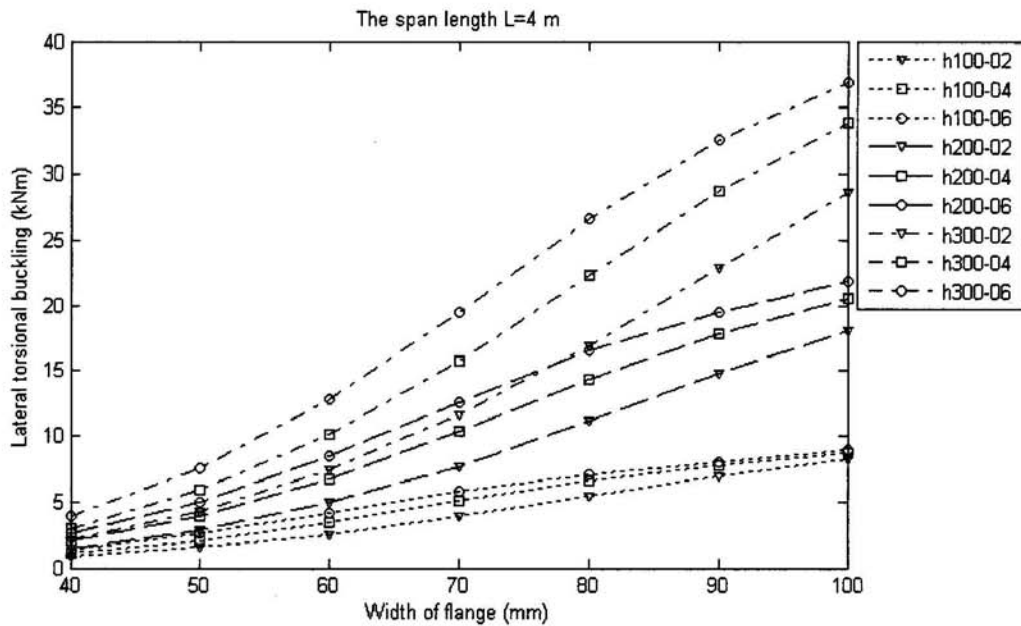


Fig. 6.4: Effects of the dimensions on the moment of lateral-torsional buckling based on BS 5950-5:1998.

6.1.5 Effects of dimensions changes on the deflection of the zed purlin

Fig. 6.5 shows the effect of dimension change on moment resistance when the deflection is considered, It can be seen that the moment resistance increases rapidly when the web depth increases. For example with the same width of flange of 70mm and ratio c_o/b_o of 0.2, when h_o increases from 200 to 300mm (increase 50%) the moment resistance increases from 12 to 28kNm (increase 133%). Compared with the case with the same depth of web, and the change of b_o , for instance $h_o = 200$ mm and b_o varies from 60 to 90mm (increase 50%). The moment resistance increases from 9 to

12kNm (increase 33%). Therefore, for the deflection constraint, the depth of web is dominant variable for determining the resistance of section.

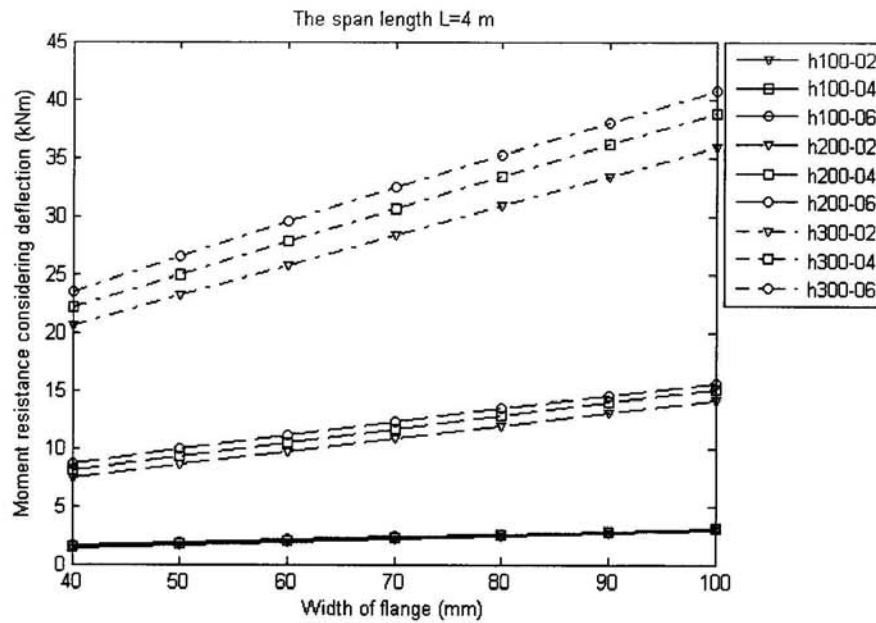


Fig. 6.5: Effects of the dimensions on the moment resistance taking into account of deflection.

6.1.6 Distortional buckling

Due to the lack of distortional buckling calculation for the purlin design in BS 5950-5:1998, similar to the channel design, the distortional buckling design is integrated in the design programme.

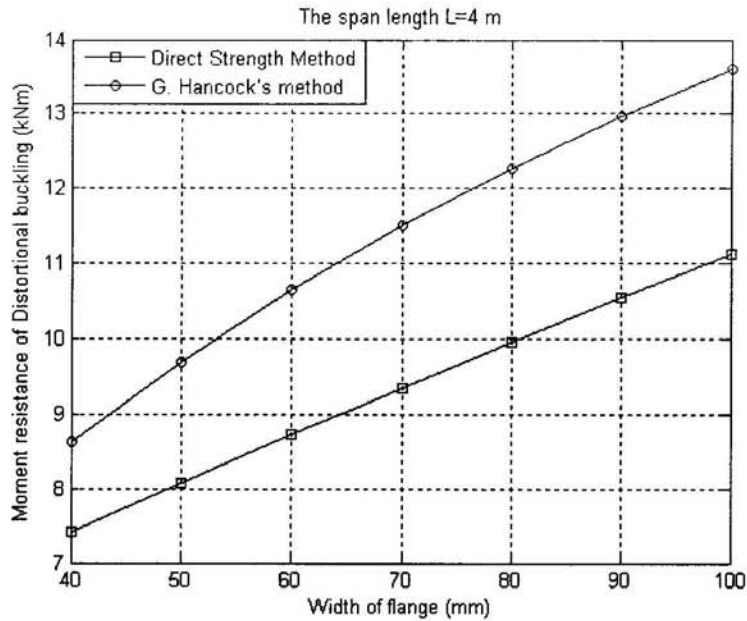


Fig. 6.6: Distortional buckling comparison.

From Fig. 6.6 and Fig. 5.10, it found that the distortional buckling behaviour of both channel and zed sections are similar. The reason is due to the same analytical model for distortional buckling of channel and zed section. Since distortional buckling in the analytical model mainly involves the rotation of the flange around the junction between the flange and the web of section.

6.1.7 Comparison of lateral-torsional buckling results

Four parametric studies identified by b_o , h_o , c_o and span length L , which are varied to investigate their effect on the moment resistance of lateral-torsional buckling calculated by three methods BS 5950-5:1998, AISI and Li's model. Considering the zed purlin restrained against rotation in any direction at the end supports with the dimension of h_o varying from 150 to 300mm, the thickness being 2 mm, and b_o varying from 40 to 100 mm, c_o varying from 15 to 60mm and the span length from 4 to 6m, From Fig. 6.7 the moment resistance of lateral-torsional buckling increases

with the increase of b_o in the three methods BS 5950-5:1998, Li model and AISI. The Fig. 6.7 shows that the results of AISI are higher than that of BS 5950-5:1998 and Li model with b_o from 40mm to 85mm, but when the width of flange is more than 85mm the moment resistance based on AISI is now lower than that of BS 5950-5:1998 and the Li model.

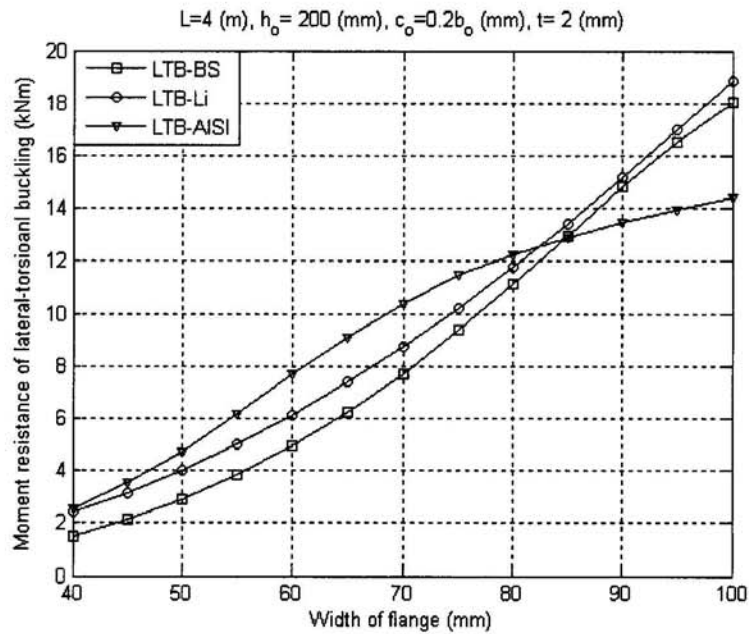


Fig. 6.7: Lateral-torsional buckling with variation of the flange width.

From Fig. 6.8, we can see that the moment resistance of lateral-torsional buckling increases in three methods with the increase of h_o . However the results calculated by AISI are the highest value. It shows that h_o improves significantly the lateral-torsional buckling of the zed section purlin calculated by AISI. However Li's model and BS 5950-5:1998 give more conservative results. Thus, we tend to use the result of BS 5950-5:1998 or Li's calculation in the optimisation programme.

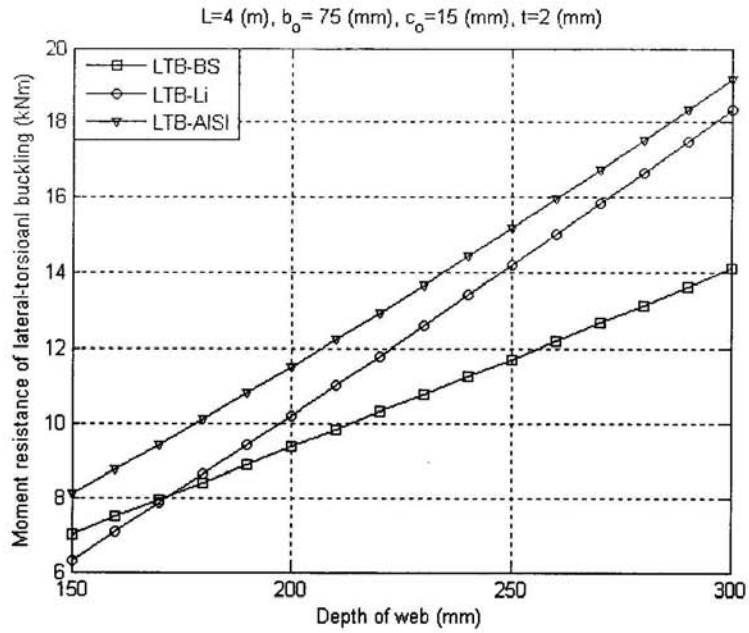


Fig. 6.8: Lateral-torsional buckling with variation of the web depth.

As can be seen from Fig. 6.9, with the same section dimensions and the span length varies, the moment resistance of lateral-torsional buckling decreases gradually with the increase of the span length. The AISI results are always the highest values.

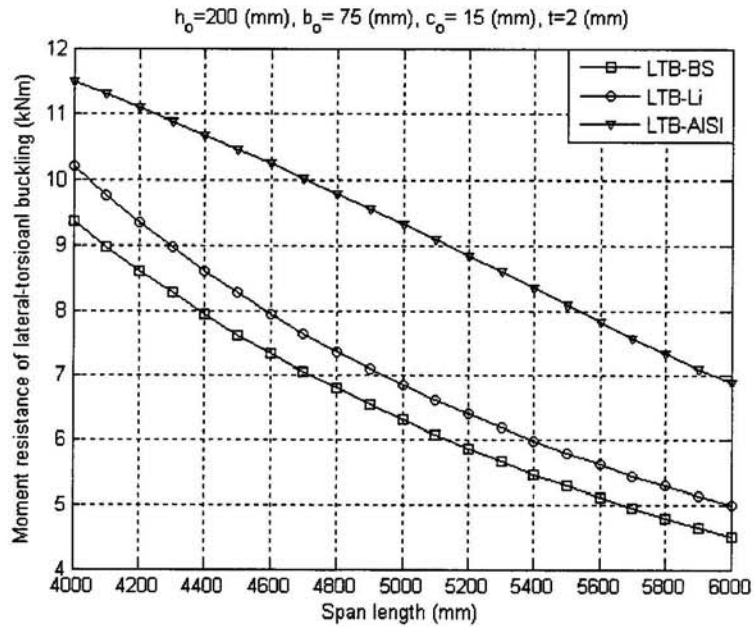


Fig. 6.9: Lateral-torsional buckling with variation of the span.

However, from Fig. 6.10 when the depth of lip varies, the results based on AISI are only highest at c_o from 15 to 25mm. And c_o from 25 to 60mm, the results of Li's

model are the highest. It indicates that in Li's model the depth of lip has more contribution to improve resistance of lateral-torsional buckling in zed purlin than other approaches. It is due the fact that in Li's model, the purlin is subjected to the gradient bending moment, the bending moments decrease from mid span to ends of the beam. There is redistribution of stiffness and stress between mid span zone and zone near supports. This makes the moment resistance of section based on Li's model is higher than that of other models.

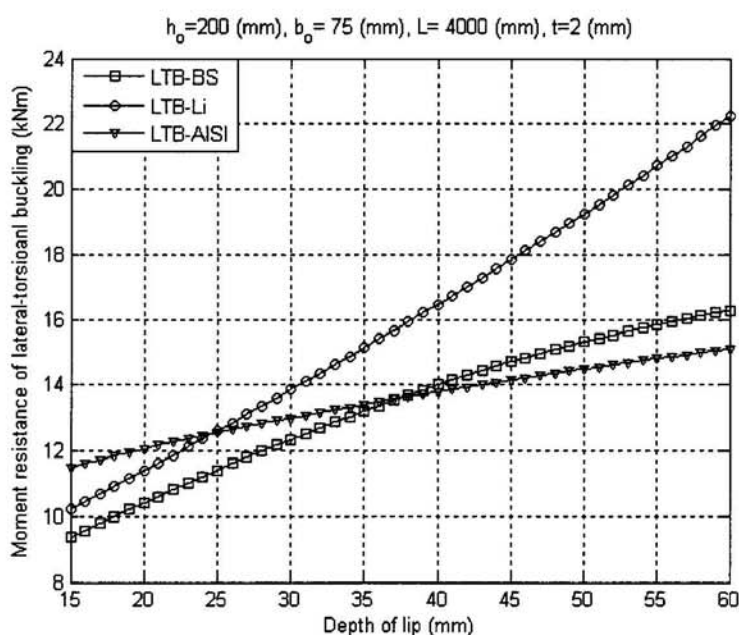


Fig. 6.10: Lateral-torsional buckling with variation of the the lip.

6.2 SELECTION OF PARAMETERS OF OPTIMISATION PROBLEM

In this section, the optimisation of section is performed for single zed purlin subjected to a uniformly distributed vertical load ranging from 2 to 4kN/m with span length between 3m and 6m. The modulus of elasticity and yield strength of the steel are taken as $E=205\text{GPa}$ and $\sigma_y = 350\text{MPa}$. The optimisation problem is performed with different constraints. Firstly, we consider the optimisation based on BS 5950-5:1998 in which local buckling, lateral buckling and deflection constraint are considered. Secondly, due to the lack of the calculation of the distortional buckling failure of BS

5950-5:1998, we include the distortional computation in the optimisation problem. The geometric constraints of the design variables are assumed as in Eq.(6.1) based on BS 5950-5:1998.

$$\frac{h_o}{t} \leq 500; \frac{b_o}{t} \leq 60; \frac{c_o}{t} \leq 50; 0.2 \leq \frac{c_o}{b_o} \leq 0.6 \quad (6.1)$$

6.3 NUMERICAL OPTIMISATION RESULTS

6.3.1 Optimisation results based on BS 5950-5:1998

Similar to the channel purlin, the description of optimisation problem and the optimisation process were presented in Chapter 4. The optimisation results are presented under plots of global optimum dimensions. Figs. 6.11 to 6.15 provide the optimum dimensions section in accordance with given span and given load case.

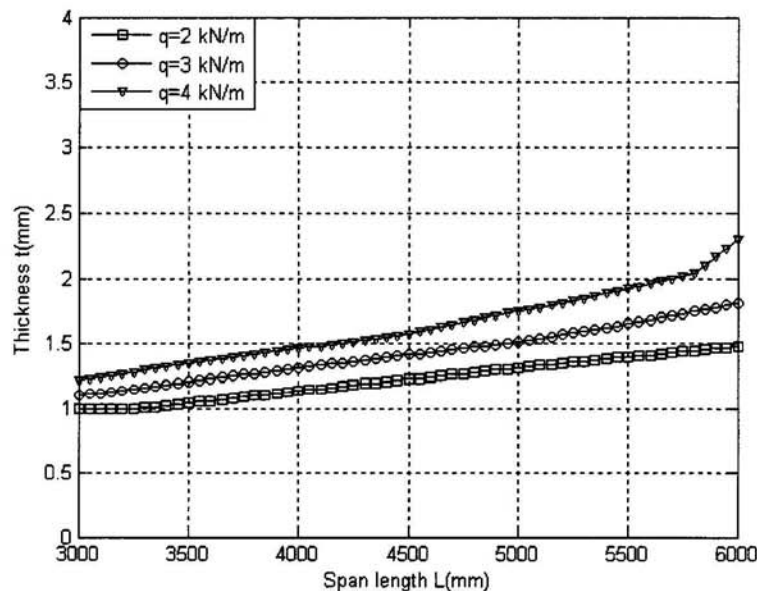


Fig. 6.11: Global optimum design thickness versus span length for un-braced zed beams based on BS 5950-5:1998.

Fig. 6.11 shows that the trend of optimum thickness of zed section is similar to the channel section shown in Fig. 5.16. For load case of 2kN/m the thickness increases

more gradually than that in the load case of 4kN/m. However for all three load cases, the thickness of section increases slowly, it demonstrates that the thickness does not contribute much to increase the resistance of section.

Fig. 6.12 demonstrate that h_o increases quickly when the span length increases from 3 to 6m. Especially for the highest load of 4kN/m, h_o reaches maximum bound of 300mm at 4.5m span, while for the channel sections shape this happened when the span is 4.7m. It indicates that the resistance strength of zed section is smaller than that of channel section. Whereas, for small load cases such as 2kN/m, h_o increases gradually. It is due to the fact that in large load cases for unrestrained beams the lateral-torsional buckling becomes more active and starts to control the capacity of section, so it evidently leads to an increase to h_o in order to improve the lateral-torsional buckling resistance.

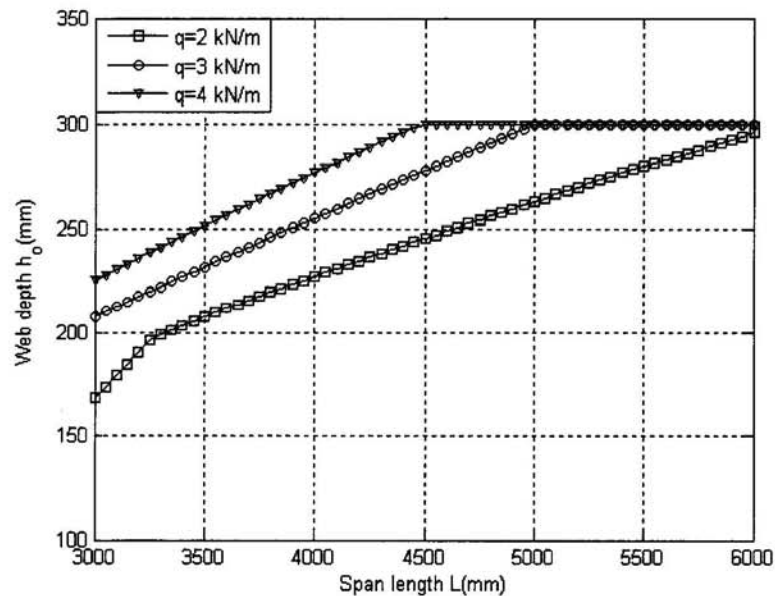


Fig. 6.12: Global optimum design web depth versus span length for un-braced zed beams based on BS 5950-5:1998.

Fig. 6.13 and Fig. 5.18 show that for three load cases the width of flange in zed section reaches the maximum bound value more quickly than that of channel sections. It is due to the fact that the major axis of a zed section makes an angle with the plane of web, so the load is not applied in the plane of the major axis. This leads to lower torsional resistance than that of a channel section with the same dimensions h_o , b_o , c_o and t .

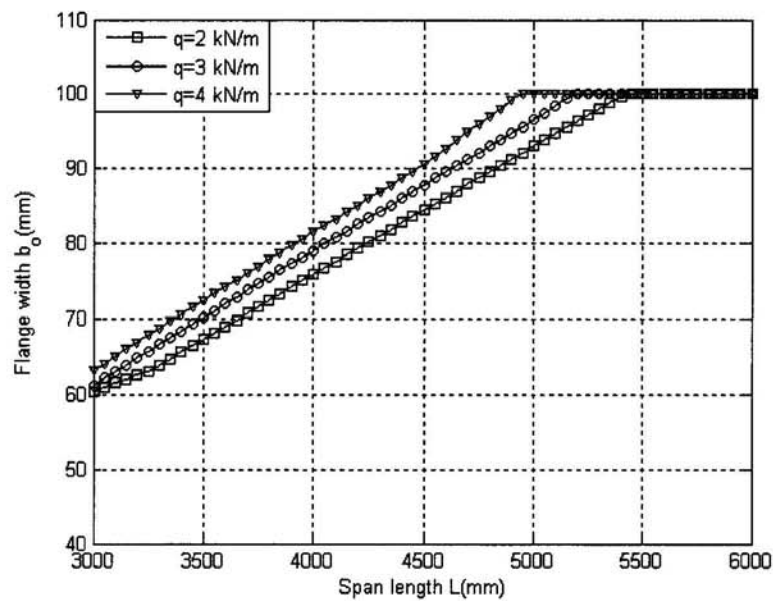


Fig. 6.13: Global optimum design flange width versus span length for un-braced zed beams based on BS 5950-5:1998.

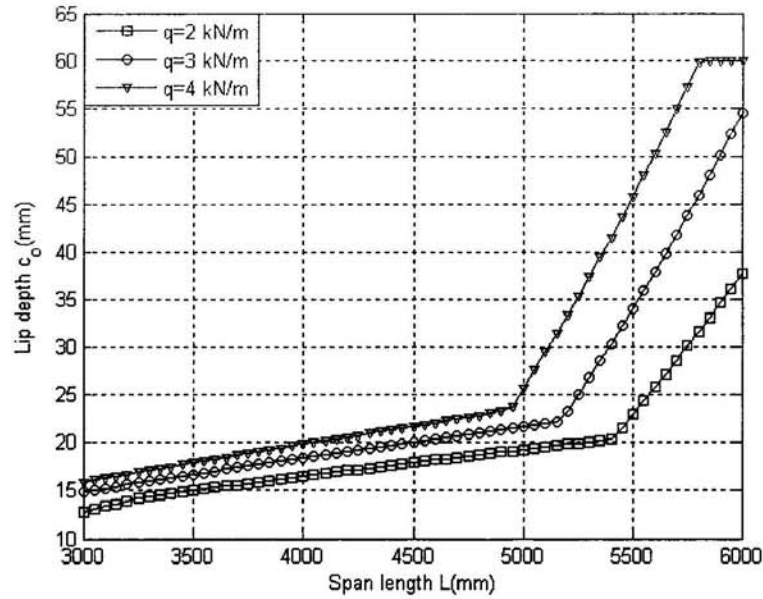


Fig. 6.14: Global optimum design lip depth versus span length for un-braced zed beams based on BS 5950-5:1998.

Fig. 6.14 shows that the depth of lip increases with span more rapidly than that of channel section shape. This is because the torsion stiffness of zed sections is lower. To overcome this, c_o of zed section tends to increase quickly to improve the section's torsional stiffness. It can be seen that when span is from 5m, c_o has the sudden change in gradient in three plots. This shows that the lip contributes significantly to increase resistance of section.

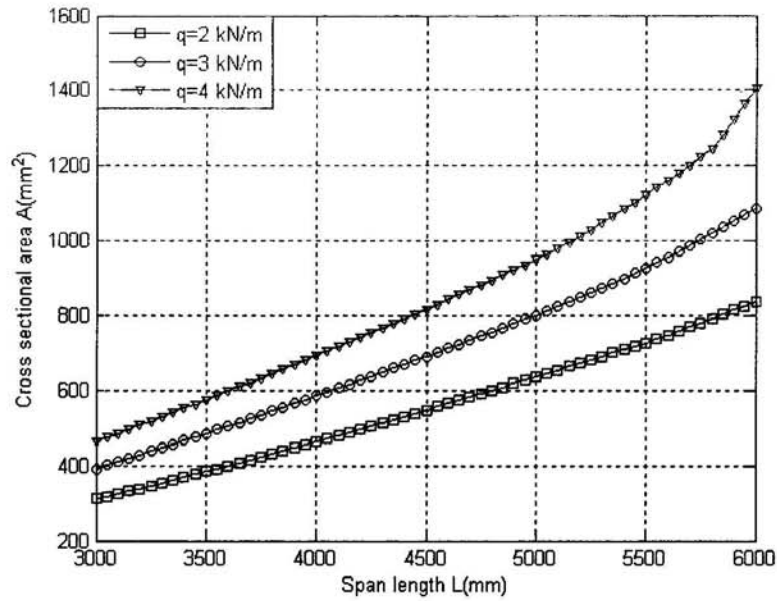


Fig. 6.15: Global optimum design cross area section versus span length for unbraced zed beams based on BS 5950-5:1998.

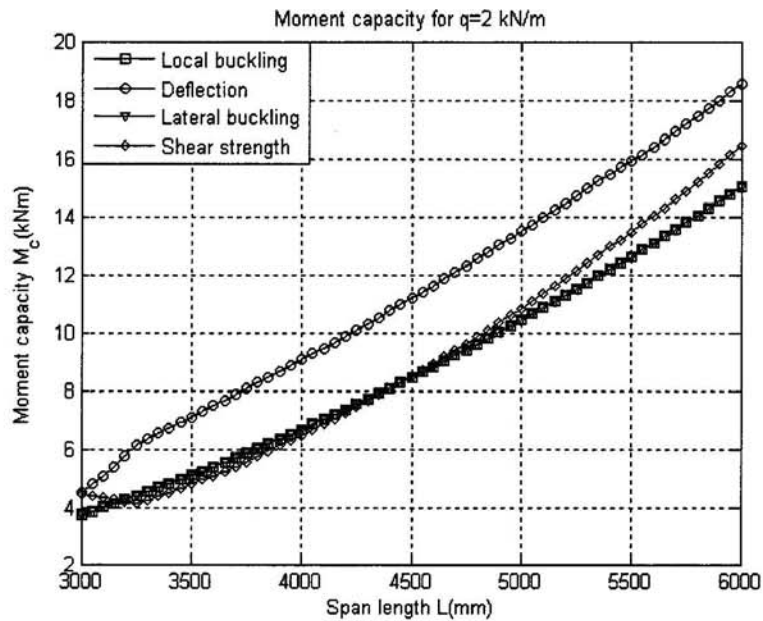


Fig. 6.16: Moment capacities of the optimised section over span length for unbraced zed beams based on BS 5950-5:1998 for $q=2 \text{ kN/m}$.

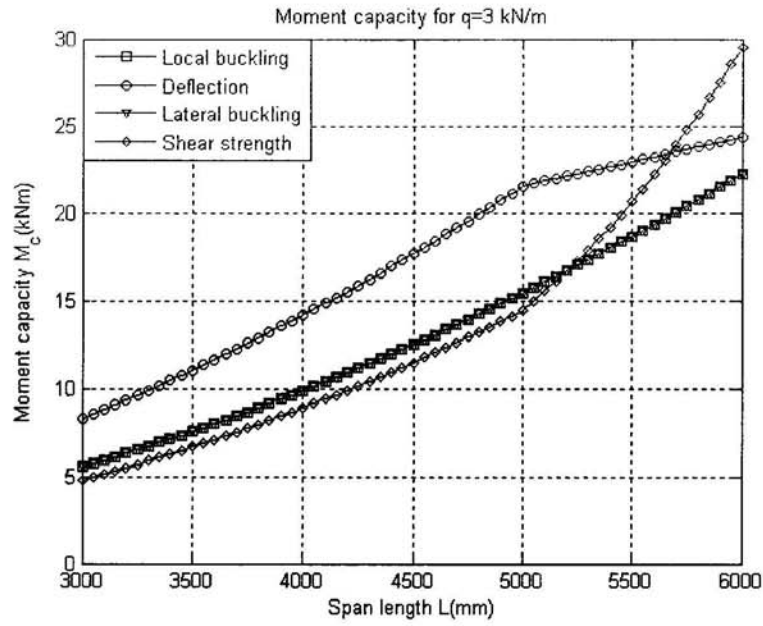


Fig. 6.17: Moment capacities of the optimised section over span length for unbraced zed beams based on BS 5950-5:1998 for $q= 3$ kN/m.

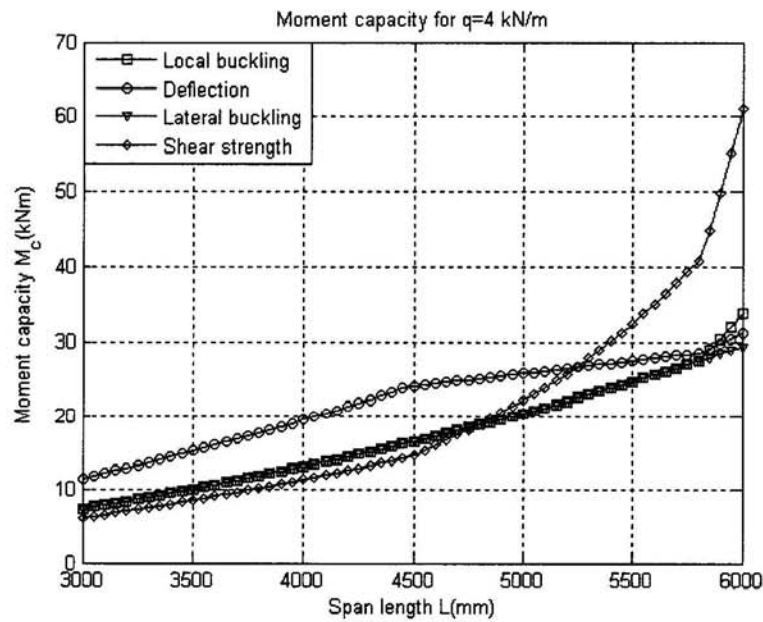


Fig. 6.18: Moment capacities of the optimised section over span length for unbraced zed beams based on BS 5950-5:1998 for $q= 4$ kN/m.

From Fig. 6.16 to 6.18, it can be seen that for all three load cases during the optimisation process, the lateral-torsional buckling moment coincides with local

buckling. As mentioned in the section 2.3, the ideal optimum section is obtained when all modes of failure of section happen at the same time. However, this case is impossible to occur due to the geometric constraints of section for practical engineering. It is a so-called naïve optimum section. In fact two modes of failure are possible to occur at the same time as shown in the results above.

6.3.2 Optimisation results based on BS 5950-5:1998 considering distortional buckling

Similar to channel sections, the zed section purlin is a symmetric section about the minor axis. Therefore, for flexural member there is only a flange in tension and other in compression. The compression flange tends to buckle in two kinds of buckling mode, namely local buckling and distortional buckling. In the case of distortional buckling, the compression flange of zed section behaves similarly to the flange of channel section, which was described in chapter 5. The flange acts as compression element and tends to rotate around the intersection between the flange and web of section. Currently, there are two efficient approaches to calculate the distortional buckling as DSM and Hancock method. Both methods are practical for hand calculation and suitable for the structural engineer. Thus, these two methods are employed in the optimisation programme to find the optimum section.

The optimum dimensions of zed purlin are presented by each individual curve form of each element of section such as thickness, flange width, depth lip and the web depth. In this study, we present the numerical optimisation results for three load cases 2kN/m, 3kN/m and 4kN/m with span length varying from 3m to 6m. However, the optimisation programme can be applied for different load cases with different spans

that the structural engineer defines. The optimum results are illustrated in Fig. 6.19 to 6.22.

Comparing optimum thicknesses of zed sections considering distortional buckling and without taking into account distortional buckling in Fig. 6.11 and Fig. 6.19, there is no difference between the two cases. It confirms the finding that the thickness of section has a very small effect on distortional buckling resistance of the zed section. Nevertheless, for each individual case the thickness of section still helps to increase distortional buckling resistance of the section, because the thickness increases gradually when span length increase.

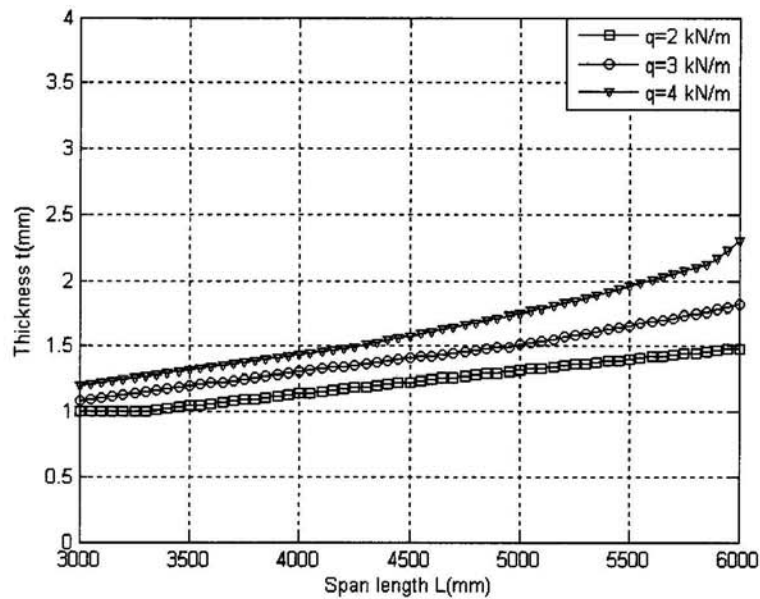


Fig. 6.19: Global optimum design thickness versus span length for un-braced zed beam based on BS 5950-5:1998 taking into account distortional buckling.

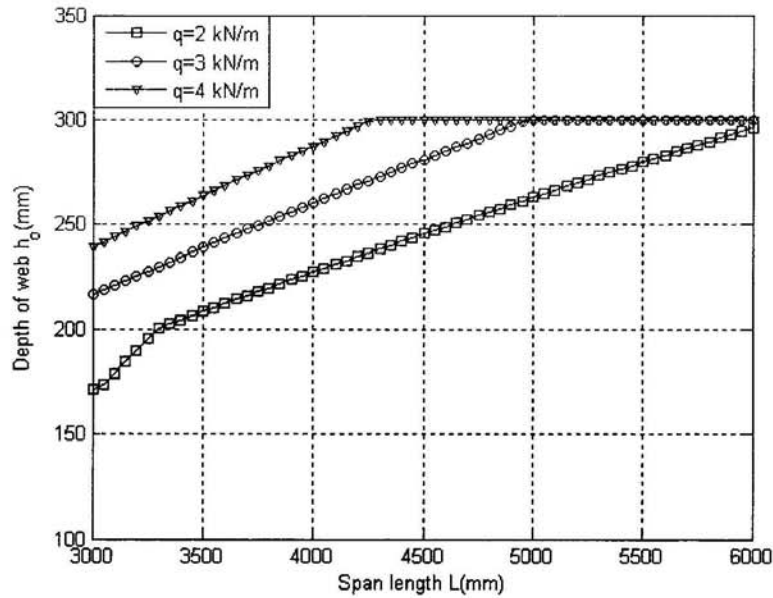


Fig. 6.20: Global optimum design web depth versus span length for un-braced beam based on BS 5950-5:1998 taking into account distortional buckling.

Comparing plots in Fig. 6.20 and 6.12, we can see that for two load cases 2 and 3kN/m, the optimum depth of web does not change, but when the load is 4kN/m the distortional buckling controls the dimension, and h_o now increases faster. To illustrate this, Fig. 6.12 shows that the depth of web reaches its maximum of 300mm at a span of 4.5m whereas in the Fig. 6.20 h_o attains 300mm at the smaller span of 4.2m . This is an important finding since it shows that there are situation where design in accordance with BS 5950:5:1998 will not be as safe as the guidance does imply.

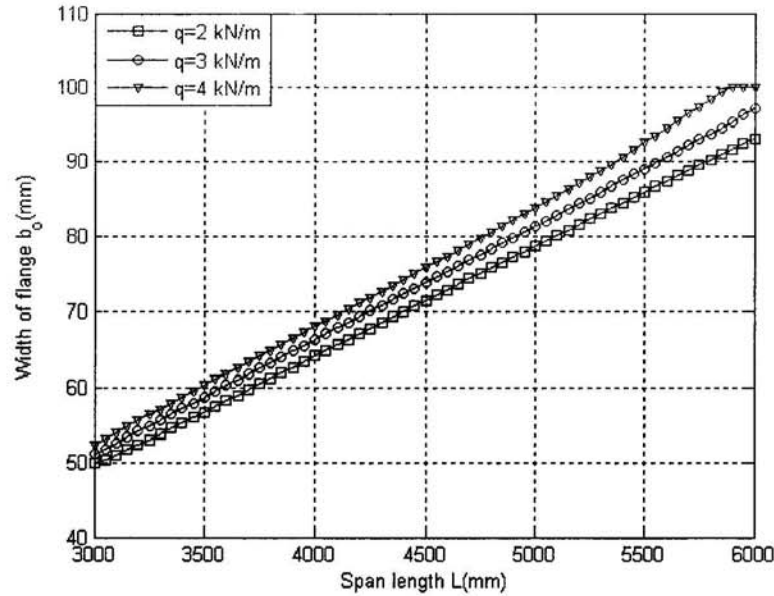


Fig. 6.21: Global optimum design flange width versus span length for un-braced zed beam based on BS 5950-5:1998 taking into account distortional buckling.

Comparing the optimum width of flange in Fig. 6.13 and Fig. 6.21, we can see evidently that the effect of the distortional buckling on the design of zed purlin, the optimum results of b_o in two cases considering distortional buckling and not considering distortional buckling are completely different. The width of flange increases faster in the case not considering the distortional buckling. For example, for load case 2kN/m, b_o reaches the maximum 100mm at span 5.4m in the case not considering distortional buckling, a flange width of 85mm when taking into account distortional buckling. It appears to be not a logical trend, when distortional buckling is considered, the width of flange should be increased more quickly when the load and the span increase. However, b_o does not increase. It is due to the fact that c_o increases more quickly when considering distortional buckling. For instance, the optimum c_o starts from 32mm at the shortest span of 3m in the case taking into account distortional buckling instead of 12mm in the case without distortional buckling and for

the largest load case 4kN/m, c_o attains the maximum value at span 5.2m instead of 5.7m in the case not considering distortional buckling. The increase of c_o helps to strengthen the stiffness of the lip to prevent vertical deflection of the lip which causes the failure of distortional buckling.

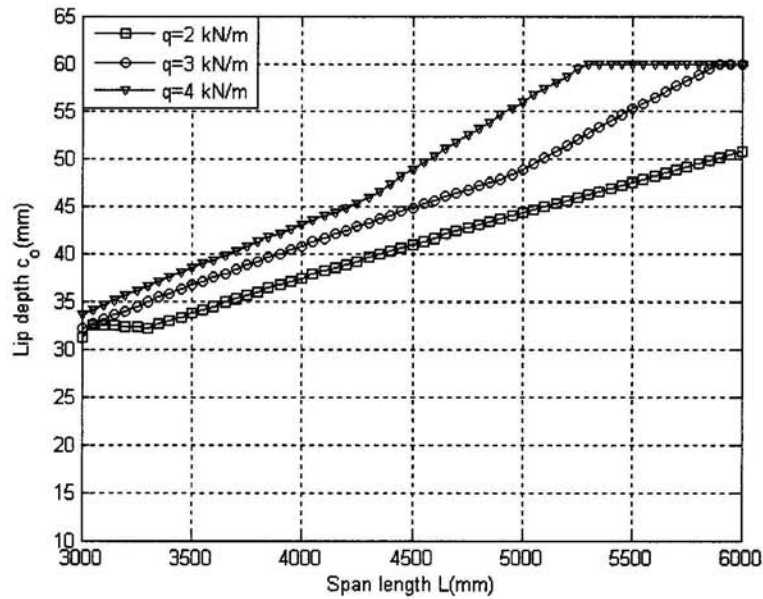


Fig. 6.22: Global optimum design lip depth versus span length for un-braced Zed beam based on BS 5950-5:1998 taking into account distortional buckling.

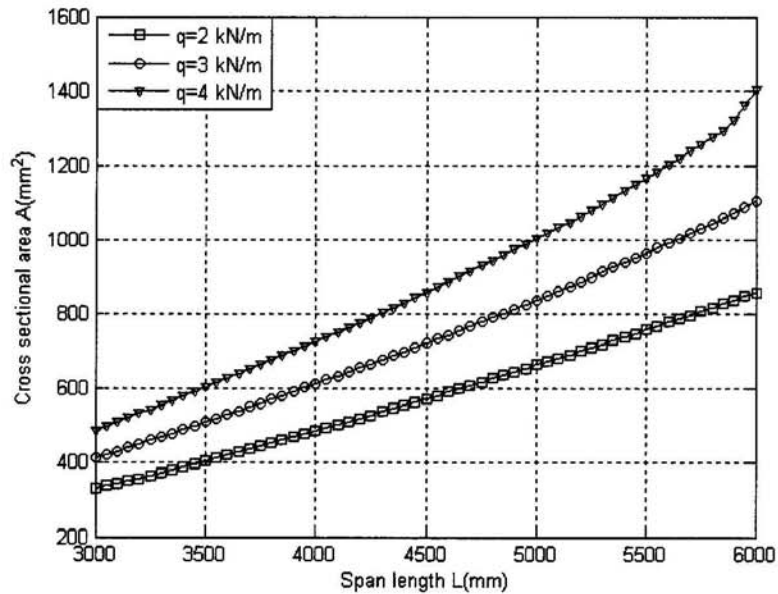


Fig. 6.23: Global optimum design cross area section versus span length for un-braced zed beams based on BS 5950-5:1998 taking into account distortional buckling.

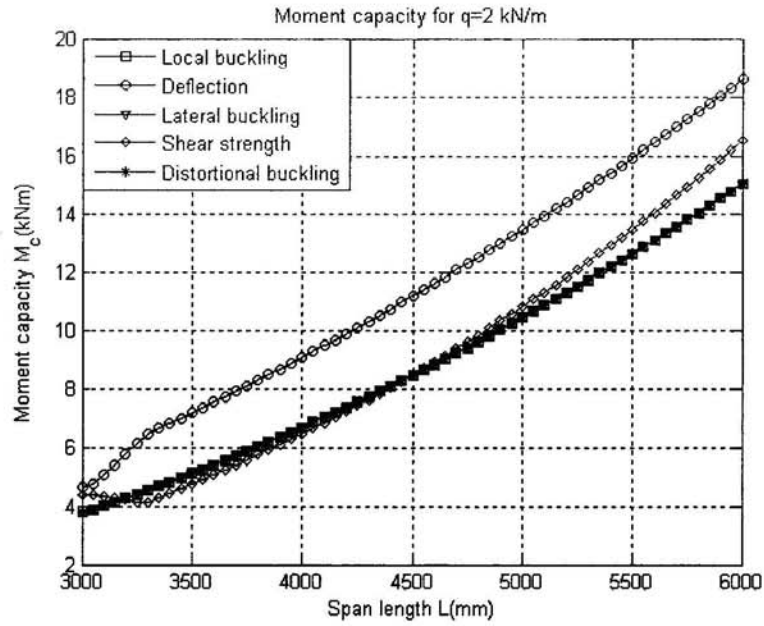


Fig. 6.24: Moment capacities of the optimised section over span length for unbraced zed beam based on BS 5950-5:1998 taking into account DB for $q=2\text{kN/m}$.

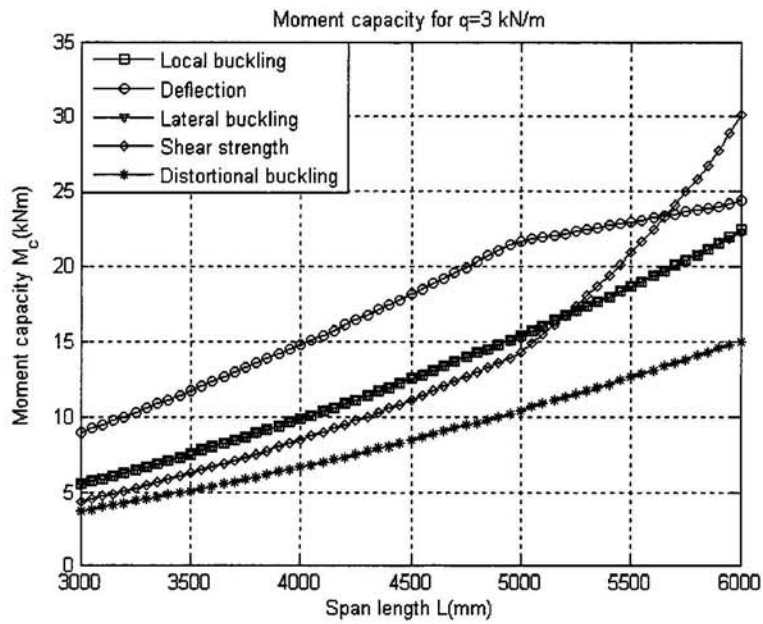


Fig. 6.25: Moment capacities of the optimised section over span length for unbraced zed beam based on BS 5950-5:1998 taking into account DB for $q=3\text{kN/m}$.

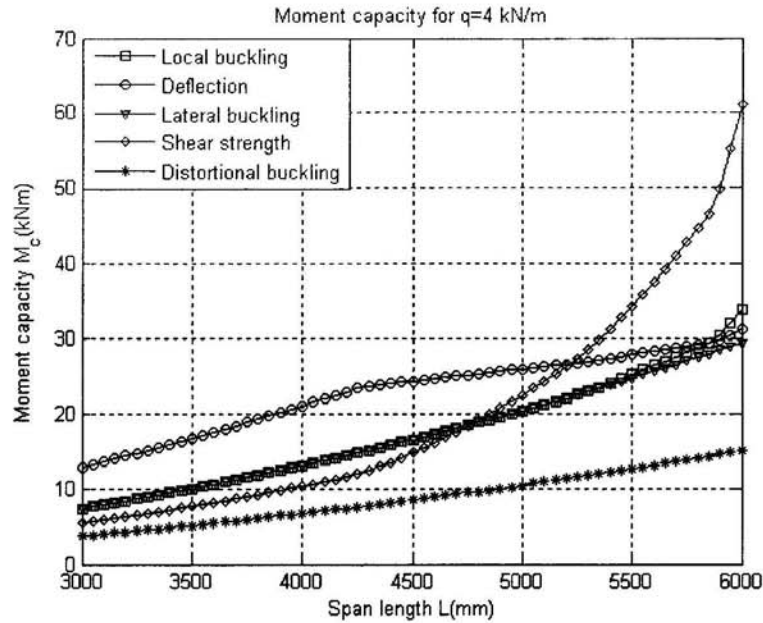


Fig. 6.26: Moment capacities of the optimised section over span length for unbraced zed beam based on BS 5950-5:1998 taking into account DB for $q=4\text{kN/m}$.

Figs. 6.24 to 6.26 show the moment capacity of section under 5 different design constraints. Fig. 6.24 shows that when $q = 2\text{kN/m}$ the optimum moment capacity is obtained when three failure modes of local buckling, lateral-torsional buckling and distortional buckling coincide. When the load increases to 3kN/m , distortional buckling mode controls the moment capacity, lateral-torsional buckling and local buckling still occur at the same as can be seen in Fig. 6.25 and Fig. 6.26. The behaviour of section through the optimisation process is investigated. In terms of structure design, the structural engineer will know which design criterion controls the capacity of the section. The designer can strengthen the section by putting more internal restraints or stiffeners to prevent the failure of section.

6.4 CONCLUSION

The result of optimum dimensions of the simply supported zed purlins which are subjected to the uniformly distributed vertical load with no restraints at the middle of

span under different loads intensities have been presented. The optimisation programme is performed for two cases with and without considering distortional buckling based on BS 5950-5:1998. It was found that the optimum thicknesses for both cases with different loads intensities are very similar. It indicates that the distortional buckling has a slight influence on the thickness of section. On the contrary, the distortional buckling affects the other dimensions of the section such as the depth of web, the width of flange and depth of lip. Furthermore, we realise that the optimum section is controlled by the moment of distortional buckling when this is considered in the design calculation.

In conclusion, the global optimum dimensions are found and the behaviour of section during the optimisation process is investigated. They can be used for a quick design for the structural engineer. For other standards or other design criteria such as with intermediate restraints etc., the optimisation programme can easily be amended to find the global optimum dimensions.

Chapter 7

7 OPTIMISATION OF THE SIGMA PURLIN SECTION

7.1 BEHAVIOUR OF A SINGLE SPAN SIGMA PURLIN

7.1.1 Introduction

In this chapter, the behaviour of Σ -shape purlins with one axis of symmetry is investigated. The purlins are simply supported beams subjected to uniformly distributed loads. The dimensions of the cross section are shown in Fig.7.1, in the figure, b_o is the width of the flange, c_o is the depth of the lip, h_o is the total height of the cross section, h_1 is the distance of the web stiffener to the top and bottom flange, h_2 is the depth of the stiffener in the plane of the web, d_s is the depth of the web stiffener perpendicular to the web plane. The parametric studies focus on the effects of position and size of the web stiffener on the section's strength capacity based on the finite strip method CUFSM by Schafer (2001). After an investigation of the size of the web stiffener, the size of the stiffener will be used in the optimisation programme.

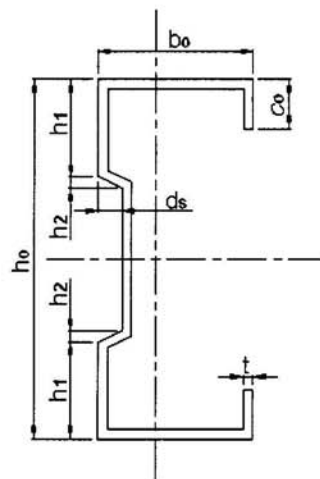


Fig.7.1: Dimension of the cross-section of the Σ -shape purlin.

7.1.2 Effect of the depth of the web stiffener in the plane perpendicular to the web on local buckling

To investigate the effect of the depth of the web stiffener in the plane perpendicular to the web, we perform a local buckling analysis based on the finite strip method CUFSM of the sample section with the dimension of a total height h_o of 300mm, the width of the flange b_o being 75mm, h_1 being 100mm and h_2 being 10mm, the ratio between d_s and width of the flange is 0.1, 0.15, 0.2, 0.3, respectively.

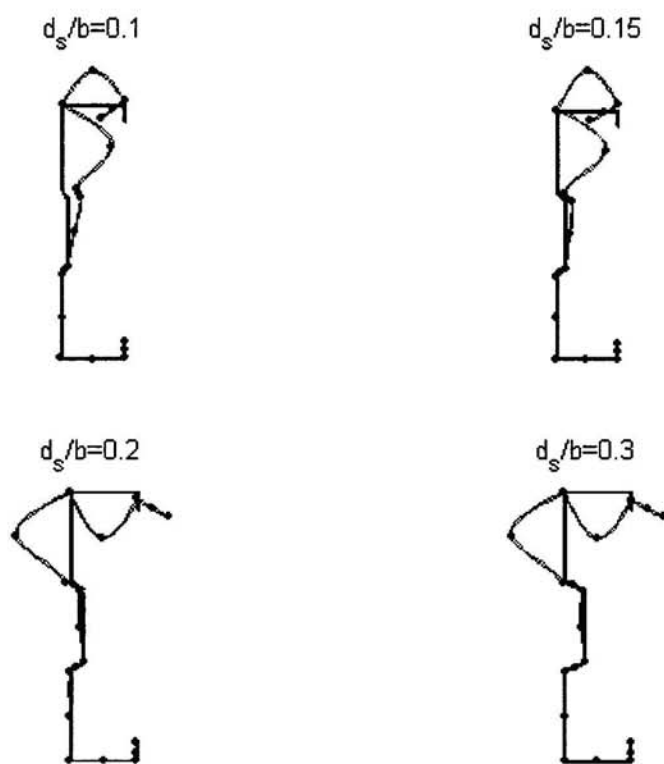


Fig. 7.2: Effect of the depth of the web stiffener on local buckling mode shape.

After running analysis for the different modes of failure from 1 to 30 and it can be seen that when depth of the web stiffener is not sufficient long identified by the ratio between d_s to b_o as 0.1, 0.15, respectively, the compression part of the web buckles as an element and the web stiffener does not work properly as like a true stiffener, while with the ratios d_s to b_o are over 0.2, the two compression part of the web

buckle locally between the web stiffener. Thus, the web stiffener works effectively as a true stiffener.

Fig. 7.3 plots the stress factor curves of the sections with different d_s . It can be seen that the deep web stiffener has higher stress factor than that of the shallow web stiffener. Thus, the web stiffener has influence on the resistance of the section.

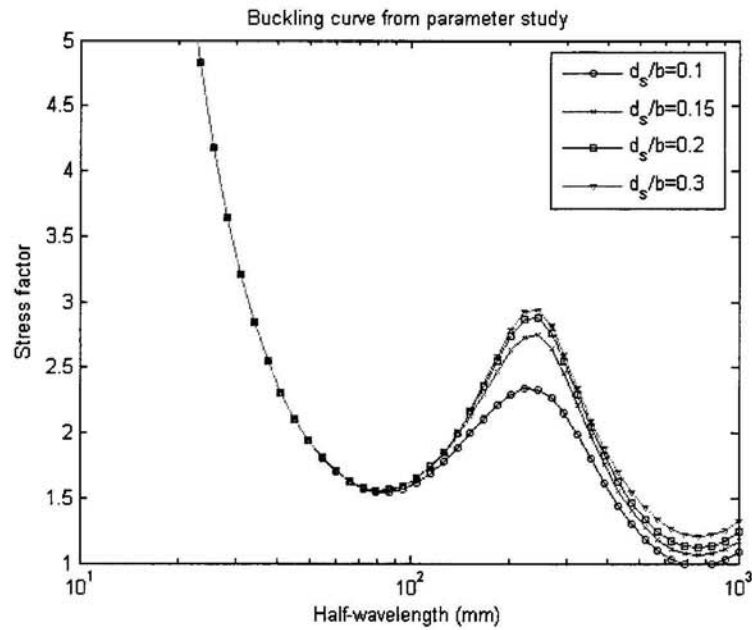


Fig. 7.3: Effect of the web stiffener on the load factor of the sigma purlin section.

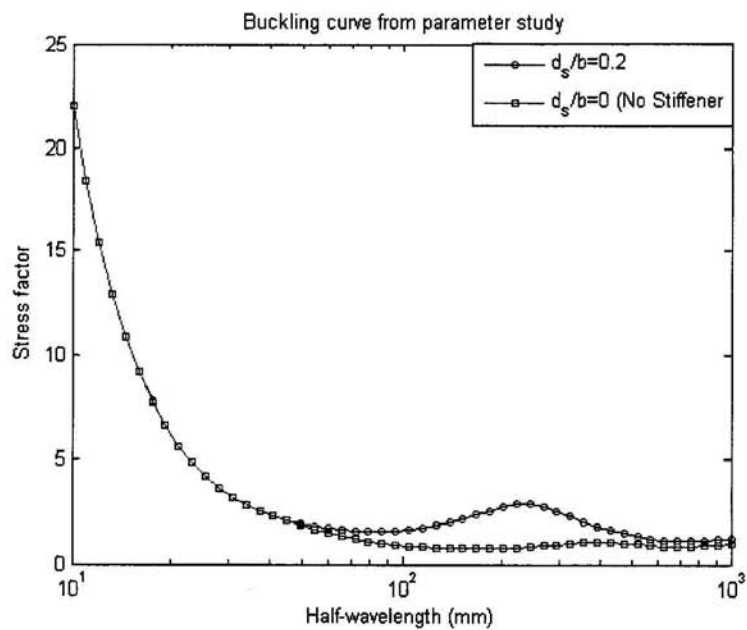


Fig. 7.4: Comparison between section with stiffener and without stiffener.

Fig. 7.4 illustrates the comparison of the stress factor between a section with and without the web stiffener. As can be seen from Fig. 7.4, the stress factor of section with the web stiffener is twice higher than that of the section without the web stiffener at the half wavelength from 100mm to 600mm.

7.1.3 Effect of the depth of web stiffener in plane of web on local buckling resistance

After determining the most efficient depth of the web stiffener perpendicular to the web which is over one fifth of the flange width, we perform the analysis of the section with fixed d_s , h_2 of the web stiffener varies from 10 to 30mm with step 5. The shapes of buckling section with the variation of h_2 are illustrated in Fig.7.5.

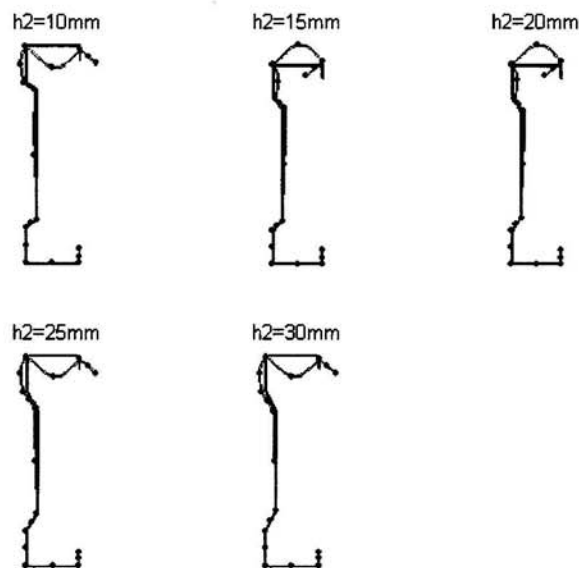


Fig.7.5: Buckling mode shape of the section with h_2 from 10 to 30mm.

From Fig.7.5, it is seen that, with the $h_2 > 20\text{mm}$, the buckling mode tends to change from local buckling to distortional buckling of the whole compression part of web.

While with a small value of h_2 such as 10mm, the local buckling occurs only on the parts above and below the web stiffener, the web stiffener is stable.

In conclusion, the value of h_2 should be small enough to avoid the web distortional buckling mode. The conventional elastic distortional buckling stress is also lower when the web distortional buckling mode occurs.

7.2 DESIGN OF SIGMA SECTION PURLIN BASED ON BS 5950-5:1998

7.2.1 General

Similar to channel and zed purlin sections, there are several factors which govern the resistance of sigma sections such as the deflection of section, the stability of section identified by local buckling, distortional buckling and the lateral-torsional buckling. The influence of section dimensions on each factor is investigated next.

7.2.2 Determination of moment capacity based on the local buckling

Local buckling occurs on the compression part of section such as the compression flange and the compression part of the web. In clause 5.2.2.2 of BS 5950-5:1998, it is indicated that in the case of sections which have stiffened webs or bending elements, the moment capacity should be determined on the basis of a limiting compressive stress in the web, p_o . This stress is used in evaluation of the effective width of the compression flange and the compressive lip. Hence, the reduced section properties and moment capacity are determined. The detailed procedure of calculation of the effective section based on BS 5950-5:1998 is presented in Section 4.3.1. Fig. 7.6 shows the model of calculating effective section of sigma section.

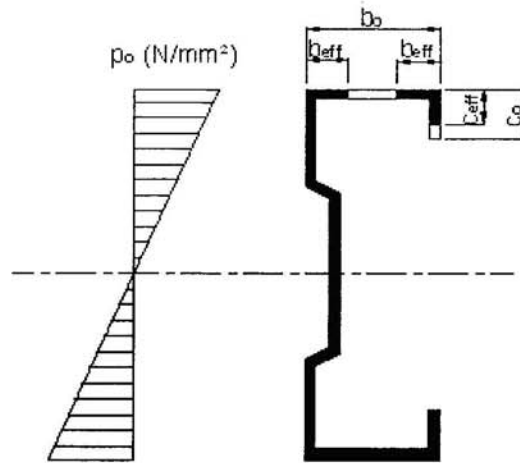


Fig. 7.6: Effective section of the Sigma purlin.

7.2.3 Effect of dimensions changes on the moment capacity

In order to investigate the effect of dimensions changes on the moment capacity of section, we perform the analysis of sections with h_o of 250mm and b_o varies in the order 50, 60, 75mm, respectively and the position of web stiffener, h_1 varies from 20 to 70 with 5mm increments. As shows in Fig. 7.7, the symbol h250-50-20-2 defines the dimensions of section as total depth of web, width of flange, depth of lip and the thickness, respectively. Fig. 7.7 shows the effect of position of web stiffener to the moment capacity of section. It is seen that the position of the web stiffener has a slight influence on the moment capacity. Following BS 5950-5:1998 the moment capacity is determined on the basis of the limiting compressive stress in the web, thus the full length of compressive web is considered. On the contrary, the influence of b_o on the moment capacity is quite important. The moment capacity increases with the increase of b_o , because the effective width of the flange increases significantly.

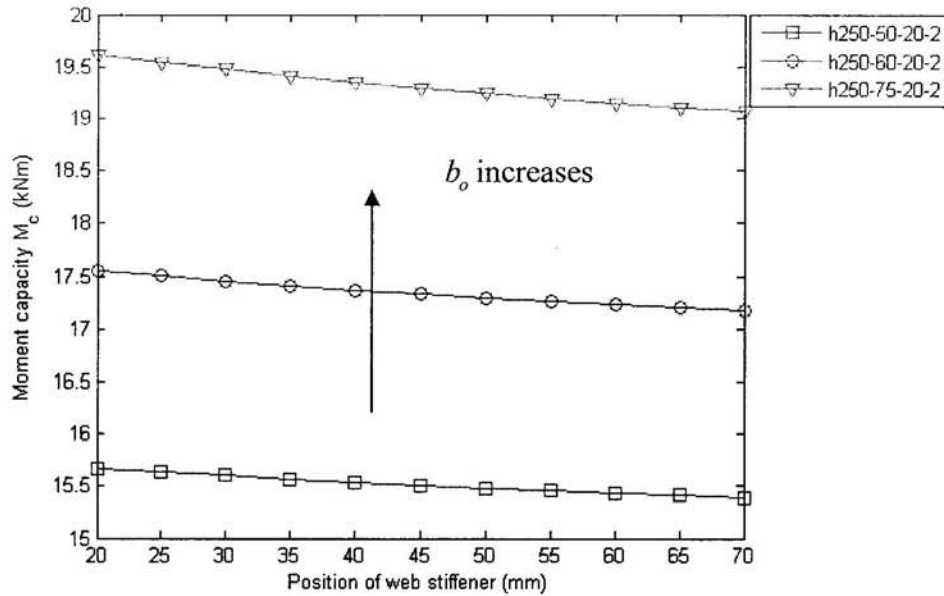


Fig. 7.7: Effect of position of web stiffener on the moment capacity.

7.2.4 Calculation of lateral-torsional buckling of sigma section

A slender beam under the action of a bending load in the plane of maximum flexural rigidity can buckle by combining a twist and a lateral movement of the cross section, unless it has continuous lateral restraints. Slender beam is manufactured from a narrow rectangular plate to form the section as channel section, zed section and sigma section. These sections have narrow flanges, which lack of both lateral flexural rigidity and torsional rigidity, and when the beams have no restraints or are restrained intermittently only, they may buckle under bending stresses considerably lower than yielding stress of the material. The low torsional rigidity is an important factor, thus the thin-walled open section, for instance channel or zeds and sigma section are also susceptible to the instability. In almost, all methods design like BS 5950-5:1998, AISI, the elastic lateral-torsional buckling moment resistance is used to calculate the nominal lateral-torsional buckling moment resistance of the open section. The elastic lateral-torsional moment depends on a lot of factors such as the type of load, loading

position, the shape of section and the lateral end restraints or intermediate lateral restraints. For this study, we only consider the simply supported purlins under the uniformly distributed vertical load applied through the shear centre, the elastic lateral-torsional buckling moment can be computed from (Allen, 1980).

$$M_e = 1.13 \frac{\pi}{l} \left[\frac{E.I_1.G.J}{\gamma} \right]^{1/2} \left[1 + \frac{E.C_w.\pi^2}{G.J.I^2} \right]^{1/2} \quad (7.1)$$

where: l : span of the purlin

E : modulus of elasticity of steel

I_1 : major second moment of section

I_2 : minor second moment of section

G : Shear modulus of steel

J : St Venant torsion constant of section

C_w : Warping constant of section

$$\gamma = \left(1 - \frac{I_2}{I_1} \right)$$

7.2.5 Comparison of the lateral-torsional buckling results

In this section, we will perform the comparison between the two design methods of lateral-torsional buckling by BS 5950-5:1998 and the direct strength method (DSM) proposed in AISI. From Fig.7.8, we realise that the flange improves significantly the lateral-torsional buckling moment resistance due to the increase of torsion rigidity of section. Also can be seen from Fig. 7.9, when the web stiffener moves toward the neutral axis of the section, the lateral-torsional moment increases up to maximum value at 90mm wide of b_o for DSM and at 110mm wide of b_o for BS 5950-5:1998 and then decreases. It indicates that it exists at a position of web stiffener at which the maximum lateral-torsional moment of the sigma section can be reached. From Fig.7.8

and 7.9 the results using BS 5950-5:1998 are always below than those using by DSM. It indicates that BS 5950-5:1998 results are more conservative than the direct strength method and are therefore safer.

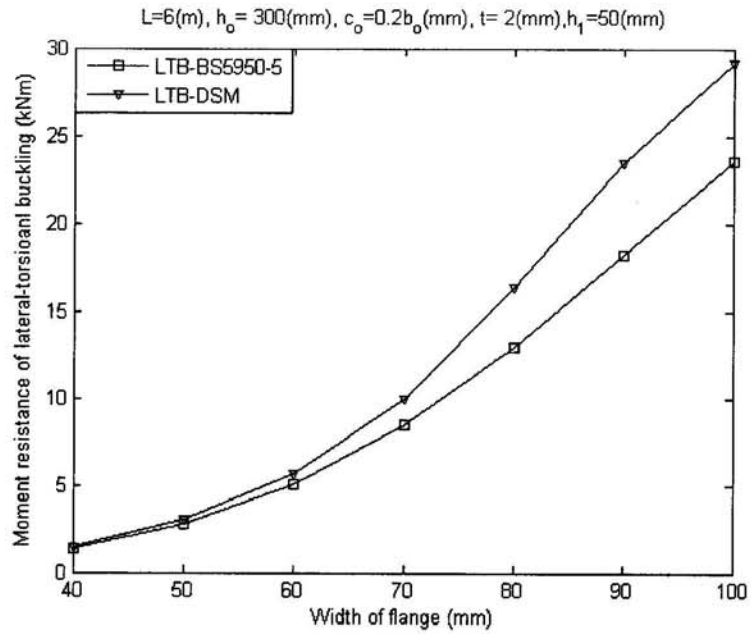


Fig.7.8: Effect of the flange to the lateral-torsional buckling.

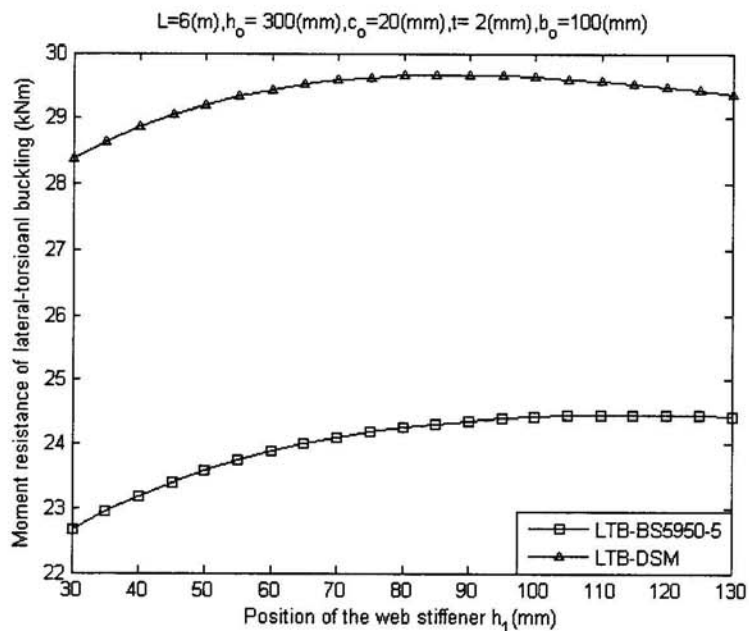


Fig. 7.9: Effect of the position of the web stiffener.

7.2.6 Distortional buckling

To understand the distortional buckling behaviour of simply supported sigma purlins subjected to the uniformly distributed vertical load, we employ the programme CUFSM of Schafer (2002) to investigate the shape mode of distortional buckling of sigma section. In this section, we execute the numerical studies with four different sections, with $h_o = 300\text{ mm}$ and $h_1 = 75\text{ mm}$, $h_2 = 10\text{ mm}$, $d_s = 0.2b_o$, b_o varies in range of 75, 85, 95, 105mm, respectively.

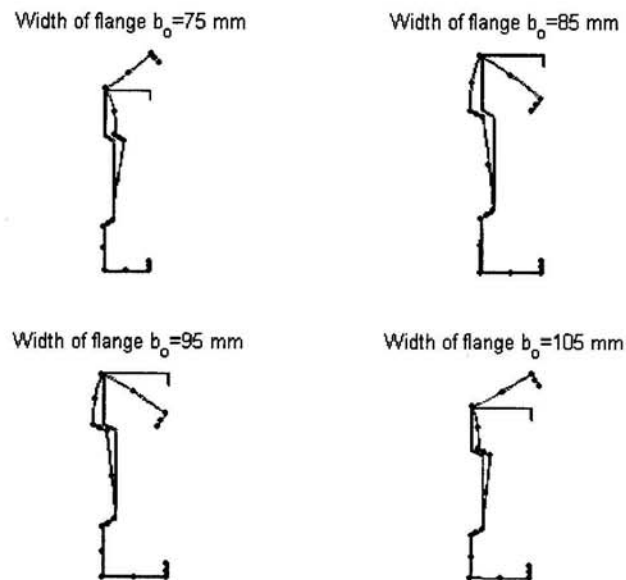


Fig. 7.10: Distortional buckling shape mode of sigma section.

From Fig. 7.10, we found that the compression flange tends to rotate around the intersection between the compression flange and the compression part of web. Therefore, the distortional buckling calculation model by Hancock's model (1995) or Schafer and Pekoz (1999) for channel section or zed section are still applicable for sigma sections. For sigma sections, because of the appearance of the web stiffener, the distortional buckling can happen on the compression part of the web. However, as the

investigation in Section 7.1.2, in order for the web stiffener to work as an efficient stiffener which can stay stable during the buckling process, the minimum length required of the web stiffener is 0.2 times of b_o . Consequently, the failure mode of distortional buckling of the sigma section involves only the rotation of the compression flange around the junction between the compression flange and the web. The models calculation of distortional buckling by Hancock's model (1995) or Schafer and Pekoz's model (1999) are presented in Chapter 4.

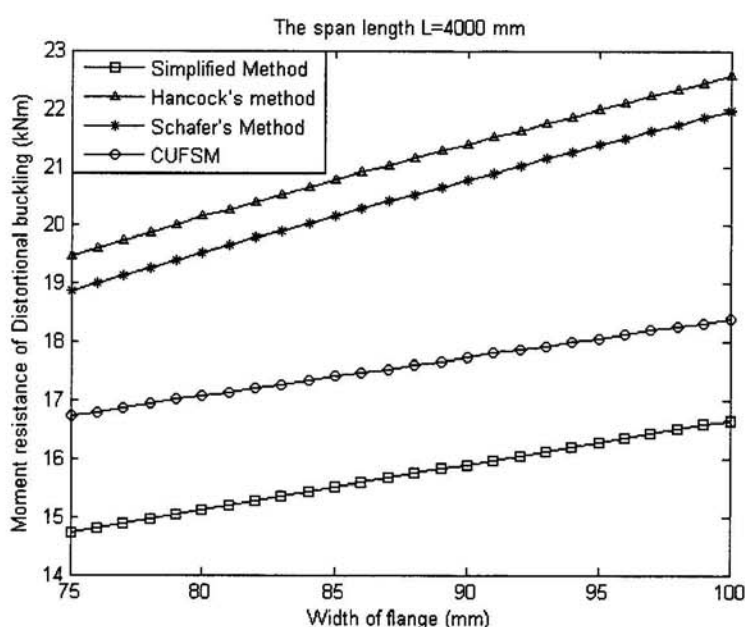


Fig.7.11: Effect of the flange width on distortional buckling of sigma section calculated by direct strength method.

Fig.7.11 illustrates the effect of b_o on the moment resistance of distortional buckling calculated by DSM in which the elastic distortional buckling moments are computed by different approaches such as CUFSM programme (2002), Hancock's approach (1995), Schafer and Pekoz'(1999) approach and simplified method of Yu (2005). The investigation is performed on the sample sigma section with 4m span length. From Fig.7.11, we found that in all methods b_o contributes significantly to the distortional

buckling strength of the section. And the simplified method of Yu (2005) gives the most conservative result. In terms of the safety aspect and practical engineering purposes, the simplified method of Yu is preferable to use.

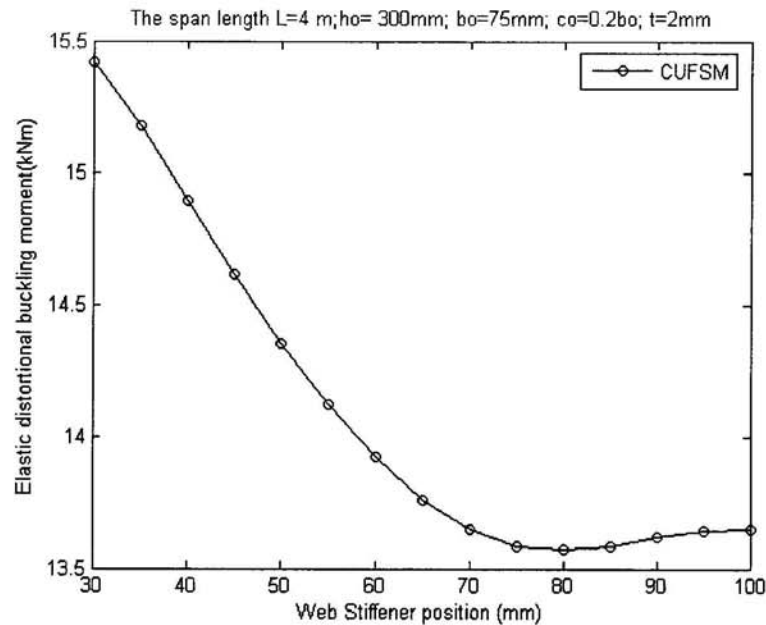


Fig.7.12: Effect of web stiffener position on the elastic distortional buckling strength.

In order to investigate the effect of the web stiffener location on the elastic distortional buckling, we use the finite strip method CUFSM (2002) to calculate the elastic distortional buckling moment. From Fig.7.12, it is said that when the web stiffener move downward to the neutral axis of section, the elastic distortional buckling decreases 15%. It proves that the web stiffener has an important influence on the distortional buckling strength of sigma sections. Thus, for the optimisation programme, we will find out the optimum location of web stiffener and also b_o to obtain the maximum distortional buckling capacity of sigma section.

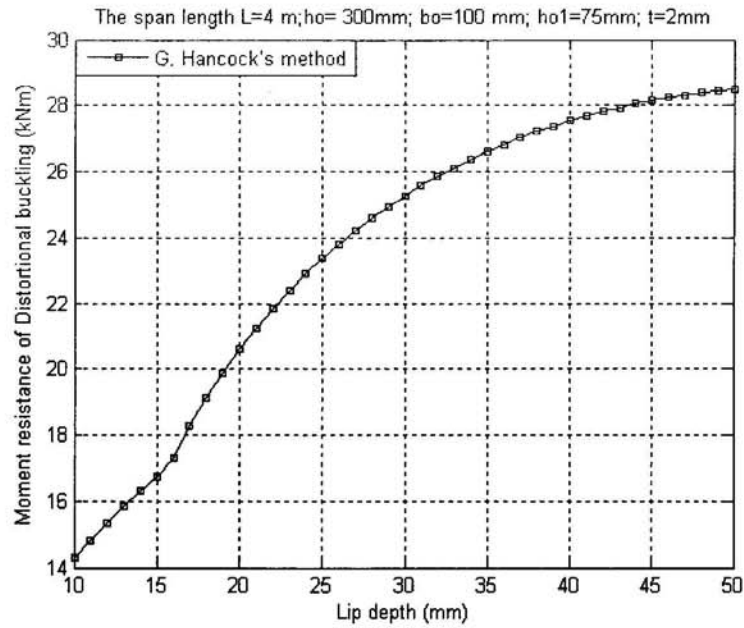


Fig. 7.13: Effect of depth of lip on the distortional buckling resistance.

Fig. 7.13 shows the effect of lip depth on the distortional buckling resistance. It can be seen that the depth of lip helps to improve the distortional buckling resistance of the section with the increase of the depth of lip, but when the ratio c_o/b_o is over 0.5, the beneficial contribution of lip depth decreases quickly. In order to understand the interaction between the elements of section, the CUFSM programme is used to investigate the effect of the lip on the elastic moment distortional buckling. In the CUFSM analysis, the whole section is modelled and so that it depicts a more realistic picture of section behaviour. Fig. 7.14 demonstrates that the depth of lip assists to increase the distortional buckling resistance at 15 to 30mm lip depth and after that the lip does not contribute to increase distortional buckling any more. It can be explained that when the depth of lip increases, at the first stage the lip will help to improve the distortional buckling of flange and then when the depth of lip reaches the limited length as 31mm at which the distortional buckling of itself starts to occur. It leads to the decrease of distortional buckling of the whole section.

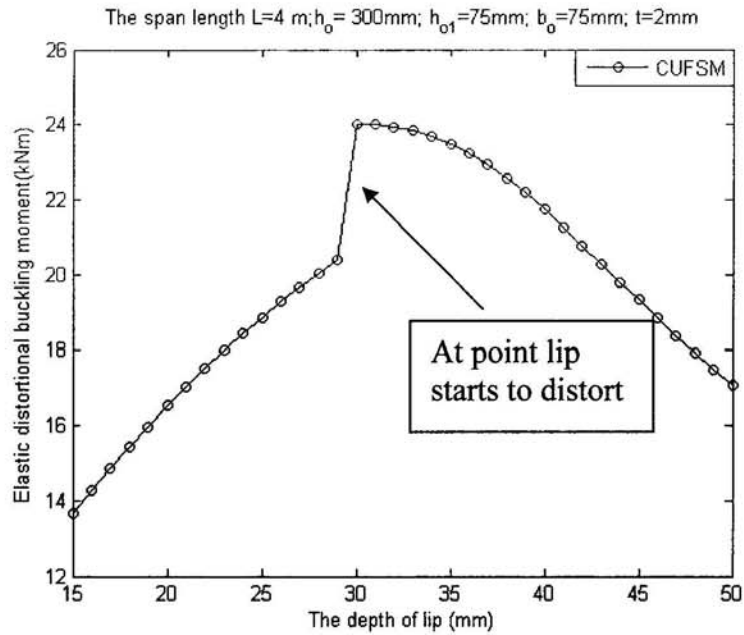


Fig. 7.14: Effect of lip depth on the distortional buckling strength.

7.3 OPTIMISATION OF SIGMA PURLIN

7.3.1 Selection of parameters

The optimisation of section is carried out for simply supported sigma beams subjected to a uniformly distributed vertical load varying from 2 to 4kN/m with the span length between 3 and 6m. The modulus of elasticity and yield strength of steel are taken as $E = 205$ GPa and $p_y = 350$ MPa . The optimisation problem is performed based on different design constraints. Firstly, we carry out the optimisation programme based on BS 5950-5:1998 in which local buckling, lateral-torsional buckling and deflection constraint and shear strength at the supports are considered. Hence, due to the lack of calculation of the distortional buckling failure of BS 5950-5:1998, we will consider the distortional buckling calculation in the optimisation programme based on the current approach by Hancock method, and the DSM presented in AISI.

7.3.2 Optimisation results based on BS 5950-5:1998

The thickness was found to not contribute too much to increase the strength capacity of section in Chapter 5 and 6. Comparing with channel section in Chapter 5, the thickness of sigma section has the similar trend as channel section, but slightly thinner than that of the channel section. It is due to the fact that the appearance of the web stiffener does help to increase the strength capacity of section. It leads to a slow increase of the thickness as shown in Fig.7.15.

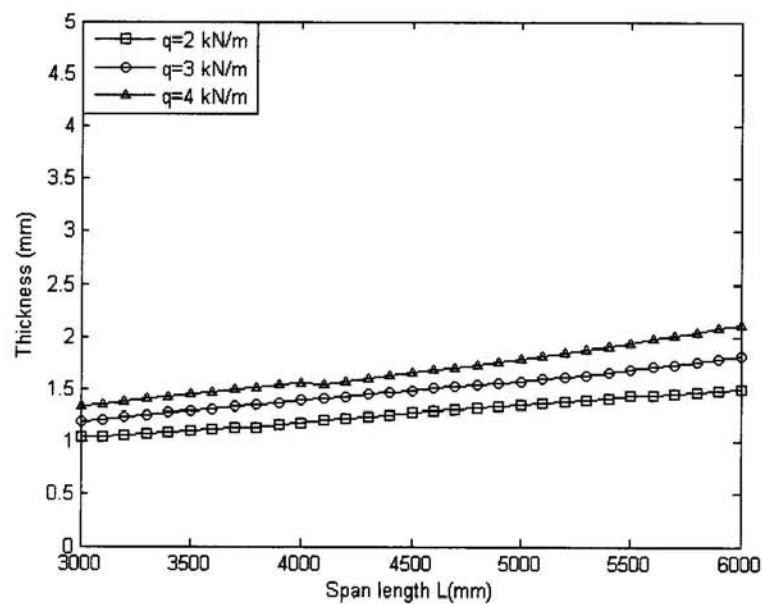


Fig.7.15: Global optimum design thickness versus span length for un-braced sigma beams based on BS 5950-5:1998.

Fig. 7.16 shows the optimum h_o versus span length for un-braced beams based on BS 5950-5:1998. Comparing the optimum h_o of channel and sigma sections which are designed based on BS 5950-5:1998, we discover that h_o of two sections are very similar even with the existence of web stiffener in sigma section. It indicates that the depth of web in the sigma section makes a significant contribution to the strength of section. Fig. 7.17 plots the optimum b_o versus span length for un-braced beams. On the contrary, it can be seen from Fig.7.17 that b_o of sigma section increases more

slowly than that of channel section, for instance with the largest load case 4kN/m the width of flange of channel increases and attains 100mm at span 5.2m, but in the sigma section the flange width increase gradually and reaches the value of 100mm wide at span 6m. Therefore, there is a balance between h_o and b_o in sigma section. Logically, in sigma section h_o should be smaller than that of channel section because of having web stiffener. However in fact, b_o of sigma section is smaller than that of channel section. It demonstrates that in sigma section with the help of web stiffener, the stiffness of section tend to move toward the web part, b_o increases more slowly to prevent local buckling in the compression flange.

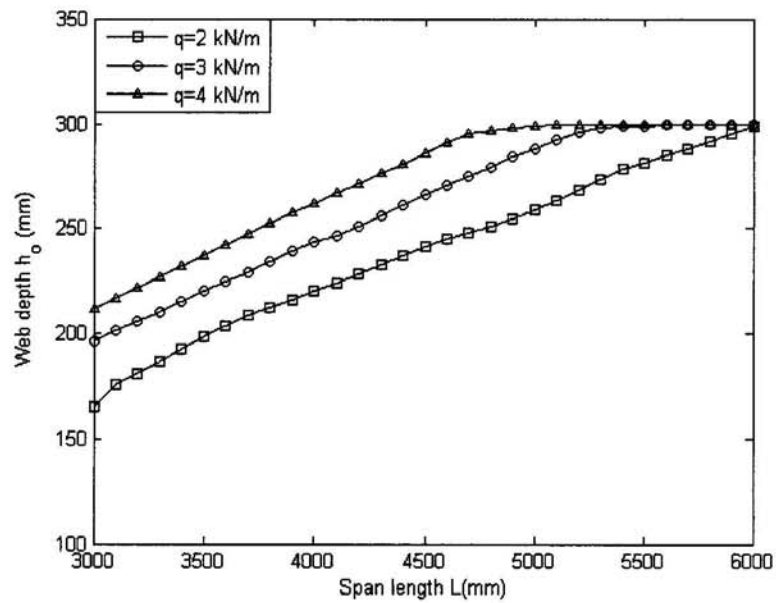


Fig.7.16: Global optimum design web depth versus span length for un-braced sigma beams based on BS 5950-5:1998.

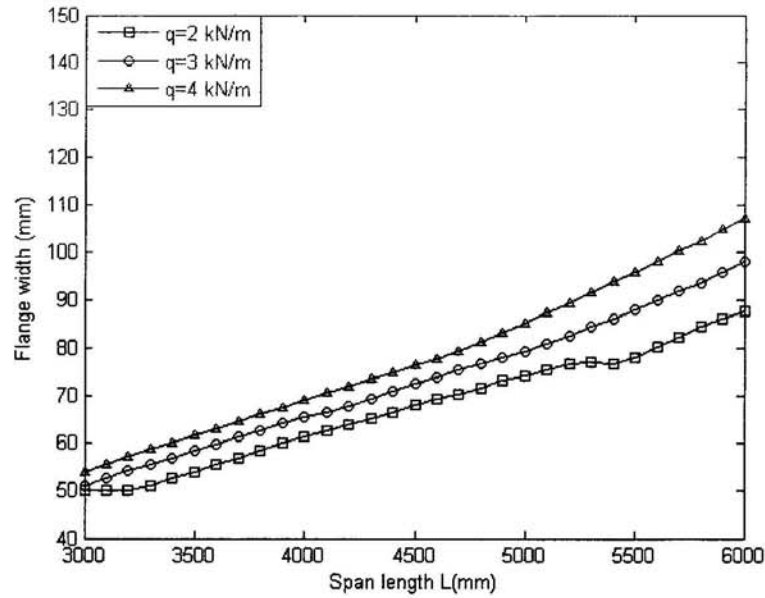


Fig.7.17: Global optimum design flange width versus span length for un-braced sigma beams based on BS 5950-5:1998.

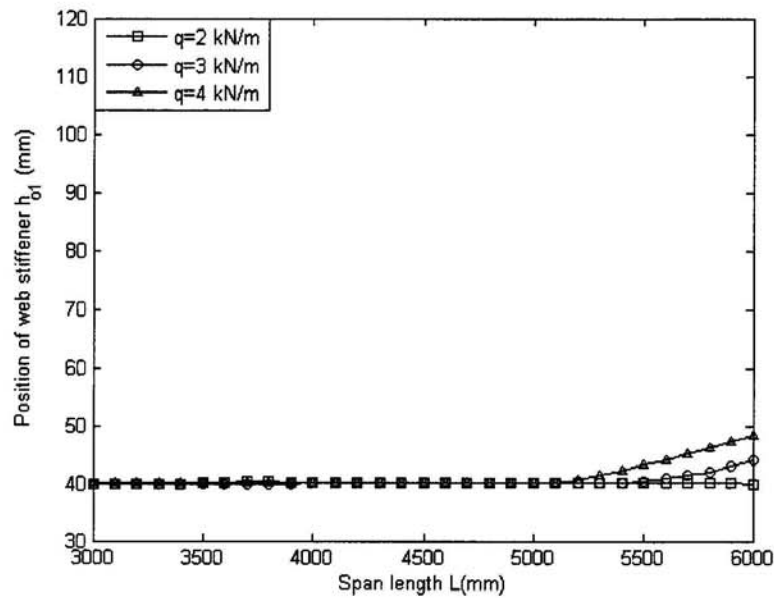


Fig.7.18: Global optimum design position of web stiffener in plane of web versus span length for sigma beams based on BS 5950-5:1998.

Fig.7.18 presents the optimum position of web stiffener. For all three load cases at the span from 3 to 5m, the position of the web stiffener does not change. It indicates that for small span the location of web stiffener does not affect the resistance of section, but when the span increases over 5m the bending moment increases and the

compression stress in the web will increase also. In order to prevent local buckling in the compression part of web, the web stiffener starts to move towards the neutral axis of section to prevent the local buckling.

Fig.7.19 shows the optimum depth of web stiffener, it was found that d_s increases gradually with the increase of span length and the load intensity. However, d_s does not reach to the upper bound of d_s . The optimisation programme found the optimum d_s which performed effectively the role of stiffener.

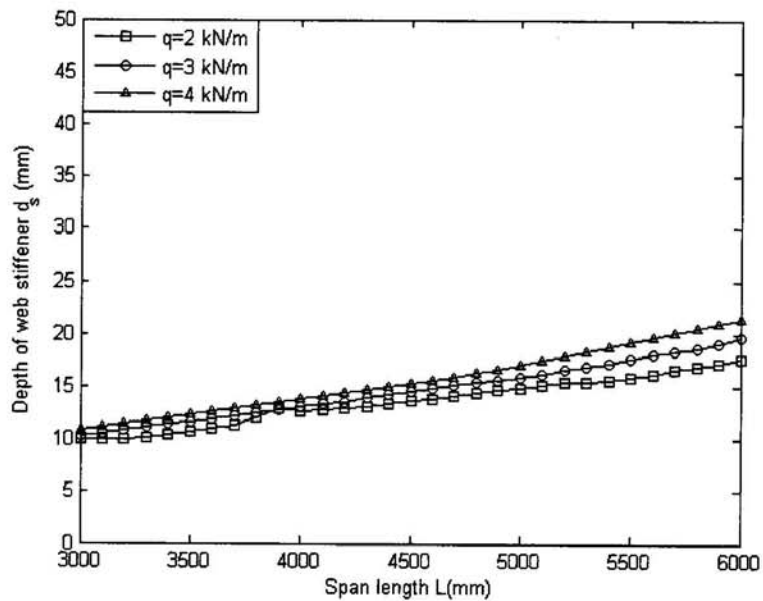


Fig.7.19: Global optimum design web stiffener depth versus span length for sigma beams based on BS 5950-5:1998.

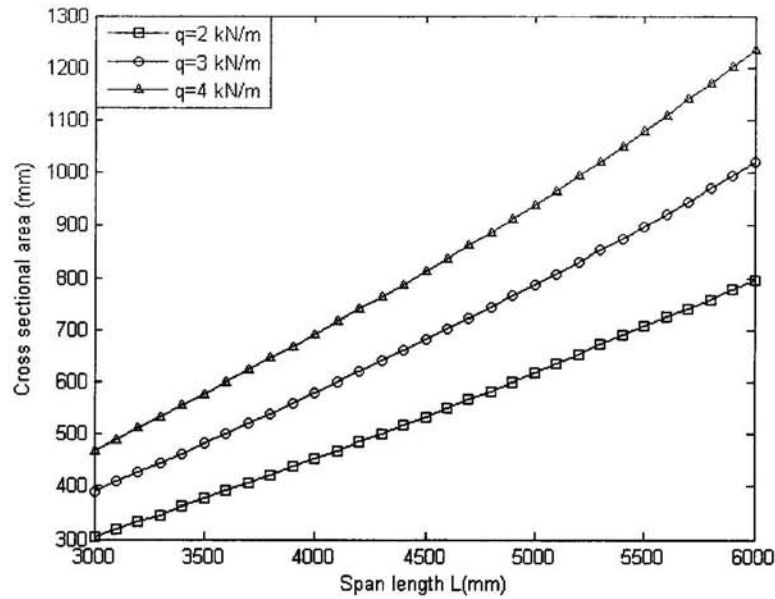


Fig.7.20: Optimum cross sectional area versus span length for sigma beams based on BS 5950-5:1998.

Comparing Fig.7.20 and Fig. 5.20, it is said that sigma section can save more material than channel section with the same load condition and the same span length. For example, at the load case of 4kN/m and 6m span length the cross sectional area is about 1400mm² for a channel section, while with the same conditions the cross sectional area is about 1250mm² for a sigma section. In conclusion, in terms of saving material a sigma section is found to be more economical than that of the channel section.

Fig.7.21 to 7.23 present the behaviour of simply supported sigma purlin subjected to uniformly distributed vertical load for three different load cases. It can be seen that the shear resistance of the section is always higher than other resistance. The optimum sections are not controlled by the shear resistance. However, the optimum sections are governed by local buckling and lateral-torsional buckling. When load intensity and span length increase, the deflection criterion becomes active and controls the optimum section, for instance when the span above 5.5m as can be seen in Fig.7.23. As

mentioned in Chapter 2, the ideal section occurs when all failure modes occur at the same time, but it is impossible to obtain that section due to the limit of the geometrical constraint. In this study, the local buckling and the lateral-torsional buckling occur at the same time.

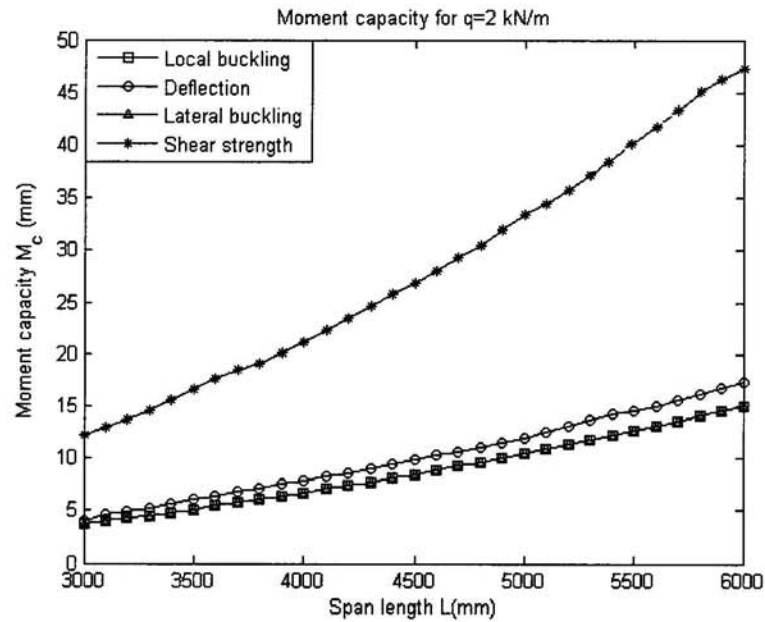


Fig.7.21: Moment capacity of the optimum section versus span length for sigma beam based on BS 5950-5:1998 for $q=2\text{kN/m}$.

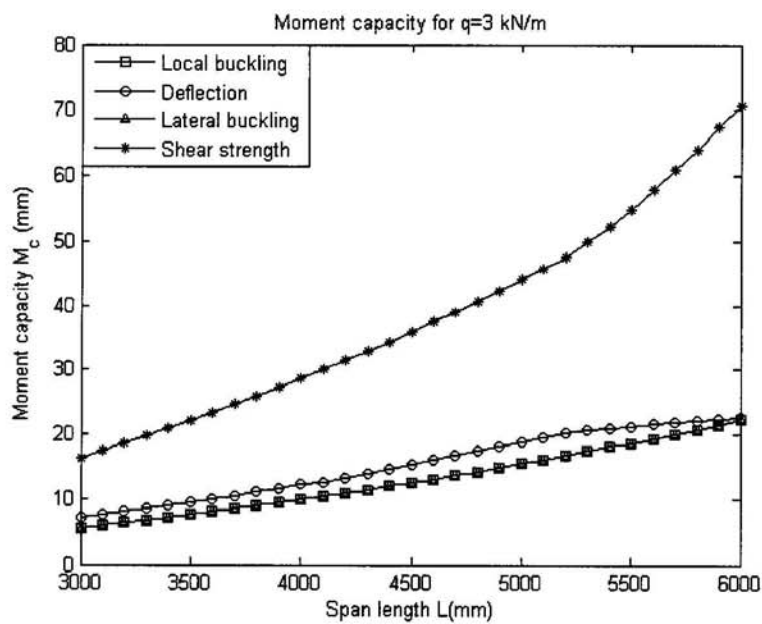


Fig.7.22: Moment capacity of the optimum section versus span length for sigma beam based on BS 5950-5:1998 for $q=3\text{kN/m}$.

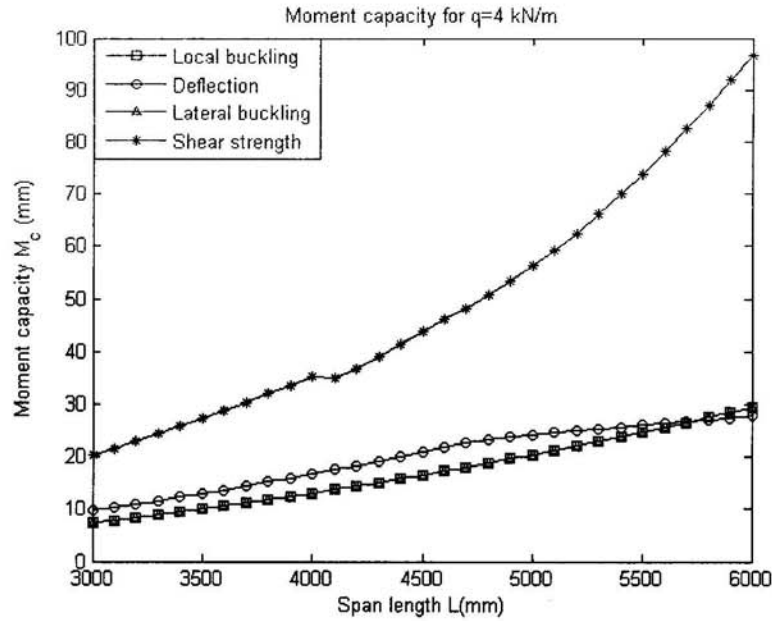


Fig.7.23: Moment capacity of the optimum section versus span length for sigma beam based on BS 5950-5:1998 for q=4kN/m.

7.3.3 Optimisation result based on BS 5950-5:1998 and considering distortional buckling

Fig.7.24 shows that the thickness of sigma section changes very slightly in both cases considering the distortional buckling and not considering the distortional buckling. It is similar to channel and zed section, the thickness does not help to improve the strength resistance of section very much.

Fig. 7.25 shows the difference of optimum h_o between sections with and without distortional buckling, it can be seen that there is slight difference of the optimum h_o in two cases. h_o increases slightly and more quickly when distortional buckling is considered. It is because in the analytical model of distortional buckling, the flange width keeps the most important role in the model, while h_o only contributes to the rotational spring stiffness at the junction between the flange and the web.

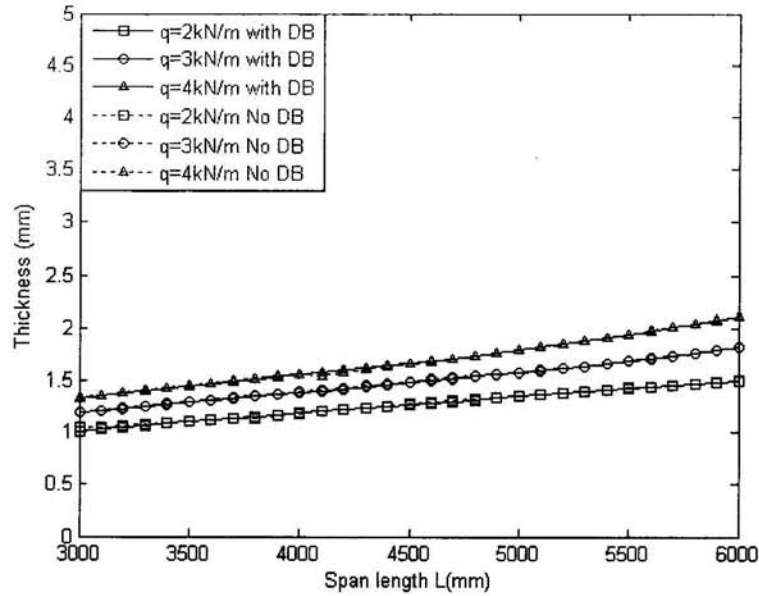


Fig.7.24: Optimum design thickness of sigma section with and without distortional buckling (DB).

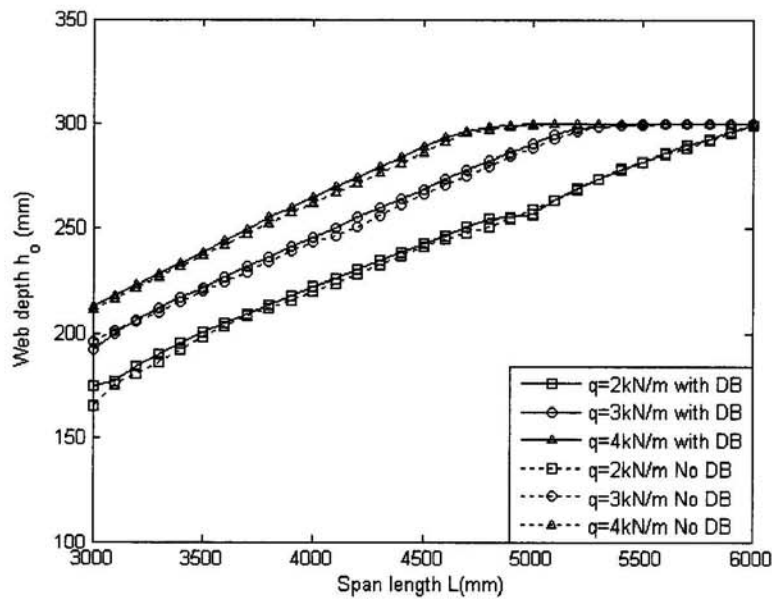


Fig. 7.25: Optimum design web depth of sigma section with and without distortional buckling (DB).

In contrast to h_o , the width of flange increases more slowly when the distortional buckling is considered. This is due to the fact that with the existence of the web stiffener, the compression part of web is much stiffer and the stress redistributes to the

web. Furthermore, b_o has a tendency to increase to the optimum value at which the distortional buckling resistance is maximum value. If b_o is over this value, the distortional buckling resistance of the section will decrease.

The position of web stiffener h_{o1} is not active until the span length increases to over 5m. It indicates that over 5m span length, the compressive stress in the web above neutral axis increase considerably due to the increase of bending moment, and the web stiffener tends to move toward the neutral axis to avoid local buckling occurring in the compression part of the web. The change of location of web stiffener is shown in Fig.7.27.

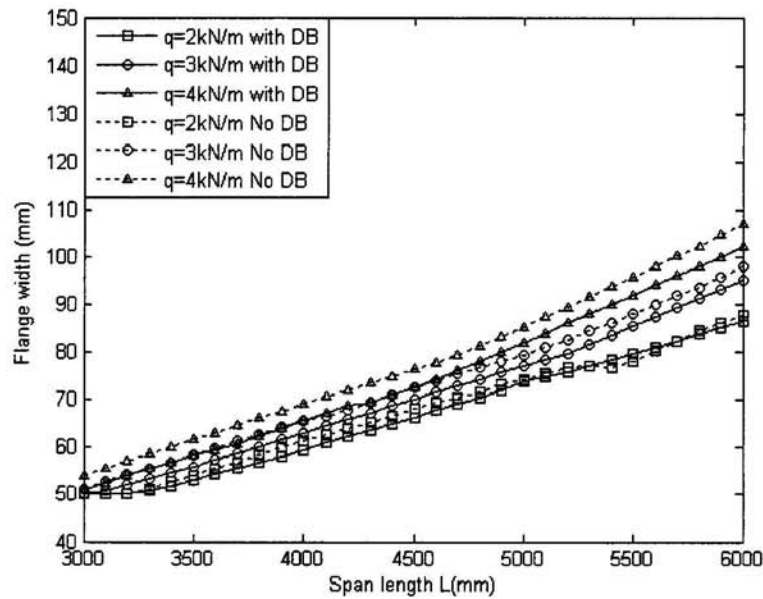


Fig.7.26: Optimum design flange width of sigma section with and without distortional buckling (DB).

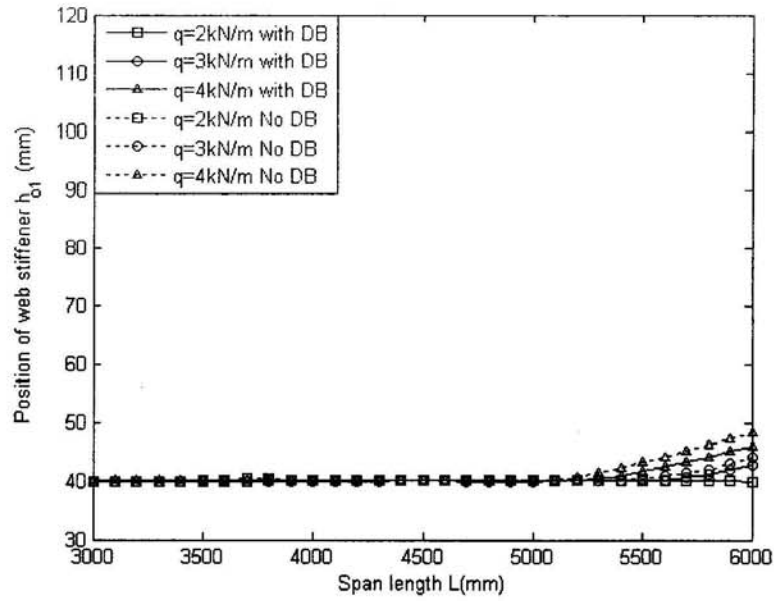


Fig.7.27: Optimum location of web stiffener of sigma section with and without distortional buckling (DB).

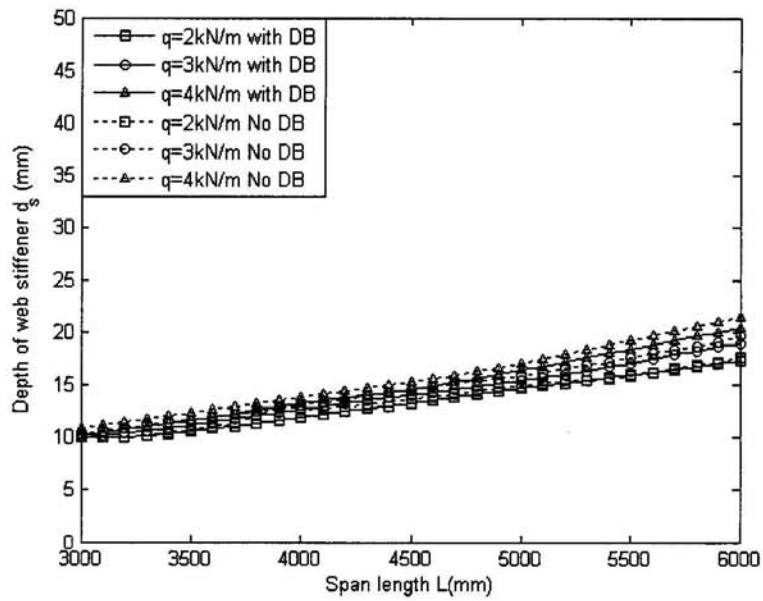


Fig.7.28: Optimum design depth of web stiffener of sigma section with and without distortional buckling.

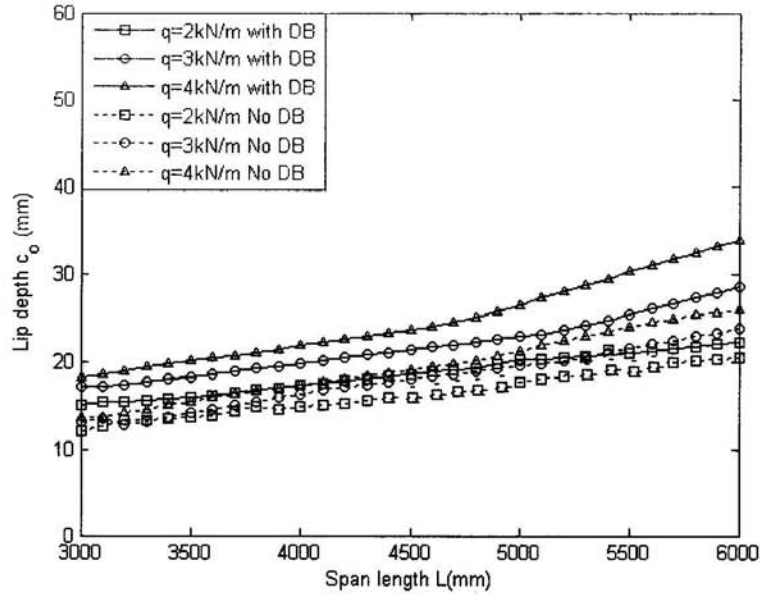


Fig.7.29: Optimum design depth of lip of sigma section with and without distortional buckling.

Fig.7.28 shows the optimum depth of web stiffener. The depth of web stiffener increases gradually with the increase of span length and load intensity. The same trend occurs with the depth of lip. However, c_o does not reach the upper bound value. It indicates that c_o attains the optimum depth.

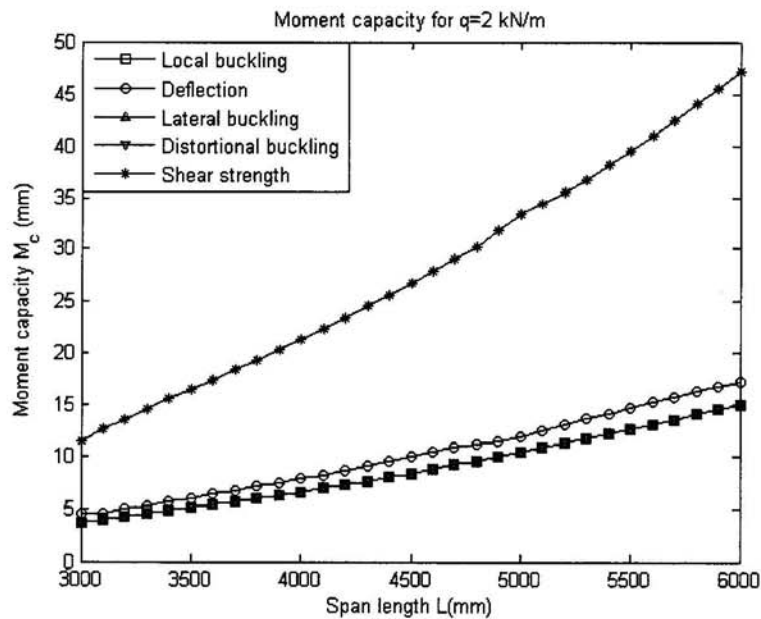


Fig.7.30: Moment capacity of the optimised section for un-braced sigma beams based on BS 5950-5:1998 considering distortional buckling for $q=2\text{ kN/m}$.

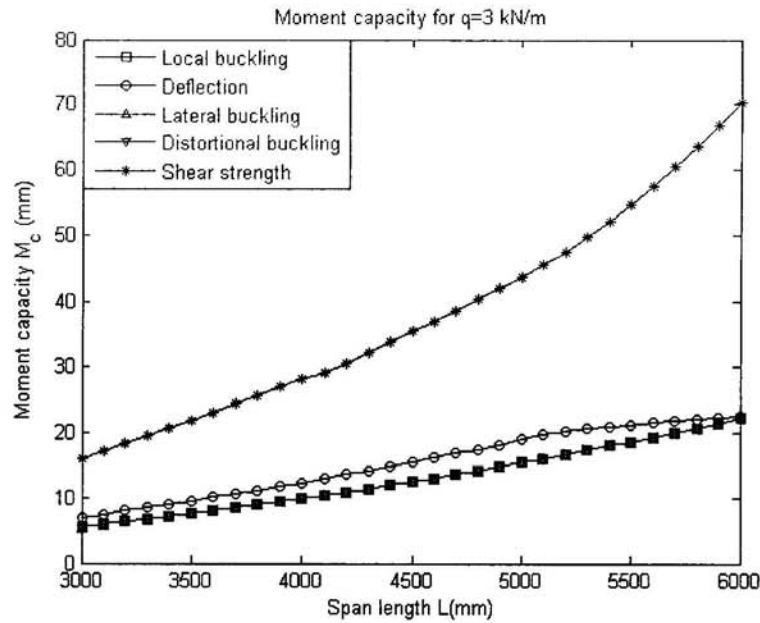


Fig.7.31: Moment capacity of the optimised section for un-braced sigma beams based on BS 5950-5:1998 considering distortional buckling for q=3kN/m.

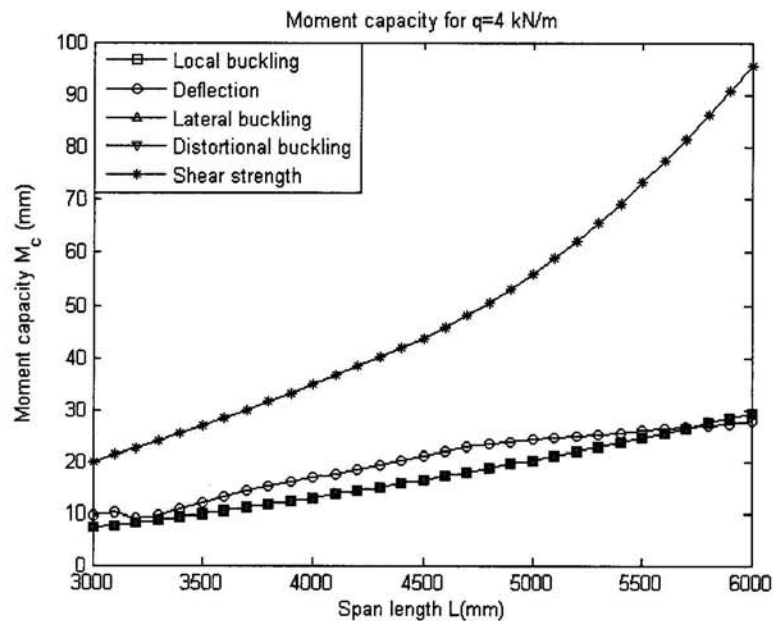


Fig. 7.32: Moment capacity of the optimised section for un-braced sigma beams based on BS 5950-5:1998 considering distortional buckling for q=3kN/m.

Fig.7.30 to 7.32 present the behaviour of section through the optimisation process and show design criterion which controls the strength of section. From the point of view of structural engineering, this information is very important because it will help

engineer to know which mode of failure will occur with section and to have engineering solution for individual case.

7.4 CONCLUSION

The optimum dimensions of a simply supported sigma beam subjected to uniformly distributed load are presented here. The objective function is the total cross sectional area which is minimised subjected to the five strength constraints identified by local buckling, deflection based on BS 5950-5:1998, lateral-torsional buckling following Allen (1980), distortional buckling calculated by DSM and the shear strength at the support. The lateral-torsional buckling and the local buckling are two criteria that mostly control the optimum result. Comparing the optimum cross sectional area of the channel section and the sigma section, we found that with the existence of the web stiffener, with the same load condition the area requirement of a sigma section is smaller than that of a channel section and a zed section. Hence, in terms of structure resistance and saving material, the sigma section is the best choice.

Chapter 8

8 CONCLUSIONS AND FUTURE RESEARCH

8.1 CHAPTER SYNOPSIS

This thesis has completed two main studies. Firstly, the investigations of the behaviour of cold-formed steel zed, channel and sigma sections of a simply supported beam subjected to the uniformly distributed load were performed. Secondly, the main aim of this thesis was to find a robust optimisation method and develop the optimisation programme to find the optimum section.

The essential work of this research has been predominately theoretical. Thus, the main methodology to perform the analysis and the investigation of the sections' behaviour as well as the optimisation procedure has been carried out using the computer programme MATLAB, which has involved an extensive range of theory development and formulation.

8.2 MATHEMATICAL MODELLING OF THE OPTIMISATION PROBLEM

Nowadays, optimisation has become a basic necessity in design activity across all major disciplines. The motivation to produce economically relevant products with embedded quality is the principal reason for optimisation. Optimisation is frequently associated with engineering design, especially so in civil engineering structures. To solve any specific optimisation problem, it is required to transform the problem into a mathematic model which can be solved by mathematical concepts as described in detail in Chapter 3. The optimisation of cold-formed steel sections is complicated by the complex and highly nonlinear nature of the rules that govern their designs. In this

thesis, the standard algorithm has been chosen for its robustness and iterative efficiency. To solve the inequality constraints of nonlinear optimisation of cold-formed steel sections, the Lagrange multiplier method and Kuhn-Tucker equation were employed.

8.3 DESIGN CONSTRAINTS OF OPTIMISATION

The optimisation problem of the cold-formed steel section is a highly nonlinear problem in which the objective function is a quadratic nonlinear function of the multi-design variables and the constraints are also inequally nonlinear. The constraints of the optimisation problem in the cold-formed steel section consist of strength, deflection and stability requirement as well as the practical geometric constraint of the design variables. For zed, channel and sigma section, the local buckling, distortional buckling and lateral-torsional buckling are given consideration, respectively. Currently, the local buckling resistance is based on formulae given in BS 5950-5:1998 and EN 1993-1-3:2006. For distortional buckling calculation used in the optimisation programme, the direct strength method employing the elastic distortional buckling is calculated by three available approaches, i.e Hancock (1995), Schafer and Pekoz (1998) and Yu (2005). In this thesis, the lateral-torsional buckling based on BS 5950-5:1998, AISI and analytical model of Li (2004) are employed.

8.4 OPTIMISATION RESULTS OF CHANNEL SECTION

The behaviour of channel shape cold-formed steel purlins is investigated in Chapter 5 using the optimisation computer programme developed in MATLAB. The investigations are carried out based on BS 5950-5:1998 with and without distortional buckling. The optimum dimensions of the simply supported channel beam which are

subjected to the uniformly distributed load with no restraint at the middle of span under different loading intensity are found. The following conclusions are made:

- Optimum thicknesses for both cases with different loading intensities are the same, which indicates that the thickness of the section has a slight influence on distortional buckling.
- On the contrary, the distortional buckling affects the other dimension of the section such as the depth of web, the width of flange and depth of lip.
- Furthermore, we realise that the optimum section is controlled by the moment of distortional buckling when distortional buckling is considered in the design calculation.

8.5 OPTIMISATION RESULTS OF ZED SECTION

The same procedure of optimisation is applied to zed sections and some conclusions are made:

- Optimum thicknesses for cases considering distortional buckling and not considering distortional buckling with different loads of intensity are the same. It indicates that same as the channel section, the thickness of section does not contribute a lot to improve the distortional buckling strength of a section.
- The web depth of zed section reaches the maximum bound value more quickly than that of channel section, but the zed section's width of flange increases more quickly than that of channel sections. It is due to the fact that the major axis of the zed section makes an angle with the plane of the web, so the load applied is not in the plane of the major axis. It leads to a strength resistance of the zed section being lower than that of a channel section with the same dimension.

- The depth of lip in cold-formed steel zed sections increases more quickly than in channel sections. This is due to the fact that the torsion stiffness of zed section is lower than that of channel sections when the load is applied not in the plane of web. Hence the depth of lip in zed sections tends to increase more quickly with the span to improve the torsional stiffness of the section
- As for the optimum section the moment lateral-torsional buckling coincides with local buckling. As mentioned in the literature review, the ideal optimum sections are obtained when all modes of section's failure happen at the same time. However, this is impractical due to the geometric constraints of the section for practical engineering. It is a so-called naïve optimum section. In fact two modes of failure are possible to occur at the same time as the results above show.

In conclusion, the global optimum dimensions are found and the behaviour of the section during the optimisation process is investigated here. They can be used for quick design by structural engineers. For other standards or other design criteria such as intermediate restraints etc, the optimisation programme can easily be amended to find the curves for global optimum dimensions.

8.6 OPTIMISATION RESULTS OF SIGMA SECTION

The optimum dimensions of a simply supported sigma beam subjected to uniformly distributed load are found here. The objective function is the total cross sectional area which is minimised and subjected to the five constraints identified, i.e. local buckling, deflection based on BS 5950-5:1998, lateral-torsional buckling following Allen (1980), distortional buckling calculated by direct strength method and the shear

strength at the support. Lateral-torsional buckling and local buckling are two criteria which control the optimum result. The following conclusions are made:

- The thickness of a section increases gradually with the increase of span length and load condition. However, the thickness does not help much to improve the strength resistance of a section.
- The optimum depth of web of a sigma section increases more quickly than that of channel and zed sections.
- The optimum width of flange of a sigma section increase more slowly than that of channel and zed sections.
- The optimum depth of lip of a sigma sections is smaller than that of channel and zed sections.
- Comparing the optimum cross sectional area of channel sections and sigma sections, we find that with the existence of web stiffeners, having the same load condition, the area requirement of the sigma section is smaller than that of channel and zed sections. Hence, in terms of structure and economising on material, the sigma section is the best choice.

8.7 HOW TO APPLY THE RESEARCH RESULTS IN PRACTICAL DESIGN

The optimisation results of channel, zed and sigma sections in this thesis are the case study of simply supported purlins subjected to the assumed uniformly distributed load applied through the shear centre of a section. The member is designed with no restraint in the span. The imposed loads are 2, 3 and 4kN/m. The results are presented under global curves of dimensions of a section versus the span varying from 3 to 4m. For example, the channel section results are read in combination of Figs 5.24 to 5.27, such as the purlin span of 4.5m and load of 3kN/m, the optimum dimensions are a

thickness of 1.4mm, a web depth of 280mm, a flange width of 70mm, lip depth of 37mm (C-280-70-1.4). The purpose of using curve form is to show clearly the behaviour of a section during the optimisation process. However, for practical design purposes, the designer can set the input with a specific span and load value and the output will be a set of optimum dimensions for the section. Hence the designer can order with the manufacturer or find a suitable section close to the optimum section in the catalogue of products.

8.8 DISCUSSION FOR FUTURE RESEARCH

This thesis consists of two parts. The first part is the study of the design of cold-formed steel open sections. The second part is to find a robust and effective method to solve the optimisation problem. In the design of purlin sections, all analysis and calculation formula in this thesis are based on the assumption that the load is applied on the top of flange and go through the shear centre of the section. In fact, the load applied has the eccentricity from the shear centre of the section. Hence in the future the design of channel, zed section and sigma section should consider the effect of load location. For local buckling in BS 5950-5:1998, the local buckling occurring at the compression part of the web is ignored by limiting compressive stress in the web. This limitation may make the design method too conservative. This leads to an underestimation of the section's capacity. Recently, the new approach has been presented by Schafer, where a consistent integration of local buckling and distortional buckling into the design of thin-walled section is proposed. The local buckling is calculated based on a semi-empirical interaction approach which considers the interaction between elements of the section expressed in terms of buckling factor $k_{\text{flange/lip}}$, $k_{\text{flange/web}}$. For distortional buckling, at the moment the available

approaches for flexural members, for instance by Hancock (1997), or Schafer (2002) and Yu (2005) are based on the assumption that the translational spring stiffness, which represents the resistance to translational movement of the flange by web element, is zero. In fact this value is not zero, so in future the model of distortional buckling can be improved. Furthermore, the effect of a web stiffener of the sigma section to the torsional restraint stiffness needs to be improved and further studied. The local buckling and distortional buckling relationship has been investigated by Schafer, but the local buckling and lateral-torsional buckling should be investigated, too.

For the optimisation programme in this thesis, the programming codes are written for optimisation of simply supported channels, zed and sigma beams subjected to uniformly distributed load only. The full study has been coded into a computer-based analysis programme (MATLAB). However, the programme can be amended to meet other optimisation problems for different kinds of cold-formed steel sections. It is suggested that the performance of the programme can be further improved by upgrading to a user friendly standalone version, which would become a more efficient tool for design engineers.

REFERENCE

- Adeli H, Park HS. 1995. A dynamic neural network model for structural optimisation-application to plastic design of structures. *Computers and Structures* 57(3):391-399.
- Adeli H, Karim A. 1997. Neural network model for optimisation of cold-formed steel beams. *Journal of Structural Engineering* 123(11):1535-1543.
- Allen H.G and Bulson P.S. 1980 *Background to buckling*. McGraw-Hill Book Company (UK) Limited.
- American Iron and Steel Institute. 1996. *Specification for the design of cold-formed steel structural members*; Washington.
- American Iron and Steel Institute. 2004. *Specification for the design of cold-formed steel structural members with commentary, Appendix 1: Design of Cold-Formed Steel Structural Members Using the Direct Strength Method*.
- AS/NZS 4600. 1996. *Standards Australia/Standards New Zealand. Cold-formed steel structures*.
- Badway Abu-Sena AB, Chapman JC and Davidson PC. 2001. Interaction between critical torsional flexural and lip buckling in channel sections. *Journal of Constructional Steel Research* 57(8):925-44.
- Beshara B and LaBoube RA. 2001. Pilot study: lateral braced C-sections under bending. *Thin-Walled Structures* 39(10):827-39.
- Bradford MA. 2000. Strength of compact steel beams with partial restraint. *Journal of Constructional Steel Research* 53(2):183-200.
- BS 5950-5. 1998. *Structural use of steelwork in building: Code of practice for the design of cold-formed sections*, BSI: Part 5. London: British Standards Institution.
- Camotim D, Silvestre N, Goncalves R. and Dinis BP. 2004. GBT analysis of thin-walled members: new formulations and applications. *International Workshop on*

Advances and Future Trends in Thin-Walled Structures Technology. Loughborough University, UK. 25 June, 137-68.

Camp C, Pezeshk S, Cao GZ. 1998. Optimised design of two dimensional structures using a genetic algorithm. *Journal of Structural Engineering* 124(5):551-559

Chu XT, Li LY and Kettle R. 2004. The effect of warping stress on the lateral-torsion buckling of cold-formed zed purlins. *Journal of Applied Mechanics* 71(5):742-44.

Chu XT, Kettle R and Li LY. 2004. Lateral-torsion buckling analysis of partial-laterally restrained thin-walled channel-section beams. *Journal of Constructional Steel Research* 60(8):1159-75.

Cheung YK. 1976. *Finite Strip Method in Structural Analysis*, Pergamon Press.

Davies JM. 2000. Recent research advances in cold-formed steel structures. *Journal of Constructional Steel Research* 55(1-3):267-88.

Davies JM and Jiang C. 1996a. Design of thin-walled beams for distortional buckling. In: 13th Int. Special Conf. on Cold-Formed Steel Structures, St. Louis, Missouri, 141-53.

Davies JM and Jiang C. 1996b. Design of thin-walled purlins for distortional buckling, In: TWS Bicentenary Conf. on Thin-Walled Structures, Strathclyde, Glasgow.

Davies JM, Leach P and Kelo E. 1995. The use of light gauge steel in low and medium rise modular buildings. In: Proc. 3rd Int. Conf. on Steel and Aluminium Structures, ICSAS'95. Istanbul.

Davies R, Pedreschi R and Sinha BP. 1996. The shear behaviour of press-joining in cold-formed steel structures. *Thin-Walled Structures* 25(3):153-70.

BS EN 1993-1-3:2006. Design of steel structures: General rules-supplementary rules for cold-formed members and sheeting. European Standard.

- El-Kassas EMA, Mackie RI, El-Sheikh AI. 2001. Using neural networks in cold-formed steel design. *Computer & Structures* 79(18):1687-1696.
- Erbatur F, Hasancebi O, Tutuncu I, Kilic H. 2000. Optimal design of planar and space structures with genetic algorithms. *Computers and Structures* 75(2):209-224
- Gotluru BP, Schafer BW and Pekoz T. 2000. Torsion in thin-walled cold-formed steel beams. *Thin-Walled Structures* 37(2):127-45.
- Grundy P. 1990. Effect of pre- and post-buckling behaviour on load capacity of continuous beams. *Thin-Walled Structure* 9(1-4):407-15.
- Hancock GJ. 1994. Design of cold-formed steel structures (To Australia Standard AS 1538-1988), 2nd ed. North Sydney, Australia: Australia Institute of Steel Construction.
- Hancock GJ. 1995. Design for distortional buckling of flexural members, In: Proc. 3rd Int. Conf. on Steel and Aluminium Structures, Istanbul. (also in *Thin-walled Structures* 1997;27:3-12).
- Hancock GJ. 1997a. The behaviour and design of cold-formed purlins. *Journal of Constructional Steel Research* 15(3):2-16.
- Hancock GJ. 1997b. Light gauge construction. *Prog Struct Engng Mater* 1(1):25-30.
- Hancock GJ. 2003. Cold-formed steel structures. *Journal of Constructional Steel Research*, 59(4): 473-487.
- Jönsson J. 1999a. Distortional warping functions and shear distributions in thin-walled beams. *Thin-Walled Structures* 33(4):245-68.
- Jönsson J. 1999b. Distortional theory of thin-walled beams. *Thin-Walled Structures* 33(4):269-303.
- Kameshki ES, Saka MP. 2001. Genetic algorithm based optimum bracing design of non-sway tall plane frames. *Journal of Constructional Steel Research* 57(10):1081-1097.

- Karim A, Adeli H. 1999. Global optimum design of cold-formed steel hat-shape beams. *Thin-Walled Structures* 35(4):275-288.
- Karim A, Adeli H. 1999. Global optimum design of cold-formed steel Z-Shape beams. *Periodical on Structural Design and Construction* 4(1):17-20.
- Karim A, Adeli H. 1999. Global optimum design of cold-formed steel I-Shape beams. *Periodical on Structural Design and Construction* 5(2):78-81.
- Kesti J and Davies JM. 1999. Local and distortional buckling of thin-walled short columns. *Thin-Walled Structures* 34(2):115-34.
- Kounousis VK and Arsenis SJ. 1998. Genetic algorithms in optimal detail design of reinforced concrete members. *Computer-Aided Civil and Infrastructure Engineering* 13:43-52.
- Laine M and Tuomala M. 1999. Testing and design of gravity loaded steel purlins restrained by sheeting. *Journal of Constructional Steel Research* 49(2):129-38.
- Lau SCW and Hancock GJ. 1987. Distortional buckling formulas for channel columns. *Journal of Structural Division, ASCE* 113(5):1063-78.
- Lee J and Kim SE. Lateral buckling analysis of thin-walled laminated channel-section beams. *Composite Structures*. 56:391-99.
- Lee J, Kim SM, Park HS, Woo BH. 2005. Optimum design of cold-formed steel channel beams using micro Genetic Algorithm. *Engineering Structures* 27(2005):17-24.
- Li LY. (1999). Test reports of cold-formed steel sections. Department of Civil Engineering, Aston University, Birmingham.
- Li LY. (2004) Lateral-torsional buckling of cold-formed zed-purlins partial laterally restrained by metal sheeting. *Thin-Walled Structures*. 42(7):995-1011.
- Liu P, Chan CM and Wang ZM. 1999. Optimal sizing/shape design of steel portal frames using genetic algorithms. *Proceedings of 2nd International conference on Advances in Steel Structures, December 15-17, Hongkong, China* 1081-1088.

- Loughlan J. 1996. The buckling of composite stiffened box sections subjected to compression and bending. *Composite Structures* 35:101-16.
- Loughlan J. 2004. Thin-Walled Structures Advances in Research, Design and Manufacturing Technology. Proceedings of the Fourth International Conference on Thin-Walled Structures in Loughborough, UK, 22-24 June.
- Loughlan J. 2004. Thin-Walled Structures Recent Advances and Future Trends in Thin-Walled Structures Technology. International Workshop in Loughborough, UK, 25 June.
- Lucas RM, Al-Bermani FGA and Kitipornchai S. 1997a. Modelling of cold-formed purlin-sheeting systems. Part 1: Full model. *Thin-Walled Structures* 27(3):223-43.
- Lucas RM, Al-Bermani FGA and Kitipornchai S. 1997b. Modelling of cold-formed purlin-sheeting systems. Part 2: Simplified model. *Thin-walled Structures* 27(4):263-86.
- Mosawi S, Saka MP. 2000. Optimum shape design of cold-formed thin-walled steel sections. *Advances In Engineering Software* 31(11):851-862.
- Papangelis J.P, Hancock G.J and Trahair N.S. 1998. Computer design of cold-formed C and Z section purlins. *Journal of Constructional Steel Research*, 46(98):1-3.
- Pekoz T. 1999. Possible future developments in the design and application of cold-formed steel. Keynote lecture, "ICSAS'99", 4th Int. Conf. Light-weight Steel and Aluminium Structures. Espoo, Finland 20-23 June.
- Pezeshk S and Camp C.V and Chen D. 2000. Design of nonlinear framed structures using genetic optimisation. *Journal of Structure Engineering* 126(3):382-388.
- Pi YL, Put BM and Trahair NS. 1998. Inelastic lateral buckling of cold-formed channel and z-section beams. Second International Conference on Thin-walled Structures. Singapore: Research and development; 205-12.

- Pohlheim, H. 1994-1997. Genetic and evolutionary algorithms: principles, methods and algorithms. Genetic and Evolutionary Algorithm Toolbox for use with MATLAB (GEATbx). http://www.systemtechnik.tu-ilmeneau.de/~pohlheim/GA_Toolbox/alindex.html
- Polyzois D and Guillory Jr L.J. 1991. Finite strip method for analysis of cold-formed purlins. *Journal of Structural Engineering* 17(1):184-204.
- Put BM, Pi YL, Trahair NS. 1998. Lateral buckling tests on cold-formed channel beams. Research Report No R767, Centre for Advanced Structural Engineering, Department of Civil Engineering, the University of Sydney, Australia.
- Put BM, Pi YL and Trahair NS. 1999. Bending and torsion of cold-formed channel beams. *Journal of Structural Engineering* 25(5):540-6.
- Rajan S.D. 1995. Sizing, shape, and topology design optimisation of trusses using genetic algorithm. *Journal of Structural Engineering* 121(10):1480-1487.
- Rajeev S, Krishnamoorth C.S. 1997. Discrete optimisation of structures using genetic algorithms based metrologies for design optimisation of trusses. *Journal of Structural Engineering* 123(3):350-358.
- Rajeev S, Krishnamoorth C.S. 1998. Genetic algorithm-based methodology for design optimisation of reinforced concrete frames. *Computer-Aided Civil and Infrastructure Engineering* 13:63-74.
- Rondal J. 2000. Cold-formed steel members and structures-general report. *Journal of Constructional Steel Research* 55(1-3):155-8.
- Rusch A and Lindner J. 2001. Remarks to the direct strength method. *Thin-Walled Structures* 39:807-20.
- Sarma K.C and Adeli H. 2000. Fuzzy genetic algorithm for optimisation of steel structures. *Journal of Structural Engineering* 126(5):596-604.
- Schikking S and Werner F. 2001. Practical design of steel frame structures using different optimisation algorithms and building codes. European Conference on Computational Mechanics, Krakow, Poland, June 26-29.

Sciuva M.D, Lomario D and Voyat J.P. 2001. Evolutionary algorithms their use in multiconstrained optimisation of laminated and sandwich plates. European Conference on Computational Mechanics, Krakow, Poland, June 26-29.

Schafer BW. 2001a. Thin-walled column design considering local, distortional and euler buckling. Structural Stability Research Council, Annual Technical Session and Meeting.

Schafer BW. 2001b. Experiments on braced thin-walled cold-formed steel C and Z beams in flexure. Recent Advances in Stability of Structural Components and Systems Combined ASCE-EMD and ASME Summer Conference, San Diego, California.

Schafer BW. 2001c. Elastic buckling analysis of thin-walled members using the classical finite strip method, CUFEM Version 2. Johns Hopkins University.

Schafer BW. 2003a. Elastic buckling analysis of thin-walled members using the classical finite strip method, CUFSM Version 2.6, Johns Hopkins University.

Schafer BW. 2003b. Advances in Direct Strength Design of Thin-Walled Members, Proceedings, Advances in Structures Conference, ASSCCA03, 22-25 June, Sydney, Australia.

Schafer BW and Pekoz T. 1998. Direct strength prediction of cold-formed steel members using numerical elastic buckling solutions. In: Thin-walled Structures, Research and Development. Proc. 2nd International Conf on Thin-walled Structure, Singapore, Dec. Elsevier, 137-44.

Schafer BW and Pekoz T. 1999a. Local and distortional buckling of cold-formed steel members with edge stiffeners flanges. ICSAS'99, 4th International Conference on Light-weight Steel Aluminium Structures, Espoo, Finland, 20-23 June, 89-97.

Schafer BW and Pekoz T. 1999b. Laterally braced cold-formed steel flexural members with edge stiffened flanges. Journal of Structural Engineering 125(2):118-27.

- Sokol L. 1996. Stability of cold-formed purlins braced by steel sheeting. *Thin-Walled Structures* 25(4):247-68.
- Tian YS, Lu TJ. 2004. Minimum weight of cold-formed steel sections under compression. *Thin-Walled Structures* 42(4):515-532.
- Timoshenko SP and Gere JM. 1961. *Theory of Elastic Stability*. McGraw-Hill Book Company, New York.
- Toma T and Wittenmann K. 1994. Design of cold-formed purlins and rails restrained by sheeting. *Journal of Constructional Steel Research* 31(2/3):149-68.
- Trahair NS and Bradford MA. 1998. *The behaviour and design of steel structures to AS4100 (3rd ed.)*, E & FN Spon, London.
- Venkataraman P. 2001. *Applied optimisation with MATLAB programming*. John Wiley & Sons, New York.
- Vinot P, Cogan S, Piranda J. 2001. Shape optimisation of thin-walled beam-like structures. *Thin-Walled Structures* 39(7):611-630.
- Walker AC. 1995. *Design and Analysis of Cold-formed Sections*. International Textbook Company Ltd., London.
- Wenyu Sun and Ya-Xiang Yuan. 2006. *Optimisation theory and methods Nonlinear programming*. Spring Science Business Media, LLC
- Ye ZM, Kettle R, Li LY and Schafer B. 2002. Buckling behaviour of cold-formed zed-purlins partially restrained by steel sheeting. *Thin-Walled Structures* 40(10):853-64.
- Ye ZM, Kettle R and Li LY. 2004. Strength analysis of cold-formed zed-purlins partially restrained by steel sheeting. *Computer & Structures* 82(9-10): 731-9.
- Young B and Hancock GJ. 2001. Design of cold-formed channels subjected to web crippling. *Journal of Structural Engineering* 127(10):1137-44.
- Yu WW. 1985. *Cold-Formed Steel Design*. J. Wiley and Sons, New-York.

A.1.3 Geometric stiffness matrix (CUFSM)

$$[K_g] = C \begin{bmatrix}
 70(3T_1 + T_2) & 0 & 70(T_1 + T_2) & 0 & 0 & 0 & 0 & 0 \\
 70(3T_1 + T_2) & 0 & 70(T_1 + T_2) & 0 & 0 & 0 & 0 & 0 \\
 70(T_1 + T_2) & 0 & 70(T_1 + T_2) & 0 & 0 & 0 & 0 & 0 \\
 70(T_1 + 3T_2) & 0 & 0 & 0 & 0 & 0 & 0 & 0 \\
 70(T_1 + 3T_2) & 0 & 0 & 0 & 0 & 0 & 0 & 0 \\
 8(30T_1 + 9T_2) & 2b(15T_1 + 7T_2) & 54(T_1 + T_2) & -2b(7T_1 + 6T_2) \\
 70(T_1 + 3T_2) & b^2(5T_1 + 3T_2) & 2b(6T_1 + 7T_2) & -3b^2(T_1 + T_2) \\
 0 & 0 & 24(3T_1 + 10T_2) & -2b(7T_1 + 15T_2) \\
 0 & 0 & 0 & b^2(3T_1 + 5T_2)
 \end{bmatrix}$$

symmetric

where: $C = \frac{b_s(m\pi)^2}{1680\alpha_s}$;

A.1.4 Coupled geometric stiffness matrix of semi-analytical finite strip method

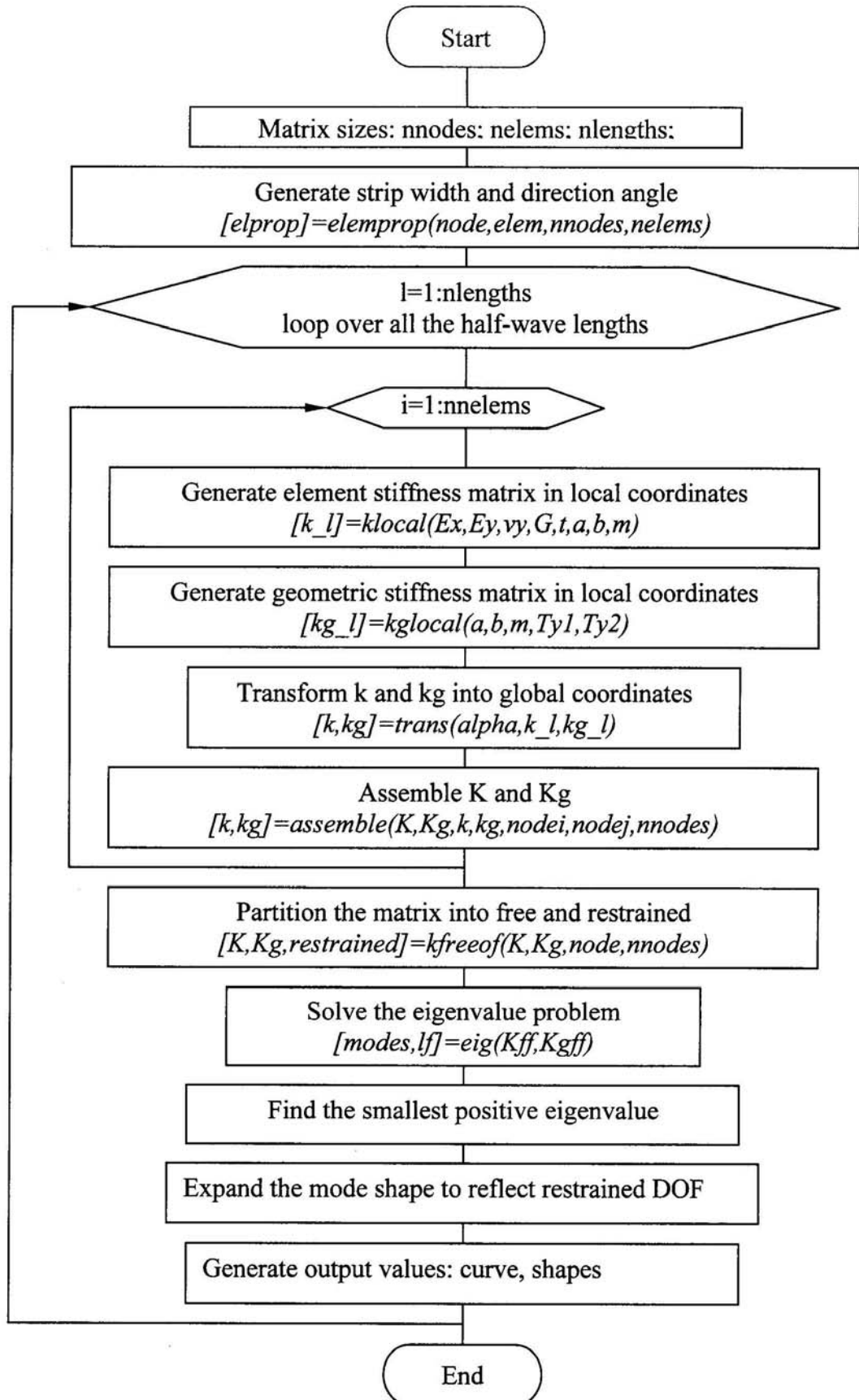
$$[K_{gmn}] = C \begin{bmatrix} 70(3T_1 + T_2)k_c & 0 & 70(T_1 + T_2)k_c & 0 & 0 & 0 & 0 & 0 \\ 70(3T_1 + T_2)k_s & 0 & 70(T_1 + T_2)k_s & 0 & 0 & 0 & 0 & 0 \\ 70(T_1 + 3T_2)k_c & 0 & 70(T_1 + 3T_2)k_c & 0 & 0 & 0 & 0 & 0 \\ 70(T_1 + 3T_2)k_s & 0 & 70(T_1 + 3T_2)k_s & 0 & 0 & 0 & 0 & 0 \\ 8(30T_1 + 9T_2)k_c & 2b(15T_1 + 7T_2)k_c & 54(T_1 + T_2)k_c & -2b(7T_1 + 6T_2)k_c & 0 & 0 & 0 & 0 \\ b^2(5T_1 + 3T_2)k_c & 2b(6T_1 + 7T_2)k_c & -3b^2(T_1 + T_2)k_c & -2b(7T_1 + 6T_2)k_c & 0 & 0 & 0 & 0 \\ 24(3T_1 + 10T_2)k_c & 24(3T_1 + 10T_2)k_c & -2b(7T_1 + 15T_2)k_c & -2b(7T_1 + 15T_2)k_c & 0 & 0 & 0 & 0 \\ b^2(3T_1 + 5T_2)k_c & b^2(3T_1 + 5T_2)k_c & b^2(3T_1 + 5T_2)k_c & b^2(3T_1 + 5T_2)k_c & 0 & 0 & 0 & 0 \end{bmatrix}$$

symmetric

$$\text{where: } C = \frac{b_s(mn)\pi^2}{210a_s}; \quad k_c = \frac{1}{a_s^3} \int_0^{a_s} (a_s y - y^2) \cos \frac{m\pi y}{a_s} \cos \frac{n\pi y}{a_s} dy = \begin{cases} \frac{1}{12} \frac{1}{(m+n)^2 \pi^2} & \text{if } (m-n) = 0 \\ \frac{1}{\pi^2} \left[\frac{1}{(m+n)^2} + \frac{1}{(m-n)^2} \right] & \text{if } (m-n) \text{ is even} \\ 0 & \text{if } (m-n) \text{ is odd} \end{cases}$$

$$k_s = \frac{1}{a_s^3} \int_0^{a_s} (a_s y - y^2) \sin \frac{m\pi y}{a_s} \sin \frac{n\pi y}{a_s} dy = \begin{cases} \frac{1}{12} + \frac{1}{(m+n)^2 \pi^2} & \text{if } (m-n) = 0 \\ \frac{1}{\pi^2} \left[\frac{1}{(m+n)^2} - \frac{1}{(m-n)^2} \right] & \text{if } (m-n) \text{ is even} \\ 0 & \text{if } (m-n) \text{ is odd} \end{cases}$$

A.1.5 Finite strip programme scheme



A.2 EXPRESSIONS OF SECTION PROPERTIES

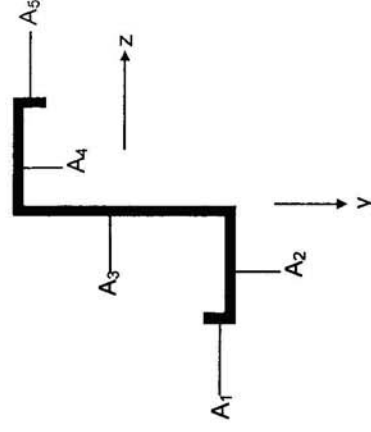
A.2.1 Zed sections

$$\Rightarrow \omega \text{ and } \bar{\omega} (= \frac{1}{k} \int \omega ds = \sum_{i=1}^5 \bar{\omega}_i)$$

A_i	Plane Element s	ω_i	$\bar{\omega}_i$
A_1	$[0 \ c]$	bs	$\frac{bc^2}{2}$
A_2	$[c \ c+b]$	$bc + \frac{h}{2}(s-c)$	$b^2(c + \frac{h}{4})$
A_3	$[c+b \ c+b+h]$	$bc + \frac{hb}{2}$	$\frac{bh}{2}(2c+h)$
A_4	$[c+b+h \ c+2b+h]$	$bc + \frac{hb}{2} - \frac{h}{2}[s - (c+b+h)]$	$b^2(c + \frac{h}{4})$
A_5	$[c+2b+h \ 2c+2b+h]$	$bc - b[s - (c+2b+h)]$	$\frac{bc^2}{2}$

Note: A_i = the individual plane element of the cross section; b, c, h = flange, lip and web width along the middle line respectively; ω = the sectorial co-ordinate; $k = 2b + 2c + h$;

$$\bar{\omega} = \sum_{i=1}^5 \bar{\omega}_i = bc + \frac{b}{2} \frac{h^2 - 2c^2 + hb}{2c + 2b + h}$$



$$\Rightarrow \text{Expression of } D_w (= \sum_{i=1}^5 D_{wi})$$

Plane Element			$D_{wi} = \int_{A_i} (\bar{\omega} - \omega_i)(y^2 + z^2) dA_i$
A_i	y	z	
A_1	$[h/2 - c \ h/2]$	b	$\frac{tbc}{24} [2c^2(c-h) + (12b^2 + 3h^2 - 6hc + 4c^2) \frac{h^2 + hb + 2bc + hc}{2c + 2b + h}]$
A_2	$h/2$	$[-b \ 0]$	$\frac{tb^2}{48} [2hb^2 + (3h^2 + 4b^2) \frac{h^2 - 4c^2 - 2hc}{2c + 2b + h}]$
A_3	$[-h/2 \ -h/2]$	0	$-\frac{tbh^3}{24} \frac{2c^2 + 2hc + hb}{2c + 2b + h}$
A_4	$-h/2$	$[0 \ b]$	$\frac{tb^2}{48} [2hb^2 + (3h^2 + 4b^2) \frac{h^2 - 4c^2 - 2hc}{2c + 2b + h}]$
A_5	$[-h/2 \ -h/2 + c]$	b	$\frac{tbc}{24} [2c^2(c-h) + (12b^2 + 3h^2 - 6hc + 4c^2) \frac{h^2 + hb + 2bc + hc}{2c + 2b + h}]$

Note: D_w is a constant.

A.2.2 Channel sections

⇒ Section properties

Centroid e_2	$b \frac{2c+b}{2c+2b+h}$
Second moment about y axis I_y	$t[2b^2c + \frac{2}{3}b^3 + \frac{2}{3}e_2^3 + e_2^2h]$
Second moment about z axis I_z	$\frac{t}{12}(8c^3 - 12hc^2 + 6h^2c + 6h^2b + h^3)$
Shear centre e_1	$\frac{tbch^2}{I_z} \left(\frac{1}{2} + \frac{b}{4c} - \frac{2c^2}{3h^2} \right)$
Torsion constant J	$\frac{t^3}{3}(2b+2c+h)$
Warping constant about shear centre C_w	$\frac{tb^2}{6}(4c^3 + 3h^2c + 6hc^2 + bh^2) - I_z e_1^2$
Warping constant about centroid $I_o = \int_A (\bar{\omega} - \omega)^2 dA$	$C_w + I_{oz} / I_z$
Sectorial product of inertia about z axis $I_{oz} = - \int_A \omega y dA$	$t \left[-bh \left(\frac{h^2}{4} - h^2 \right) + \frac{2b'}{3} h^3 \left(\frac{h^3}{8} - h^3 \right) - \frac{bh^2}{4} (b+2e_2) - \frac{e_2 h^3}{12} \right]$

Note: b, c, h = flange, lip and web width along the middle line respectively;

$b' = b - e_2$; $h' = d/2 - c$; $e = e_1 + e_2$;

$$A = t(2b + 2c + h);$$

ω and $\bar{\omega}$ are given next.

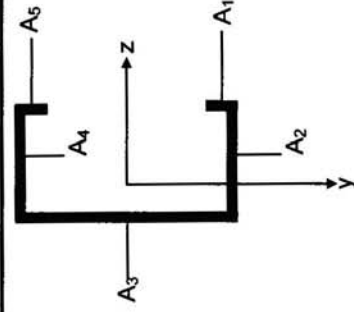
$\Rightarrow \omega, \bar{\omega}$ and $\omega_s, \bar{\omega}_s$

A_i	Plane Element s	ω_i	$\bar{\omega} - \omega_i$	ω_{si}	$\bar{\omega}_s - \omega_{si}$
A_1	$[0 \ c]$	$-b's$	$-bh + b'y$	$-b''s$	$-bh + b''y$
A_2	$[c \ c+b]$	$-b'c - \frac{h}{2}(s-c)$	$-he_2 - \frac{h}{2}z$	$-b''c - \frac{h}{2}(s-c)$	$\frac{h}{2}(e_1 - e_2) - \frac{h}{2}z$
A_3	$[c+b \ c+b+h]$	$-b'c - \frac{hb}{2} - e_2[s - (b+c)]$	$-e_2y$	$-b''c - \frac{hb}{2} + e_1[s - (b+c)]$	e_1y
A_4	$[c+b+h \ c+2b+h]$	$-b'c - e_2h - \frac{h}{2}[s - (c+h)]$	$he_2 + \frac{h}{2}z$	$-b''c + e_1h - \frac{h}{2}[s - (c+h)]$	$-\frac{h}{2}(e_1 - e_2) + \frac{h}{2}z$
A_5	$[c+2b+h \ 2c+2b+h]$	$-2e_2h - b'(s - 2b)$	$bh + b'y$	$2e_1h - b''(s - 2b)$	$bh + b''y$

Note: A_i = the individual plane element of the cross section;

$$b'' = b + e_1; \quad k = 2b + 2c + h;$$

$$\bar{\omega} = -b'c - \frac{h}{2}(b + e_2); \quad \bar{\omega}_s = -b''c - \frac{h}{2}(b - e_1).$$



A.2.3 Sigma section or arbitrary open section

In view of the complexity of sigma sections and arbitrary open sections, the MATLAB codes were written by Schafer (1997) to determine the section properties.

- The gross properties of the section are determined by the function below:

function [A,xcg,zcg,Ixx,Izz,Ixz,thetap,I11,I22]=grosprop(node,elem)

```
%[A,xcg,zcg,Ixx,Izz,Ixz,thetap,I11,I22]=grosprop(node,elem)
```

```
%Input
```

```
%node=[# x z DOFX DOFZ DOFY DOF0 stress]
```

```
%elem=[# i j t]
```

```
%Ouput
```

```
%
```

```
A=0;; Ax=0;; Az=0;; Axx=0;; Azz=0;; Axz=0;
```

```
Ixx_o=0;; Izz_o=0;; Ixz_o=0;
```

```
for k=1:length(elem(:,1)) % number element of section
```

```
  ni=elem(k,2);
```

```
  nj=elem(k,3);
```

```
  t=elem(k,4);
```

```
  xi=node(ni,2);
```

```
  xj=node(nj,2);
```

```
  zi=node(ni,3);
```

```
  zj=node(nj,3);
```

```
  %
```

```
  delx=xj-xi;
```

```
  delz=zj-zi;
```

```
  theta_xx=pi/2-atan2(delz,delx);
```

```
  theta_zz=theta_xx+pi/2;
```

```
  xcg_elem=1/2*(xi+xj);
```

```

zcg_elem=1/2*(zi+zj);
L_elem=sqrt(delx^2+delz^2);
A_elem=t*L_elem;
Ixx_elem=1/12*t*L_elem*(t^2*(sin(theta_xx))^2 + L_elem^2*(cos(theta_xx))^2);
Izz_elem=1/12*t*L_elem*(t^2*(sin(theta_zz))^2 + L_elem^2*(cos(theta_zz))^2);
Ixz_elem=1/12*t*L_elem*(t^2*sin(theta_xx)*cos(theta_xx) + ...
                L_elem^2*cos(theta_xx)*sin(theta_xx));
%
A=A + A_elem;
Ax=Ax + A_elem*xcg_elem;
Az=Az + A_elem*zcg_elem;
Axx=Axx + A_elem*xcg_elem*xcg_elem;
Azz=Azz + A_elem*zcg_elem*zcg_elem;
Axz=Axz + A_elem*xcg_elem*zcg_elem;
Ixx_o=Ixx_o + Ixx_elem;
Izz_o=Izz_o + Izz_elem;
Ixz_o=Ixz_o + Ixz_elem;
%
end
xcg=Ax/A;
zcg=Az/A;
Ixx=Ixx_o + Azz - A*zcg^2;
Izz=Izz_o + Axx - A*xcg^2;
Ixz=Ixz_o + Axz - A*xcg*zcg;
thetap=180/pi*1/2*atan2(-2*Ixz,Ixx-Izz);
I11=1/2*(Ixx+Izz) + sqrt( (1/2*(Ixx-Izz))^2 + Ixz^2 );
I22=1/2*(Ixx+Izz) - sqrt( (1/2*(Ixx-Izz))^2 + Ixz^2 );

```

- Sectional properties of thin-walled members

```

function [Cw, J, Xs, Ys, w, Bx, By, B1, B2]=Warp(node,elem)
%[A,xcg,zcg,Ixx,Izz,Ixz,thetap,I11,I22]=grosprop(node,elem);
%Cw, J, Warping function,
%Xs ,Ys Shear center location

```

```

% J torsion constant
% w sectorial co-ordinate.
%Input
%node=[# x z DOFX DOFZ DOFY DOF0 stress]
%elem=[# i j t]
n=length(node(:,1));

```

```

%Basic Section Properties

```

```

% Area lengths, coordinates etc

```

```

t=elem(:,4);
x=node(:,2);
y=node(:,3);
A=0;
for i=1:n-1
    l(i)=sqrt((x(i+1)-x(i))^2+(y(i+1)-y(i))^2);
    Ai(i)=t(i)*l(i);
    x_(i)=(1/2)*(x(i)+x(i+1));
    y_(i)=(1/2)*(y(i)+y(i+1));
    dx(i)=x(i+1)-x(i);
    dy(i)=y(i+1)-y(i);
    A=A+Ai(i);
end

```

```

%Centroid

```

```

xc=0;
yc=0;
for i=1:n-1
    xc=xc+(1/A)*t(i)*l(i)*x_(i);
    yc=yc+(1/A)*t(i)*l(i)*y_(i);
end

```

```

%Moments of Inertia, Torsion constant

```

```

J=0;
Ixc=0;

```

```

Iyc=0;
Ixyz=0;
for i=1:n-1
    J=J+(1/3)*l(i)*t(i)^3;
    Ixc=Ixc+((y_(i)^2*Ai(i)+(1/12)*dy(i)^2*Ai(i)));
    Iyc=Iyc+((x_(i)^2*Ai(i)+(1/12)*dx(i)^2*Ai(i)));
    Ixyz=Ixyz+((x_(i)*y_(i)*Ai(i)+(1/12)*dx(i)*dy(i)*Ai(i)));
end
Ixc=Ixc-yc^2*A;
Iyc=Iyc-xc^2*A;
Ixyz=Ixyz-yc*xc*A;
%Principal moments of inertia
Imax=(1/2)*((Ixc+Iyc)+sqrt((Ixc-Iyc)^2+4*Ixyz^2));
Imin=(1/2)*((Ixc+Iyc)-sqrt((Ixc-Iyc)^2+4*Ixyz^2));
Th_p=1/2*(atan2(-2*Ixyz,(Ixc-Iyc)));

%Transform into new coordinates about principal axes
for i=1:n
    XY=[(x(i)-xc) (y(i)-yc); (y(i)-yc) -(x(i)-xc)]*[cos(Th_p);sin(Th_p)];
    X(i)=XY(1);
    Y(i)=XY(2);
end

%Shearflow and Shear center
VX(1)=0;
VY(1)=0;
for i=1:n-1
    dX(i)=(1/l(i))*abs(X(i)*Y(i+1)-X(i+1)*Y(i));
    dY(i)=(1/l(i))*abs(X(i)*Y(i+1)-X(i+1)*Y(i));

    if (Y(i)*(X(i+1)-X(i)))<(X(i)*(Y(i+1)-Y(i)))
        dlX(i)=1;
    else if (Y(i)*(X(i+1)-X(i)))>(X(i)*(Y(i+1)-Y(i)))
        dlX(i)=-1;
    end
end

```

```

else if (Y(i)*(X(i+1)-X(i)))==(X(i)*(Y(i+1)-Y(i)))
    dLX(i)=0;
end
end
end

if (X(i)*(Y(i+1)-Y(i)))<(Y(i)*(X(i+1)-X(i)))
    dLY(i)=1;
else if (X(i)*(Y(i+1)-Y(i)))>(Y(i)*(X(i+1)-X(i)))
    dLY(i)=-1;
else if (X(i)*(Y(i+1)-Y(i)))==(Y(i)*(X(i+1)-X(i)))
    dLY(i)=0;
end
end
end

VX(i+1)=VX(i)+Ai(i)*(Y(i+1)+Y(i))/2;
VY(i+1)=VY(i)-Ai(i)*(X(i+1)+X(i))/2;
end

Xs=0;
Ys=0;
if Imax~=0
    for i=1:n-1
        Xs=Xs+(-1/Imax)*dLX(i)*dX(i)*l(i)*(VX(i)+(1/6)*Ai(i)*(Y(i+1)+2*Y(i)));
    end
end
if Imin~=0
    for i=1:n-1
        Ys=Ys+(-1/Imin)*dLY(i)*dY(i)*l(i)*(VY(i)-(1/6)*Ai(i)*(X(i+1)+2*X(i)));
    end
end

%Warping funcions and Warping Constant
X_s(1)=X(1)-Xs;

```

```

Y_s(1)=Y(1)-Ys;
ws(1)=0;
wa(1)=0;
ws_=0;

for i=1:n-1
    X_s(i+1)=X(i+1)-Xs;
    Y_s(i+1)=Y(i+1)-Ys;
    ds(i)=(1/l(i))*abs(X_s(i)*Y_s(i+1)-X_s(i+1)*Y_s(i));
    if (Y_s(i)*(X(i+1)-X(i)))<(X_s(i)*(Y(i+1)-Y(i)))
        dls(i)=1;
    else if (Y_s(i)*(X(i+1)-X(i)))>(X_s(i)*(Y(i+1)-Y(i)))
        dls(i)=-1;
    else if (Y_s(i)*(X(i+1)-X(i)))==(X_s(i)*(Y(i+1)-Y(i)))
        dls(i)=0;
    end
end
end
ws(i+1)=ws(i)+ds(i)*l(i)*dls(i);
ws_=ws_+(1/A)*Ai(i)*(ws(i+1)+ws(i))/2;
end

xx(1)=0;
for i=1:n
    w(i,1)=ws_-ws(i);
end

Cw=0;
for i=1:n-1
    dw=w(i+1)-w(i);
    wa=w(i);
    Cw=Cw+t(i)*(wa^2*l(i)+(1/3)*dw^2*l(i)+wa*dw*l(i));
end

```

```

%Monosymmetry Parameters Bx and By
B1=0;
B2=0;
for i=1:n-1
    Xa=X(i);
    dX=X(i+1)-X(i);
    Ya=Y(i);
    dY=Y(i+1)-Y(i);

    B1=B1+Ai(i)*1/12*(3*dY*dX^2+3*dY^3+4*Ya*dX^2+12*Ya*dY^2+8*dY*Xa*dX+
    12*Ya*Xa*dX+18*Ya^2*dY+6*dY*Xa^2+12*Ya*Xa^2+12*Ya^3);

    B2=B2+Ai(i)*1/12*(3*dX^3+3*dX*dY^2+12*Xa*dX^2+4*Xa*dY^2+8*dX*Ya*dY+
    18*Xa^2*dX+12*Xa*Ya*dY+6*dX*Ya^2+12*Xa^3+12*Xa*Ya^2);
end
B1=(1/Imax)*B1-2*(Ys);
B2=(1/Imin)*B2-2*(Xs);

X=x-xc*ones(n,1);
Y=y-yc*ones(n,1);
Bx=0;
By=0;
for i=1:n-1
    Xa=X(i);
    dX=X(i+1)-X(i);
    Ya=Y(i);
    dY=Y(i+1)-Y(i);

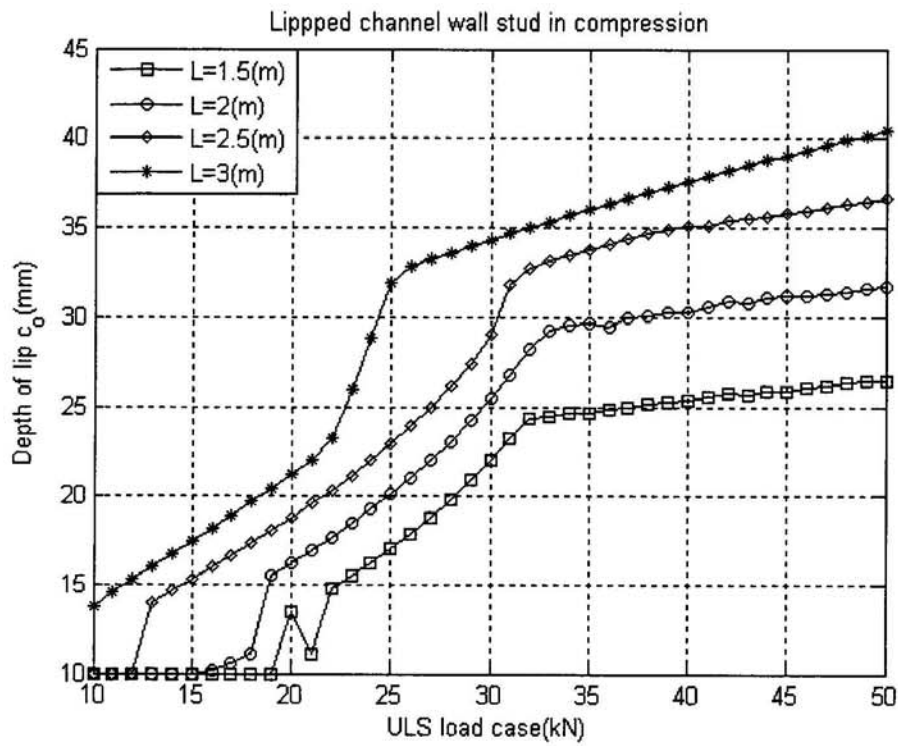
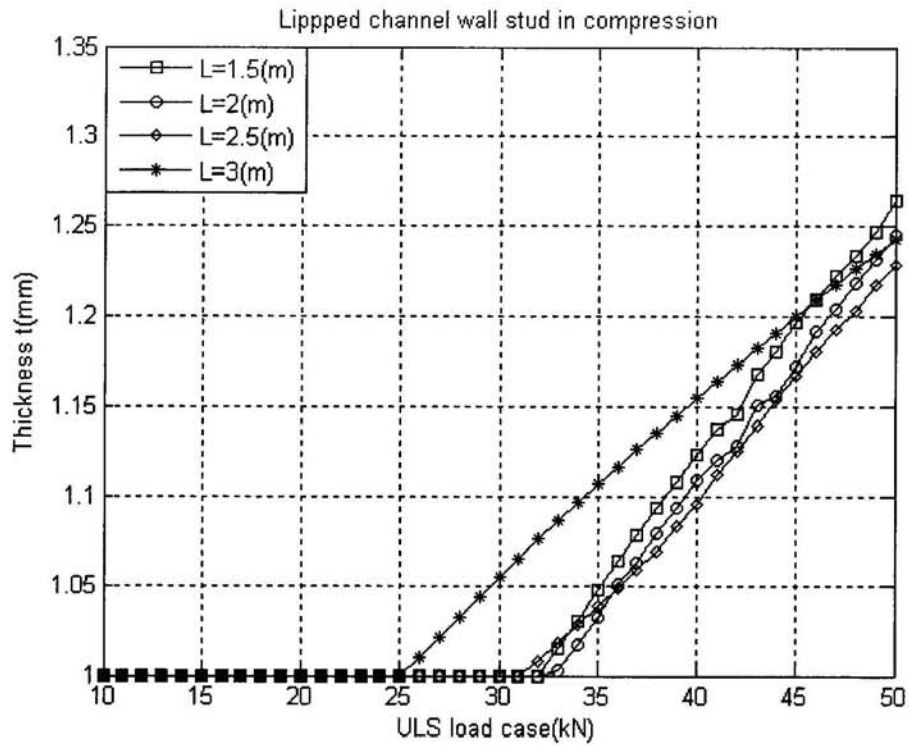
    Bx=Bx+Ai(i)*1/12*(3*dY*dX^2+3*dY^3+4*Ya*dX^2+12*Ya*dY^2+8*dY*Xa*dX+
    12*Ya*Xa*dX+18*Ya^2*dY+6*dY*Xa^2+12*Ya*Xa^2+12*Ya^3);

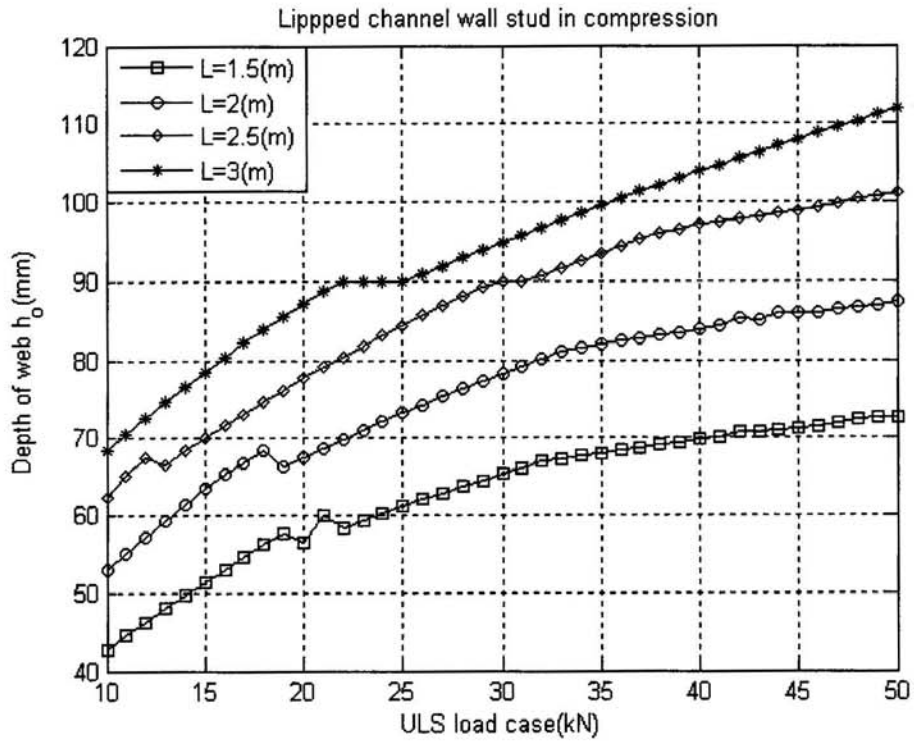
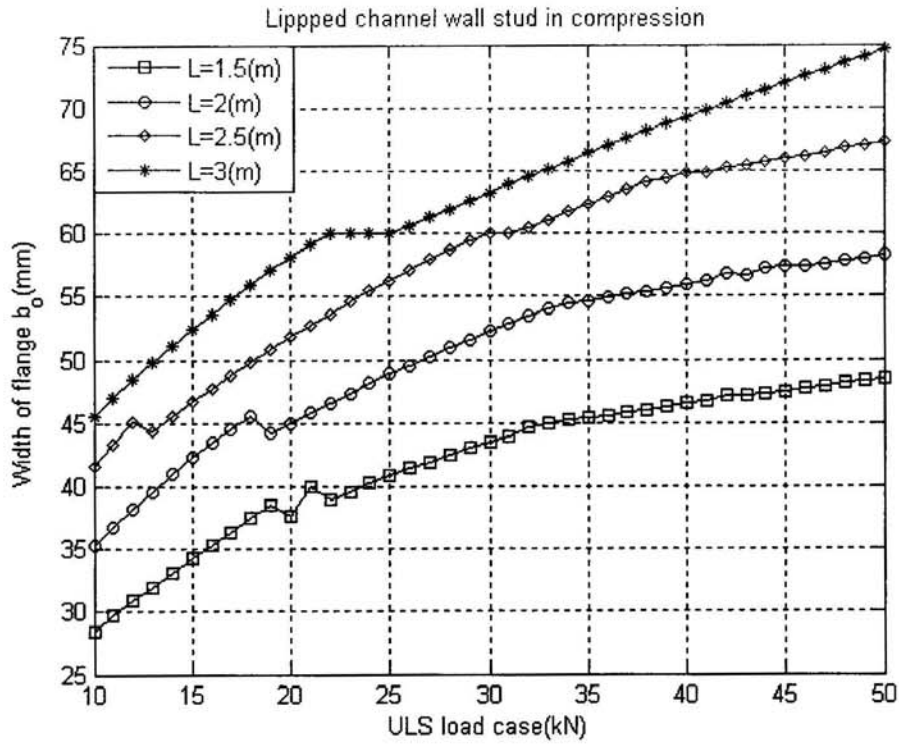
    By=By+Ai(i)*1/12*(3*dX^3+3*dX*dY^2+12*Xa*dX^2+4*Xa*dY^2+8*dX*Ya*dY+
    18*Xa^2*dX+12*Xa*Ya*dY+6*dX*Ya^2+12*Xa^3+12*Xa*Ya^2);
end
Bx=(1/Ixc)*Bx-2*(Ys);
By=(1/Iyc)*By-2*(Xs);

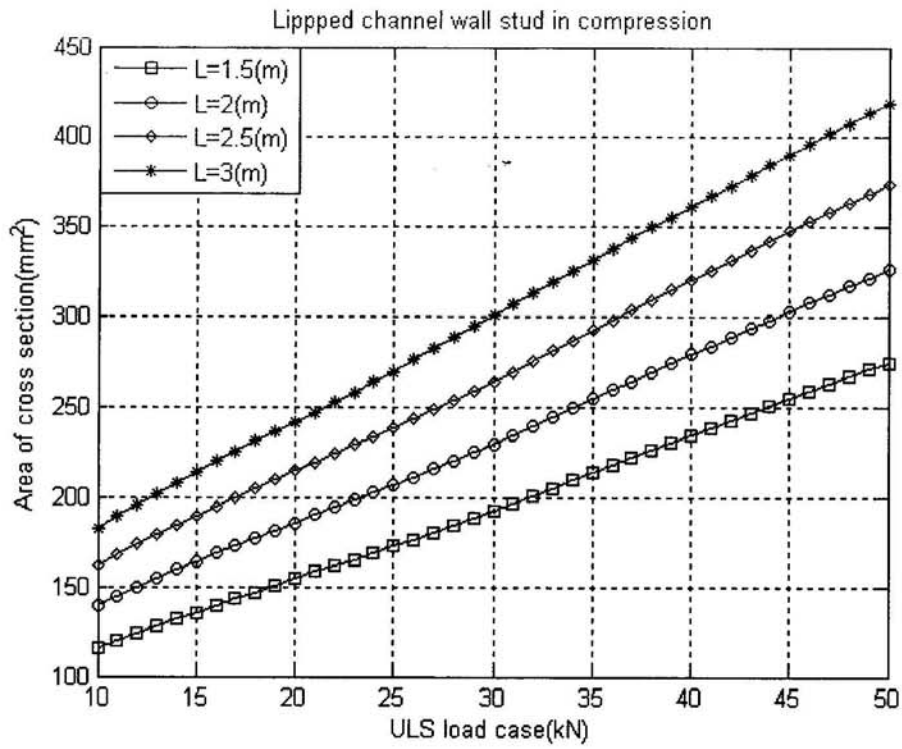
```

A.3 NUMERICAL OPTIMISATION RESULTS

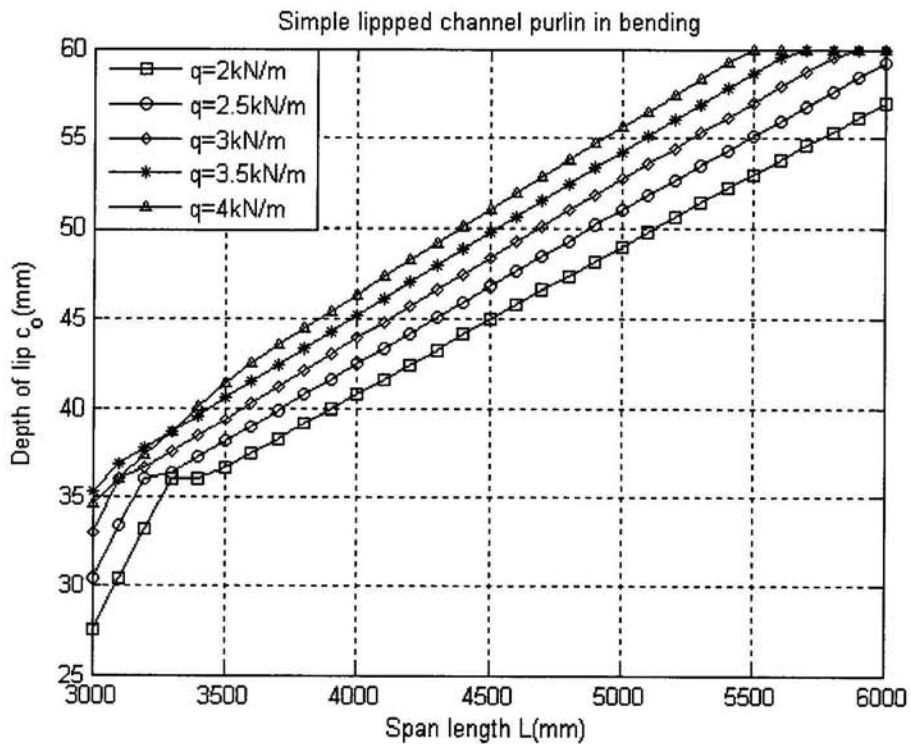
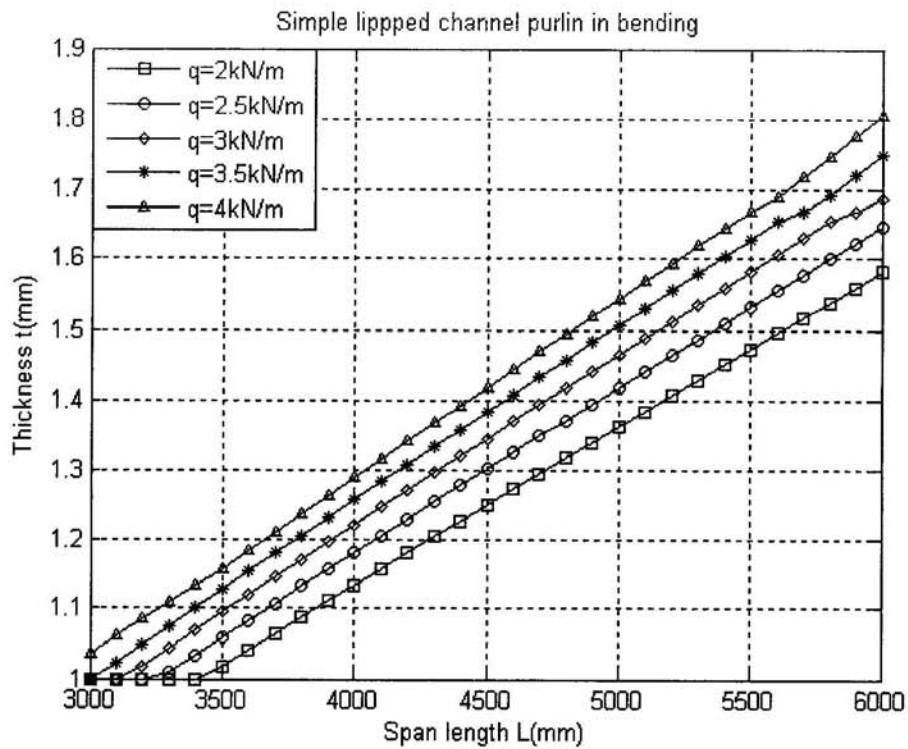
A.3.1 Steel lipped channel wall stud in compression based on EN 1993-1-3:2006

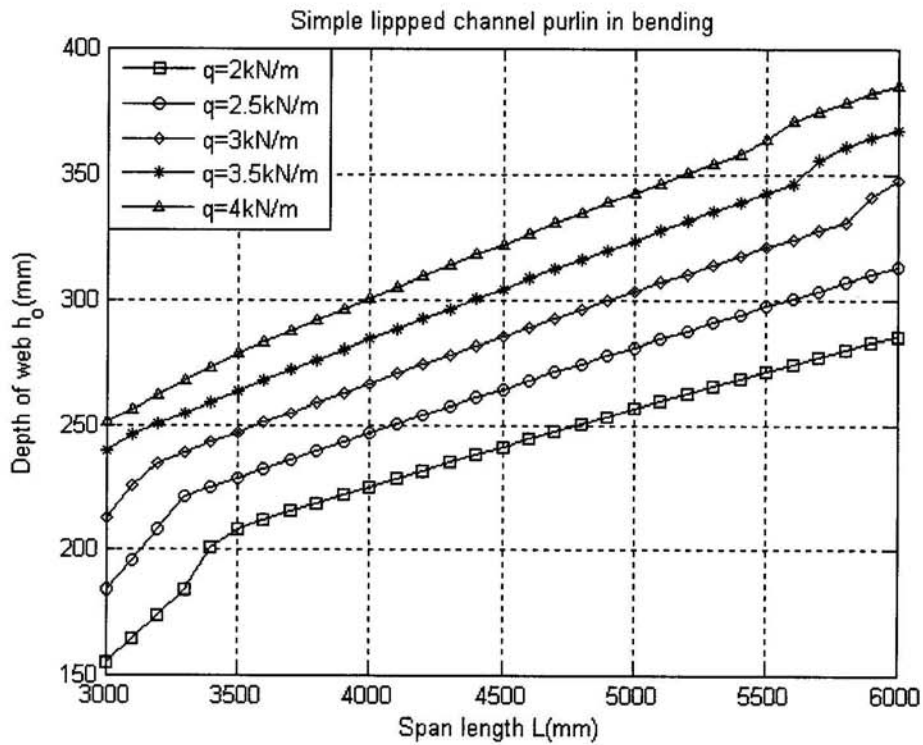
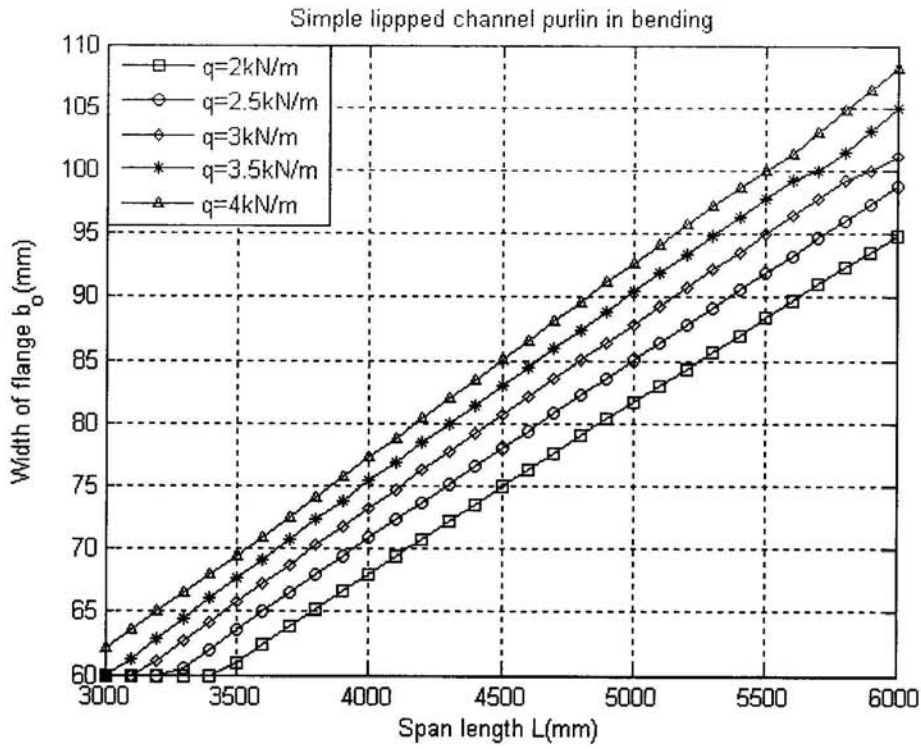


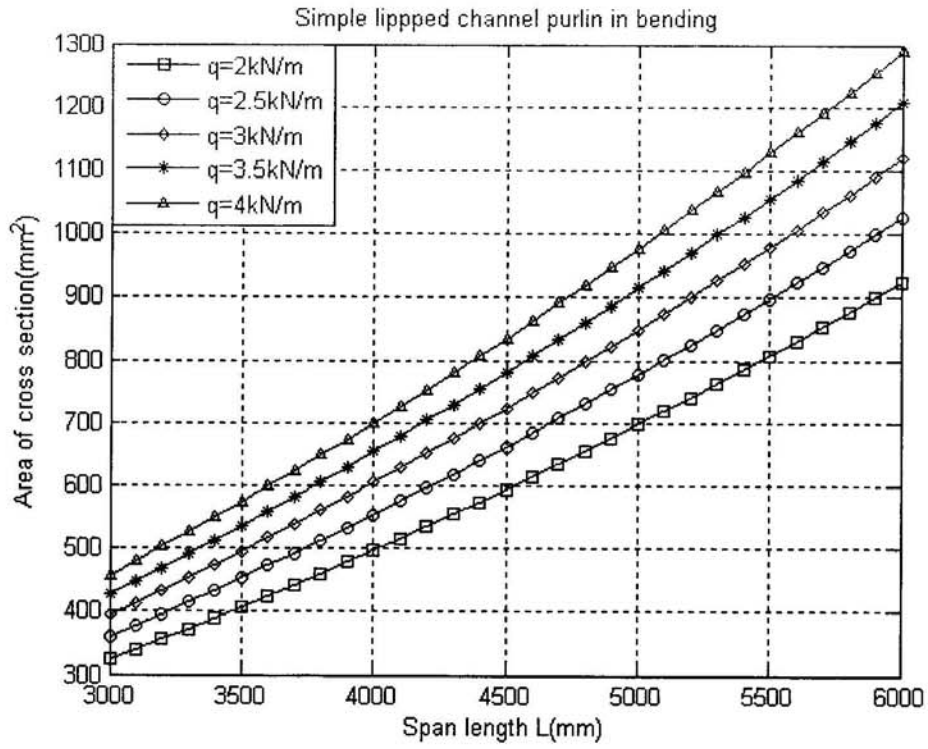




A.3.2 Simple steel lipped channel purlin in bending based on EN 1993-1-3:2006







A.4 PUBLICATIONS

1. Xiao-ting Chu, Long-yuan Li, Roger Kettle and Dinh-Tuan Tran, Local buckling behaviour of partially restrained cold-formed steel sections. *Building and Environment*. (Submitted in Jul 2004)
2. Tuan Tran, Long-yuan Li, Global optimisation of cold-formed steel channel sections. *Thin-Walled Structures*. 2006(44):399-406.